IFC-based Analysis of Present and Future Thermal Comfort using Building Energy Performance Simulation and Computational Fluid Dynamics

Von der Fakultät für Bauingenieurwesen der Rheinisch-Westfälischen Technischen Hochschule Aachen zur Erlangung des akademischen Grades einer Doktorin der Ingenieurwissenschaften genehmigte Dissertation

vorgelegt von

Veronika Elisabeth Richter

Berichter: apl. Prof. Dr.-Ing. Jérôme Frisch
Univ.-Prof. Dr.-Ing. Christina Johanna Hopfe

Tag der mündlichen Prüfung: 23. Juni 2025

Abstract

Mitigating the impacts of climate change on ecosystems and humans requires reducing greenhouse gas emissions. To achieve this reduction, political organizations such as the European Union (EU) have established targets for emission reductions, which are ratified nationally. In recent years, Germany has failed to meet its targets, partly due to the energy consumption of buildings driven by their heating and cooling demands. Suitable simulations allow for capturing the dynamic thermal performance of buildings, which can be used not only to evaluate energy efficiency but also to predict indoor thermal comfort as a driving factor in the operation of Heating, Ventilation, and Air Conditioning (HVAC) systems. However, previous research has criticized the model setup for Building Energy Performance Simulations (BEPS) and Computational Fluid Dynamic (CFD) simulations for requiring high manual effort, limiting their use in the decision-making process on energy-efficient building design. These simulations also lack interoperability within collaborative processes with the Building Information Modeling (BIM) approach.

Therefore, this dissertation presents approaches for the automated setup of BEPS and CFD models within a BIM-based design process of buildings using the open data exchange format IFC as a representation of BIM data. The proposed methods address current challenges in the automated transformation of IFC data into simulation model input. The IFC-based BEPS setup uses template-based enrichment for building constructions and zone usage to compute the thermal performance of the building at hourly resolution over a full year, including air and surface temperatures, heat fluxes, heating and cooling loads, and energy consumption. The BEPS results of a selected timestep are used to define the boundary conditions for the IFC-based CFD simulation. This CFD simulation is then used to calculate the indoor air distribution, which can be further used to optimize the operation of the HVAC systems. These IFC-based simulations form the basis for an IFC-based thermal comfort setup, which uses an extension of the template-based zone-usage enrichment for personal comfort parameters. This combined approach allows for efficiently evaluating static, local, and adaptive thermal comfort. Based on the evaluation of the annual hourly BEPS results, spaces with a high risk for thermal discomfort are evaluated in detail on their local thermal comfort through CFD. This combination enhances the reduction of computational cost by selecting only critical cases for an in-depth CFD analysis, while the overall building thermal performance is evaluated using BEPS.

The proposed approaches are applied to evaluate the impact of climate change on the energy efficiency and thermal comfort of indoor environments on different spatio-temporal scales. In addition, future energy demand and thermal comfort are predicted, and the performance of available heating and cooling capacities is evaluated under future weather conditions. Within this dissertation, the evaluation of the results for a non-residential building under future weather conditions resulting from the IPCC scenario SSP5-8.5 for the year 2050 indicate a doubling of the cooling capacity requirements, leading to an increase of cooling energy consumption of 400% and a reduction of the heating energy consumption of 30%. The presented approach on automated IFC-based simulations allows for assessing the dynamic effects in a building's thermal performance while considering both the current and the future climatic conditions. This consideration then enables evaluating the performance over the building's life cycle, supporting a paradigm shift in decision-making in the building design. By predicting future heating and cooling loads, a significant step towards an optimized, energy-efficient, comfortable building design will be achieved, providing high thermal resilience to the impact of climate change.

Kurzfassung

Um die Auswirkungen des Klimawandels auf Ökosysteme und Menschen abzumildern, müssen die Treibhausgasemissionen reduziert werden. Um diese Reduzierung zu erreichen, haben politische Organisationen wie die Europäische Union (EU) Ziele für die Emissionsreduzierung festgelegt, die auf nationaler Ebene ratifiziert werden. In den letzten Jahren hat Deutschland seine Ziele verfehlt, was unter anderem auf den Energieverbrauch von Gebäuden durch deren Heiz- und Kühlbedarf zurückzuführen ist. Geeignete Simulationen ermöglichen die Erfassung der dynamischen thermischen Performance von Gebäuden, die nicht nur zur Bewertung der Energieeffizienz, sondern auch zur Vorhersage des thermischen Komforts in Innenräumen als treibender Faktor für den Einsatz von Heizungs-, Lüftungs- und Klimaanlagen (HLK) verwendet werden kann. In früheren Forschungsarbeiten wurde jedoch kritisiert, dass der Modellerstellung für thermisch-energetische Gebäudesimulationen (engl.: Building Energy Performance Simulation, BEPS) und Strömungssimulationen (engl.: Computational Fluid Dynamic, CFD) ein hoher manueller Aufwand vorausgeht, was ihre Verwendung im Entscheidungsprozess für energieeffiziente Gebäudedesigns einschränkt. Außerdem mangelt es diesen Simulationen an der Interoperabilität innerhalb kollaborativer Prozesse mit dem Building Information Modeling (BIM)-Ansatz.

Daher werden in dieser Dissertation Ansätze zur automatisierten Erstellung von BEPS- und CFD-Modellen innerhalb eines BIM-basierten Planungsprozesses von Gebäuden unter Verwendung des offenen Datenaustauschformats IFC als Repräsentation von BIM-Daten vorgestellt. Die entwickelten Methoden adressieren aktuelle Herausforderungen bei der automatisierten Umwandlung von IFC-Daten in Simulationsmodelle. Das IFC-basierte BEPS-Setup verwendet eine vorlagenbasierte Anreicherung für Gebäudekonstruktionen und Zonennutzung, um die thermische Leistung des Gebäudes in stündlicher Auflösung über ein ganzes Jahr zu berechnen, einschließlich der Luft- und Oberflächentemperaturen, Wärmeströme, Heiz- und Kühllasten und des Energieverbrauchs. Die BEPS-Ergebnisse eines ausgewählten Zeitschrittes werden verwendet, um die Randbedingungen für die IFC-basierte CFD-Simulation zu definieren. Die CFD-Simulation berechnet die Raumluftverteilung, die zur Optimierung des Betriebs der HLK-Anlagen verwendet werden kann. Diese IFC-basierten Simulationen bilden die Grundlage für ein IFC-basiertes Setup zur Analyse des thermischen Komforts, das eine Erweiterung der template-basierten Zonen-Nutzungsanreicherung für persönliche Komfortparameter verwendet. Dieser kombinierte Modellerstellungsansatz ermöglicht eine effiziente Bewertung des statischen, lokalen und adaptiven thermischen Komforts. Basierend auf der Auswertung der jährlichen stündlichen BEPS-Ergebnisse werden Räume mit einem hohen Risiko für thermische Unbehaglichkeit detailliert hinsichtlich ihres lokalen thermischen Komforts mittels CFD bewertet. Diese Kombination trägt zur Reduzierung der Rechenkosten bei, da nur kritische Fälle für eine detaillierte CFD-Analyse ausgewählt werden, während die thermische Performance des Gesamtgebäudes mit BEPS bewertet wird.

Diese entwickelten Ansätze zur Bewertung der Gebäudeperformance auf verschiedenen räumlichen und zeitlichen Ebenen werden bei der Bewertung der Auswirkungen des Klimawandels auf die Energieeffizienz und den thermischen Komfort von Innenräumen angewandt. Darüber hinaus werden der zukünftige Energiebedarf und die thermische Behaglichkeit vorhergesagt und die Performance der aktuellen Heiz- und Kühlkapazitäten unter zukünftigen Wetterbedingungen bewertet. Im Rahmen dieser Dissertation ergab die Auswertung der Ergebnisse für ein Nichtwohngebäude unter zukünftigen Wetterbedingungen, die sich aus dem IPCC-Szenario

SSP5-8.5 für das Jahr 2050 ergeben, eine Verdoppelung der erforderlichen Kühlkapazitäten, was zu einem Anstieg des Kühlenergieverbrauchs um 400% und einer Reduzierung des Heizenergieverbrauchs um 30% führt. Mit dem vorgestellten Ansatz automatisierter IFC-basierter Simulationen zur Bewertung der dynamischen Auswirkungen auf die thermische Performance eines Gebäudes werden sowohl die aktuellen als auch die zukünftigen klimatischen Bedingungen berücksichtigt, um die Performance über den Lebenszyklus des Gebäudes zu bewerten und einen Paradigmenwechsel bei der Entscheidungsfindung in der Gebäudeplanung zu unterstützen. Durch die Vorhersage zukünftiger Heiz- und Kühllasten wird ein bedeutender Schritt in Richtung eines optimierten, energieeffizienten und komfortablen Gebäudedesigns erreicht, das eine hohe thermische Resilienz gegenüber den Auswirkungen des Klimawandels bietet.

Acknowledgments

This dissertation was created during my time at the Institute of Energy Efficiency and Sustainable Building (E3D) at RWTH Aachen University. Major parts of this thesis are based on my work in the projects BIM2SIM (grant number 03ET1562A) and BIM2Praxis (grant number 03EN1050A). Computations were performed with computing resources granted by RWTH Aachen University under projects rwth1588 and rwth1762. I am deeply grateful for the support and advice of the people around me. I would like to express my gratitude, even though I am unable to put it into words, and I apologize to those people I forgot to include in the following lines.

First and foremost, I would like to thank my doctoral supervisor apl. Prof. Dr.-Ing. Jérôme Frisch for his unwavering support and guidance. Your support began during my Master's studies, when I was still working as a student assistant at E3D. At that time, you introduced me to Vlado, who subsequently made it possible for me to complete a research stay at Stanford while still pursuing my Master's degree. During my time as a research associate, you were a constant source of wisdom and advice for all kinds of challenges I encountered throughout my research. I greatly value our collaboration, particularly your consistently reliable feedback, which I always received at the agreed-upon time. I don't know how you do it, but your quick responses to all organizational and technical requests have been tremendous support. For all these reasons, I was delighted when you became a professor, and I am honored to be the first person to have the privilege of completing my doctoral examination under your supervision.

I would also like to thank my second examiner, Univ.-Prof. Dr.-Ing. Christina Hopfe. I appreciate your supportive manner and your very honest, constructive feedback. You believed I could complete my doctoral thesis within a timeframe that I wouldn't have trusted myself to achieve. For that, I am very grateful.

I also owe great thanks to my institute director at E3D and chair of the examination committee, Univ.-Prof. Dr.-Ing. habil. Christoph van Treeck. You started the journey of my doctorate with me before allowing me to move to Jérôme's supervision. I greatly value your wealth of experience, as well as your support and backing during public appearances outside the institute.

My interest in building energy performance emerged during my cooperative Bachelor's studies at FH Westküste. At my industry partner emutec GmbH, I would like to thank my former department head Alexander Seider, representing all my colleagues there, who always patiently lent an open ear to me and my technical questions.

During my Bachelor's studies, I received a scholarship from the German Academic Scholarship Foundation, which first motivated me to pursue my Master's degree at RWTH Aachen University and financed my research stay at Stanford. I am very grateful for this support as well.

I thank you, Professor Vladimir (Vlado) Bazjanac, for inviting me to Stanford University for a research stay during my Master's studies. Your advice to "do something meaningful" in my dissertation significantly contributed to sharpening my research focus. I am grateful for my time at Stanford, the work at CIFE with Professor Martin Fischer and his research group, and for being able to get a first taste of the research world. I am thankful for the friendships that formed during that time and continue to this day.

For the support during my doctoral studies, I would also like to thank the support services at RWTH Aachen University. At a smaller university, such continuous writing consultation as I received from Fabian Rempfer would probably not have been feasible. Through the TandemDOK mentoring program and the subsequent Mastermind program, I not only met supportive fellow sufferers but also my mentor Professor Svenja Carrigan. I thank you for your open ear, your honest advice, and the insights into your own experiences in academia, which helped me tremendously.

The substantive work on my doctorate was significantly influenced by my project partners in the research projects BIM2SIM and BIM2Praxis. I would particularly like to thank David Jansen, without whose contribution the bim2sim tool would not be what it is today. I also thank Thomas Tian for his support with OpenFOAM and the BIM HVAC Tool. I would also like to thank the national and international collaborators within the groups of IBPSA Project 1, IEA EBC Annex 91, and VDI 2552 Part 11.9 for the fruitful discussions on the IFC-based data exchange for dynamic simulations.

I also thank my current and former colleagues at E3D for both the in-depth technical discussions and the interdisciplinary conversations, in alphabetical order: Oliver Abele, Linus Cuypers, Lukas Drexler, Elisabeth Hirt, Anna Hochberger, Erik Fichter, Sonja Herzogenrath, Qirui Huang, Anna Langenbeck, Clara-Larissa Lorenz, Alexander Miehlich, Maximilian Schildt, Daniel Schmitz, Maxim Shamovich, Marc Syndicus, Alexander Warthmann, and all the others.

Beyond the professional world, there are many people who closely accompanied me during the completion of my dissertation. First, I thank my friends in Hamburg for your understanding and for supporting me from afar, even though I hardly showed my face this past year. I thank the current and former board members of the Union of Baptist Churches (BEFG) in Germany for tolerating my workload and for praying for me. I also thank my Aachen friends, and particularly my church small groups, for bearing the temporal and emotional pressure with me.

Last but not least, I would like to thank my family, who have accompanied me much longer than just during my studies and doctorate. I thank my grandmother for being a constant role model with her positive attitude toward life's challenges. I thank Aunt Bärbel and Ernst for their interest in my work and their encouraging words to persevere. I thank my parents for inspiring me to grow beyond myself, and my sister for her open ear. I thank my partner Martin for our own little support group for completing our dissertations. You gave me the peace I needed to finish this work.

I am infinitely grateful to all of you.

Aachen, June 2025

Veronika Richter

Contents

List of Figures

List of Tables

List of Algorithms

Nomenclature

Latin Symbols

Symbol	Description	Unit
A	(surface) area	m^2
b	body forces, three-dimensional	N
c	specific heat capacity	J/(kgK)
c	speed of sound	m/s
d	thickness	m
f	force, three-dimensional	N
k	thermal conductivity	W/(mK)
l	(characteristic) length	m
m	mass	kg
$\dot{m}$	mass flow	kg/s
Ma	Mach number	—
n	surface normal, three-dimensional	—
n	air exchange rate	h^{-1}
Pr	Prandtl number	—
q	heat flux density	W/m^2
R	thermal resistance	m^2K/W
Re	Reynolds number	—
S	surface	m^2
t	time	s
T	temperature	K
T	stress tensor, three-dimensional	N/m^2
U	thermal transmittance	$W/(m^2K)$
v	velocity, three-dimensional	m/s
v	(characteristic) velocity	m/s
$\bar{v}$	mean velocity	m/s
V	volume	m^3

Greek Symbols

Symbol	Description	Unit
α	absorptance coefficient	—
α	thermal diffusivity	m^2/s
Δ	difference	—
ϵ	emissivity	—
Γ	diffusivity	m^2/s
λ	thermal conductivity	$W/(m\,K)$
μ	viscosity	$Pa\,s = N\,s/m^2$
ν	momentum/kinematic diffusivity	m^2/s
ϕ	intensive property	—
Φ	heat flux	W
Φ	extensive property	—
ϱ	reflectance coefficient	—
ρ	density	kg/m^3
τ	transmittance coefficient	—
θ	temperature	°C
ϑ	temperature	°C

Subscripts

Abbreviation	Description
air	air
beam	beam, direct
cond	conductive
c	convective
ci	convection, indoor
ce	convection, external
conv	convective
CM	control mass
CV	control volume
fsky	fictitious sky
inf	infiltration
int	internal
lw	long-wave

Continuing on the following page

Subscripts

Abbreviation	Description
op	operative
out	outdoor
r	radiative
rad	radiative
rm	running mean
sw	short-wave
surf	surface
tot	total
vent	ventilation

Acronyms

AoA	Age of Air
BBSR	Bundesinstitut für Bau-, Stadt- und Raumforschung, engl.: Federal Institute for Research on Building, Urban Affairs, and Spatial Development
BEM	Building Energy Model
BEPS	Building Energy Performance Simulation
BIM	Building Information Modeling
BMI	Body Mass Index
CC	Climate Change
CFD	Computational Fluid Dynamics
CMIP	Coupled Model Intercomparison Project
DR	Draught Risk
EBC	Energy in Buildings and Communities Programme
EEG	Erneuerbare-Energien-Gesetz, engl.: Renewable Energy Law
EnEfG	Energieeffizienzgesetz, engl.: Energy-Efficiency Law
EU	European Union
GCI	Grid Convergence Index
GCM	General Circulation Model
GEG	Gebäudeenergiegesetz, engl.: Building Energy Law
GHG	Greenhouse Gas
GUI	Graphical User Interface
HVAC	Heating, Ventilation and Air Conditioning
IDD	EnergyPlus Input Data Dictionary
IDF	EnergyPlus Input Data File
IDS	Information Delivery Specification
IEA	International Energy Agency
IFC	Industry Foundation Classes

IWU	Institut Wohnen und Umwelt, engl.: Institute for Housing and Environment
LCA	Life Cycle Assessment
LIC	Line Integral Convolution
MVD	Model View Definition
NA	(German) National Appendix
NRMSE	Normalized Root Mean Square Error
PCS	Personal Comfort System
PD	Percentage Dissatisfied
PMV	Predicted Mean Vote
PPD	Predicted Percentage of Dissatisfied
RCM	Regional Climate Model
RCP	Representative Concentration Pathway
RH	Research Hypothesis
RMSE	Root Mean Square Error
ROM	Reduced Order Method
RQ	Research Question
SB	Space Boundary
SSP	Shared Socio-economic Pathway
TC	Thermal Comfort
TMY	Typical Meterological Year
TMYx	Typical Meterological Year
TRY	Test Reference Year
UBEM	Urban Building Energy Modeling
UHI	Urban Heat Island

1 Introduction and Problem Statement

1.1 Motivational Background

Humans caused global warming of 1.1 °C from 1850 to 2020 through the emission of Greenhouse Gases (GHGs), and notably, 42% of cumulative GHG emissions from 1850 to 2019 occurred after 1990 [IPCC23]. This increase is one reason for the intensified local weather and climate extremes worldwide, causing harm to ecosystems and the human population [IPCC23]. In response, national [KSG24], European [EUEE, EUEPBD], and global efforts [UN15], aim to reduce the overall and building-specific CO_2 emissions to mitigate climate change.

In Germany, the current building stock accounted for about a third (i.e., 732.28 TWh=32.3% in 2023 [AGEB24]) of the nation's total energy consumption, resulting from the use of heating and hot water. Furthermore, this building stock contributed 16% (i.e., 105 Mio t-CO_2–equivalent) to the national carbon footprint in 2024 [Ago25], exceeding the maximum limit of carbon emissions by 8%, set by the German Climate Protection Law [KSG24]. As a result, this sector requires further emission reductions to meet the 2030 target of 67 Mio t-CO_2–equivalent [KSG24].

Although international and national policies have long focused on reducing CO_2 emissions to mitigate global warming [UN15, Eur21, EUEE], the energy crisis triggered by sanctions against Russia and the resulting surge in fossil fuel prices led to renewed, albeit temporary, attention to energy efficiency in Germany. As a result, to address the high costs and potential shortages of fossil fuels, the German government provided regulations such as lowering indoor air temperatures [EnSikuMaV] and optimizing heating systems [EnSimiMaV]. These regulations heightened awareness of indoor thermal comfort and sparked discussions about acceptable minimum indoor air temperatures, which could be compensated by adapting clothing [SKCK23].

This conversation on indoor thermal comfort was even started prior to the recent energy crisis when indoor thermal comfort was affected by increased natural ventilation aiming to mitigate the airborne spread of COVID-19. Several studies addressed indoor thermal comfort within classrooms and university buildings, focusing specifically on indoor air quality and thermal comfort [ALES21, MCRM21, MRV+22]. Some research also addressed the energy consumption caused by the increased natural ventilation [MAKH22], while others proposed new methods for radiant cooling combined with natural ventilation to reduce energy consumption [ACT+21].

While both the energy crisis and the increased ventilation during COVID-19 temporarily affected indoor thermal comfort, it is also increasingly influenced by global warming and associated climate changes, leading to an increased risk of summertime overheating of indoor environments. Avoiding the risk of overheating is crucial to maintaining work performance in offices,

as cognitive task performance is reduced with higher air temperatures [LLGX24].

The impacts of climate change should be considered throughout a building's lifecycle, to mitigate the impact on human well-being, visualized in Figure 1.1. Mitigation measures include optimizing building envelopes in building design and retrofit to enhance thermal resilience, as well as incorporating renewable energy supply [IPCC23].

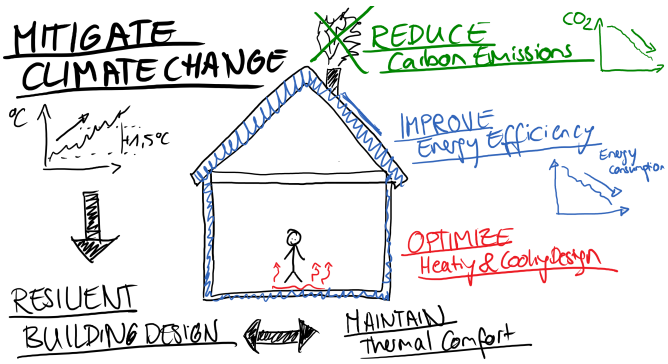

Figure 1.1: Mitigate the impact of climate change through resilient building design.

Current building codes and performance metrics primarily focus on the assessment of building energy consumption and carbon emissions, while disregarding discomfort in future climate scenarios [DDWAZ25]. As a result, thermal comfort is often neglected in the design process of buildings and indoor environments, despite its growing importance in the context of climate change. Current standards, such as [DIN16798-1], address thermal indoor environments primarily for large residential and non-residential buildings, while [DIN4108-2] provides higher thresholds for acceptable over-temperature degree hours for residential buildings (1200 Kh/a) than for non-residential buildings (500 Kh/a). Although thermal comfort is today to some extent integrated into building certifications [LEEDv5, DGNB23], occupancy ratings on thermal comfort often fail to meet acceptability criteria in office buildings [KSA18].

The profound analysis of indoor environments requires detailed indoor simulations, which utilize Building Energy Models (BEMs) as model-based representations of the physical processes in the indoor environment. However, the setup of these simulation models requires a lot of manual effort [MJvT+22] and does not automatically consider design changes. The setup process is thus too cost-expensive [Baz08] to be applied throughout all design stages of a building. The introduction of the concept of Building Information Modeling (BIM)[1] promises the standardized data exchange in the exchange format Industry Foundation Classes (IFC), which could be applied to automatically generate such BEM for Building Energy Performance Simulation (BEPS) [Baz08], and even automatically incorporate design changes. The IFC-based automated generation of these simulation models has its requirements and challenges [MOBR13], which need to be addressed and solved. Once the IFC-based setup of simulation models is established, simulations can be performed in all design stages, operation, and refurbishments of buildings,

[1] BIM describes the process creating, maintaining, and utilizing a digital representation of a building, i.e., a Building Information Model. This model typically represents a geometric and semantic representation of building objects [BKKB18], cf. Section 1.2.1.

to evaluate and support design decisions. This supports the energy-efficient design of thermally comfortable buildings, which incorporates the effects of climate change right from the design phase. Once an IFC-based setup of simulation models is available, new environmental conditions can be simulated with moderate effort, such as the requirement for increased ventilation to reduce the spread of pandemic infections or measures to maintain local thermal comfort while reducing the indoor air temperatures.

On the basis of this motivational background, this dissertation proposes methods for the automated IFC-based setup of building simulation models for BEPS and Computational Fluid Dynamics (CFD) to enhance the model-based assessment of energy efficiency and thermal comfort. These methods are evaluated using historical and future weather data to evaluate the impact of climate change.

1.2 Introduction to the Underlying Concepts

This section provides a brief introduction to the underlying concepts of BIM, BEPS, CFD, and thermal comfort, which are used in this dissertation and are further described in depth in the respective chapters. These concepts form the basis for defining the research questions in the following section.

1.2.1 Building Information Modeling and Industry Foundation Classes

Building Information Modeling (BIM) is a comprehensive methodology for the digital design of buildings that supports the continuous collaboration between stakeholders throughout the building's lifecycle. The BIM method utilizes digital workflows and digital building data representations to prevent information losses throughout the building work stages [BKKB18], illustrated in Figure 1.2. The work stages are typically defined for each country individually, e.g., in Germany according to [HOAI2021], and in the United Kingdom according to [RIBA20]. A subset of the work stages are the design stages, ranging from conceptual design to detailed design (e.g., design stages 3 to 5 as defined by [HOAI2021], and stages 2 to 4 as defined by [RIBA20]).

The resulting BIM model commonly provides a three-dimensional representation of the building, including relationships between individual elements and properties. This geometric model is enriched with additional semantic data, e.g., describing construction types, materials, occupancy schedules, and also costs. The BIM model cannot only store requirements for the building design but also data for operation, maintenance, and retrofitting, covering the whole life span of a building. [BKKB18]

In the design phase of buildings, BIM supports the design coordination between stakeholders, e.g., in clash detection. The BIM model enhances the integration of building simulations by providing geometry and material parameters, which can be further used in, e.g., building

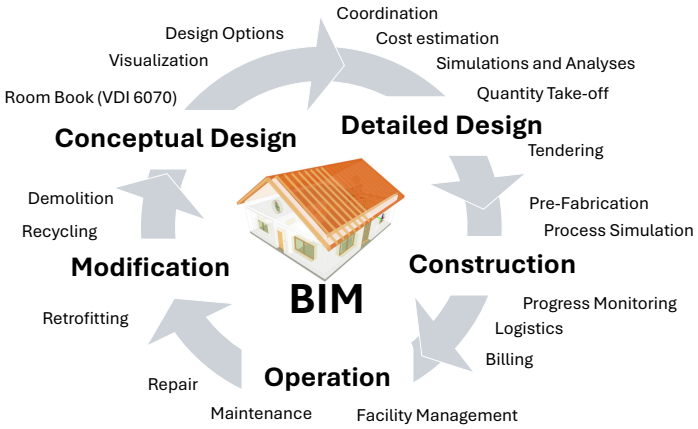

Figure 1.2: Building Information Modeling (BIM), a continuous process through the building lifecycle, holding all building data within a Building Information Model for the phases of conceptual and detailed design, the construction, operation, and modification. Adapted from [BKKB18].

performance or lighting simulations. By shifting design efforts to the earlier design phases through digital 3D modeling, the building's design can be optimized from an early design phase regarding performance and costs, reducing the risk of high costs for design changes in detailed planning phases. The data exchange requirements can be specified in different ways, e.g., by defining the Level of Development (LOD, combining the Level of Geometry (LOG) and Level of Information (LOI)), which describes the detail of semantic or geometric data, but also its design maturity or reliability. [BKKB18]

The type and extent of the application of the BIM approach within a project is visualized in Figure 1.3. It can be defined by the terms *little* and *big* BIM. Little BIM is defined as the application of the BIM method within a single construction domain or a single stakeholder, while big BIM describes the application of BIM throughout all domains and the whole building life cycle. This description of the extent of the BIM usage is combined with the declaration of the interoperability of the applied software framework. *Closed* BIM describes the use of proprietary software using proprietary data exchange format, while *open* BIM supports the use of individual software products by using open data exchange formats. The open data exchange format IFC, standardized in [DIN16739], has been developed for this purpose by the non-profit organization *buildingSMART* for the non-proprietary data exchange. [BKKB18]

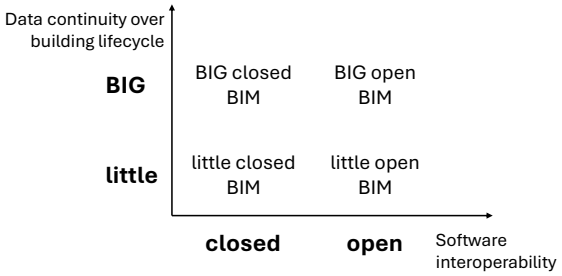

Figure 1.3: Interoperability and extent of the BIM usage within a project.

1.2.2 Building Energy Performance Simulation

Building Energy Performance Simulation (BEPS) are used to assess the dynamic energetic performance of buildings, mainly resulting from thermal heat transfer processes, and thus provide a broad range of applications that span the full bandwidth of a building's lifecycle. In recent research, BEPS is applied (1) to enhance a performance-driven building design and retrofit

optimization by supporting decision-making towards energy-efficient design optimization, (2) to represent the current calibrated state of a building's systems for further model-based optimizations to increase energy efficiency to reduce energy cost and emissions, (3) for the integration in digital twins, (4) to assess the performance of Urban Building Energy Modeling (UBEM), or (5) to predict the interaction between buildings and the grid for the integration of renewable energy sources [PZL+23]. Analyzing the building's performance during the design reduces the risk of additional cost in the operational phase [HL11]. Besides the evaluation and optimization of individual building performance, BEPS is additionally applied to evaluate the effectiveness of building energy standards on the existing building stock in terms of resulting energy savings [HL11].

Depending on its use case, the building thermal performance is assessed on different spatio-temporal scales. These include single- or multi-zone approaches for predicting heating and cooling loads, detailed evaluations on individual building components to assess heat and moisture transport, as well as in-depth analysis of air distribution in individual spaces using a CFD analysis with a high spatio-temporal resolution [vTr10]. The energy performance of buildings is influenced by transient effects, which are induced by heat and mass transfer [Cla01]. These physical effects include conduction, convection, and radiation, and are affected by the building's geometry, construction, materials, air exchange (infiltration, natural or mechanical ventilation), outdoor environment conditions, the building's location and surroundings, internal gains, and the building's operation and control [Cla01]. The computational assessment of these effects requires an appropriate setup of a Building Energy Model (BEM), including all relevant aspects of the building depending of the spatio-temporal scope of the simulation. The setup of a BEM for the use in BEPS requires a geometric representation of the building, which includes the dimension and orientation of building parts [vTr10]. The BEM can be derived from the BIM exchange format IFC to reduce manual effort for model setup while reducing human errors [Baz09]. For the evaluation of BEPS for an annual timeframe with a temporal resolution ranging from seconds to a few hours, the spatial geometry is roughly discretized on a zonal level [vTr10]. Here, the energy balances are solved for the aforementioned physical effects, including a one-dimensional heat transfer through building components between the individual zones of a multi-zone model [vTr10].

1.2.3 Computational Fluid Dynamics

Computational Fluid Dynamics (CFD) is applied to optimize Heating, Ventilation and Air Conditioning (HVAC) design to improve indoor air quality and thermal comfort [ZZW+22], to evaluate different ventilation systems regarding thermal comfort [ALNK24], to improve thermal comfort in large office spaces in the operational phase [SLS+20], or to evaluate user-controlled local thermal systems such as chairs [SCA+17]. Advanced CFD applications require high computational resources and can therefore not be economically executed on common office computers [MTC+20].

While BEPS assumes a homogeneous air distribution in each space that can be simplified to a single computational node, CFD simulations require a subdivision of the space into small volumes using a computational mesh to calculate a high-resolved air distribution within the space [THZS18]. Therefore, these simulations require a detailed representation of the space geometry [vTr10]. While IFC models can already be utilized to provide geometry for CFD applications [Fic22], engineering companies still criticize the manual effort for model healing and pre-processing that is required, e.g., for reducing the model complexity to reduce computational time, or for fixing small gaps in models to ensure the required airtightness [MJvT+22]. Since CFD simulations are sensitive to the definition of their boundary conditions, which usually cannot be generated from internal algorithms of common CFD applications, these boundary conditions can be calculated using a coupling between BEPS and CFD [THZS18]. This coupling process enhances the calculation of natural convection as well as natural and mechanical ventilation [ZC05, WW09].

1.2.4 Thermal Comfort

An overall acceptable indoor thermal comfort is the driving factor for the operation of HVAC systems in buildings [KZS+18]. As the HVAC operation accounts for more than 30% of Germany's total energy consumption [AGEB24], optimizing indoor thermal comfort is crucial for the energy-efficient design of buildings, which supports the further reduction of GHG emissions of the building stock.

A human's thermal comfort is determined by the thermal balance of its body and its surroundings [Fan70]. This heat balance is affected by the human's condition, i.e., activity level and clothing, but also by the environmental conditions, such as air conditions (temperature, velocity, humidity) and radiant temperature [ISO7730]. Based on these parameters, the human's thermal comfort can be estimated using the Predicted Mean Vote (PMV) as a measure of the mean thermal sensation of a group of people, which is further used to predict the rate of dissatisfaction of this group, defined as the Predicted Percentage of Dissatisfied (PPD) [ISO7730]. These metrics have initially been proposed by [Fan70], and are included in national and international standards on indoor thermal comfort and indoor environmental quality [ISO7730, ASH55, DIN16798-1]. These standards additionally include local thermal comfort measures that predict dissatisfaction from local thermal imbalances caused by uncomfortable floor temperatures, radiant asymmetry caused by surface temperatures, vertical air temperature differences, or Draught Risk (DR), induced by local differences in the air velocity [ISO7730]. While these measures are mainly designed for predicting thermal comfort in mechanically ventilated environments, metrics on adaptive thermal comfort [ASH55, DIN16798-1] include the human's adaptation (i.e., behavioral, physiological, psychological [dB98]) to longer periods of high outdoor temperatures, which impact the indoor temperature in naturally ventilated buildings. In these buildings, occupants have shown higher acceptability for increased indoor air temperatures than in mechanically ventilated buildings, where they have limited control over the ventilation [dB98]. For the computation of thermal comfort, some parameters can

be assessed using appropriate BEPS approaches, i.e., radiant asymmetry and floor surface temperatures, while other measures, such as vertical temperature differences and DR, require a higher spatial resolution using CFD [vTr10].

The aforementioned metrics are often criticized for several reasons, which are (1) their limited accuracy for thermal comfort predictions for individuals or small groups of people, as static (PMV, PPD) and adaptive measures are developed for comfort predictions for large groups of people neglecting the diverse physiological conditions of individuals, (2) the complex nature of PMV input parameters, resulting in parameter simplifications to avoid high measurement costs in real-world settings, and (3) these metrics do not adapt to individual thermal preferences in specific use cases. These limitations are addressed by personal comfort models that consider individual comfort feedback using data-driven approaches. These models are transferable to control Personal Comfort System (PCS). These PCS are heating and cooling systems, e.g., integrated into office chairs, that are controlled according to the individual's personal comfort demands. [KZS+18]

Another scale of individual thermal comfort is addressed by the use of thermo-physiological models that have been developed over the last decades [FLS99, TKN+02, Zha03b, Str11, Wöl17]. These models include the representation of the human's metabolic system to predict local thermal sensation and comfort for individual body parts and global sensation and comfort of a human body [Str11].

1.3 Research Questions

On the basis of the motivational background and the underlying concepts, the following Research Questions (RQs) are formulated, addressing the conceptual and detailed building design stages (cf. Figure 1.2, i.e., design stages 3 to 5 as defined by [HOAI2021], and stages 2 to 4 as defined by [RIBA20]):

RQ 1: How can both, BEPS and CFD simulations, be integrated into an IFC-based BIM workflow to increase the accessibility to dynamic building analysis for energy efficiency and thermal comfort?

RQ 2: How can current challenges in the simulation model setup (i.e., manual effort, availability and quality of data) be addressed to enhance seamless automated integration of IFC-based simulations?

RQ 3: How can IFC-based BEPS and CFD approaches be computationally efficiently combined to evaluate the energy efficiency and thermal comfort of buildings, especially related to climate change?

These RQs are addressed in the four main chapters of this dissertation and focus on IFC-based BEPS, IFC-based CFD, IFC-based thermal comfort, and the application of these methods to assess the climate change impacts during the design phase. Each chapter introduces specific Research Hypotheses (RHs), formulated on the basis of identified gaps in related research and

aligned with the corresponding RQs. The relationships between RQs and RHs are visualized in the Appendix, Figure A.1. These RHs underpin the proposed methodology, which is tested individually and collectively to evaluate the RQs.

1.4 Outline of Dissertation

This dissertation introduces a workflow for transforming IFC to CFD models using boundary conditions from IFC-based BEPS. The resulting IFC-based BEPS and CFD models are used to assess building energy efficiency and indoor thermal comfort. The developed approaches are further evaluated under the impact of projected climate change scenarios.

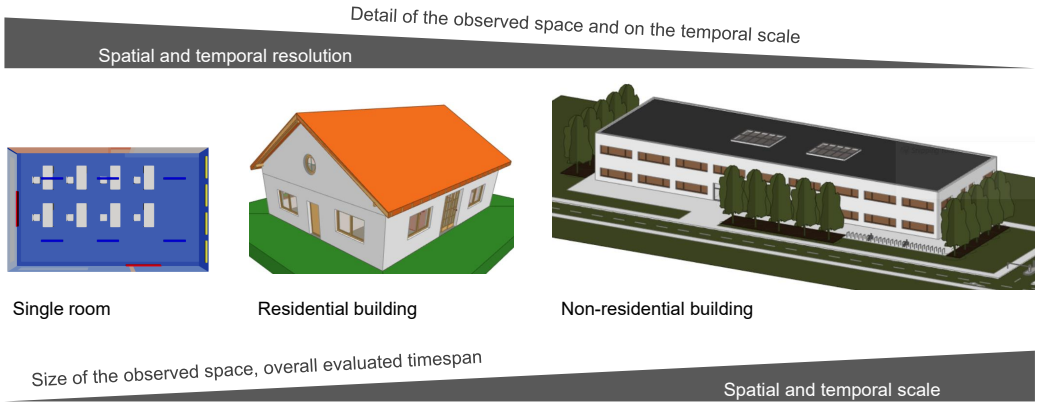

Figure 1.4: Spatial and temporal scales as well as spatial and temporal resolutions for evaluation of the proposed methods.

The proposed methods are evaluated across varying applicable temporal and spatial scales, as illustrated in Figure 1.4. CFD simulations calculate spatially high-resolved air distributions at an individual room level (i.e., comparatively small spatial scale and high spatial resolution) for a specific timestep of interest (i.e., small temporal scale, high temporal resolution). In contrast, BEPS supports an evaluation the annual (i.e., large temporal scale) thermal performance results of the building in hourly steps (i.e., low temporal resolution), represented as the individual mean results for each building surface and space (i.e., large spatial scale, low spatial resolution). The applicability of these methods is demonstrated on both residential and non-residential buildings.

Figure 1.5 depicts the structure of this dissertation. Chapter 2 introduces the IFC-based BEPS workflow. Chapter 3 builds on this workflow an describes the method for IFC-based CFD. Chapter 4 further extends the workflow by incorporating a method for IFC-based thermal comfort assessment. Chapter 5 focuses on the combination of all proposed IFC-based approaches, used to assess the impact of climate change scenarios on the decision making process in the building design. Chapter 6 provides a discussion on the limitation of the proposed method. Chapter 7 and Chapter 8 provide the conclusion and outlook, respectively.

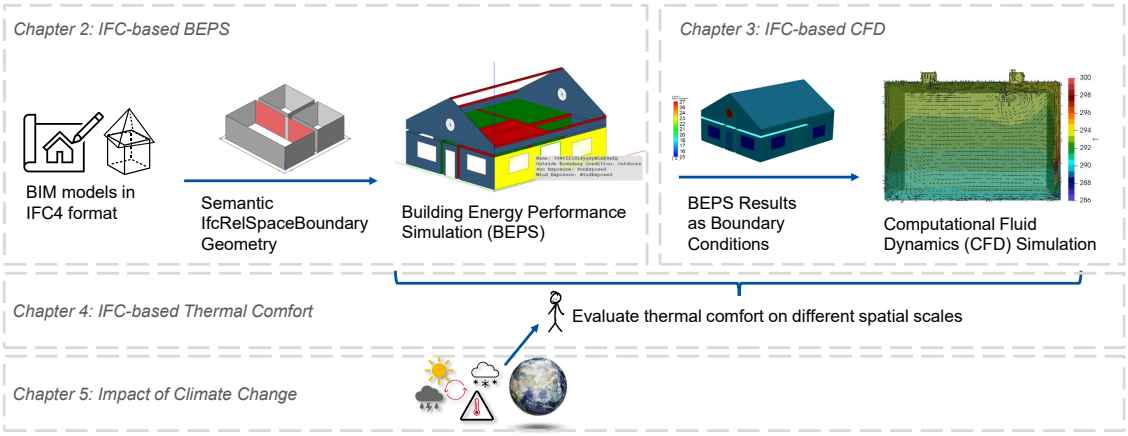

Figure 1.5: IFC-based analysis of indoor spaces: A combined approach for the IFC-based setup of BEPS and CFD to enhance thermal comfort assessment and evaluate the impact of climate change.

2 IFC-based Building Energy Performance Simulation

With the goal of enhancing the accessibility of dynamic BEPS within BIM workflows, the open data exchange format IFC provides the required data on the building design. These data can be leveraged to develop automated simulation model setup processes. This chapter introduces a process of IFC-based BEPS with EnergyPlus. While Section 2.1 introduces the fundamentals of BEPS, Section 2.2 then describes the relevant data exchange formats and software tools. Section 2.3 subsequently provides a comprehensive review of the related research in this field. This section also provides the definition of a preliminary research gap and the resulting RHs, discussed in Section 2.3.4, which guide the development of the proposed methodology. Section 2.4 focuses on the methodology used in this dissertation and addresses both, methods for the BEPS generation (Section 2.4.1), and the algorithms for the validation and correction of errors hindering the automated BEPS setup (Section 2.4.2). Based on this methodology, Section 2.5 presents the implementation of the *PluginEnergyPlus*, while Section 2.6 presents a stand-alone validation tool. Section 2.7 ultimately provides the evaluation of both, the *PluginEnergyPlus* and the validation tool. Section 2.8 concludes this chapter, providing an evaluation of the defined RHs.

The methods developed in this chapter form the foundation for the IFC-based CFD approach, presented in Chapter 3. The CFD models using the open-source Kernel OpenFOAM are further enriched with the boundary conditions precomputed from the IFC-based BEPS approach.

2.1 Fundamentals of Building Energy Performance Simulation

Simulations in buildings can be distinguished on different use cases, which include steady-state heat balance simulations, dynamic multi-zone simulations, and detailed simulations on fluid dynamics, radiation and heat conduction [vTr10]. These approaches vary in both, their spatial (e.g., building component, zone, whole building) and their temporal (i.e., duration: e.g., single timestep, day, week, year; step size: calculated at e.g., every second, minute, hour) resolution [vTr10]. Thus, these approaches can be combined on both scales to meet the requirements of the individual simulation objective.

Such building simulations require an abstract representation of the building in form of a BEM, which represents the geometric and semantic information of a building. The BEM has to be setup to meet a specific simulation objective: While district energy demand simulations may only require a rough estimation of individual building volumes and statistically enriched construction parameters [RLM+18], BEPSs on a building or even individual room-scale require geometric information on the position of walls inside and outside of the simulated building. For

very detailed simulations on heat transfer, the geometric properties of the complete building may be irrelevant, while the individual layers of the wall, or even thermal bridges have to be modeled with a high detail. This dissertation focuses on the BEPS of individual buildings with hourly temporal resolution with the maximum time-span of a year, and thus, requires information on the building geometry, as well as on the general building construction.

2.1.1 Heat Transfer Mechanisms

The profound knowledge on the heat transfer mechanisms in buildings is critical for understanding BEPS. This introduction gives a rather qualitative overview of the physical heat transfer processes inside and around buildings. For a quantitative overview and details on the mathematical background see [vTr10].

According to the second law of thermodynamics ('principle of irreversibility'), heat flows in the direction from higher to lower temperature, aiming to reach equilibrium [MSBB14]. The heat flow rate Φ, also called heat flux, is defined as the transferred heat Q by time t

$$\Phi = \frac{dQ}{dt}, \tag{2.1}$$

which can be expressed in a non-differential form $\Phi = Q/t$ for heat flux in steady state [Pin21]. The heat transfer mechanisms are conduction, convection, and radiation, as displayed in Figure 2.1.

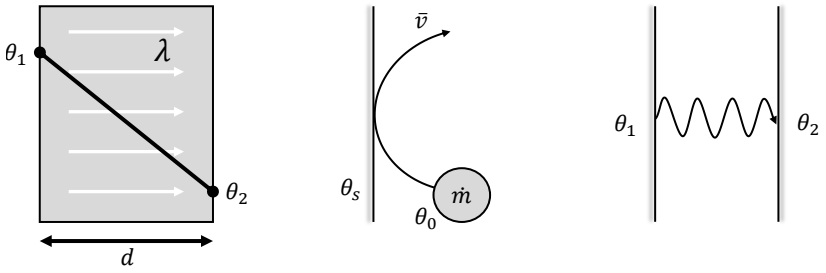

(a) Conduction (b) Convection (c) Radiation

Figure 2.1: Heat Transfer Mechanisms, adapted from [vTr10].

Conduction

Conduction is applicable for heat transfer in a material and for connected materials [Wil22]. It describes the process of heat exchange through oscillating electrons, which collide with free electrons that are randomly diffusing through a (typically solid) material [Pin21]. The conduction can be defined according to Fourier's law for the steady state, i.e., only spatial but no temporal variations are considered [Pin21]. The heat flux can be formulated for a simplified one-dimensional heat transfer through a wall as the heat flux Φ per surface area A, also called

heat flux density q [Wil22, Pin21]:

$$q = \frac{\Phi}{A} = -\lambda \frac{d\theta}{dx}. \tag{2.2}$$

Here, the heat flux density scales with the heat conductivity λ of the material, as well as with the rate of temperature change $d\theta$ with respect to its spatial position dx. Looking at Figure 2.1a, representing the cross-section of a wall with the thickness d, a surface area A, the surface temperatures θ_1 and θ_2, and the heat conductivity λ, the heat flux Φ can be discretized in a steady-state condition [Wil22]:

$$\Phi = \lambda \frac{\theta_1 - \theta_2}{\Delta d} A. \tag{2.3}$$

A general introduction to discretization approaches is given in the introduction to numerical methods in Section 3.1.3 for the application in the field of CFD.

The heat conduction through a building element is characterized by the ratio of element thickness d and thermal conductivity λ defined as the thermal resistance $R = d/\lambda$ [Pin21]. The inverse of the sum of the thermal resistances (R_{tot}) of all element and boundary layers (R_i) of an element result in the total thermal transmittance U [DIN6946], called U-value:

$$U = 1/R_{\text{tot}} = 1/\sum_{i=1}^{n} R_i. \tag{2.4}$$

Convection

Convective heat transfer describes the heat transfer between an element and a fluid. The convective heat flux at a surface, visualized in Figure 2.1b, depends on the convective heat transfer coefficient h_c, the mean flow velocity $\bar{v}$ and the resulting mass transport $\dot{m}$, the temperature gradient between the surface θ_s and adjacent fluid θ_0, as well as the roughness of the surface [Wil22, vTr10]. The friction between fluid and surface causes a fluid velocity v_s of zero directly at the surface, resulting in a boundary layer due to the viscosity of the fluid, where both the velocity and temperature gradually change from the condition at the surface (v_s, θ_s) to the mean condition of the fluid ($\bar{v}$, θ_0) outside the boundary layer [Pin21]. The convective heat flux density can thus be defined as [Pin21]:

$$q = h_c(\theta_s - \theta_0). \tag{2.5}$$

Convection can be distinguished into natural and forced convection, depending on their driving forces. The driving forces for natural convection are mainly temperature differences, while forced convection results from air velocities due to wind or mechanical ventilation [vTr10]. For the application in buildings, the international standard [DIN6946] provides convective heat transfer coefficients for surfaces in indoor environments h_{ci} based on the direction of convective flow (upwards: $h_{ci} = 5.0\,\text{m}^2\,\text{K/W}$, horizontal: $h_{ci} = 2.5\,\text{m}^2\,\text{K/W}$, downwards: $h_{ci} = 0.7\,\text{m}^2\,\text{K/W}$). For external surface convection, the external convective heat transfer coefficient h_{ce} is calculated based on the wind speed v, i.e., $h_{ce} = 4 + 4 \cdot v$ [DIN6946].

Radiation

Radiation, visualized in Figure 2.1c, describes the heat exchange between elements through electromagnetic forces, resulting from surface temperature differences $\Delta T = \theta_1 - \theta_2$ of these elements. Radiation can be distinguished into shortwave (i.e. solar radiation) and longwave radiation (i.e., radiative heat transfer between elements). [Wil22, vTr10]

The radiant heat transfer at a surface is characterized by the radiative heat transfer coefficient $h_r = \epsilon \cdot h_{r0}$, where ϵ is the hemispherical emissivity of the surface, and h_{r0} is the radiative coefficient for a black body surface. The radiative and convective heat transfer coefficients are combined to the surface resistance $R_s = 1/(h_c + h_r)$, which adds to the total thermal resistance of building elements and its resulting U-value (cf. Equation 2.4). [DIN6946]

Heat Transfer in Buildings

All previously introduced heat transfer mechanisms can be observed in- and outside of a building, as illustrated in Figure 2.2 for the example of a building thermal zone.

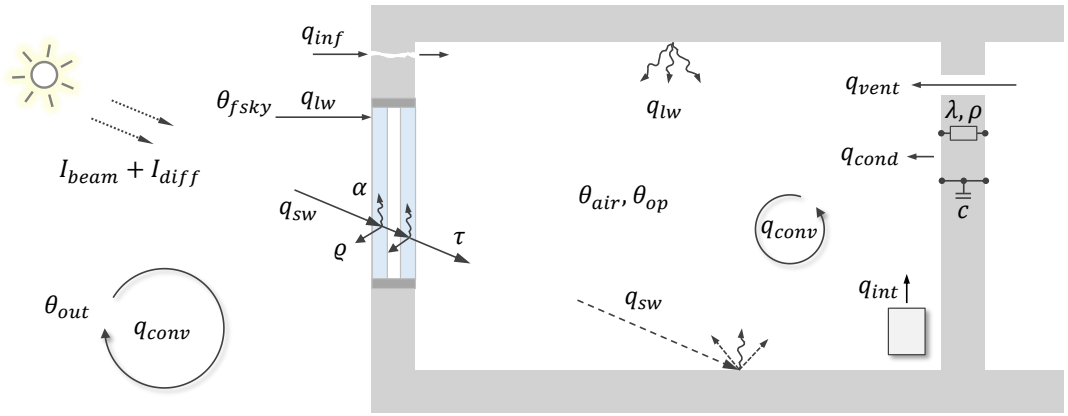

Figure 2.2: Heat transfer mechanisms related to a thermal zone, adapted from [vTr10].

The sun emits shortwave radiation q_{sw}, which is defined by the sum of the direct or beam (I_{beam}) and diffuse radiation (I_{diff}) [vTr10]. The solar position and the incident angle of the solar irradiance vary due to the time of the day and season. The solar shortwave heat flux q_{sw} is only partially transmitted (transmittance coefficient τ) into the thermal zone, but also reflected (reflectance coefficient ϱ) and absorbed (coefficient α). The fictitious sky temperature θ_{fsky} is used to compute the longwave heat transfer of the environment q_{lw}. Long wave radiation q_{lw} applies to the heat exchange between the building exterior and interior. The outside temperature is considered as θ_{out}, and the indoor air temperature as θ_{air}. The operative temperature θ_{op} represents the weighted mean of the indoor air temperature and the mean radiant temperature of the surrounding surfaces, while the weights are defined based on the prevailing air velocity, e.g., equal weights are applied for low air velocities $v < 0.2\,\text{m/s}$ [ASH55]. The environment convective heat flux q_{conv} is a forced convection due to wind. The indoor convective heat flux q_{conv} is considered as forced convection if a mechanical ventilation system is available, and

as natural convection otherwise. The thermal zone has further heat fluxes due to infiltration from the outside q_{inf} and, if available, from mechanical ventilation q_{vent}. Heat transfer through walls is considered as conductive heat flux q_{cond}, depending on the heat conduction λ, the density ρ, and the specific heat capacity c. Inside the walls, heat storage effects are observed due to absorption [vTr10]. Internal heat fluxes q_{int} represent internal heat gains from electric equipment, lighting, occupants, but also from internal heating and/or cooling devices.

2.1.2 Introduction to the Concept of Space Boundaries

A simplified representation of a building's geometry can be obtained by defining so-called Space Boundaries (SBs). [Bjö92] provides an early, general definition of these boundaries. He defines Space Boundaries (SBs) as

> "An abstract concept which represents a part of the infinitesimally thin skin which surrounds a space or enclosing structures that bounds it. Subspaces can in addition to physical boundaries also have imaginary space boundaries."[Bjö92]

This definition was considered in the context of a variety of purposes within buildings, such as construction management, evaluating building constructions against regulatory standards, and calculating heating demands.

[Baz10] states SB requirements specifically for the use in BEPS, considering the energetic aspects of buildings. While [Baz10] categorized SBs in up to five levels, this dissertation only considers the SB levels 1, 2a, and 2b, which align with the representation in the open BIM-Standard IFC (cf. Section 2.2.1 for further information on the representation in IFC4).

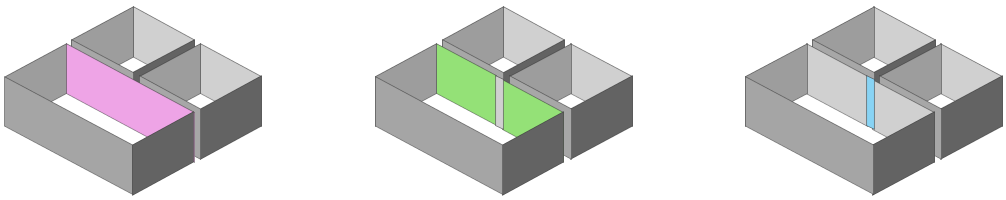

(a) 1st Level (b) 2nd Level, Type 2a (c) 2nd Level, Type 2b

Figure 2.3: 1st and 2nd level space boundaries.

Figure 2.3 displays these three types of SBs. The simplest level of SBs is represented by the first level (Figure 2.3a). According to [Baz10], the first-level SBs are defined by the full section of a modeled wall that is visible from its corresponding zone. These boundary representations do not consider any heat transfer to adjacent zones within the building.

To model heat transfer to adjacent thermal zones or building elements, second-level boundaries are used. These consider changes on the opposite side of the corresponding building elements, given by changes in the building construction or adjacent zones. Second-level boundaries of type 2a (Figure 2.3b, Level 2 according to [Baz10]) represent the sections of first-level SBs, which transfer heat to an adjacent zone of the building exterior. SBs of type 2b (Figure 2.3c, Level 3

according to [Baz10]) define second-level SBs, which do not represent heat transferring surfaces to adjacent zones, since opposite of the 2b SB is a building element, but no thermal zone. Level 4 and 5 according to [Baz10] can for simplicity be classified as special cases of type 2b, with no direct heat transfer to adjacent zones due to adjacent building elements (Level 4) and tilted surfaces (Level 5).

2.1.3 Input Requirements for Building Energy Performance Simulations

From the previous introductions on the heat transfer mechanisms in buildings in Section 2.1.1 and Figure 2.2 and on the geometric representation of heat transferring surfaces in form of SBs in Section 2.1.2, a list of general input requirements for BEPS can be derived. The input requirements include data on

- **Building geometry**: Geometric representation of the heat-transfer surfaces of a building, e.g., represented by SBs,
- **Building construction**: Information on the building materials and construction to calculate heat transfer and heat storage inside buildings,
- **Boundary conditions**: Information on the boundary conditions at the surrounding surfaces, e.g., heat transfer to another zone or the outdoor environment, or adiabatic conditions without heat transfer,
- **Internal loads**: Information on internal heat sources. This includes knowledge on heat transfer from electric equipment, machines, occupants, and heating and cooling devices,
- **Heating and cooling schedules**: Information on the operation of the building, in terms of schedules for setpoint temperatures of thermal zones,
- **Environmental parameters**: Weather (e.g., outdoor temperature, solar radiation, wind speed, humidity), location and orientation of the building, external shadings,
- **General simulation settings**: Simulation period, temporal resolution, solvers,
- **Simulation outputs**: Definition of output variables for further evaluation of results.

Using these parameters for setting up a BEPS, the thermal dynamic behavior of the building can be estimated depending on the input weather files. As opposed to static calculations on energy demands, this dynamic simulation is able to consider heat storage effects, as well as interzonal heat transfer, which, however, depends on the choice of BEPS kernel. The BEPS kernel includes the computational algorithms for solving the building physics equations for performing a BEPS. In this dissertation, EnergyPlus is used as the computational kernel for BEPS, which is introduced in Section 2.2.2.

2.1.4 Regulations and Standards for Energy Efficiency and Heating and Cooling Load Calculations

For the design of energy-efficient buildings, several laws, regulations, and standards apply. According to [Eur21], European buildings account for 40% of the total consumed energy, which

results in 36% of the energy-related greenhouse gas emissions.

Table 2.1 lists European and German laws and directives aiming for energy-efficiency and carbon neutrality. The European Union (EU) presented the 'European Green Deal' in 2019 with the aim of net-zero greenhouse gases in 2050 while securing a resource-independent economic growth [EUECL]. This finally lead to the 'European Climate Law' [EUECL], regulating climate neutrality in the EU by 2050 and also setting targets for 2030 greenhouse gas reductions. To meet these goals, the energy-efficiency directive [EUEE] has been renewed to support the European independent energy supply without fossil fuels by defined energy saving obligations.

Table 2.1: German and international law for energy-efficient building design.

Directive	Year	Title	Reference
2021/1119/EU	2021	Regulation establishing the framework for achieving climate neutrality ('European Climate Law')	[EUECL]
2023/1791/EU	2023	Directive on energy efficiency	[EUEE]
2024/1275/EU	2024	Directive on the energy performance of buildings	[EUEPBD]
KSG	2024	Bundes-Klimaschutzgesetz	[KSG24]
EEG	2024	Gesetz für den Ausbau erneuerbarer Energien (Erneuerbare-Energien-Gesetz - EEG 2023)	[EEG23]
EnEfG	2023	Gesetz zur Steigerung der Energieeffizienz in Deutschland (Energieeffizienzgesetz - EnEfG)	[EnEfG23]
GEG	2024	Gesetz zur Einsparung von Energie und zur Nutzung erneuerbarer Energien zur Wärme- und Kälteerzeugung in Gebäuden (Gebäudeenergiegesetz - GEG)	[GEG24]

[EUEPBD] is a response to accomplish these energy-efficiency goals and greenhouse gas reduction for buildings. The directive requires national building renovation plans for each EU member state to establish zero-emission buildings by 2050. By 2030, all new constructed buildings should be zero-emission buildings. Apart from a defined minimum requirement path for reducing the energy consumption of building stock, the directive sets the goal to accomplish the average primary energy use towards a zero-emission building stock by 2050. The Annex 1 of the directive states minimum requirements for the calculation of the energy performance in buildings, requiring a monthly, hourly or sub-hourly computation to consider time varying effects inside the buildings, such as thermal capacity or internal loads. The calculation approach should be defined in national directives. [EUEPBD]

These European directives are reflected in German laws. The Bundesklimaschutzgesetz (KSG, engl.: German National Climate Law) [KSG24] defines national goals for climate action to reduce the greenhouse gases compared to 1990 by 65% until 2030 and by 88% until 2040. Zero-emission should be reached by 2045, negative emissions should be reached by 2050. To support these goals, the national Erneuerbare-Energien-Gesetz, engl.: Renewable Energy Law (EEG) [EEG23] aims for 80% of renewable energy in the production of electric power, measured by the gross consumption of electric energy. The corresponding national law to the EU law for energy-efficiency [EUEE] is the German Energieeffizienzgesetz, engl.: Energy-Efficiency Law (EnEfG) [EnEfG23]. The German Gebäudeenergiegesetz, engl.: Building Energy Law (GEG) [GEG24] corresponds to the EU Law on building energy efficiency [EUEPBD]. The GEG defines the national path for the reduction of energy consumption in buildings and regulates the

calculation of building performance by referring to [DINV18599-1].

Table 2.2 and Table A.1 list standards and regulations for the performance and energy efficiency of buildings and building design. The European Directive [EUEPBD] refers to multiple standards, mainly from the standard series DIN/ISO 52xxx (see Table A.1) to calculate and rate the energy performance of buildings. However, even though national annexes are available, these standards are currently not applicable for the use under German law [DIN52000-1, DIN52003-1, DIN52010-1, DIN52016-1, DIN52018-1, ISO52120-1], which has also been elaborated by [dena24]. Two of those by [EUEPBD] referred standards outside of the DIN/ISO 52xxx series remain applicable under German Law, which are [DIN17423] on determining primary energy factors and CO_2 emission coefficients and [DIN16798-1] on indoor climate.

Table 2.2: German and international regulations and standards for energy-efficient building design, adapted and extended from [vTFW+21].

Regulation	Year	Title	Reference
DIN EN 17423	2021	Energy performance of buildings - Determination and reporting of Primary Energy Factors (PEF) and CO_2 emission coefficient - General Principles	[DIN17423]
DIN EN 16798-1	2022	Energy performance of buildings - Ventilation for buildings - Part 1: Indoor environmental input parameters for design and assessment of energy performance of buildings addressing indoor air quality, thermal environment, lighting and acoustics	[DIN16798-1]
DIN V 18599-1	2018	Energy efficiency of buildings - Calculation of the net, final and primary energy demand for heating, cooling, ventilation, domestic hot water and lighting - Part 1: General balancing procedures, terms and definitions, zoning and evaluation of energy sources	[DINV18599-1]
DIN EN 12831-1	2017	Energy performance of buildings - Method for calculation of the design heat load - Part 1: Space heating load	[DIN12831-1]
DIN 4108-2	2013	Thermal protection and energy economy in buildings - Part 2: Minimum requirements to thermal insulation	[DIN4108-2]
VDI 2078	2015	Calculation of thermal loads and room temperatures (design cooling load and annual simulation)	[VDI2078]
VDI 6007	2015, 2012, 2015	Calculation of transient thermal response of rooms and buildings - Modelling of rooms, windows and solar radiation	[VDI6007-1, VDI6007-2, VDI6007-3]
VDI 6020	2022	Requirements to be met by calculation methods for the simulation of thermal-energy efficiency of buildings and building installations	[VDI6020]
ASHRAE 140	2020	Method of Test for Evaluating Building Performance Simulation Software	[ASH140]

Instead of applying the standards referenced by European law, the GEG refers to [DINV18599-1] as national reference for calculation of energy performance. This standard provides twelve parts for the calculation of energy efficiency ratings of buildings. However, while [DINV18599-1] provides regulations for the energy performance rating of buildings, several other standards are available for the system sizing of individual components in a specific thermal zone inside a building [DIN16798-1, DIN4108-2, DIN12831-1, VDI2078]. The European standard [DIN16798-1] provides requirements for the indoor environmental quality of buildings for application in the building design process, including heating and cooling setpoints and limits for thermal comfort. The fundamental requirements on thermal insulation, thermal bridges, and on heat protection are standardized in [DIN4108-2]. For static calculations of the design heat load of spaces, [DIN12831-1] is applied in Germany. Similarly, the [VDI2078] applies for calculating design

cooling loads but applies a simplified 2-capacity model according to [VDI6007-1], referred to as lumped capacitance model (i.e., lumping all capacities of building components with temperature asymmetry to neighboring spaces, and lumping capacities of adiabatic components (temperature symmetry using $\Delta\theta < 4\,\mathrm{K}$) [VDI2078]), combined with a standardized process for considering cooling design periods. This simplified calculation approach of [VDI2078] may produce sufficient results for many use cases and has the advantage of low computational cost [GNH+22].

§ 33 GEG allows for dynamic BEPS approaches instead of the calculation approach defined in [DINV18599-1] for special cases where prior knowledge of thermal behavior is insufficient. For these dynamic simulations, the same boundary conditions need to be applied as for the usual standardized approach. The two major guidelines that apply for dynamic BEPS in Germany are VDI 6007 and [VDI6020]. VDI 6007 [VDI6007-1, VDI6007-2, VDI6007-3] provides an approach for dynamic building simulation, which is also applied in [VDI2078]. However, this approach includes a simplified calculation that is validated using the validation approaches of [VDI6020], which are strongly aligned with the simulation approaches presented in VDI 6007. [GNH+22] claim that [VDI6020] is too closely designed for validation of VDI 6007 that other, more detailed physical simulation approaches cannot be validated with [VDI6020] even though they may be closer to reality. Another validation approach for simulation tools is provided by [ASH140]. [DSFvT23] evaluated their Reduced Order Method (ROM) that builds upon VDI 6007 using [ASH140]. Their model resulted in substantially higher heating and cooling loads than the compared simulation tools, but it is not clear from the study how much these deviations result from VDI 6007 and how much they are caused by other model adaptations made in the setup process of their ROM.

2.2 Data Exchange and Software Tools

This section introduces the relevant data exchange formats and software tools used in the methodology of IFC-based BEPS. This includes brief introductions to IFC as Open BIM standard, to EnergyPlus and related tools, and to the open-source *bim2sim* tool, which is used as a framework for implementing the IFC-based simulations in this dissertation.

2.2.1 IFC as Open BIM Standard for Use in BEPS

Various BIM formats are available for data exchange, both proprietary data formats developed by the software vendors and open-BIM exchange formats. The two most common open-BIM exchange formats are green building XML (gbXML), and Industry Foundation Classes (IFC). A recent study has shown that both IFC- and gbXML-based BEM processes have interoperability issues [BPDSFB21]. However, as the IFC format has a broader field of application compared to gbXML, and gbXML uses a centerline positioning of Space Boundaries (SBs) [PWO+18], this dissertation uses IFC as input format. The IFC standard is defined in [DIN16739] and is

published by buildingSMART international. The latest official standard is IFC4.3 ADD2, but in industry, the outdated IFC2x3 TC1 (released in 2007) standard is still the most frequently used standard [NAOKS21, MJvT+22]. This dissertation focuses on the IFC4 ADD2 TC1 standard, since later updates mainly include infrastructural extensions,[1] which are not considered within the scope of BEPS. The IFC4 ADD2 TC1 standard is further referred to as IFC if not otherwise specified.

This introduction to IFC only presents the most important concepts for this dissertation; a full introduction is provided by buildingSMART.[2] The IFC data schema is described as a relational construct out of entities. IFC files are commonly represented in a STEP file, which supports the relational nature of IFC data. All IFC instances inherit from the *IfcRoot* class, which holds the attribute of a unique *GlobalId* for all IFC entities, but also the *OwnerHistory*, *Name*, and an attribute for a *Description*.[3] Figure 2.4 displays the composition and placements of an *IfcSite*, *IfcBuilding*, *IfcBuildingStorey*, *IfcSpace*, and their related *IfcProducts*, e.g., building elements, such as *IfcWall* and *IfcSlab*. The placement of the building is relative to the placement of the site, and the placement of the storey is relative to the building. The placement of the products contained in the building or storey is relative to either the building or the storey, respectively.

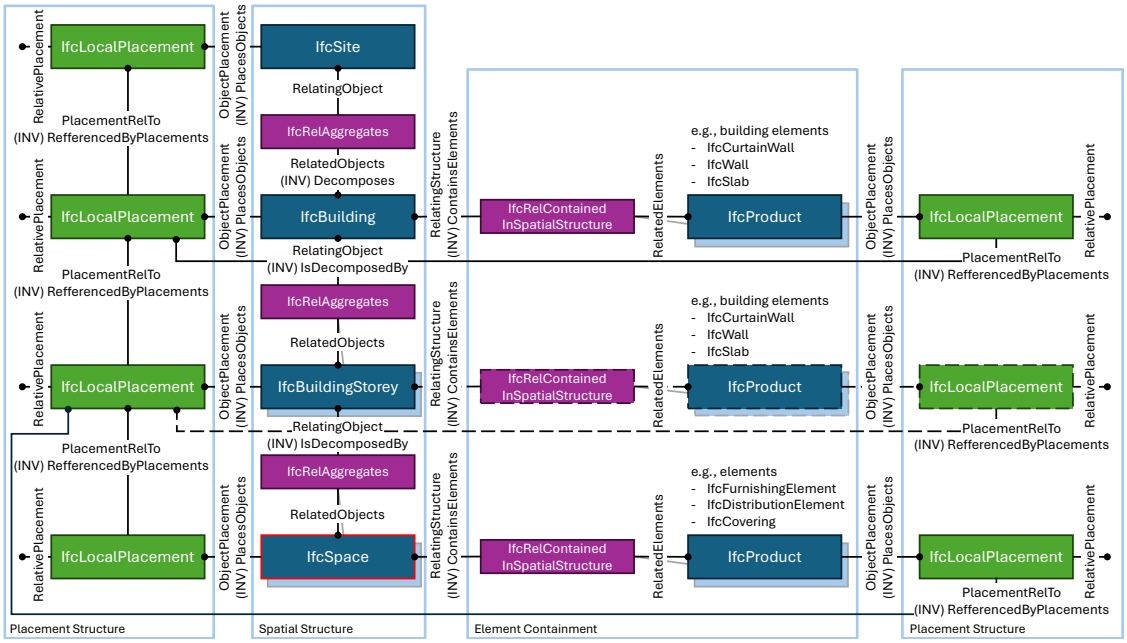

Figure 2.4: Composition and placements of site, building, storeys, spaces, and products within the IFC4 add2 TC1 standard.[4]

[1] IFC Release Notes: https://technical.buildingsmart.org/standards/ifc/ifc-schema-specifications/ifc-release-notes/, accessed on May 19, 2025.

[2] IFC4 add2 TC1 standard: https://standards.buildingsmart.org/IFC/RELEASE/IFC4/ADD2_TC1/HTML/, accessed on May 19, 2025.

[3] IfcRoot in the IFC4 add2 TC 1 standard: https://standards.buildingsmart.org/IFC/RELEASE/IFC4/ADD2_TC1/HTML/link/ifcroot.htm, accessed on May 19, 2025.

[4] Building and Space Composition in the IFC4 add2 TC1 standard, adapted from https://standards.buildingsmart.org/IFC/RELEASE/IFC4/ADD2_TC1/HTML/link/ifcbuilding.htm and https://standards.buildingsmart.org/IFC/RELEASE/IFC4/ADD2_TC1/HTML/link/ifcspace.htm, accessed on May 20, 2025.

The placement of the spaces and their contained products is relative to the related storey of the space. *IfcObject*[5] entities with their subclasses, such as *IfcProduct*, can hold *IfcPropertySets* which are used to define further properties of these products.[6]

The IFC standard includes a representation of SBs (cf. Section 2.1.2). For the use cases of both simulation methods in this dissertation, BEPS and CFD, SBs are required as heat transfer surfaces between thermal zones and surface boundary conditions on the boundaries of the computational domain, respectively. Thus, only second-level boundaries are discussed in this section. The *IfcRelSpaceBoundary2ndLevel* parameters are represented in the IFC4 ADD2 TC1 data schema as displayed in Table 2.3, which is adapted from [MJvT+22] and the buildingSMART documentation.[7]

Table 2.3: Representation of *IfcRelSpaceBoundary2ndLevel* in the IFC4 data schema.

Position	Attribute	Type	Cardinality
IfcRoot			
1	GlobalId	IfcGloballyUniqueId	required
2	OwnerHistory	IfcOwnerHistory	optional
3	Name	IfcLabel	optional
4	Description	IfcText	optional
IfcRelSpaceBoundary			
5	RelatingSpace	IfcSpaceBoundarySelect	required
6	RelatedBuildingElement	IfcElement	required
7	ConnectionGeometry	IfcConnectionGeometry	optional
8	PhysicalOrVirtualBoundary	IfcPhysicalOrVirtualEnum	required
9	InternalOrExternalBoundary	IfcInternalOrExternalEnum	required
IfcRelSpaceBoundary1stLevel			
10	ParentBoundary	IfcRelSpaceBoundary1stLevel	optional
	InnerBoundaries	IfcRelSpaceBoundary1stLevel @ParentBoundary	S[0:N]
IfcRelSpaceBoundary2ndLevel			
11	CorrespondingBoundary	IfcRelSpaceBoundary2ndLevel	optional
	Corresponds	IfcRelSpaceBoundary2ndLevel @CorrespondingBoundary	S[0:1]

The cardinality corresponds to the number of allowed relationships per object.
N represents an undefined limit of the cardinality.

Within the IFC data schema, the *IfcRelSpaceBoundary* class is further subdivided in the subclasses *IfcRelSpaceBoundary1stLevel* and *IfcRelSpaceBoundary2ndLevel*. Before the introduction of these subclasses in the IFC4 standard (up to IFC2x3), distinguishing between 1st and 2ndLevel subclasses was only possible through usage of 1stLevel and 2ndLevel descriptions in the *Name* field (Position 3 in Table 2.3), while the Positions 10 and 11 were introduced in IFC4. Within the IFC4 scheme, the description entity (Position 4) is no longer required due to the provided subclasses. However, no proprietary tools are currently known that can export SBs representing these subclass entities, even though these tools provide a certified IFC4 export. All proprietary

[5] IfcPropertySet in the IFC4 add2 TC 1 standard: https://standards.buildingsmart.org/IFC/RELEASE/IFC4/ADD2_TC1/HTML/link/ifcobject.htm, accessed on May 19, 2025.
[6] IfcPropertySet in the IFC4 add2 TC 1 standard: https://standards.buildingsmart.org/IFC/RELEASE/IFC4/ADD2_TC1/HTML/link/ifcpropertyset.htm, accessed on May 19, 2025.
[7] *IfcRelSpaceBoundary2ndLevel* in the IFC4 ADD2 TC1 schema: https://standards.buildingsmart.org/IFC/RELEASE/IFC4/ADD2/HTML/link/ifcrelspaceboundary2ndlevel.htm, accessed on May 19, 2025.

exported SBs are provided in the data format of the IFC2x3 schema (Positions 1-9). Proper *IfcRelSpaceBoundary2ndLevel* entities are only known to be provided by scientific SB tools, as proposed by [Fic22, LGR17]. The column *Cardinality* in Table 2.3 defines if the attribute is either required or optional or defined as specific set.

The SB class in IFC is inherited from the *IfcRoot* class, which provides the *GlobalId* as a unique identifyer. A description of the boundary type (Type 2a or 2b) is stated in the the *Description* field (Position 4 in Table 2.3). This description field is not specific to the SB class, but also inherited from *IfcRoot*.

The following attributes are specific to the *IfcRelSpaceBoundary* class. The *RelatingSpace* (Position 5) references the enclosed room or space that is enclosed by the SB entity. This enclosed space can be represented by an *IfcSpace* (cf. Figure 2.4) but also as *IfcExternalSpatialElement*. An *IfcSpace* represents a physical space within the building, which is enclosed by either physical or virtual boundaries. An *IfcExternalSpatialElement* considers the building's surroundings as its enclosing space, represented by the outdoor air or the ground. The position of an *IfcRelSpaceBoundary* is defined relative to the position of its *RelatingSpace*. A *RelatedBuildingElement* (Position 6) refers to a physical or virtual construction that is bounded by the SB entity. The *ConnectionGeometry* (Position 7) holds the geometric representation of the SB. The attribute *PhysicalOrVirtualBoundary* (Position 8) describes if the bounded building element is virtual or physical, and thus, if the boundary is a physical or virtual SB. The *InternalOrExternalBoundary* (Position 9) attribute describes, if the bounded part of the related building element has an outside boundary condition that refers to the building interior (*INTERNAL*) or the building exterior (*EXTERNAL*), or to the ground (*EXTERNAL_EARTH*).

The *ParentBoundary* (Position 10), which is used to define the parent surface of boundaries, represents the underlying wall/slab boundary for an opening boundary (i.e., window, door). This attribute is introduced for the SB subclass *IfcRelSpaceBoundary1stLevel*. From the parent attribute, this parent-child relationship can be accessed by the derived attribute *InnerBoundaries*, which is defined as a set of 0 to N boundaries, i.e., a parent boundary can be referenced by an unlimited number of child boundaries.

The subclass representing 2ndLevel SBs in IFC4 (*IfcRelSpaceBoundary2ndLevel*) inherits from the 1stLevel subclass. In addition to the previously described attributes, this subclass holds the *CorrespondingBoundary* attribute (Position 11), which references another 2ndLevel SB. This attribute is used to define pairs of SBs, e.g., for the heat transfer across thermal zones through the related building element. The *IfcRelSpaceBoundary* represents a relational IFC entity, is not a subclass of *IfcObject*, and can currently (i.e., in the IFC4 data schema) be referenced by *IfcPropertySet* entities. Each corresponding boundary can be accessed by the derived attribute *Corresponds*, which is limited to a set of either no or one boundary.

2.2.2 EnergyPlus and Related Tools

A variety of BEPS computation kernels and user interfaces are available. This dissertation uses the open-source EnergyPlus Kernel for simulation, while the EnergyPlus Input Data Files (IDFs) are generated using the Python tools eppy[8] and geomeppy[9] .

EnergyPlus was proposed by [CLW+01] as a new simulation kernel combining the features of the previous DOE-2 and BLAST simulation kernels. EnergyPlus was initially written in Fortran 90 and designed as a computational kernel without Graphical User Interface (GUI), where third-party developers were invited to develop their GUI already in the beta test phase [CLW+01]. Today, the major parts of EnergyPlus are written in C++.[10] EnergyPlus uses a heat balance model that assumes for simplicity that the air in a thermal zone is uniformly well-mixed and thus only uses one computational node per zone, as opposed to high resolution CFD simulations. The heat balance model further relies on simplifying assumptions for the zone surfaces: these surfaces are assumed to have uniform surface temperatures and irradiation, diffuse radiation, and a one-dimensional heat conduction. The calculation of internal loads, the air distribution, and energy supply is fully integrated into the heat balance model and thus non-sequentially executed. [CLW+01]

The EnergyPlus Simulation requires three major inputs: 1) the EnergyPlus Input File IDF, which defines the building to be simulated including all geometry, materials, and simulation settings, 2) the Input Data Dictionary (IDD), defining the structure of the IDF at runtime, and 3) the weather file. For the evaluation of the simulation results, additionally the desired output files and formats need to be specified. [CLW+01]

Eppy[8] is a Python scripting tool to read and write IDF files in Python. Geomeppy[9] is an extension of eppy that allows the setup and manipulation IDF geometry. Both tools are used in this dissertation. Due to dependencies issues, both tools are included as forks[11,12] in the *bim2sim* repository. In this dissertation, EnergyPlus Version 9.4.0 is used.

2.2.3 Introduction to the *bim2sim* Tool

This section is an adapted excerpt from [RSFvT23]. The *bim2sim* tool [JMM+21, MJvT+22] is implemented using a modular structure, is published open-source,[13] and provides the framework for multiple IFC-based simulation approaches. It is developed for supporting engineers through the automated setup of IFC-based simulation models, including a template-based enrichment of missing data. The resulting simulation models only require minor manual corrections and drastically reduce the effort for model setup compared to conventional setup

[8] Santosh, P. et al., eppy: https://github.com/santoshphilip/eppy, accessed on May 19, 2025.
[9] Bull, J. et al., geomeppy: https://github.com/jamiebull1/geomeppy, accessed on May 19, 2025.
[10] EnergyPlus on github: https://github.com/NREL/EnergyPlus, accessed on May 19, 2025.
[11] eppy fork in the *bim2sim* environment: https://github.com/BIM2SIM/eppy, accessed on May 19, 2025.
[12] geomeppy fork in the *bim2sim* environment: https://github.com/BIM2SIM/geomeppy/tree/fix_dependencies, accessed on May 19, 2025.
[13] *bim2sim* tool on github: https://github.com/BIM2SIM/bim2sim, accessed on June 09, 2025.

processes [MJvT+22].

The modular plugin-based structure of the open-source *bim2sim* framework is displayed in Figure 2.5 for the BEPS plugins *PluginEnergyPlus*, *PluginTEASER*, and the HVAC plugin *PluginAixLib*. The initial *bim2sim* framework included additional plugins with prototypical implementations for exporting CFD boundary conditions for use in the commercial CFD software ANSYS FLUENT (Version 2022 R2) and for the support of Life Cycle Assessment (LCA) [MJvT+22]. Currently, an additional plugin for dynamic co-simulation of BEPS and HVAC is under development. From these plugins, only the BEPS approaches fall in the scope of this dissertation, using EnergyPlus and the Modelica as simulation backends, respectively. These plugins share the initial steps of loading the IFC data, initializing IFC elements and their relations, and enriching missing data. These shared steps of BEPS pre-processing are followed by the plugin-specific generation of simulation input data according to the requirements of the respective simulation backend.

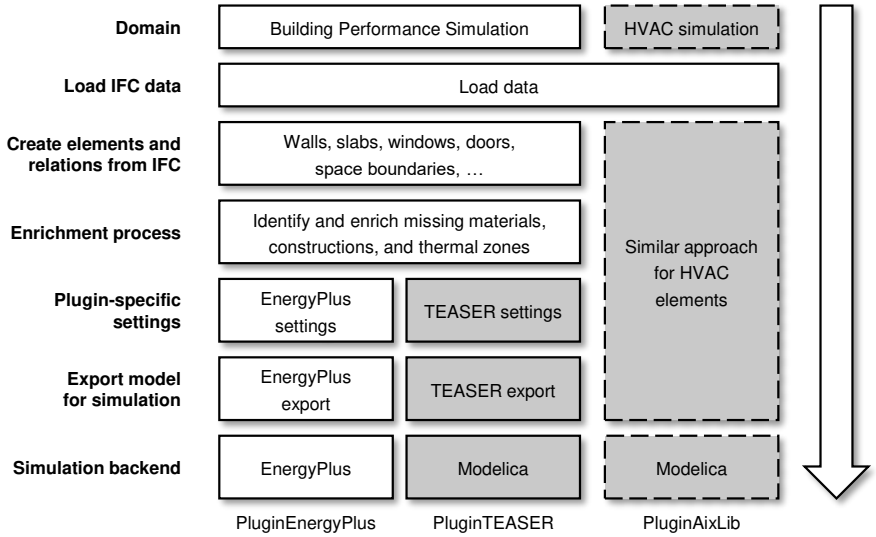

Figure 2.5: Simplified representation of the main *bim2sim* workflow; for Building Performance Simulation including the *PluginEnergyPlus* (white) and the *PluginTEASER* (gray, solid line), and for HVAC simulations the *PluginAixlib* (gray, dashed line). Adapted from [RSFvT23].

The data enrichment of materials, constructions, and zone-usage relies on a template-based enrichment process using archetypal templates, which were initially created for the enrichment within the reduced-order simulations of TEASER [RLM+18]. Within these templates, the zone-usages are derived from applicable German standards [DINV18599-10, VDI2078] and extended by the internal load profiles defined in [SIA2024] (cf. TEASER Documentation[14]). For the enrichment of the building envelope, TEASER provides data sets from different sources,[15] e.g., representing the German building stock clustered in archetypes based on their construction year provided by Institut Wohnen und Umwelt, engl.: Institute for Housing and Environment

[14]TEASER Documentation, use conditions: https://rwth-ebc.github.io/TEASER//master/docs/code/teaser.logic.buildingobjects.html#teaser.logic.buildingobjects.useconditions.UseConditions, accessed on June 04, 2025.

[15]TEASER Documentation, building archetypes: https://rwth-ebc.github.io/TEASER//master/docs/archetypes.html, accessed on June 04, 2025.

(IWU) [LDKB05], or representing the latest energy-efficient building design standard, as defined by KfW [KfW20].

Individual simulation settings can be set prior to the execution of the *bim2sim* tool for each example using *sim_settings*. The available *sim_settings* are assigned for the general use for all available plugins as *BaseSimSettings*, e.g., for setting a weather file path or for the setup of instances. Additionally, *sim_settings* can be defined for the general use in BEPS across all BEPS plugins, e.g., if the building should be cooled or heated. Furthermore, plugin-specific *sim_settings* can be declared.

2.3 Related Research

The related research analysis on IFC-based BEPS is clustered in the two major fields of 1) IFC-based BEPS presented in Section 2.3.1 and 2) the challenges in IFC-based data exchange and model quality for BEPS applications discussed in Section 2.3.2. On the basis of these fields in related research, a preliminary conclusion on the research gap in this field is drawn in Section 2.3.3, followed by the definition of Research Hypotheses (RHs) in Section 2.3.4, which are then addressed by the IFC-based BEPS methodology in Section 2.4.

2.3.1 IFC-based Building Energy Performance Simulation

This section presents an overview on related research using IFC-based approaches for the automated generation of BEM used in BEPS, which represents a brief summary of the review prepared for [JRM+24]. The evaluated research focuses on dynamic BEPS, such that steady-state BEPS approaches, e.g., PassivBIM as an IFC integration [CHM15] for the PHPP tool,[16] are not considered. Research that solely focuses on the generation of second-level Space Boundaries (SBs) has been extensively reviewed in related research [Fic22, MEL23], and is out of scope for this dissertation.

Following the suggestion in the initial EnergyPlus proposal in 2001 [CLW+01] that IFC models could be used to automate BEPS generation, a variety of IFC-based BEPS approaches have been proposed over the years. The evaluated research for this dissertation, summarized in Table 2.4, includes approaches that generate BEPS models from existing IFC data but also approaches that include additional pre-processing steps (e.g., SB generation, validation, correction). The results are compared to the latest version of the *bim2sim* framework, included in the last row of the table.

The evaluated studies have different input requirements. Only half of the approaches clearly state the use of the IFC4 standard, while others use an older or not referenced IFC version. While two of the studies do not consider SBs for their implementations [ARHZ15, CDGC21], many other studies include the generation of SBs [Baz08, GLG+15, Cao18, NIK+17, NRTRT19, GKLR19,

[16] PHPP, Passivhaus-Projektierungspaket: https://passiv.de/de/04_phpp/04_phpp.htm, accessed on May 20, 2025.

Table 2.4: IFC-based BEPS approaches from related research (chronologically ordered), R: Required, G: Generation, Y: Yes, -: No / not applicable. Empty fields are not clearly stated in literature. Adapted from [JRM+24].

Reference	Name	IFC Version	Spaces	SB	Enrichment	BEPS	HVAC	CFD	Modularity	open-source	Implementation
[Baz08]		IFC	G	G	manual	EnergyPlus	-	-	Y	-	-
[OSR+11]	SimModel	IFC	R	R	template	EnergyPlus	-	-	Y	-	XML
[ARHZ15]		IFC2x3/IFC4	R	-		COMETH	COMETH	-	-	-	-
[GLG+15]		IFC2x3/IFC4	R	G	-	EnergyPlus, TRNSYS	-	-	-	-	- , Matlab
[Cao18]	SimModel+	IFC	G	G		Modelica	Modelica	-	Y	-	Python, C++
[ASK18]	Ifc2Modelica	IFC4	R	R	spreadsheet	Modelica	Modelica	-	partially	-	Python, ifcopenshell
[NIK+17, NRTRT19]	CoTeTo/ BIM2Modelica	IFC2x3	R	G	template & manual	Modelica	-	-	-	Y	Python, JModelica
[GKLR19]		IFC4	R	G	SimModel XML	SimModel XML, EnergyPlus	-	-	-	-	-
[RMM20]	OsmSerializer	IFC2x3	R	G	OpenStudio	OpenStudio / EnergyPlus	-	-	-	Y	Java
[CDGC21]		IFC4	R	-		EnergyPlus, eQuest	Y (for BEPS)	-	-	-	Java
[NPW+23]	SIM-VICUS	IFC2x3/IFC4	R	G	template & manual	Nandrad, EnergyPlus	local / districts	-	Y	Y	C++
[CDCC23]	AutoBPS-BIM	IFC2x2	R	R		EnergyPlus	EnergyPlus	-	-	-	-
[MEL23]		IFC4	G	G	template	EnergyPlus (not executed)	-	-	-	-	-
bim2sim framework	*bim2sim*	IFC4	R	R	template & manual	EnergyPlus, Modelica	Modelica	partially	Y	Y	Python, ifcopenshell

RMM20, NPW+23, MEL23], for which most of the studies rely on existing representations of IFC spaces. Several studies claim the challenging pre-processing of IFC data for simulation purposes due to missing or incorrect SBs or other consistency errors [Baz08, GLG+15, LGR17, GKLR19, MEL23].

The generated BEM requires additional information, which cannot be derived from IFC. The studies named either a manual or template-based enrichment, a combination of both, spreadsheet enrichment, or software-internal enrichment. The applied simulation kernels for BEPS are dominated by the use of EnergyPlus, followed by Modelica. Half of the analyzed approaches considered some type of additional HVAC simulation within their approaches. None of these studies included a support for CFD simulations. The modularity of the approaches is limited, and only a minority is published open-source. The implementations are mainly based on Python, C++, and Java.

[Baz08] proposed the initial IFC-based BEPS workflow to reduce the modeling errors caused by manual model setups and decisions of design engineers. Using the presented Geometry Simplification Tool (GST), he reduced the model setup time of BEPS by 80%, even if manual post-processing for HVAC systems and simulation settings were still needed. Further methods for SB generation, validation, and correction are presented by [GLG+15, LGR17, GKLR19] as parts of the Common Boundary Intersection Projection (CBIP) algorithm.

This brief introduction to related research on IFC-based BEPS generation found that multi-domain approaches are sparse, as these approaches mainly focus on a single specific BEPS domain. IFC4-based approaches for co-simulation of building and HVAC systems or supporting CFD simulations are not available. For an extended review of this presented research, see [JRM+24].

2.3.2 IFC-based Data Exchange and Model Quality for BEPS Applications

As previously identified, the issue of inconsistencies in the input IFC data has been observed for the use case of automatic generation of IFC-based BEPS. Therefore, this section continues with an analysis of related research on IFC model quality, as well as an in-depth analysis on error

categories, potential errors, error handling, and error detection in the transformation process of automated IFC-based BEPS generation.

Related Research on IFC Model Quality

This section summarizes the findings from related research on model quality presented in [JRM+24]. The quality of IFC data frequently causes interoperability issues in the data exchange for the setup of BEPS. [DBCD+22] found that geometric issues (64%) and data loss (48%) were the most common problems arising along with a lack of interoperability in related research, requiring an increased manual effort for manual pre- and post-processing in the setup of BEPS models. Even though SBs have been identified as key for the IFC-based BEPS transformation two decades ago [Baz08], buildingSMART-IFC4-certified tools still fail to export SBs (i.e., ALLPLAN [Fic22]), or export them with an insufficient representation of second-level SBs (i.e., ARCHIAD, Autodesk Revit) [MJvT+22].

To define and control the data exchange of IFC data, buildingSMART provided the concept of Model View Definitions (MVDs), which explicitly declares the exchange requirements of IFC data. While MVDs were developed in previous research [PWO+18, ASK18], these are mostly not available open-source [Fic22] and have limited support by proprietary software [MEL23]. Recently, buildingSMART proposed the concept of Information Delivery Specification (IDS) [bui23], which can not only define the requirements on the existence of IFC entities such as MVDs but additionally provides semantics to define requirements for individual attribute values. However, even if MVD and IDS allow a detection of semantic and syntactic errors in the IFC data exchange, they fail to detect errors in geometry and consistency. Therefore, to ensure the quality of SBs for the use in BEPS, related research has analyzed the potential further error risks [Fic22], proposed validation and correction algorithms [LGR15, YL17, YL20, KNO+20, RFA+21], and implemented these in validation tools [LGKR18, LES20, YL21b, RMF+22]. The implementation of the *IFC2IDFValidationTool* [RMF+22] for the validation of IFC, IDF, and the transformation process is part of this dissertation (cf. Section 2.6).

Besides the lack of geometric quality in IFC data, the quality of the semantic data is also frequently an issue when preparing IFC-based BEPS models. [MEL23] enriched material and construction parameters using a default parameter set and stated the need for a user interface for manual enrichment of IFC data. [MDRPM23] developed an approach for semantic enrichment for facility management using virtual reality and IDS checking. [BS20] developed an approach to fill missing, partly missing, or incorrect semantic data using clustered requirements from building codes in the field of security, fire, access, and maintenance. Their approach could be extended for applicable codes on energy-efficent building design.

The review of related research highlighted the need for further improvements of IFC model quality, along with suitable algorithms and approaches for evaluating and correcting these models. Further research on error categories, as well as on validation and correction algorithms, is discussed in the following sections.

Handling Errors in IFC

The following analysis on current approaches for handling errors in IFC is adapted from the review presented in [RMF+22]. The errors observed in the IFC data on SBs in related research [YL17, MSP18, FRFvT21, RFA+21] allow for clustering into four main categories, namely (1) syntax, (2) semantics, (3) geometry, (4) consistency [YL21b]. The strategies for handling these errors vary in related research. While several algorithms are available to generate a full new set of SBs [vTR07, RB15, LGR17, Fic22, MEL23], the application of these algorithms may still produce erroneous SBs caused by unexpected modeling choices of the IFC modeler. Another option is the validation of existing SBs [LGR15, YL17, YL20, YL21b, KNO+20] as a basis for a manual correction of the detected SB errors in the original authoring tool that exported the SBs. The access to tools that allow a visual validation of SBs is scarce. The FZKViewer[17] has a rudimentary representation of SBs, which does not allow for an individual selection of SBs or a detailed view on vertices and surface normals, but includes some inbuilt validation and correction algorithms, e.g., a collinear point detection. [YL21b] developed a prototypical user interface for a limited geometric SB validation, aswell as an mvdXML for syntactic validation.

Algorithms for the (semi-)automatic correction are less common in related research, as most research focuses on the generation of the full set of SBs, risking additional computational overhead. [LGR15] algorithmically fix surface orientations of SBs within closed shells as part of their research on general corrections in IFC data. [RFA+21] present correction algorithms to remove collinear and coincident vertices for the transformation of IFC to EnergyPlus IDF, which are developed within the scope of this dissertation and further described in the following section. The only IFC viewer that is known to visualize SBs on a vertex level was presented in [RMF+22], also within the scope of this dissertation. The viewer is described in Section 2.6.

Handling Errors in EnergyPlus

While the availability of tools for validating and correcting IFC SBs is limited, the availability of respective tools for EnergyPlus is even further reduced. EnergyPlus [USDoE21] includes inbuilt methods to validate the compliance of an input IDF with the respective EnergyPlus Input Data Dictionary (IDD), which defines the applicable limits and bounds for individual EnergyPlus objects. The compliance check is executed during runtime, where additionally invalid references are checked, leading to a potentially long list of errors and warnings in the EnergyPlus output error file. Locating the errors in the IDF model is time-consuming due to the lack of error visualization, which, however, can be supported by the open-source tool OpenStudio (open-source user interface for EnergyPlus). Another option for model visualization is the use of proprietary software, such as the Euclid Plugin for SketchUp,[18] which provides an improved visualization compared to OpenStudio. This plugin provides some inbuilt correction algorithms, e.g., for correcting surface orientations. However, this plugin requires the positions

[17] KIT IAI, FZKViewer (Version 6.1): https://www.iai.kit.edu/1310.php, accessed on June 09, 2025.
[18] Big Ladder Software LLC, https://bigladdersoftware.com/projects/euclid/, accessed on June 09, 2025.

of SBs to be located at the centerline of constructions, which is not compatible with the IFC SBs placed on the interior surface (cf. Figure 2.3), and is thus not compatible with the developments within this dissertation.

Transformation Validation

The related research on the transformation validation of IFC-based BEPS processes using EnergyPlus was initially presented in [RMF+22]. The following paragraph is an adapted excerpt from this work.

When transforming IFC SBs for BEPS, geometric requirements may differ for the model setup for the EnergyPlus input IDF. Herein, the geometrical definitions are often stricter than defined in the IFC standard. Some differences in definition were identified in the requirements relating to the number of vertices in an opening, convexity, and the representation of inner loops within surfaces [RFA+21]. The available research is sparse for the validation of the IFC to IDF transformation itself. [RMM20] evaluate the resulting space and building element volumes of IDFs generated from different sources. Another common validation approach within the development of BEPS tools is the validation using [ASH140], which states an acceptable range of the simulation results for given use cases. [Ric19] evaluated the impact of geometric inaccuracies and errors in the EnergyPlus input using various metrics, distinguishing between multiple granularity levels. However, the mentioned approaches do not analyze the transformation of IFC SBs in detail. [RMF+22]

2.3.3 Preliminary Conclusion on Research Gap in IFC-based BEPS

From the analysis of related research, two research gaps are identified. These gaps address (1) the field of IFC-based BEPS and (2) the IFC-based data exchange and model quality.

Research Gap 1: From the analysis of existing IFC-based BEPS approaches, it can be concluded that IFC4-based open-source generation of BEPS and specifically of EnergyPlus models is unavailable.

> *Explanation:* An IFC-based BEPS is critical for developing further multi-domain IFC-based simulation approaches, such as co-simulation and CFD analysis. If the IFC-based generation of simulation models is not available, the repetitive costs of setting up these simulation models in the design stage of buildings are too high. Thus, the design and system optimization potential of dynamic simulations is not used, and only standardized static calculations are performed for system sizing. This may result in inefficient system sizing and increased costs for system optimizations during building operation. If no BEPS is applied in the design stage, more detailed approaches like co-simulation and CFD analysis cannot be applied or only with a high manual effort, since these require BEPS as part of the simulation (co-simulation) or for setup of boundary conditions (CFD).

Research Gap 2: The analysis of related research on IFC-based data exchange and model quality revealed the need for error handling to meet the requirements for IFC-based BEPS model setup.

> *Explanation:* The geometric quality of IFC-based model setup is found to be one of the main challenges, besides errors in the categories syntax, semantics, and consistency. To increase the robustness, especially towards incorrect geometry, two main options exist: 1) Generation of new SB geometry if SBs are missing or incorrect, e.g., using the IFC2SB Tool [Fic22], and 2) geometric correction and enrichment. The latter is addressed in this dissertation. The model quality is critical to the BEPS results, and thus is the quality of the input IFC model. The IFC model quality varies with the capabilities of the authoring tool, but also with the modelers and their knowledge on IFC and best practices on the modeling for the purpose of IFC export. A variety of errors can apply, ranging from geometric gaps, duplicate vertices, incorrect or missing attributes (e.g., SBs defined as internal instead of external), or consistency errors, such as SBs defined on the centerline of the surface, neglecting the positional requirements of the IFC schema. To overcome these errors, IFC-based BEPS processes need to include strategies to robustly handle and correct faulty geometries. However, even automated setup processes for BEPS models still require expert knowledge to evaluate the resulting model quality and the results. The presented approaches can only assist in reducing the manual effort for model setup and for handling design changes.

2.3.4 Research Hypotheses

The following two RHs are concluded from the identified research gaps in response to the RQs defined in Section 1.3 and visualized in Figure A.1:

RH BEPS 1: The automatic transformation of IFC Space Boundaries to Building Energy Performance Simulation models improves the Building Energy Performance Simulation usability across all design stages of buildings. The usability is enhanced by drastically reducing the manual effort for model setup through transforming and enriching IFC-based data.

RH BEPS 2: The transformation of erroneous or incomplete IFC4 Space Boundaries into Building Energy Performance Simulation models involves correction and enrichment approaches. The transformation process requires validation to evaluate the model quality.

RH BEPS 1 addresses RQ 1 by presenting an approach for integrating BEPS into an IFC-based BIM workflow. While RH BEPS 1 also touches on challenges formulated in RQ 2 by addressing the model setup efforts, RH BEPS 2 specifically focuses on these challenges associated with achieving seamless integration of IFC-based BEPS by proposing correction and enrichment approaches. The following methodology for the transformation of IFC-based BEPS is designed to fulfill these research hypotheses by presenting a robust approach for IFC-based generation

of BEPS models. The developed methods are included in the development of the *bim2sim* plugin *PluginEnergyPlus* and the *IFC2IDFValidationTool* for the evaluation of IFC, IDF, and transformation quality. Both the tool and the plugin are evaluated through two use cases to prove these RQs.

2.4 Methodology for Setting up IFC-based BEPS

In this dissertation, BEPS models are set up based on a BIM model in the data format IFC. The following methods for model generation were developed to integrate in the *bim2sim* toolchain for the use within the *PluginEnergyPlus* (Section 2.5). However, model validation and correction algorithms were mainly developed to be integrated in a standalone validation tool (*IFC2IDFValidationTool*, Section 2.6), due to higher computational costs caused by intensive geometric computations. Thus, validation should be performed seperately from the general IFC-based BEPS setup to avoid computational overhead.

This section starts with a general introduction on the methodology of transforming IFC to BEPS models using the EnergyPlus kernel. On the basis of these fundamental requirements, algorithms for validation and correction of IFC, IDF, and their transformation process are presented.

2.4.1 Transforming IFC to EnergyPlus

This section represents an adapted and extended translation of [MJvT+22]. Space boundaries (cf. Section 2.1.2) and their representation in the IFC data schema (cf. Section 2.2.1) are fundamental requirements for the IFC-based BEPS workflow, here further discussed using the BEPS software EnergyPlus (cf. Section 2.2.2).

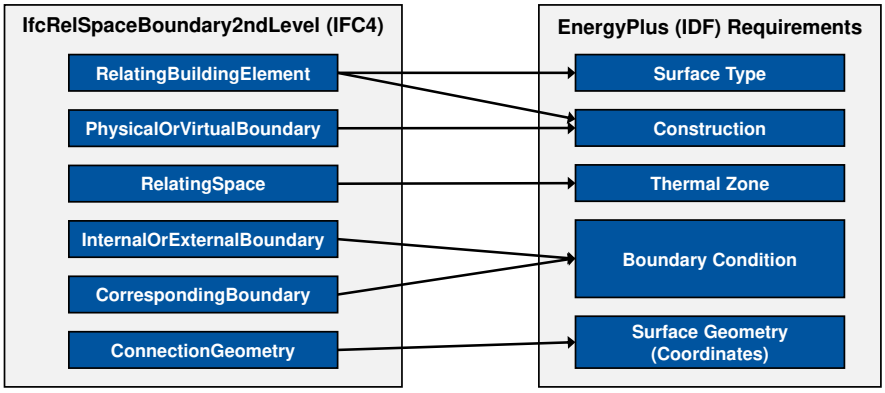

Figure 2.6: Mapping of IFC data schema to EnergyPlus input requirements, adapted from [MJvT+22].

Figure 2.6 displays the mapping of IFC entities to the input requirements of EnergyPlus and its input data format IDF. The *RelatedBuildingElement* in the IFC data schema allows the classification of surface types (e.g., wall, floor/ceiling, openings) and constructions (i.e., construction

layers and materials), which are a requirement for the definition of semantic EnergyPlus geometry. To correctly define a construction for the EnergyPlus model, the value of the *PhysicalOrVirtualBoundary* attribute is taken to determine if a boundary is virtual (i.e., must be defined as "Air Wall" in EnergyPlus, which supports the exchange of air between thermal zones) or if its material is determined by the physical related building element.

The reference of the relating space from IFC can be directly transformed to the corresponding thermal zone in the IDF. Here, further attributes and property sets of the relating space can be used to define further details in the IDF regarding internal loads and control (e.g., heating and cooling setpoints). The boundary conditions in the EnergyPlus model can be defined by combining the data from *InternalOrExternalBoundary* and the *CorrespondingBoundary* attributes. As the latter are only rarely available, the corresponding boundary information should be enriched using geometric algorithms before further processing of the boundary conditions in the EnergyPlus input file. Combining the data of these attributes enables the identification of heat transfer surfaces between thermal zones in EnergyPlus, as well as boundary conditions for outdoor air and ground in the IDF setup.

Finally, the geometric representation of surfaces in the IDF can be obtained from the *ConnectionGeometry* of the space boundary in IFC. Here, as the IFC standard allows the definition of inner loops within space boundaries, the space boundary geometry may require to be transformed to a single polygon (if the hole in the boundary is valid, cf. Figure 2.9) or the inner loop has to be removed (if the hole includes an opening surface) in order to generate a valid EnergyPlus input model.

2.4.2 Algorithmic Validation and Correction

As already derived from related research in Section 2.3.2, errors occur in the process of generating EnergyPlus Input Data Files (IDF) from IFC, which can be grouped in different categories: (1) syntax errors, (2) semantic errors, (3) geometric errors, (4) consistency errors, and (5) conversion or translation issues due to differences in the data schema definitions of IFC and IDF [YL21b, RFA+21, RMF+22]. In related research, several studies focus on identifying erroneous space boundaries in IFC files [LGR15, YL17, YL20, YL21b, RFA+21, RMF+22], while [MSP18, RFA+21, RMF+22] also addressed the errors caused by transformation of IFC to IDF files. In Appendix A.3, examples for common errors arising from translating IFC SBs to the EnergyPlus input format IDF are described.

While syntax and some semantic errors (i.e., missing references) can be easily spotted by evaluation of the data schema and the input data requirements, other semantic (i.e., incorrect values), geometric, and consistency errors require an advanced geometric analysis of detailed IFC geometry. [RFA+21, YL21b, YL20, YL17, RMF+22] proposed several algorithms for syntax, semantic, and geometric validation and correction for the use case of IFC-based generation of IDF files. Even though the IFC schema includes a parameter for *CorrespondingBoundary* since IFC4, no proprietary architectural IFC authoring tool is known to define this relationship,

which is crucial for defining heat transfer between thermal zones. Currently, only scientific algorithms that create IFC4 space boundaries [Fic22, LGR17, MEL23, YL21a] and the Blender AddOn Bonsai[19] are capable of writing a complete set of IFC4 compliant space boundaries.

A correct set of matching corresponding space boundaries is visualized in Figure 2.7. An algorithm (cf. Appendix A.3, Algorithm A.1) is developed to match corresponding 2ndLevel SBs in a given IFC file by leveraging the relation of SBs to their related building element. Boundaries are matched based on their surface area and distance. Using this algorithm, the computational overhead of generating a full new set of space boundaries "from scratch" is avoided.

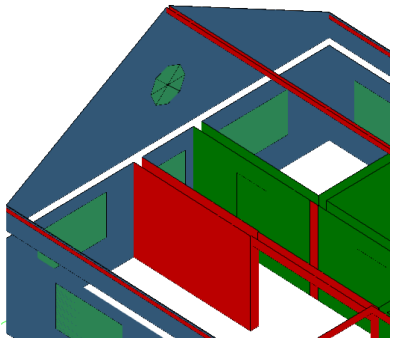

Figure 2.7: Corresponding space boundaries in the FZK Haus showing the boundary conditions in EnergyPlus. Corresponding surfaces are set to be adiabatic (red) if both are within same thermal zone, and set to be a heat transferring surface (green) otherwise. [RFA+21]

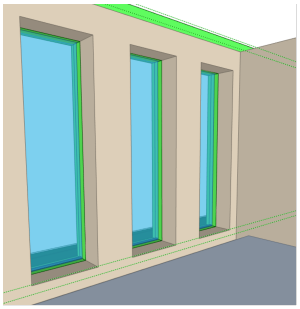

Figure 2.8: Example of a hybrid wall, modeled in Autodesk Revit. [RFA+21]

[RFA+21] additionally presented a semantic algorithm to determine the parent-child relationship between openings and hybrid modeled walls composed of individual walls placed directly next to each other instead of a single wall with multiple layers (Figure 2.8). In this case, the opening space boundary may be attached to a different element than the space boundary of the wall, such that additional matching is required for automatic translation to EnergyPlus.

Further geometric validation and correction algorithms addressed by [RFA+21] are visualized in Figure 2.9. These include an algorithm to ensure coplanarity of matching parent-child surfaces (i.e., openings and walls), an algorithm to remove inner loops of space boundaries by triangulation and reconstruction to fulfill the geometric requirements of EnergyPlus Input files, as well as an algorithm to remove collinear and coincident vertices from polygons.

[RMF+22] addressed the validation and correction of IFC and IDF files, as well as the validation of the IFC to IDF transformation process. Their algorithm developed for validating the airtightness of spaces provides higher computational efficiency and reduced complexity compared to a ray-tracing algorithm presented by [YL20]. The proposed algorithm by [RMF+22] topologically sews all SBs within a given space to determine free edges within the set of sewed SBs. The application of the sewing operation topologically connects all faces that share a common edge. The resulting free edges are used for error visualization and as a basis for automatically closing

[19] Bonsai Add-on for Blender (former BlenderBIM): https://bonsaibim.org/, accessed on May 20, 2025.

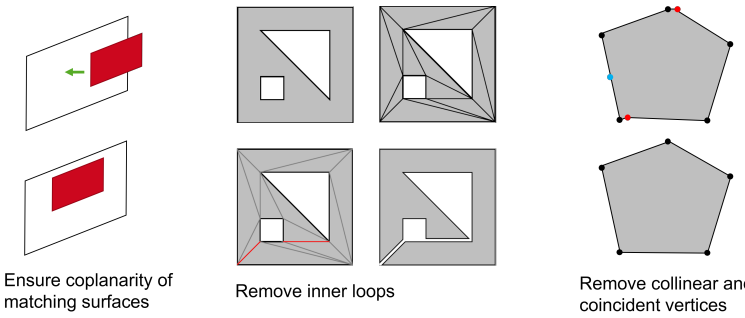

Figure 2.9: Algorithms for geometric validation and correction. [RFA+21]

these gaps by generating a void-filling shape before splitting it into its convex sub-shapes. This sewing-algorithm is only applied for visualization purposes in the validation tool (Section 2.6), while a different algorithm is included in the *PluginEnergyPlus* (Section 2.5) for internal correction of non-airtight space boundaries (cf. Appendix A.3, Algorithm A.2). The approach presented in Algorithm A.2 initially checks if the total area of all space boundaries in a space differs from the space surface area. If the difference is above a threshold, all space boundary shapes are cut from the space shape, to obtain a single shape that fills all gaps in the set of space boundaries. This shape is split in individual non-convex faces and converted into new space boundary instances for use in the *bim2sim* tool.

This proposed methodology for adding space boundaries does not work for centerline-modeled space boundaries where the shape of the space only reaches to the surface of the building components. However, for those cases, e.g., generated by Autodesk Revit, no 2b boundaries are required due to the position of the space boundaries on the centerline of building elements, and no gaps have been observed so far in the resulting centerline IFC SBs during the handling of IFC files in the projects BIM2SIM[20] and BIM2Praxis.[21]

The approach for validating surface normal orientations of individual SBs is applied according to the method by [YL21b] and further described based on an adapted excerpt from [RMF+22]. The prerequisite for this approach is a closed set of SBs. Thus, gaps within the space (Figure 2.10) must be filled (e.g., by an airtightness validation and correction). To validate if the surface normal $\vec{n}$ points outward of the space, a point p on the respective surface is moved along the direction of the

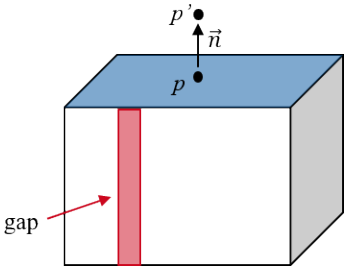

Figure 2.10: Validation of surface normal orientation: All gaps (red) within a space must be closed (space must be airtight), before the surface normal orientation of a SB (blue) can be validated. [RMF+22]

[20] BIM2SIM Project, "Development of methods for the generation of simulation models using Building Information Modeling data", grant number 03ET1562A: https://enargus.de/pub/bscw.cgi/?op=enargus.eps2&q=03ET1562A&m=1&v=10&s=13&id=387474, accessed on May 20, 2025.

[21] BIM2Praxis Project, "Integration of methods for the creation of simulation models based on Building Information Modeling in practice", grant number 03EN1050A: https://enargus.de/pub/bscw.cgi/?op=enargus.eps2&q=03EN1050A&m=1&v=10&s=13&id=8714122, accessed on May 20, 2025.

surface normal $\vec{n}$ by a small distance (e.g., 10 mm) and named p'. If the point p' lies outside the space polyhedron, the surface normal $\vec{n}$ correctly points outside the space. The small distance must be larger than the model's precision to identify if the point p' is outside the space correctly. If the space polyhedron is non-convex and the distance is chosen too large, p' may be inside the space even if the surface normal is correctly pointing outward the space. [RMF+22]

The transformation validation, originally presented in [RMF+22], focuses on the building geometry, which is a translated representation of the *IfcRelSpaceBoundary2ndLevel* entities in the IDF. Here, the building's geometric properties (i.e., area and zone volume) are analyzed on both the global building- and individual zone-scale, evaluating the Root Mean Square Error (RMSE) and Normalized Root Mean Square Error (NRMSE). Additionally to the geometric validation, the total number of entities per surface type (e.g., wall, window, door) is compared to identify surface type inconsistencies hinting at translation errors. [RMF+22]

2.5 *PluginEnergyPlus*: IFC-based BEPS using EnergyPlus

The *PluginEnergyPlus* integrates into the *bim2sim* tool (cf. Section 2.2.3) as a plugin for BEPS using the simulation kernel EnergyPlus (cf. Section 2.2.2). For more detailed insights into the implementation, please see the *bim2sim* GitHub Repository.[22]

Figure 2.11 adds detail to the general *bim2sim* workflow (cf. Figure 2.5). In Figure 2.11, the workflow steps are broadly clustered into the steps (1) to (8) and their substeps using alphanumeric labels. The *bim2sim* kernel provides general tasks for loading the IFC (1), creating *IfcProduct*s (2), setting up space boundaries (3), enriching materials and use conditions (4), and post-processing of BEPS (i.e., EnergyPlus) results (8). The steps (1) and (2) are common steps for all *bim2sim* simulation domains, including BEPS, LCA, and HVAC simulations. Steps (3), (4) and (8) are currently only used within the BEPS simulation domain, including the *PluginEnergyPlus*. Specific to the *PluginEnergyPlus* are steps (5) to (7), which create and export the EnergyPlus Input File IDF (5), export IDF data for post-processing (6), and run the EnergyPlus simulation (7).

This dissertation focuses on the steps (3) and (5), as (3) contains the handling of space boundaries (3), which are critical for the geometric setup of the EnergyPlus model, and (5) contains the transformation algorithms developed for the *PluginEnergyPlus*. Therefore, most of the methods presented in Section 2.4 resolve in the substeps (A), (B), and (C) of the creation of SBs (3), and in the setup of the EnergyPlus IDF (5) with their substeps (A) to (F) as visualized in Figure 2.11.

After loading the IFC file into the *bim2sim* environment (1), the *IfcProduct*s, (e.g., walls, doors, spaces, ...) are created as instances within *bim2sim* (2). These instances form the basis for setting up the *bim2sim* space boundary instances. The process of creating space boundaries (3) addresses the translation of IFC SBs into the *bim2sim* structure, which can be divided into three major tasks: (A) the creation of space boundaries based on the provided IFC data, (B) the addition of missing space boundaries to fill gaps within the sets of space boundaries, and (C) a

[22] *bim2sim* on GitHub: https://github.com/BIM2SIM/bim2sim, accessed on June 09, 2025.

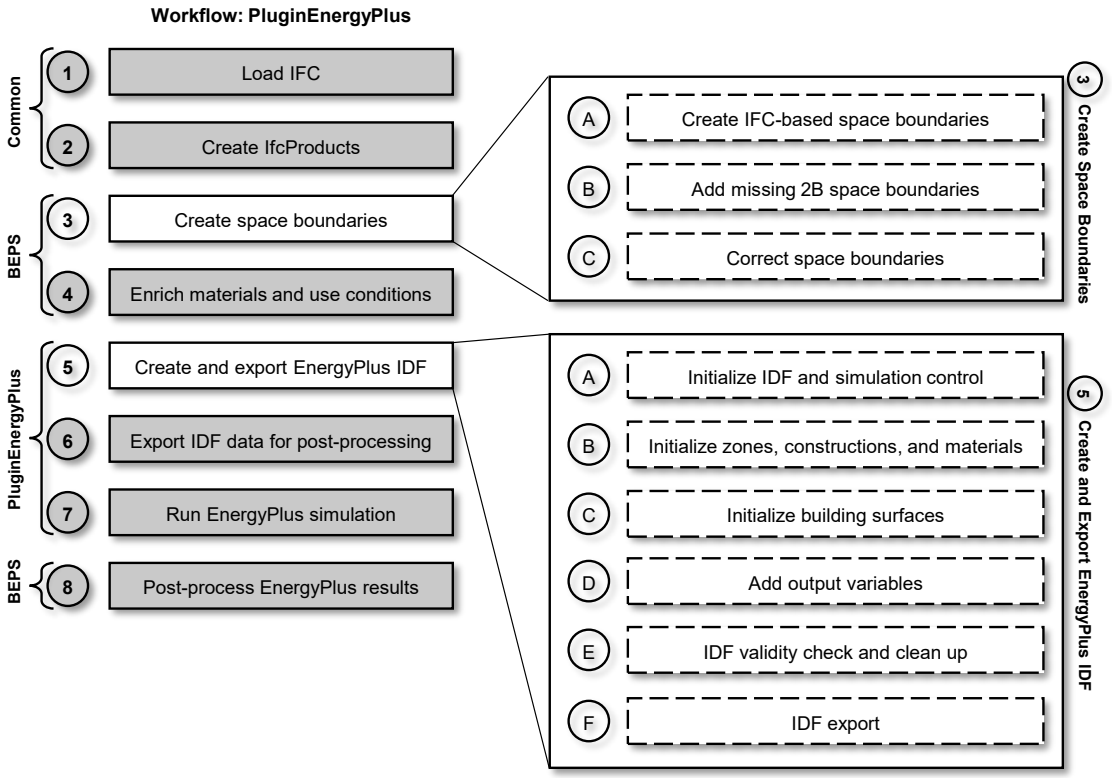

Figure 2.11: Workflow of the *PluginEnergyPlus* within the *bim2sim* tool.

correction of space boundaries.

2.5.1 Create Space Boundaries

For Substep (A) of Step (3) in Figure 2.11, the *IfcProduct*-based instances created in Step (2) are a prerequisite. Some geometric corrections are directly applied within the geometric setup (A), while additional corrections require the full set of generated space boundaries and are handled in Substep (C). Depending on the type of the *RelatingSpace*, the *bim2sim* instances of the space boundaries are either created as *SpaceBoundary* instance, if relating space is an *IfcSpace*, or created as *ExtSpatialSpaceBoundary*, if the relating space is a *IfcExternalSpatialElement*. *SpaceBoundary* instances are critical for setting up the heat transferring surfaces within BEPS, while *ExtSpatialSpaceBoundary* instances can be leveraged to determine shading elements of overhangs such as balconies. Additionally, the global position of the space boundaries is determined by the position of their *RelatingSpace*s (cf. Section 2.2.1).

This information on the position of the SB is used for setting up its geometry from the *ConnectionGeometry* of the *IfcRelSpaceBoundary* entity. In the process of setting up the geometry, an algorithm directly checks for coincident and collinear points within the polygons, as well as for inner loops within the shapes, which are not allowed in EnergyPlus. The coincident and collinear points are removed as presented in Figure 2.9 according to [RFA+21]. The inner loops occur in some authoring tools to represent the voids for openings (windows, doors), which are

neither legal within the IFC schema nor in the EnergyPlus representation of surfaces. However, some of these inner loops are valid, e.g., in slabs within a multi-storey atrium. Within the setup of the space boundary geometry the setup algorithm checks if the inner loop is potentially valid. Currently, the simplified assumption is made that inner loops within subtypes of *IfcWall* are always invalid as these most likely contain windows or doors. All other inner loops, e.g., in *IfcSlab*s, are considered to be valid and transformed into a single polygon according to Figure 2.9. For a detailed algorithm on removing the inner loops see [RFA+21]. In further research, inner loops should be considered with more detail, as with the current implementation, inner loops within roofs containing windows are considered as valid inner loops. A potential algorithm would check if the inner loop is filled with an opening element that contains a building element. If only a virtual element is contained in this opening element, the inner loop is valid, if a building element is included, the inner loop is invalid.

The instances of building parts (e.g., walls) are linked to the space boundary instances as *RelatedElement*s. Within this first substep, the relation between parents (e.g., walls) and their openings (e.g., windows, doors), is also determined. Within this process, also hybrid modeled walls (cf. Figure 2.8) are considered to define parent-child relationships to avoid errors within other algorithms that rely on relations between building parts.

The information on corresponding space boundaries, i.e., heat transferring surface pairs between thermal zones, is implemented as an attribute of the *SpaceBoundary* class. The matching of the corresponding boundaries follows the implementation of Algorithm A.1 in Appendix A.3. All these relations between space boundaries and other *bim2sim* instances are required for further creation and correction of space boundaries in substeps (B) and (C).

Substep (B) creates additional space boundaries to close gaps within each set of space boundaries per space according to Algorithm A.2 in Appendix A.3. Since missing space boundaries have been observed in IFC models generated from ARCHICAD, where only 2b space boundaries have been missing, these added space boundaries are labeled as 2b space boundaries. These space boundaries are considered as adiabatic in the setup of BEPS models. To improve this process, a type verification for these space boundaries should be applied to determine whether the generated space boundaries should be considered as 2a or 2b space boundaries. However, the currently implemented approach of generating 2b space boundaries provides a workaround for the requirement of watertight simulation models, e.g., required for a subsequent CFD analysis as presented in Chapter 3.

Substep (C) applies additional corrections to the created *SpaceBoundary* instances, which can be disabled by a general *sim_setting*. These SB corrections include moving children (openings) to their parent space boundary surfaces (parents) to ensure coplanarity of these surfaces (cf. Figure 2.9), fixing of surface orientations (cf. Figure 2.10 and [RMF+22]), and the decomposition of non-convex space boundaries into a set of convex boundaries [RFA+21] for a correct shadowing calculation within EnergyPlus. The latter correction can also be enabled by a *sim_setting*.

2.5.2 Create and Export an EnergyPlus IDF File

The creation and export of the EnergyPlus IDF file within the *PluginEnergyPlus* (Step (5) in Figure 2.11) consists of multiple functions, which can be grouped for simplicity into the six substeps (A) to (F). Substep (A) sets the path of the EnergyPlus IDD based on a *sim_setting* and initializes the IDF file based on a minimal example IDF, which is included in the sample files that come with the full EnergyPlus installation. Additionally, the default schedules are imported, and the weather file and general simulation controls are initialized based on their *sim_setting*s.

Substep (B) contains the setup of zones, materials and constructions. These are initialized first right after the basic IDF initialization, as they are referenced by the building surfaces created in Substep (C). For each *IfcSpace* within the given IFC file, an EnergyPlus *Zone* is initialized. Within the initialization process of the zone, further zone-related settings for heating and cooling, infiltration and ventilation, and internal loads are set up. The heating and cooling setup contains the declaration of heating and cooling schedules and setpoints according to the IFC import in steps (1) and (2), and the enrichment of use conditions in Step (4). These heating schedules are used to control indoor air temperature as default, which allows an optional setting to an operative temperature control to meet the requirements of thermal comfort analysis as described in Section 4.5. The infiltration and natural ventilation are setup according to the *sim_setting*s and the enrichment of use conditions in Step (4). A similar procedure is also applied for the setup of the internal loads, consisting of the definition of internal loads through occupants, electric equipment, and lighting. For these internal loads, the enrichment process provides maximum and related fractional 24 h load profiles.

Substep (C) initializes the building surfaces, but also the shadings from external space boundaries. According to the precomputed parameters from steps (1) through (4) and the knowledge on parent and child SBs, either building surfaces (*BuildingSurface:Detailed*) or fenestration surfaces (*FenestrationSurface:Detailed*) are created. The surface types of the building surfaces are chosen according to the previously created *bim2sim* instances of *IfcProduct*s. Here, the *RelatedBuildingElement* of each SB is evaluated on its class type. For walls, roofs, doors, and windows, the corresponding type in EnergyPlus is assigned. For the assignments of floors and ceilings, the position of the SB within the *IfcSpace* is evaluated, using the position within the space and the surface normal orientation. Furthermore, the boundary conditions are assigned. All SBs of the type '2b' are assigned to be adiabatic, while all SBs providing a corresponding boundary are assigned to have a *Surface* boundary condition representing a heat transferring boundary to an adjacent zone. Floor surfaces without a related bound are assigned to a *Ground* boundary condition, while all other boundaries without related bound are considered to be external. The construction and materials are also assigned according to the *bim2sim* pre-processing. In a final step, the surface geometry is assigned to the object. Within this step, the number of vertices of the surface polygon is evaluated, as opaque surfaces in EnergyPlus are only allowed to have 120 vertices, and fenestration can only have four vertices. If the surface has more vertices than allowed, the shape is evaluated if it is circular and then triangulated, or approximated with a simpler shape with fewer vertices.

Shading surfaces from external space boundaries are directly transformed into EnergyPlus shading elements. Apart from external shading elements, window shading control can be added by use of the respective *sim_setting*. If the window shading is applied, it is activated by default for incident radiation > 150 W/m^2 (simplification of requirements defined in [DIN4108-2]), in case the indoor air temperature is 2 K larger than the heating setpoint temperature. This 2 K range is introduced to use solar gains on winter days, when the operative temperature control may result in larger indoor air temperatures to meet the operative temperature setpoints, caused by low surrounding surface temperatures.

Substep (D) adds the output variables according to a list from *sim_setting*s, which enables the user to select the desired outputs. These outputs are clustered in outdoor conditions, zonal temperature conditions, internal gains, zonal setpoints and infiltration and ventilation data.

Substep (E) applies an internal validity check for the IDF before the export and applies an automatic cleanup combined with a warning for the user to later-on double-check and verify the removed objects. Here, any fenestration is removed that does not provide information on a parent building surface, as well as fenestration that has an adiabatic surface as a parent. These cases would cause a crash within the EnergyPlus simulation. Subsequently, the shading control settings are checked for unavailable fenestration surfaces, which have been removed or not created during setup. Additionally, tiny building and shading surfaces are removed, if their surface area is below a certain threshold (here: 0.01 m^2).

Finally, Substep (F) saves the IDF file using the project file name to the export path within the *bim2sim* project directory.

2.6 *IFC2IDFValidationTool*: Validate Input, Output, and Transformation

Once the *PluginEnergyPlus* was executed, the quality of the transformation process and of the resulting BEPS model (i.e., IDF) needs to be assessed. For a successful execution of the *PluginEnergyPlus*, a suitable quality of 2ndLevel *IfcRelSpaceBoundary* has to be ensured prior to the execution of the *PluginEnergyPlus*. The implementation of the *IFC2IDFValidationTool* assists in validating the input, output, and transformation of the IFC-based EnergyPlus workflow of the *bim2sim* tool. This validation process is designed as a separate validation tool to assist in ensuring the data quality within the *PluginEnergyPlus*, but this validation tool can also be applied to any other IFC-based EnergyPlus workflow.

The proposed validation tool addresses the IFC model quality for the use in BEPS, such that the included algorithms focus on the validation of SBs. The validation of SBs is not listed in the documentation of common proprietary validation tools (e.g., Solibri[23]). The IfcCheckingTool[24] evaluates the semantic and syntactic correctness of IFC files, but is not available open-source.

[23] Solibri Documentation, Space Validation: https://help.solibri.com/hc/en-us/articles/1500004738222-202-Space-Validation, accessed on May 20, 2025.
[24] IfcCheckingTool, developed by KIT IAI: https://www.iai.kit.edu/english/1649.php, accessed on May 20, 2025.

This tool provides a text-based validation output that states the error in combination with the location in the IFC file, but no graphical output is provided. The KITModelViewer[25] is a model viewer that supports open-standard 3D models, such as IFC, gbXML, and CityGML. Focusing on the IFC functionality, the viewer also includes model checking functionalities, but the representation of space boundaries for validation purposes is limited.

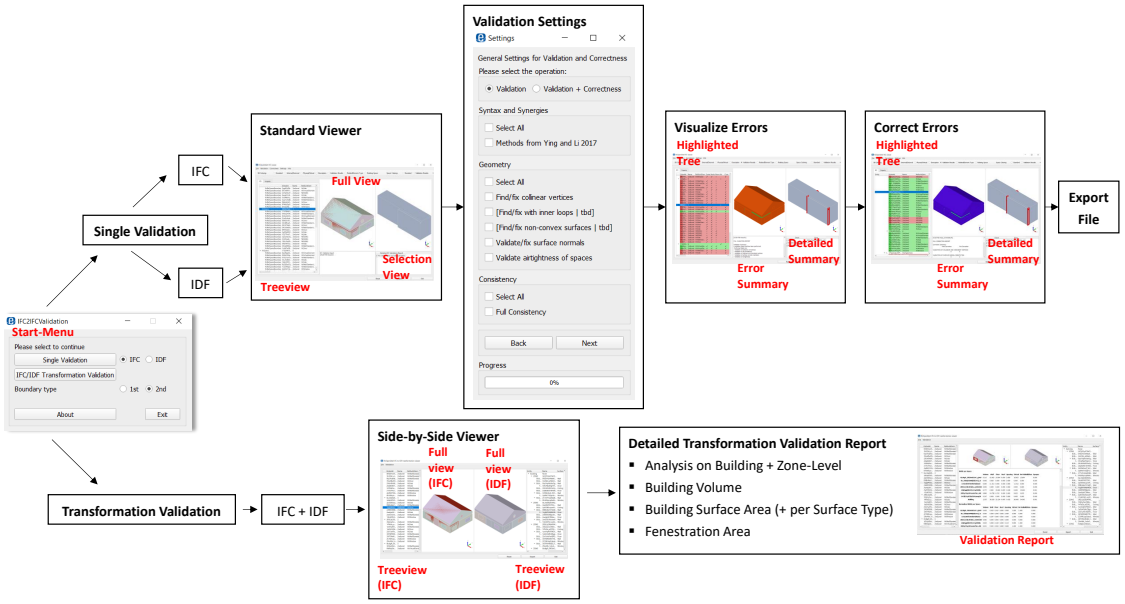

Figure 2.12: An overview of the user-interaction workflow for single validation and transformation validation, adapted from [RMF+22].

The *IFC2IDFValidationTool* has therefore been developed to provide a combined SB viewer and validation tool and is implemented on the basis of an IFC Viewer originally provided by IfcOpenShell.[26] The underlying methodology for the implementation of the *IFC2IDFValidationTool* is presented in Section 2.4.2, addressing its initial publication in [RMF+22]. As presented in [RMF+22], the tool addresses three types of validation: (A) the validation of IFC input files for the transformation to a BEPS model, (B) the validation of IDF files before executing an EnergyPlus simulation, and (C) the validation of the automated transformation process from IFC to IDF to ensure a correct representation of the IFC model in BEPS. The user-interaction workflow in Figure 2.12 represents an updated version of the initial development presented in [RMF+22]. The workflow of the *IFC2IDFValidationTool* is split in two major parts, the single validation and the transformation validation, which can be selected in the start menu of the tool. The single validation is applied to either an IFC (A) or an IDF (B) file, while the transformation validation (C) applies a comparison of the transformation of an IFC to an IDF file and therefore requires two matching files of the same building. The following sections describe the requirements for the single validation processes and the transformation validation process.

[25] KITModelViewer, developed by KIT IAI: https://www.iai.kit.edu/english/4561.php, accessed on May 20, 2025.
[26] IfcOpenShell: https://ifcopenshell.org, accessed on May 20, 2025.

2.6.1 Single Validation

The single validation tool is built to assist with profound space boundary validation supported by a detailed representation of individual space boundary geometries and their errors. The single validation for both IFC and IDF files within the *IFC2IDFValidationTool* mainly rely on the same algorithms, which only require minor modifications for the specifications in the respective IFC and IDF data schemas.

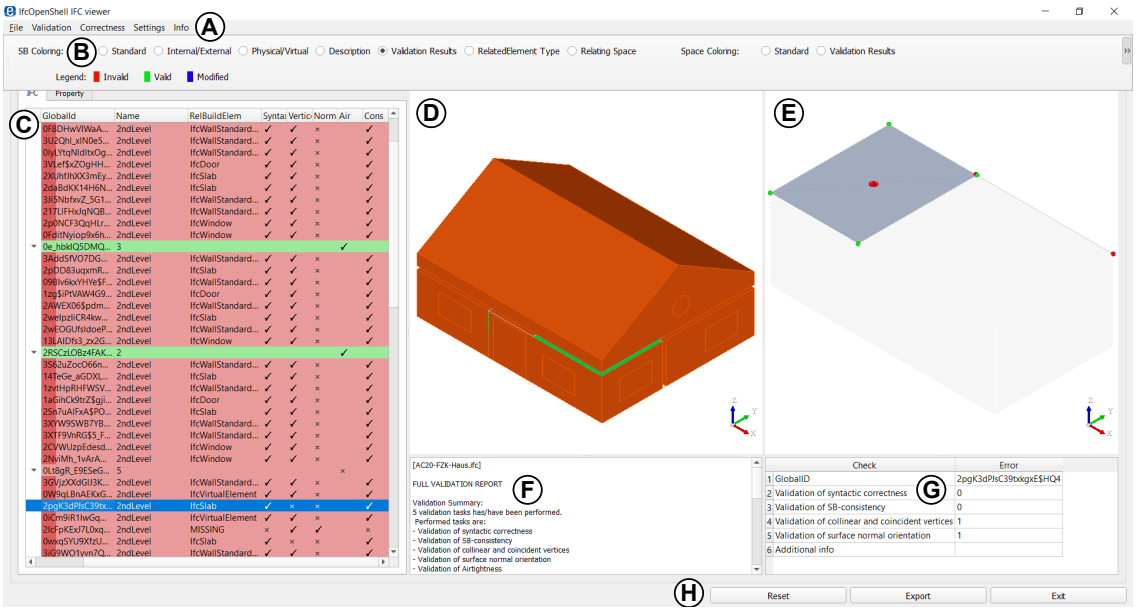

Figure 2.13: Single validation of an IFC file in the *IFC2IDFValidationTool*. Tool parts: Main Menu (A); Choose color scheme for space boundaries (B); Tree view of IFC entities (C); Viewer for SBs and spaces (D); Detailed viewer for individual space boundaries, surface normals and vertices (E); Validation report (F); Detailed validation report of selected space boundary (G); Export and reset options (H).

The top part of Figure 2.12 represents the user workflow of the single validation, which applies for both file types. Starting in the start menu, the file type is chosen, the file is loaded, and the tool's main window opens up. As displayed for IFC in Figure 2.13, the main window consists of a treeview (C), a view on the full building (D) and a selection view on the current selected space boundary (E). On the top (B), the coloring of the space boundaries in the full view can be chosen. An example for a selection of the coloring options is visualized in Figure 2.14.

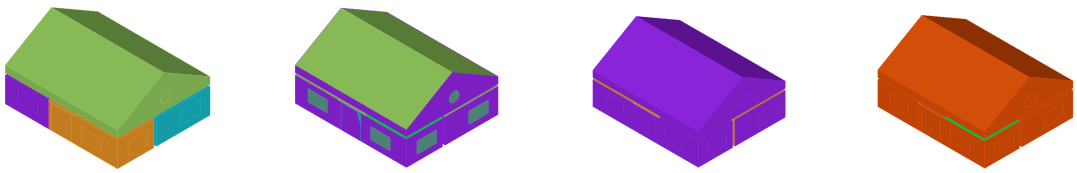

(a) Related spaces; random colors per space.

(b) Related elements; walls: violet, roof: green, windows: blue.

(c) Internal: orange, external: violet.

(d) Validation results; valid: green, invalid: red, corrected: blue.

Figure 2.14: Space boundary coloring in the full view of the single validation tool.

Within the main window (Figure 2.13), the validation settings (A) allow to choose from validation algorithms in the categories syntax, geometry, and consistency, as introduced in Section 2.4.2. Once the validation has been applied (cf. Figure 2.13), the errors are highlighted in the treeview (C) and can additionally be highlighted in the full view (D) of the viewer. Below the full view in the center of the tool, the validation report (F) is displayed, and below the selection view, a detailed validation report (G) for the current selected element is shown. If required, geometric corrections can be selected in the validation settings menu (A). Finally, the corrected files can be exported (H).

IFC File Validation

If the single validation process is applied for IFC files, validation algorithms are available for syntax, geometric, and consistency checks (cf. Section 2.4.2 and [RMF+22]). Geometric validation includes the validation of airtightness of spaces, the detection of collinear and coincident vertices in space boundary shapes, as well as the validation of surface normals. The implemented correction algorithms can sufficiently remove collinear and coincident vertices, and correct surface normal orientations. The airtightness of spaces is only validated but not corrected within this tool, as the addition of these gap-filling space boundaries requires additional elaboration on the correct type (2a, 2b) and boundary conditions (e.g., internal, external, adiabat) of the new SBs, which is not yet included in validation tool. However, a similar algorithm is implemented in the *bim2sim* tool itself (cf. Section 2.4.2) and could be transferred to the validation tool in further research.

IDF File Validation

The validation of IDF files is designed especially for the needs of IDF files generated from the *bim2sim PluginEnergyPlus*. As the *bim2sim* workflow already includes correction algorithms, the validation and correction algorithms within the stand-alone validation tool have only partially been implemented, but can be added in further research. The IDF validation focuses on geometric errors within the IDF file. Similar to the IFC validation, the IDF validation supports the validation of airtightness, collinear and coincident vertices, and surface normals. Vertices and surface normals can also be corrected in IDF format. However, the export of corrected IDF files is not yet implemented, as the quality of the generated IDF files from the *bim2sim* tool provides an overall sufficient quality, which is ensured by the applied correction algorithms for the IFC file that is used as input for the IFC-based BEPS process (i.e., the IDF generation).

2.6.2 IFC to IDF Transformation Validation

For the transformation validation from IFC to IDF, both models require the same set of IFC *GlobalId*s as unique identifiers for the matching of building components. Figure 2.15 displays the exemplary transformation validation example for the FZK Haus. On the left, the IFC tree

view (A) and the IFC model (B) are shown. The resulting IDF from the *bim2sim PluginEnergyPlus* is displayed in viewer (C) and tree view (D) on the right.

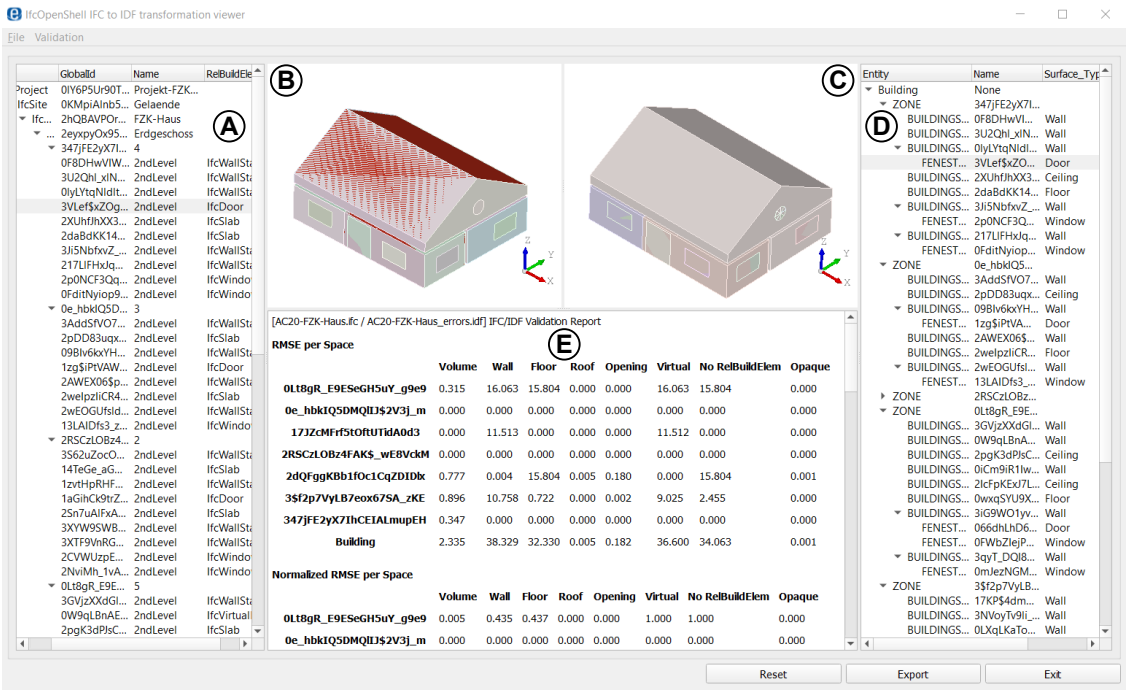

Figure 2.15: Transformation Validation. IFC tree view (A), IFC viewer (B), IDF viewer (C), IDF tree view (D), transformation validation report (E).

Once the validation is applied, the bottom report panel (E) displays the validation results. As described in [RMF+22], the validation report includes the evaluation of the RMSE and NRMSE per space and surface type, and missing and conflicting matches in the surface types between IFC and IDF elements. Finally, the report states the number of items per space, to assist with identifying potential mismatching entities in specific spaces.

2.7 Application and Testing of the *IFC2IDFValidationTool* and the *PluginEnergyPlus*

The following section presents two simple use cases to test the implementation of the *PluginEnergyPlus* and the *IFC2IDFValidationTool*. The testing process, visualized in Figure 2.16, starts with the introduction of the input data in Section 2.7.1, followed by the validation of the model input, output, and transformation in Section 2.7.2, and closes with the evaluation of the BEPS results on different spatio-temporal scales in Section 2.7.3. This application of the proposed methods leads to the evaluation of the proposed research hypotheses in Section 2.8.

As the presented *PluginEnergyPlus* is only a part of a larger framework that is proposed, implemented, tested, and evaluated within this dissertation, the further chapters provide use cases for more complex buildings and application scenarios.

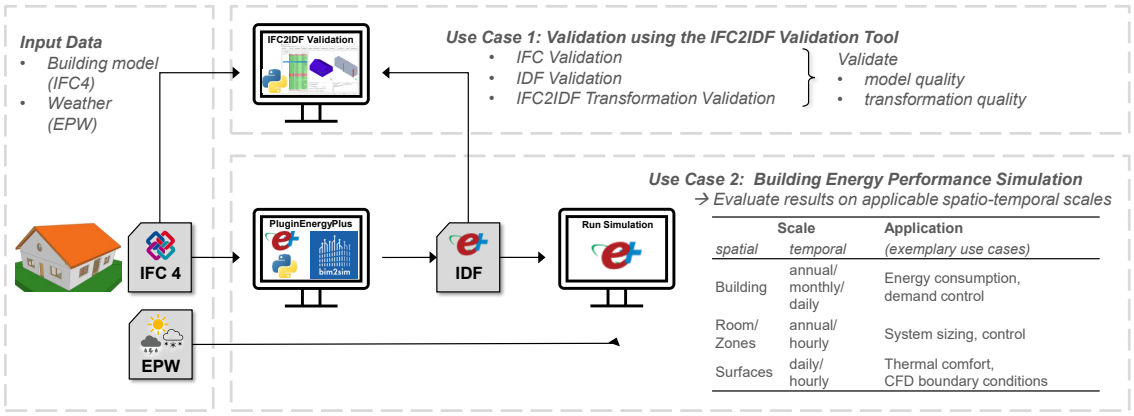

Figure 2.16: Overview on the application and testing of the IFC-based BEPS.

2.7.1 Use Case Introduction: FZK Haus

The proposed and implemented methods are evaluated on the use case of the FZK Haus displayed in Figure 2.17, which is an IFC4 single family house provided by KIT, IAI[27] modelled in the proprietary authoring tool ArchiCAD. The FZK Haus is used as input for the *bim2sim PluginEnergyPlus*, which uses the template-based enrichment as described in Table 2.5, using adapted heating and occupancy schedules as applied in [RSFvT23].

(a) FZK-Haus (b) Ground floor (EG) (c) First floor (OG)

Figure 2.17: View and floor plans of the FZK-Haus. Thin lines visualize virtual boundaries.

Using the template-based construction enrichment of Table 2.5, i.e., an IWU[28] heavy construction constructed in 1960, the resulting U-values are displayed in Table 2.6. The selected year of 1960 represents a common construction year in the building stock in Germany, since 36% of the residential buildings have been built between 1946 and 1977 [dena23]. Interior doors have the same thermal transmittance as exterior doors, but apply different convective coefficients due to internal conditions. For simplicity, external windows have a combined U-value of glass and frame. The air exchange rates (cf. Table 2.5) in this use case are adapted from the applied TEASER templates. In the evaluation of thermal comfort (Section 4.7) and climate change impact (Section 5.4), a different natural ventilation approach is applied, which is implemented

[27] FZK Haus (IFC4), provided by Institute for Automation and Applied Informatics (IAI) / Karlsruhe Institute of Technology (KIT): https://www.ifcwiki.org/index.php?title=KIT_IFC_Examples, accessed May 21, 2025.

[28] The TEASER-templates used for template-based enrichment of the building's envelope provide different data sets. In this use case, a data set based on simplified envelope parameter calculations is used, provided by IWU [LDKB05], https://rwth-ebc.github.io/TEASER//master/docs/archetypes.html#singlefamilydwelling, accessed on June 04, 2025.

lateron according to [DIN4108-2]. Additional parameters on the building use conditions are stated in Appendix A.10.1. In the current use case, only the bathroom setpoint temperature differs from the schedule displayed in Figure A.32, as the current use case applies a heating setpoint of 24 °C instead of 22 °C.

Table 2.5: Use case setup: General settings.

Parameter	Value	Unit/Format
Building	AC20-FZK-Haus	IFC4
Total Floor Area	208.55	m^2
Construction	IWU heavy, 1960	
Windows	Double-glazed wooden windows	
Weather Location	Cologne/Bonn Airport	
Shading	None	
Infiltration	0.2	1/h
Ventilation	Winter: 0.2	1/h
	Summer: 1.0	1/h
	Overheating: 3.0	1/h
Heating / Cooling	Heating, no cooling	

Table 2.6: Use case setup: U-values.

	U-value [W/(m^2 K)]
Outer Walls	1.267
Ground Floor	1.979
Roof	2.165
Inner Walls	1.613
Inner Floors	1.632
Inner Doors	1.157
Exterior Doors	1.291
Windows	2.706

The use case building is simulated using the TMYx (2007-2021) weather data of Cologne/Bonn Airport, provided by Climate.OneBuilding.[29] The outdoor air temperature for this location, which ranges from −9 °C to 35 °C, is displayed as heatmap in the Appendix, Figure A.3. Additional parameters of this weather file are discussed in Section 5.4 and additional statistics are presented in Appendix A.11.

2.7.2 Use Case 1: Validation using the IFC2IDF Validation Tool

Prior to converting IFC files into simulation input, e.g., in the application of the *bim2sim* framework, the quality of the IFC file has to be validated. Similarly, before any efforts are invested into the evaluation of the simulation results, the quality of the resulting IDF and the corresponding transformation from IFC to IDF has to be evaluated.

IFC Validation

Before the IFC4 model of the FZK-Haus is used for automated IFC-based BEPS generation in the *PluginEnergyPlus*, the quality of the IFC file has to be ensured. While the general geometric setup of an IFC model can be evaluated in common free or proprietary IFC viewers, space boundaries can be usually neither visualized, nor analyzed in these tools. Therefore, within this use case, the IFC validation is executed using the IFC2IDF Validation tool, introduced in Section 2.6. Figure 2.18 displays the validation tool in the validation process of the FZK-Haus. The treeview (left) gives an overview on the error types per space boundary (syntax,

[29] climate.onebuilding.org [LC22], weather data for Cologne/Bonn Airport, TMYx (2007-2021): https://climate.onebuilding.org/WMO_Region_6_Europe/DEU_Germany/NW_Nordrhein-Westfalen/DEU_NW_Koln.Bonn.AP.105130_TMYx.2007-2021.zip, accessed May 21, 2025.

collinear/coincident vertices, surface normals, consistency). For each space, the airtightness is evaluated. The detailed viewer on the right highlights the erroneous inward-pointing surface normal in red.

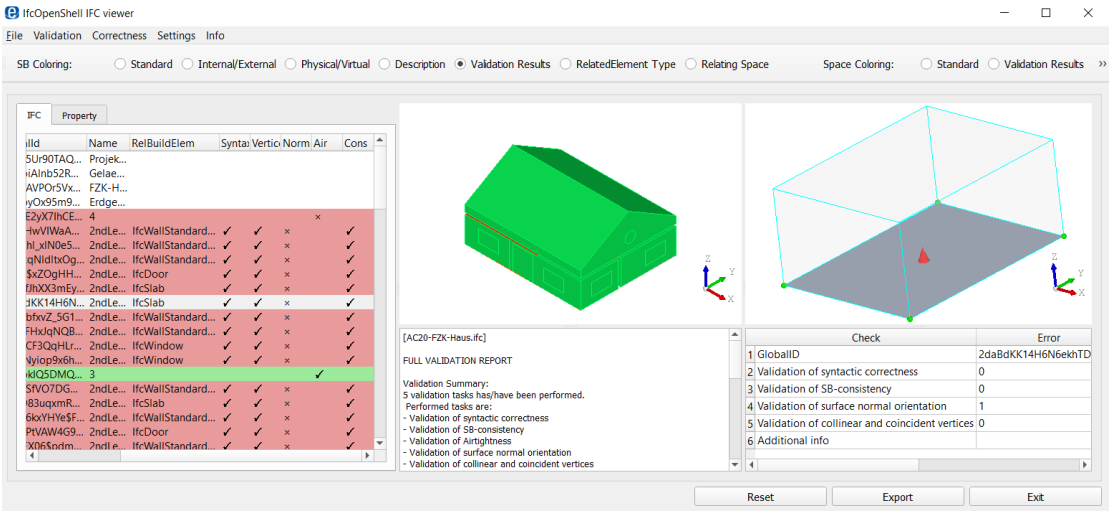

Figure 2.18: Space boundary validation of the FZK-Haus IFC4 file.

A total of 81 space boundaries was evaluated. Five space boundaries show syntax errors, as these have no relation to a related building element. The space boundaries of four out of seven spaces do not form an airtight shell. Only eight space boundaries have a correctly orientated surface normal. All of these correctly oriented space boundaries have either a missing or a virtual related building element. Thus, there seems to be a systematic error within the authoring tool ArchiCAD. Seven space boundaries show collinear and/or coincident vertices.

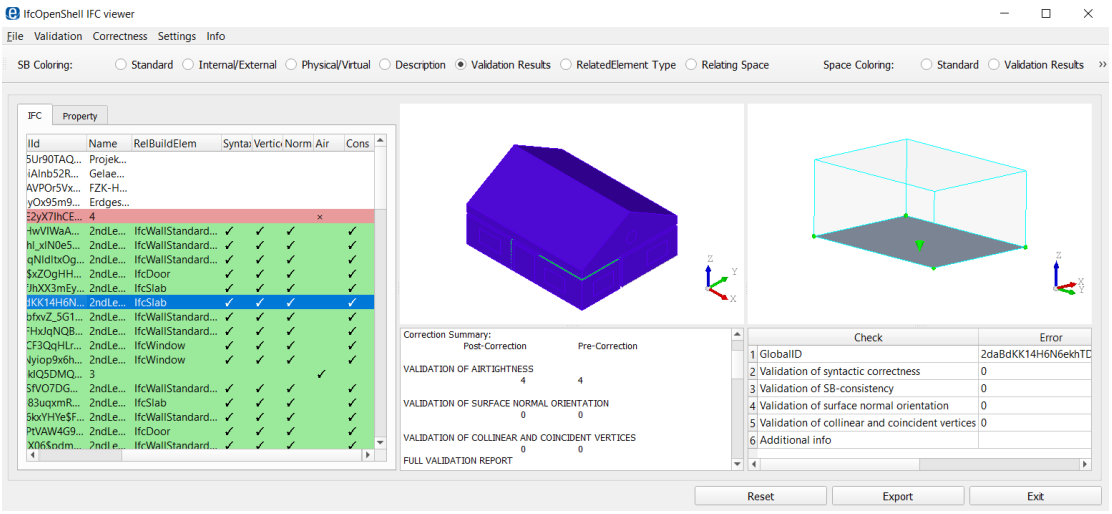

Figure 2.19: Space boundary correction of the FZK-Haus IFC4 file.

Once the validation is performed, the surface normal and vertex errors can automatically be corrected within the validation tool. Figure 2.19 displays the corrected FZK-Haus, including an updated treeview (left), all corrected surfaces highlighted in blue (full view, center), the corrected surface normal (detailed view, right), and a summary of the corrections (bottom

center). This corrected IFC4 model allows for an export to a new IFC4 file. Apart from this IFC correction in the validation tool, the *bim2sim* tool and its *PluginEnergyPlus* includes algorithms to correct these errors before converting it to EnergyPlus IDF.

For the FZK-Haus use case building, the *IFC2SB* tool [Fic22] was tested to generate a set of space boundaries with a higher quality. The validation is presented in the Appendix, Figure A.4. The new set of generated space boundaries shows syntax errors regarding their corresponding space boundaries for 108 out of 191 total space boundaries. It has to be noted that the original use case FZK-Haus did not contain this information and has thus not been tested. Also, these erroneous surfaces have fairly small surface areas, which may be one reason even for algorithmic validation failure. The evaluations on airtightness, syntax (aside from corresponding boundaries), and surface normals show no errors. However, for 24 space boundaries collinear and/or coincident vertices were detected, which partially result from the high spatial resolution of space boundaries that was generated by [Fic22]. As an example, the circular window in the detailed view in Figure A.4 was detected to hold coincident vertices, caused by the large amount of polygon vertices defining the window shape.

Even though the general space boundary quality of the *IFC2SB* tool is better than the original FZK-Haus space boundaries, the *IFC2SB* tool does not include the virtual space boundaries that are included in the original model. The new model combines four of the seven original spaces to a single space due to missing virtual boundaries, resulting in a total of four spaces. Thus, the original FZK-Haus is kept for further analysis of the IFC-based BEPS process in this dissertation, as it allows for an analysis of a broader range of spaces with individual usages.

IDF Validation

The validation of the IDF file is started by a visual check of the overall geometry. The validation tool also allows for a visual analysis of the surface types and constructions, as visualized in Figure 2.20. Here, the focus is on a first impression of the correctly assigned different constructions per surface type, visualized by different colors, e.g., showing that the exterior and interior walls have different construction types.

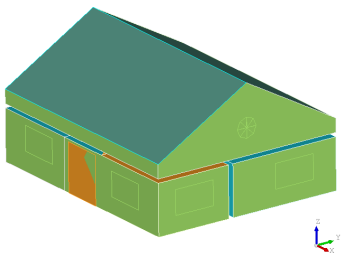

Figure 2.20: Visual validation of the construction types in the resulting IDF file.

The geometric analysis of the IDF file reveals less errors compared to the analysis of the IFC file. For the IDF, no airtightness errors are observed, as the *bim2sim* tool adds all missing 2b boundaries as adiabatic surfaces. Four out of 102 surfaces show errors on collinear and/or coincident vertices, which can automatically be corrected, cf. [RMF+22]. In the resulting IDF, only three surface normal errors are detected by the tool. A visual evaluation of these detected surfaces revealed that the errors are detected false positive, which hints at an error in the implementation. All of these false positive detected surface normal errors occur for surfaces that have a neighboring surface with

the same surface normal in the same space. The detection error may be caused by an incorrectly computed bounding box for these neighboring faces or by errors in the geometric computations due to precision errors. The IDF Validation allows for an automatic correction of all detected errors. The incorrect detection of surface normals though underlines the importance of visual human verification of detected errors before applying automatic correction algorithms. In the present case, only the vertex errors should be corrected. The small amount of errors within this IDF file is a precondition for a sucessfull simulation.

Transformation Validation

The transformation validation results are similar to the elaboration in [RMF+22]. The transformation validation compares the resulting surface areas in the IDF to the input IFC space boundary surfaces. For the FZK-Haus, the major differences in the surface areas results from additional adiabatic surfaces, which correspond to the missing 2b space boundaries in the input IFC. The total error in opaque surface areas has a RMSE of 8.585 m^2 (NRMSE=0.012 m^2, normalized to the total opaque surface area), which mainly results from the missing adiabatic walls on the first floor and the corridor. A major difference in the mapping of surface types is caused by the missing connection to virtual elements for the virtual space boundaries in the IFC, such that these surfaces had no RelatedBuildingElement. Minor surface area errors (RMSE=0.18 m^2) result from the triangulation of the circular windows in the first floor, which resulted in a larger number of windows in the IDF file compared to the IFC file. A detailed analysis of the transformation results can be found in [RMF+22], which shows only minor deviations to the model transformation in this dissertation as they are analyzing the same IFC input model.

2.7.3 Use Case 2: Building Energy Performance Simulation

The simulation results are generated using the use case setup described in Section 2.7.1. The total simulated annual energy consumption for this use case is 35.04 MWh/a (=168.03 kWh/(m^2 a)), consisting of 31.31 MWh/a (=150.14 kWh/(m^2 a)) heating energy and 3729.74 kWh/a for electricity (lighting and equipment). The high heating energy demand results from the poor insulation of the building from the 1960's (cf. U-values in Table 2.6), and roughly complies with a typical heating energy consumption of a single family house for this construction year.[30]

The calculation of maximum daily heating demand in Figure 2.21a can be used during the design phase of a building to evaluate the sizing of the heating system. This heating demand calculation already includes a reduction by the internal loads within the building and is influenced by the choice of weather file. Thus, for a profound sizing, e.g., of a heat pump using simulation, the internal loads and the influence of the weather (i.e., extreme weather scenarios) should be evaluated to prevent over-/undersized systems. Figure 2.21b displays the monthly heating

[30] i.e., 163.4 kWh/(m^2 a) for construction years between 1958-1968 according to the TABULA WebTool: https://webtool.building-typology.eu/, accessed on May 21, 2025.

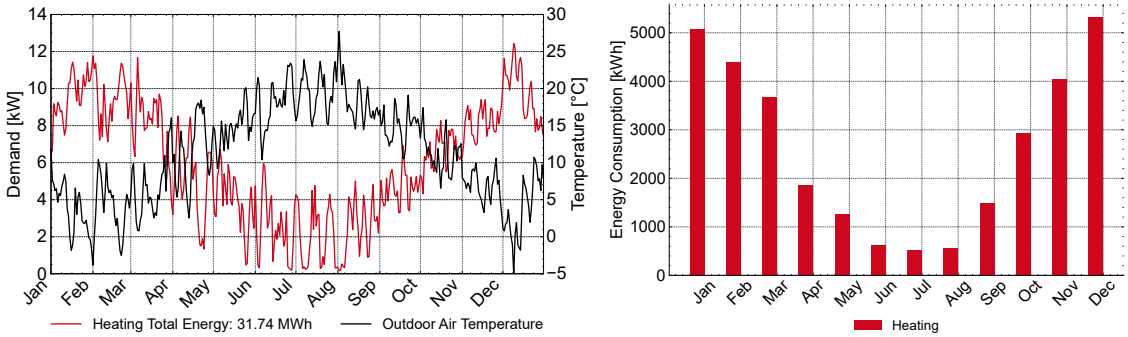

(a) Maximum daily heating demands and daily mean outdoor air temperature, Maximum demand of 13.25 kW on December 9

(b) Heating energy consumption per month

Figure 2.21: Daily heating demands and monthly heating energy consumption of the FZK-Haus using TMYx (2007-2021) weather data of Cologne/Bonn Airport.

energy consumption. This plot reveals that the heating system is operating even during the summer months, even though it would be turned off in most of the households.

Figure 2.22 displays the simulation results with higher detail. The maximum heating demands per space are shown in Figure 2.22a. The area-specific heating demands range from 43.5 W/m^2 in the corridor to 78.9 W/m^2 in the bathroom, which is reasonable considering the maximum heating setpoint temperatures of 18 °C and 24 °C in these rooms respectively (cf. Appendix, Figure A.2 and Appendix A.10.1).

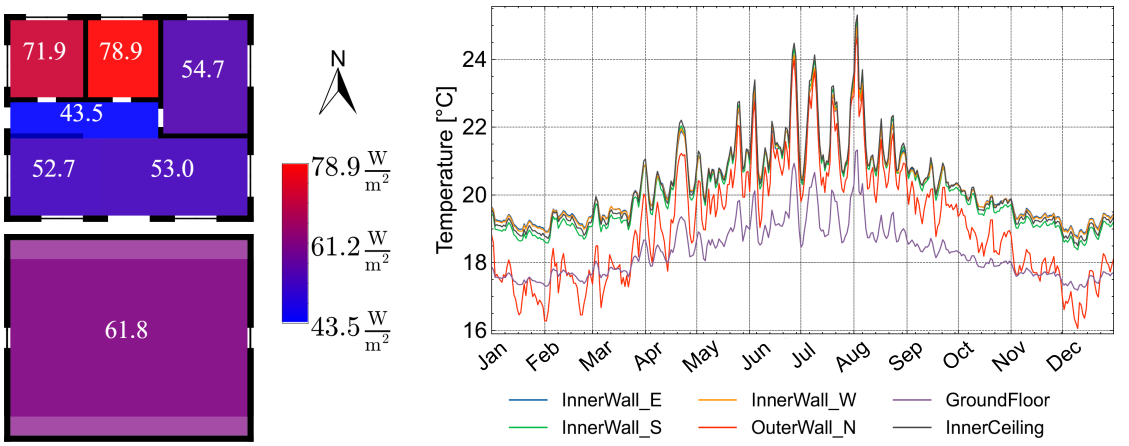

(a) Maximum heating demand per area per room; Top: ground floor, bottom: first floor

(b) Annual indoor surface temperatures in bathroom, daily mean values

Figure 2.22: Detailed results on heating demands and surface temperatures.

Figure 2.22b visualizes the inner surface temperature distribution within the bathroom, which is the room with the highest setpoint temperature (24 °C) of the house. The outer wall of the bathroom faces north, so the solar gains are small. The outer wall is the coldest wall during the winter and shows the highest temperature variability. The ground floor has the second lowest temperature, but less temperature fluctuations due to the smaller temperature fluctuations in

the ground. The temperatures of the inner walls are higher and have similar temperatures, but the south wall has the lowest temperature as it bounds to the corridor, which has a setpoint temperature of 18 °C and thus a large temperature difference to the bathroom temperature. The individual surface temperatures and their corresponding heat fluxes are a basis for the setup of boundary conditions for CFD in Chapter 3 and further investigations of thermal comfort in Chapter 4. A tabular overview on all BEPS results is included in Appendix A.11.

2.8 Evaluation and Summary of the Research Hypotheses

This section evaluates the RH on IFC-based BEPS defined in Section 2.3.4 under the scope of the RQ in Section 1.3, visualized in Figure A.1. A methodology was presented for an automated transformation of IFC4 models to BEPS simulation input for the open-source kernel EnergyPlus. The application of this use case in the previous Section 2.7 proves that the model transformation can be applied automatically. This supports the first research hypotheses RH BEPS 1 proposed in Section 2.3.4, as the automated process of BEPS model transformation allows the seamless integration of simulation approaches starting from the initial IFC-based design stage. The presented transformation approach included only minor manual effort in the transformation process, e.g., the choice of applicable *sim_setting*s within the setup of the simulation in the *PluginEnergyPlus*. These advances successfully provide a solution approach for the integration of IFC-based BEPS into the BIM workflow in response to the RQ 1. However, the presented approach still requires minor manual effort, as it uses template-based enrichment for materials and schedules, which have to be adapted for real-world use cases.

Apart from the IFC-based BEPS itself, RH BEPS 2 addressed the lack of model quality within the input data. The erroneous input IFC was successfully transformed to an EnergyPlus input IDF model used for simulation, although the initial IFC validation revealed a set of non-airtight SBs with incorrect surface normals and vertex errors. The internal *bim2sim* algorithms successfully corrected these errors in the transformation stage, as the analysis of the resulting IDF has proven. The IDF is analyzed for errors visually and algorithmically, followed by the transformation analysis. This multi-layer validation allows for profound error detection to validate the previous automatic transformation of the models securely. These challenges of missing and erroneous data for BEPS setup were identified in response to RQ 2 and were successfully addressed by applying the proposed enrichment, validation, and correction algorithms.

The proposed BEPS methods rely on the open-source *bim2sim* framework and its plugin-based structure, which includes the applied methods for template-based enrichment of materials and use conditions. The presented IFC-based BEPS approach currently has limited capabilities to include IFC-based materials, constructions, and use conditions, as its integration has not been in the focus of recent *bim2sim* tool developments, and thus lack testing and robustness. Design changes in materials, constructions, and use conditions can thus not be evaluated using the automated process of IFC-based simulations. However, design decisions on the building geometry can be assessed, as well as material choices that comply with the pre-defined set of templates,

which provide constructions for the German building stock, as well as recent constructions like the KfW standard. Use-case-specific requirements on building usage and constructions can be evaluated using modifications from the existing templates or own templates that follow the required structure.

While the evaluation of the use cases was successful, the proposed methods still require further research to improve the robustness of the underlying algorithms. As mentioned in the implementation of the approaches, a simplification for the inner loop removal was applied, which fails to detect inner loops in roofs. This simplification requires manual modifications of the resulting EnergyPlus IDF, as these roof shapes are likely to be split into convex shapes (cf. Figure 2.9, center), resulting in an error in the surface area in the generated model, causing inaccuracies in the results. Additionally, a type verification for gap-closing SBs should be added, to account for heat transfer through these bounds. Currently, these SBs are considered as adiabatic. For the approximation of circular shapes, the *IFC2IDFValidationTool* revealed a mismatch in the resulting surface areas. Here, the triangulation algorithm should be adapted to match the original surface shapes. Window frames are currently not considered in the IFC-based BEPS setup, which requires manual correction, and further development within the *PluginEnergyPlus*. The effect of external shadings is evaluated in Section 4.7.2, as well as mechanical ventilation and cooling. The *IFC2IDFValidationTool* requires further development on the export of the corrected models and a correction of the IDF algorithm for validating surface normal orientations. Both the IFC and IDF validations should be extended for automated syntactic checks to comply with the underlying IFC schema and the EnergyPlus IDD, respectively. For the validation of the input requirements of the IFC, the buildingSMART IDS format can be used to evaluate the existence of required entities and properties in the IFC for the BEPS setup, but the IDS check does not cover the geometric and consistency validation. The presented transformation validation of the IFC to IDF validation has not been found in related research and presents a novel type of validation for the IFC-based setup of BEPS using EnergyPlus IDF files, but can be further extended for the evaluation of other BEPS input files that rely on the IFC GlobalID as unique identifier of space boundaries.

Additionally, the BEPS results have not been validated with data from case studies. Further research should address validation approaches for IFC-based model setup, including approaches to enhance calibration. Future development should also consider the automated integration of IFC-based HVAC data for an accurate definition of HVAC systems within the BEM. While the current implementation supports the effect of external shadings generated from external SBs (cf. Section 4.7.2), other external shadings that are not included in the IFC, e.g., neighboring buildings, cannot automatically be included in BEPS and require further manual post-processing. In further research, these buildings could be included from applicable city models, e.g., using the CityGML format, to include shadings automatically.

3 IFC-based Computational Fluid Dynamics

CFD has a broad range of applications in the field of building design, operation, thermal comfort, and building safety, which allow for integration of BIM models [KWW+22]. This chapter proposes a method to reduce the manual effort for setting up CFD models and simulations. The CFD model is set up using an IFC-based approach to generate the required surface geometries for automated meshing. For setting up the boundary conditions, heat fluxes and temperatures are used based on the IFC-based BEPS presented in Chapter 2.

In this chapter, Section 3.1 provides the CFD fundamentals, while Section 3.2 introduces the applied software tools. Section 3.3 examines existing research to identify gaps that are leading to the research hypotheses (see Section 3.3.4). To test these hypotheses, Section 3.4 proposes a methodology for IFC-based CFD model setup using precomputed boundary conditions from building energy performance simulations. Section 3.5 presents the implementation as *bim2sim PluginOpenFOAM*, while Section 3.6 covers testing and evaluation. Finally, Section 3.7 evaluates the methods against the defined research hypotheses.

3.1 Fundamentals of Computational Fluid Dynamics

This introduction to CFD is written to gain a brief overview on the fundamental principles required to perform an IFC-based CFD. This section does not provide a complete introduction into the principles of CFD. Please consider applicable resources for a full introduction, e.g., [AM02, FPS20, Gha23, Joh16].

3.1.1 Conservation Laws

The physics of fluid flow is based on three fundamental principles of conservation, namely the conservation of mass, momentum, and energy [AM02]. The conservation laws of mass and momentum form the base of the definition of the Navier-Stokes-Equation, which is used to solve fluid flow problems.

The conservation of mass, i.e., the mass m of a given control mass does not change over time t, is mathematically defined as [FPS20]

$$\frac{\mathrm{d}m}{\mathrm{d}t} = 0. \tag{3.1}$$

As the momentum on a control mass is impacted by external forces $\mathbf{f}$, the conservation of momentum is defined as

$$\frac{\mathrm{d}(m\mathbf{v})}{\mathrm{d}t} = \sum \mathbf{f}, \tag{3.2}$$

where the change in the velocity **v** of the control mass over time is the response on the sum of all acting forces **f**. The bold notation of symbols such as **f** and **v** denotes three-dimensional components of these properties. [FPS20]

It is further distinguished between extensive and intensive properties, where intensive variables are independent of the actual amount of a matter (e.g., density ρ (mass per volume) and velocity **v** (momentum per mass)), and extensive properties are their counterparts depending on the amount of matter (e.g., mass, momentum) [FPS20]. The variables defining the fundamental equations are mainly intensive [FPS20]. The conservation of mass and momentum can be expressed in a general integral form, where the extensive property Φ is defined by the relation of the conserved intensive property ϕ inside the control mass, and can be computed as

$$\Phi = \int_{V_{\mathrm{CM}}} \rho\phi \mathrm{d}V, \tag{3.3}$$

where $\phi = 1$ for mass conservation, $\phi = \mathbf{v}$ for momentum conservation, and V_{CM} denotes the volume of the control mass. Equation 3.3, denoted in the control mass form, can also be expressed for a control volume, which can further be transformed in the left-hand side of each conservation equation, leading to

$$\frac{\mathrm{d}}{\mathrm{d}t}\int_{V_{\mathrm{CM}}} \rho\phi \mathrm{d}V = \frac{\mathrm{d}}{\mathrm{d}t}\int_{V_{\mathrm{CV}}} \rho\phi \mathrm{d}V + \int_{S_{\mathrm{CV}}} \rho\phi(\mathbf{v}-\mathbf{v}_{\mathrm{s}})\cdot\mathbf{n}\mathrm{d}S, \tag{3.4}$$

where V is the volume and S is the enclosing surface of a control volume CV, **n** is the outward-oriented normal of S_{CV}, and $\mathbf{v}_{\mathrm{s}}$ is the velocity of a moving control volume surface ($\mathbf{v}_{\mathrm{s}} = 0$ if surface is fixed). This equation is called the *Control Volume Equation* or the *Reynold's Transport Theorem*. It defines that the change in the extensive property Φ is defined by the change of the property inside the control volume and its net flux through the surface of the control volume. [FPS20]

From Equations 3.1 and 3.4 ($\phi = 1$) can now be derived the integral form of the mass conservation equation (i.e., continuity equation)

$$\frac{\partial}{\partial t}\int_{V} \rho \mathrm{d}V + \int_{S} \rho\mathbf{v}\cdot\mathbf{n}\mathrm{d}S = 0, \tag{3.5}$$

where the time derivative is now a partial derivative due to the fixed control volume (i.e., $\mathbf{v}_{\mathrm{s}} = 0$), and the integral notation is simplified for volume V and surface S of the control volume. [FPS20]

The conservation of momentum can also be expressed in an integral form considering Equations 3.2 and 3.4 ($\phi = \mathbf{v}$). The sum of forces introduced in Equation 3.2 can be expressed as a combination of surface forces and body forces. The surface forces can be expressed by the stress tensor **T** describing the momentum transport, which is influenced by the static pressure, fluid velocities and viscosity, as well as the deformation tensor. Body forces are denoted as **b**. This

leads to the following integral form of momentum conservation:

$$\frac{\partial}{\partial t}\int_V \rho \mathbf{v} \mathrm{d}V + \int_S \rho \mathbf{v}\mathbf{v} \cdot \mathbf{n} \mathrm{d}S = \int_S \mathbf{T} \cdot \mathbf{n} \mathrm{d}S + \int_V \rho \mathbf{b} \mathrm{d}V. \tag{3.6}$$

The set of equations of mass and momentum conservation (Equations 3.5 and 3.6) are called *Navier-Stokes equations*, which are usually solved numerically, as the solution of these coupled, non-linear equations is complex. [FPS20]

The third conservation equation is the energy equation. Similar to the previous derived equations, the conservation of a scalar quantity ϕ can be denoted as

$$\frac{\partial}{\partial t}\int_V \rho \phi \mathrm{d}V + \int_S \rho \phi \mathbf{v} \cdot \mathbf{n} \mathrm{d}S = \sum f_\phi. \tag{3.7}$$

Here, f_ϕ denotes the transport of the scalar quantity ϕ. One transport mechanism is the diffusion transport

$$f_\phi^{\mathrm{d}} = \int_S \Gamma \nabla \phi \cdot \mathbf{n} \mathrm{d}S, \tag{3.8}$$

which is a gradient approximation, e.g., for heat diffusion (*Fourier's law*) and mass diffusion (*Fick's law*), where Γ denotes the diffusivity of the scalar quantity. The conservation of scalar properties can be expressed in a generic form as

$$\frac{\partial}{\partial t}\int_V \rho \phi \mathrm{d}V + \int_S \rho \phi \mathbf{v} \cdot \mathbf{n} \mathrm{d}S = \int_S \Gamma \nabla \phi \cdot \mathbf{n} \mathrm{d}S + \int_V q_\phi \mathrm{d}V, \tag{3.9}$$

where q_ϕ describes a volumetric source or sink of the scalar quantity ϕ. [FPS20]

From these equations, considering the case of incompressible flows and a constant specific heat capacity of the fluid, the energy equation can be expressed as a convection-diffusion equation depending only on the temperature T:

$$\frac{\partial}{\partial t}\int_V \rho T \mathrm{d}V + \int_S \rho T \mathbf{v} \cdot \mathbf{n} \mathrm{d}S = \int_S \frac{\mu}{\mathrm{Pr}} \nabla T \cdot \mathbf{n} \mathrm{d}S, \tag{3.10}$$

where μ is the fluid viscosity and the Prandtl number $Pr = \frac{\nu}{\alpha} = \frac{c_p \mu}{k}$ [Joh16] defines the ratio between momentum diffusivity $\nu = \frac{\mu}{\rho}$, also called kinematic viscosity, and thermal diffusivity $\alpha = \frac{k}{\rho c_p}$ (thermal conductivity k, specific heat capacity c_p). [FPS20]

3.1.2 Fluid Characteristics

The previously introduced Navier-Stokes equations are represented in a generic form that supports the spatio-temporal variation of all fluid and flow properties. However, most often for liquids, but also for gases with a Mach number ($Ma = \frac{v}{c}$, v: flow speed, c: speed of sound in fluid) below 0.3, the density can be assumed as constant, and thus, these fluids can be considered as *incompressible*. [FPS20]

Indoor air flows often include heat transfer, such that the small temperature changes in the

fluid affect their properties and cause fluid motion, called buoyancy. In case the temperature differences have only a minor effect on the density, the density can be considered as constant, except for the density in the body forces term **b** (here: gravitation) in the momentum equation (Equation 3.6). This assumption of constant density is called *Boussinesq Approximation*. The approximation causes errors of about 1% for air temperature differences below 15 K but may cause larger errors for larger temperature differences. [FPS20]

The Reynolds number is defined as $Re = \rho \frac{vl}{\mu}$ (v: characteristic velocity, l characteristic length, μ: viscosity), where a small Re represents *laminar* flow, while a large Re represents *turbulent* flow. As an example, in pipes, $Re < 2000$ usually represent laminar flows, $Re > 4000$ turbulent flows, with a transition region showing mixed properties in between. [Joh16]

3.1.3 Numerical Methods

Fluid flow equations require numerical methods to approximate a solution since they cannot be solved analytically. In order to apply these methods, the continuous problem must first be discretized, i.e., transformed into a discrete problem. This discretization results in a large set of nonlinear algebraic equations that require iterative solution procedures due to their inherent nonlinearity. These equations are subsequently solved using a suitable finite approximation scheme. [FPS20]

Accordingly, the computational domain is partitioned into subdomains by defining a grid. Once this grid is established, different finite approximation schemes can be applied to iteratively solve the nonlinear equations. Before the numerical solution can be obtained, suitable boundary and initial conditions have to be defined for the grid. The numerical solution and its procedure can be evaluated by common numerical solution properties, e.g., consistency, stability, and convergence, which are described at the end of this section. Existing numerical solvers can be used to apply the numerical approximation of the results. [FPS20]

Numerical Grids

Before a numerical solution can be computed for a given domain, the domain is discretized by a numerical grid, also called mesh. From the variety of available numerical grids, three are to be named in this introduction: (1) structured or regular grids, (2) block structured grids, and (3) unstructured grids. [FPS20]

The *structured grid* (cf. Figure 3.1a) is the simplest grid structure, as the lines and positions of grid points can be numbered consecutively and are thus uniquely defined by two indexes in 2D and three indexes in 3D spaces. Thus, each grid point has four or six neighboring points in 2D and 3D, respectively. This simple structure is suitable for simple geometries and supports a straightforward implementation of numerical solution schemes. However, this approach is not suitable for complex geometries, as the grid points may be unevenly distributed. In the case of long cells, the convergence of the numerical solution may be negatively affected. [FPS20]

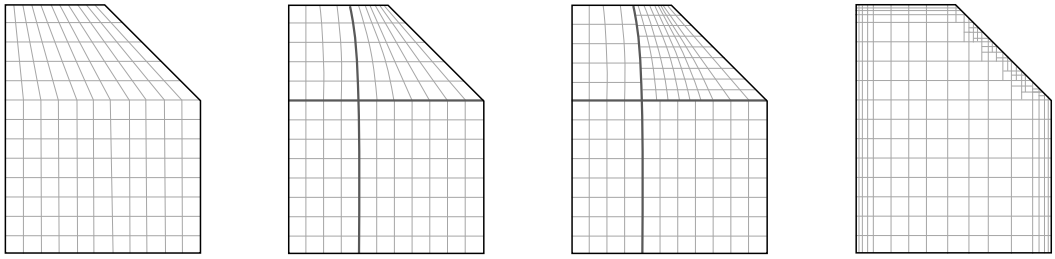

(a) structured (b) block, conform (c) block, non-conform (d) unstructured

Figure 3.1: Numerical grids. Adapted from [FPS20]

The second grid type is the *block-structured grid*, where the solution domain is subdivided into at least one coarse and one fine level. The coarse level subdivides the domain into large blocks, in which structured grids are inserted on a finer level. Figure 3.1b shows such a block-structured grid, where the vertical edge (bold line) between the blocks was transformed to a curved line due to smoothing operations and the interfaces between the blocks are conform, i.e., their grid points match. Block-structured meshes also allow for non-conform interfaces, as displayed in Figure 3.1c, which enables the definition of grids for shapes with a higher complexity. The definition of a high-quality block-structured grid is time-consuming, while block-structured grids with non-conform interfaces require advanced implementation of solution algorithms. [FPS20]

The most flexible grid types are *unstructured grids*. These grids do not restrict the number of neighboring grid cells, so they are suitable for any kind of geometric complexity. Figure 3.1d represents a combination of a hexahedral grid with local grid refinements and prism layers at the side and top surfaces, suitable for adapting to curved surfaces. This grid type requires an explicit definition of the grid connectivity. Unstructured grids are commonly used with finite-element and finite-volume solution approaches, which are introduced in the following section. [FPS20]

Finite Approximations

The applicability of finite approximation schemes depends on the choice of the numerical grid type [FPS20]. The *finite difference* method solves the conservation equations for each point in the grid by applying finite difference schemes [Gha23]. This method requires a structured grid containing nodes that are explicitly described by a set of indexes as shown in Figure 3.2a. The fundamental principle of derivatives

$$\left(\frac{\partial \phi}{\partial x}\right)_{x_i} = \lim_{\Delta x \to 0} \frac{\phi(x_i + \Delta x) - \phi(x_i)}{\Delta x} \tag{3.11}$$

can be extrapolated to a set of finite difference schemes (e.g., *forward*, *backward*, *central*) as displayed in Figure 3.2b [FPS20], which take different neighboring grid points into account for approximating the solution. The derivative $\frac{\partial \phi}{\partial x}$ at a grid point on a curve (cf. *exact* in Figure 3.2b),

describes the gradient of the curve in that point, which is equal to the gradient of the tangent in the curve. Depending on the shape of the curve, the size of the Δx, and the choice of the approximation scheme, the solution of the approximation is more or less accurate. [FPS20]

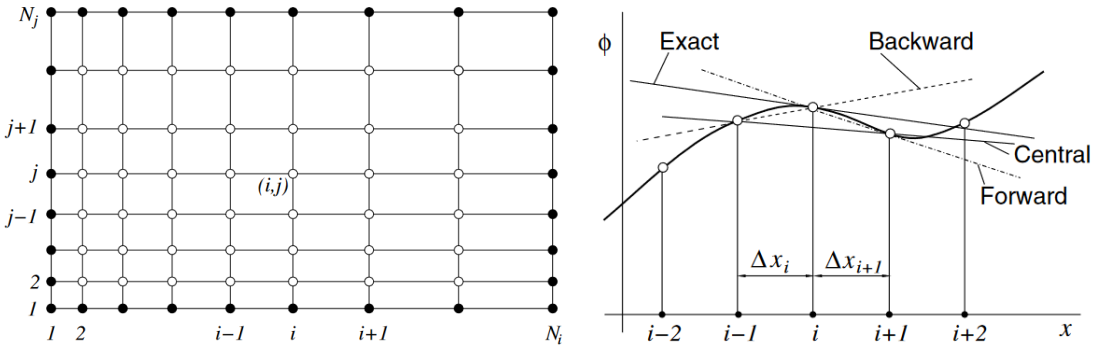

(a) Finite difference 2D grid (b) Finite difference schemes

Figure 3.2: Finite difference grid and schemes [FPS20]. Reproduced with permission from Springer Nature.

In the *finite volume* approach, the conservation equations (cf. Equation 3.9) are solved for control volumes instead of grid points [Gha23], where the grid itself now forms the boundaries of the volumes, displayed in Figure 3.3a [FPS20]. This conservation equation applies to both, the individual control volumes, but also to the whole computational domain. The surface integrals have to be approximated. Each control volume has four (2D) or six (3D) surfaces with neighboring control volumes for the simplified case of a Cartesian grid as displayed in Figure 3.3b. The net flux over the surface of a volume is defined as the sum of the flux over the individual surfaces. The values on the surfaces of the volumes are interpolated. The finite volume approach has no restrictions on the type of grids and is thus applicable to complex geometric domains. However, the control volumes cannot overlap. [FPS20]

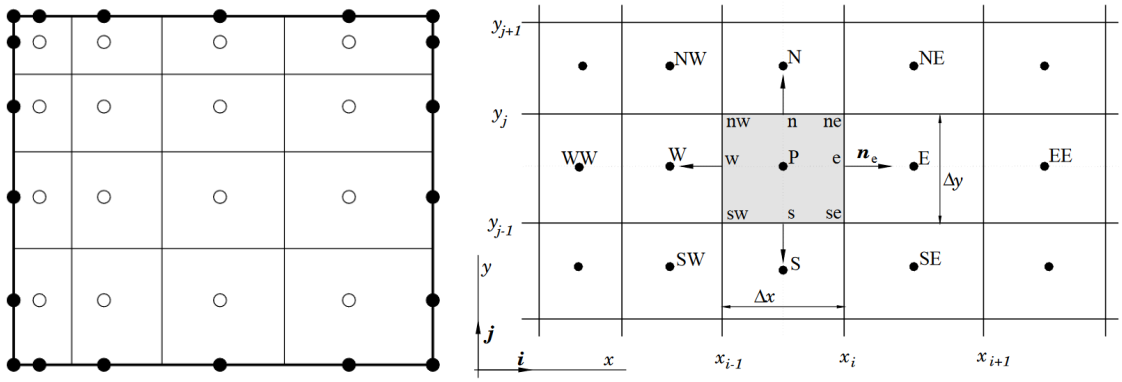

(a) Finite volume 2D grid (b) Finite volume notation in 2D grid

Figure 3.3: Finite volume 2D grid and notation [FPS20]. Reproduced with permission from Springer Nature.

The requirements on the computational domain and the grid for the *finite element* method are similar to the finite volume approach. The main difference to the finite volume approach is the weighting of the equations using a weight function before the integration is applied [FPS20].

Comparing the three numerical schemes, the choice of the scheme strongly depends on the complexity of the computational domain to balance the flexibility of the numerical grid and the accuracy of the results [LO18]. As the finite volume approach provides appropriate accuracy and flexibility for common CFD applications, it is most commonly applied for spatial discretizations in CFD software industry [Gha23].

Initial and Boundary Conditions

The iterative solution procedure requires an initialization with appropriate values. In steady-state simulations, the computational domain is commonly initialized with constant velocity (either zero or non-zero), pressure, and temperature, since the initialization of the computational domain affects the convergence rate of the solution but does not affect the converged solution. For unsteady simulations, the initial conditions significantly affect the accuracy of the overall solution, as errors at initial timesteps are propagated to later timesteps. [FPS20]

To define the boundaries of the computational domain, three types of boundary conditions are defined in steady-state problems. For the *Dirichlet* boundary condition, a variable ϕ on the boundary is defined by constant (i.e., fixed) values. For the *Neumann* boundary condition, the derivative of the variable ϕ is defined by a constant value. The third type of boundary conditions is a *mixed type* boundary condition, also called *Robin* boundary condition. The mixed boundary condition is defined by a weighted combination of a Dirichlet and Neumann Boundary Condition. [AM02, Joh16]

Quality of Numerical Solutions

The quality of numerical processes and solutions can be evaluated using different criteria, which are briefly introduced here. *Consistency* is defined by the *truncation error*, which is the error between the discretized and the exact solution. A method is called *consistent*, if the truncation error tends to zero for an infinitesimal small mesh distance. The *stability* criterion is met, when the numerical method does not increase the error in the solution process, e.g., that it does not diverge in iterative processes. The general *convergence* criterion is fulfilled, when the solution of the numerical method tends to the exact solution for decreasing grid size. However, as both the stability and convergence are highly dependent on the boundary conditions for non-linear problems, the convergence is evaluated, for example, by repeating the calculations for different grid sizes. This procedure allows for testing for a *grid-independent solution*. The *conservation* criterion evaluates if the conservation equations are preserved in cases where no sources or sinks are prevalent in the computational domain. The conservation should apply to both local control volumes in case of volumetric discretization and the global domain over all local volumes. The criterion of *boundedness* describes that quantities are within proper bounds. These bounds are either caused by physical laws, e.g., properties like density must be positive. Also, if no sinks or sources are present, properties like temperatures must

not exceed or fall below the temperatures of the domain boundaries. Boundedness cannot be guaranteed numerically, but unboundedness may be a sign for a too coarse mesh that needs further refinement. The definition of fluid flow problems must be realizable such that it is possible to obtain physically valid solutions, which is covered by the *realizability* criterion. Finally, as all numerical methods only produce approximate solutions, the *accuracy* should be evaluated. Thus, numerical solution lead to three types of systematic errors: (1) *modeling errors*, (2) *discretization errors*, and (3) *iteration errors*, which are often called *convergence errors*. [FPS20]

Coupling Approaches

To initialize the boundary conditions and to set initial values of the CFD computational domain, these parameters can either be set to fixed values, but also be pre-computed by a BEPS, as introduced in Chapter 2. The methods for coupling pre-computed BEPS and CFD can be categorized into three approaches [vTr10], visualized in Figure 3.4:

- *direct coupling*: BEPS and CFD are combined into a single system such that the equations for airflow and heat transfer are solved in a fully integrated approach.
- *sequential approach*: BEPS and CFD are solved sequentially for each timestep such that the results of BEPS are used as initial conditions for CFD within the same timestep. If executed for multiple timesteps, small timesteps are required to avoid oscillations. This approach is also called 'ping-pong' approach [Hen95].
- *iterative approach*: The results of BEPS and CFD are computed iteratively for each timestep until convergence is reached for the current timestep. Due to the iterative approach the timesteps can be larger than for the sequential approach. However, the iterative approach requires an increased computational effort. This approach is also called 'onion' approach [Hen95].

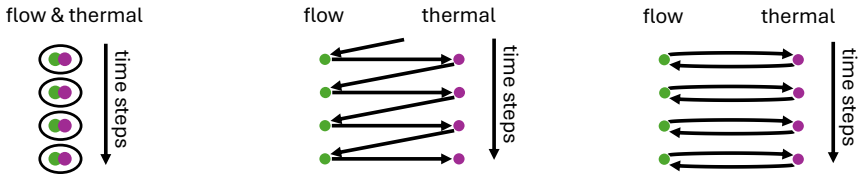

(a) Direct coupling (b) Sequential (ping-pong) (c) Iterative (onion)

Figure 3.4: Visualization of coupling approaches of BEPS (thermal) and CFD (flow), adapted and extended from [Hen95].

3.2 Data Exchange and Software Tools

This section introduces the OpenFOAM kernel as open-source computational kernel for CFD simulations in this dissertation, as well as Paraview as a tool for visualizing the CFD meshing and simulation results.

3.2.1 OpenFOAM and Related Tools

The open-source tool OpenFOAM (**Open**-source **F**ield **O**peration **A**nd **M**anipulation) has been developed for solving a variety of problems in the field of continuum mechanics, and thus, it is applied in a broad field of industries and research. OpenFOAM provides modular tools for processing these engineering problems, including tools for pre- and post-processing, and is extensible by users due to its open-source modular structure, written in C++.[1]

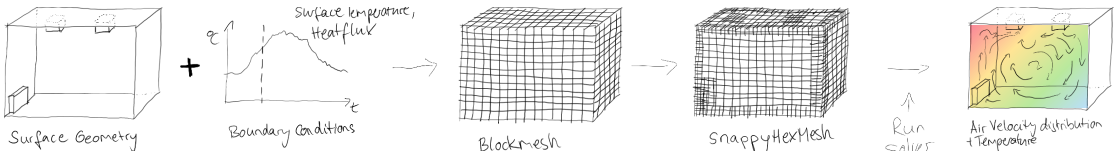

Figure 3.5: Sketch of the OpenFOAM input requirements and processes.

An overview on the OpenFOAM input requirements and the processes are given in Figure 3.5. The first basic input requirement is a computational domain that is fully enclosed by surrounding surfaces without gaps (i.e., airtight), where further geometries have to be defined within the space if applicable. For each of the surfaces, boundary conditions have to be applied, e.g., surface temperatures and heat fluxes, such that sources and sinks are well defined within the computational domain. On the basis of these data inputs, the computational domain can be subdivided into smaller subsets, which are defined by a mesh. For the computational domain, first, a structured mesh is defined using the *blockMesh* tool of OpenFOAM, which is then refined using the *snappyHexMesh* tool to account for complex geometries within the domain. Using the refined mesh and the defined boundary conditions, a numerical solver can be applied to solve for the spatially high-resolved solution over the domain, e.g., air velocity and temperature distribution.

The following introduction to OpenFOAM provides more details on (1) the basic input data structure for OpenFOAM simulations, (2) the meshing process and requirements, (3) definition of boundary conditions and physical properties, (4) the OpenFOAM solvers and their requirements, and (5) OpenFOAM parsing in Python.

Input Data Structure for OpenFOAM

OpenFOAM requires a specific structure for providing the input data files. The structure of the data input[2] can be broadly categorized into *system* data (i.e., control and solver settings), *constant* data (i.e., mesh data and physical properties), and *time series* data (i.e., initial and boundary conditions), visualized in Figure 3.6 [RvTF24].

[1] OpenFOAM Documentation, fundamentals: https://doc.openfoam.com/2312/fundamentals/about/, accessed on May 22, 2025.
[2] OpenFOAM Documentation, file structure: https://www.openfoam.com/documentation/user-guide/2-openfoam-cases/2.1-file-structure-of-openfoam-cases, accessed on May 22, 2025.

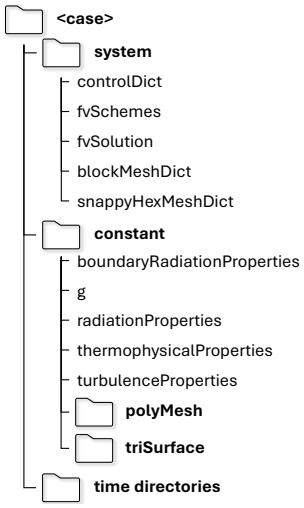

Figure 3.6: OpenFOAM input file structure, adapted from OpenFOAM Documentation.[2]

Meshing in OpenFOAM

The *blockMesh* tool generates structured hexahedral meshes. This procedure is defined by the *blockMeshDict*, which is located in the *system* directory,[3] cf. Figure 3.6. The blockMeshDict provides vertices, edges, blocks, and boundary for the blockMesh generation. The *vertices* define the eight outer vertices of the blockMesh, which are per default connected by straight *edges*, if not defined otherwise. In the *blocks* section, the vertices are combined to form a hexahedral block. In this section of the blockMeshDict, the number of cells in the x, y and z directions of the blockMesh are stated, as well as the cell expansion ratio in each direction if applicable. The *boundary* section defines the boundary of the domain as faces based on the defined vertices, which can be combined to patches for the further application of boundary conditions with individual patch names, or defined as geometric walls. In the simplest case, which is also applied in this dissertation, the boundaries of the defined box are considered as a single *boundingbox* of type wall.[4]

If the blockMesh is further processed in snappyHexMesh, the *cell aspect ratio* should be near 1 (i.e., nearly cubic shape) to support a fast snapping procedure. Each geometric surface inside the domain that should be considered in the meshing process must be cut by the block mesh grid; surfaces inside a single grid cell are not considered within the further refinement process using snappyHexMesh.[5]

The settings for the *snappyHexMesh* tool are defined in the *snappyHexMeshDict*, also located within the *system* directory (cf. Figure 3.6). snappyHexMesh further requires the surface data

[3] OpenFOAM Documentation, blockMesh: https://doc.openfoam.com/2312/tools/pre-processing/mesh/generation/blockMesh/blockmesh/, accessed on May 22, 2025.
[4] OpenFOAM Documentation, blockMesh: https://www.openfoam.com/documentation/user-guide/4-mesh-generation-and-conversion/4.3-mesh-generation-with-the-blockmesh-utility, accessed on May 22, 2025.
[5] OpenFOAM Documentation, snappyHexMesh: https://www.openfoam.com/documentation/user-guide/4-mesh-generation-and-conversion/4.4-mesh-generation-with-the-snappyhexmesh-utility, accessed on May 22, 2025.

files in the a triangulated format, e.g., STL,[6] located in *constant/triSurface* directory, as well as a hexahedral mesh, typically generated by the blockMesh tool and located in *constant/polyMesh* directory. The snappyHexMeshDict consists of five sub-dictionaries and additional global settings. The sub-dictionaries define the geometry, the castellated mesh, the surface snapping, layer addition, and the mesh quality.[5]

The *geometry* sub-dictionary defines triangulated surfaces on the basis of the files in the triSurface directory, but also searchable objects regions within the domain that can be used as refinement regions.[6] The *castellatedMeshControls* is a sub-dictionary that specifies the subdivision of the blockMesh and applies surface and region refinements. This sub-dictionary includes settings on the *locationInMesh*, which defines any point inside of the resulting mesh, but also global settings for the number of resulting mesh and refinement cells. Each surface defined in the geometry section needs a definition of its surface refinement in the *refinementSurfaces* sub-dictionary of the castellatedMeshControls. Here, the minimum and maximum refinement levels for each surface relative to the blockMesh are defined. The maximum refinement level is used at intersections of surfaces, while the minimum refinement is applied for the surface in general. Similarly to the refinementSurfaces, *refinementRegions* are defined for imported geometries or defined searchableBoxes. These refinementRegions follow the same principle of refinement levels as the surface refinements, but additionally hold a refinement mode, which defines if the region should be refined inside, outside, or with a distance to the defined region.[5]

Further parameters for the control of snappyHexMesh are defined in the snappyHexMeshDict sub-dictionaries *snapControls*, *addLayersControls*, and *meshQualityControls*,[5] which are not further addressed in this dissertation as the default values were used.

Parametrization of Models

Apart from subdividing the computational domain into smaller subsets using the meshing procedure, the OpenFOAM model also requires an appropriate definition of boundary conditions and underlying physical principles for solving the conservation equations.

The provided boundary conditions in OpenFOAM can be categorized into the three categories basic, constraint, and derived. *Basic* boundary conditions describe basic boundary conditions as described in Section 3.1.3, e.g., *fixedValue*, *fixedGradient*, *mixed*, and *zeroGradient*. The *constraint* boundary conditions represent geometrical constraints, e.g., cyclic or symmetric boundaries, which are not applied in this dissertation. The *derived* boundary conditions are designed for specific applications, e.g., the *inletOutlet* boundary condition that is used for air inlets and outlets as it is able to handle reversed flow.[7] For modeling indoor environments with heat fluxes on the wall, the *externalWallHeatFluxTemperature* is used to define the boundary by

[6] OpenFOAM Documentation, snappyHexMesh geometry: https://www.openfoam.com/documentation/guides/latest/doc/guide-meshing-snappyhexmesh-geometry.html, accessed on May 22, 2025.

[7] OpenFOAM Documentation, boundary conditions: https://www.openfoam.com/documentation/user-guide/5-models-and-physical-properties/5.1-boundary-conditions, accessed on May 22, 2025.

fixing the power, heat flux, or heat transfer coefficient.[8] Boundary conditions are defined in the time directory, commonly defined as '0' (=zero) directory, for each individual boundary condition in separate files. The file names express the name of the variable, e.g., T for temperature, U for velocities, p for pressure.

In the constant directory, the general *thermophysicalProperties*, *turbulenceProperties*, and gravity *g* are defined. Additionally, for the use cases in this dissertation, the radiation model (e.g., fvDOM, P1) is defined in the *radiationProperties* globally for the domain. While P1 integrates the radiation throughout the domain, leading to a smooth distribution of radiation, fvDOM applies a ray traycing approach, which is more computationally expensive but provides more accurate results. Other approaches, e.g., OpenFOAM's view factor approach for radiation, are not considered in this dissertation. Individual radiation properties of surfaces are defined in the *boundaryRadiationProperties*.

Running OpenFOAM Simulations

All dictionaries for solving the numerical systems and controling the simulation are located in the system directory. While the spatial discretization of the domain is addressed by the refined mesh using snappyHexMesh, the temporal discretization is handled in the *controlDict*. Here, start- and endtime, and step-size are defined, but also the *writeInterval* parameters for the simulation outputs are controlled. The discretization of equations is defined in the *fvSchemes* dictionary for different types of discretizations (e.g., *ddtSchemes*: time discretization schemes, *gradSchemes*: gradient schemes, *divSchemes*: divergence schemes) either as default scheme or for the individual calculated properties. The *fvSolution* dictionary requires the definition of the pressure-velocity coupling algorithm, e.g., SIMPLE (steady-state) or PIMPLE (instationary), but also the linear solver settings for field parameters, which include solver, smoother, and tolerance settings.[9]

Parsing OpenFOAM files in Python

The open-source Python tool *butterfly*,[10] provided by Ladybug Tools is used for parsing OpenFOAM input files within the *bim2sim* environment. To comply with the requirements of the *bim2sim* developments, a slightly modified fork has been created for the use in the *bim2sim* environment.[11]

[8] OpenFOAM Documentation, externalWallHeatFluxTemperature: https://doc.openfoam.com/2306/tools/processing/boundary-conditions/rtm/derived/thermal/externalWallHeatFluxTemperature/, accessed on May 22, 2025.
[9] OpenFOAM Documentation, quick start: https://doc.openfoam.com/2312/quickstart/, accessed on May 22, 2025.
[10] butterfly by Ladybug Tools: https://github.com/ladybug-tools/butterfly, accessed on May 22, 2025.
[11] butterfly fork in the *bim2sim* environment: https://github.com/BIM2SIM/butterfly/tree/1-updates-for-usage-in-bim2sim, accessed on May 22, 2025.

3.2.2 Paraview

In this dissertation, Paraview[12] is used for visualizing all steps of the OpenFOAM pipeline. The STL files that are used as a basis for generating the meshes can be loaded and analyzed, as well as the blockMesh and generated refined mesh using snappyHexMesh. During and after simulation, the exported simulation results (e.g., air velocity and temperature distribution) can be visualized and evaluated for plausibility.

3.3 Related Research

The analysis of related research for the design of IFC-based CFD generation is split into two parts. First, the existing research is examined for the use case of the IFC-based model setup itself. In a second step, available research is analyzed that couple BEPS and CFD to define their respective boundary conditions, as the BEPS-based initialization of IFC-based CFD models is a major part of the proposed methodology. The analysis of related research revealed four research gaps, which are reduced to two research hypotheses as a basis for the proposed methodology in this chapter.

3.3.1 IFC-based CFD

This section focuses on BIM-based approaches for setting up CFD simulations and provides an overview of the use of IFC-based workflows for CFD in related research and industry. Parts of this section are adapted and extended excerpts from [RvTF24].

Reviews on the BIM-CFD transformation process in related research consider only proprietary data exchange and fail to address open data exchange [ZLWZ23, KWW+22]. Additionally, two recent studies [WWQ24, LH24] use BIM-based CFD setup for optimizing indoor airflow. However, both did not use IFC for data exchange, but another exchange format (SAT) and native Revit data transfer, respectively. In Germany, especially in public construction projects, the software landscape of project participants is diverse and cannot be limited to specific proprietary software. Standardized data exchange formats (mainly IFC as the data exchange format for BIM processes) are required for data exchange between project participants. Therefore, this dissertation focuses on IFC-based model generation for CFD purposes.

Related research has developed different methods for the IFC-based setup of CFD models. [NKNR14] introduce an early IFC-based (IFC Versions 1.5.1 and 2x) approach to setting up CFD models using results of multi-zone thermal building simulations as boundary conditions. [PCN+19] present their approach for an IFC-based CFD setup applied for outdoor airflow simulations using their own CFD solver. They use IFC models exported from Revit and apply surface healing to improve the meshing process, but they do not state any details on the handling of the IFC file itself. Other studies present IFC-based CFD setups creating the CFD geometry based on

[12] Paraview: https://www.paraview.org/, accessed on May 22, 2025.

IfcProducts [LCLZ21, LPJK21, PKLC20]. However, these studies disregard the use of *IfcRelSpaceBoundary* entities. In their studies on IFC-based CFD model setups with OpenFOAM, [LPJK21] and [PKLC20] focused on geometric simplification, as well as optimization and validation of grids.

IfcRelSpaceBoundary geometry has been used within the BIM2SIM Project [MJvT+22] to set up indoor airflow CFD models for ANSYS Fluent. In addition, the meshing for OpenFOAM has been exemplary evaluated for building surroundings. [HR24] utilize these SBs from the *bim2sim* tool to propose a methodology for automatically improving mesh refinements for a composition of IFC-based entities. The resulting meshes were evaluated for mesh quality and simulation performance using OpenFOAM.

The application scenarios for IFC-based CFD in related research focused on indoor airflow, thermal comfort, and fire simulations. [LCLZ21, LPJK21] tested their approaches on the simulation of indoor airflow (i.e., temperature distribution and velocities). [MJvT+22] applied the IFC-based CFD setup to prove a pressure differential system and the scenario of smoke control in a staircase. [RLS+23] analyzed the required IFC entities for thermal comfort on different simulation scales, and they named the CFD simulation as the approach with the highest requirements on IFC data availability.

To gain insights into the use of CFD software in industry, [MJvT+22] analyzed the IFC import capabilities of available CFD software. Out of 13 analyzed software and kernels, five software tools did not provide any IFC import capabilities, two were capable of importing Autodesk Revit geometries, two imported IFC through an additional intermediate software, three supported a direct import of the outdated IFC2x3, and only the BIM HVACTool supported the import of both IFC2x3 and IFC4 files. All software with IFC import capabilities require license fees, and thus have limited applicability in research, also due to their limited access for adaptations in open-source projects.

Apart from the software analysis, [MJvT+22] did a survey in 14 companies that offer CFD simulations for construction projects. Five of these companies named thermal comfort as the most frequently requested use case. Other companies named indoor airflow analysis, including an analysis of air velocities and air temperatures as their most frequent case of application, which are also a major indicator for thermal comfort applications. Regarding data exchange, eight companies have experience with IFC data. However, most common format of data exchange is pdf, and less frequently other CAD data exchange formats such as dwg and dxf. The most commonly reported issue with handling IFC data was the content of these files. In this respect, seven out of nine companies claimed the high complexity of the models, requiring high manual effort of pre-processing for CFD purposes. Five companies remarked issues with the airtightness of models, i.e., the resulting model surfaces had gaps. Eight companies named the pre-processing (i.e., creation, preparation, and simplification) of model geometry as the most time-consuming step in the model. Three companies each named the mesh generation and the definition of boundary conditions to require the largest part of the setup time. [MJvT+22]

While [MTC+20] claimed that CFD applications are too computationally cost-expensive to be applied on common office computers of building design engineers, [LRW22] underlined the importance of CFD-knowledge of engineers that apply CFD analysis. Both factors limit CFD accessibility in building design, leaving BEPS as the more viable option for the broader engineering community.

3.3.2 Coupling BEPS and CFD

Early coupling approaches of BEPS and CFD have already been proposed in 1990s and 2000s [Neg95, Bea00, ZC15, Zha03a, Dju05, ZC05]. [Neg95] and [Bea00] developed an integration of CFD simulation using the CFD solver *dfs* for the BEPS software ESP-r,[13] which exchanges data between the computational domains for each timestep.

[ZC15, Zha03a] introduce different coupling mechanisms for data exchange between BEPS and CFD, distinguishing forms of *static* (i.e., sequential), *dynamic* (i.e., iterative), and *bin* (i.e., pre-computed) coupling based on the type of interaction between the simulation algorithms, cf. Section 3.1.3. [ZC15] developed a prototype of a quasi-dynamic coupling for EnergyPlus and CFD, i.e., BEPS surface temperatures and heating loads are used as boundary conditions for CFD, which returns air temperature and heat transfer coefficients to EnergyPlus in reverse. This procedure is repeated for every (hourly) timestep of BEPS. [Zha03a] and [ZC05] validated these coupling approaches, finding that full dynamic coupling achieved the highest accuracy, while static and bin coupling methods proved most computationally efficient while still maintaining reasonable result quality.

While the previous coupling approaches focused on integrated, internal coupling of simulation domains, [Dju05] proposed an external coupling approach to improve long-term maintenance and to support further development of the computational methods within each computational domain. The external coupling approach incorporates the solution of CFD and BEPS in separate software environments, while previous approaches proposed software-integrated (i.e., internal) solutions.

[THZS18] classified the exchanged data between CFD and BEPS into *interface* and *state* data. The interface data defines the conditions on the boundaries of the domain, while the state data defines the state inside a computational domain. They distinguish the data exchange according to the direction of data exchange. Most of the data exchange from BEPS to CFD can also be applied bi-directionally, including the exchange of surface temperatures and envelope heat fluxes, and air flow conditions (velocity, pressure, temperature) at openings to the computational domain. The conditions of the building surroundings are computed in BEPS for CFD due to the incorporation of weather depending simulations in BEPS. Data exchange from CFD to BEPS includes convective heat transfer coefficients, state data of indoor conditions (e.g., thermal comfort (i.e., PPD, PMV as introduced in Chapter 4), temperature, air velocity, humidity

[13] Environmental Systems Performance - Research (ESP-r): https://www.strath.ac.uk/research/energysystemsresearchunit/applications/esp-r/, accessed on May 22, 2025.

distribution), but also local outdoor air profiles and microclimate. [THZS18]

The field of application for coupled BEPS and CFD simulations is broad. Recent approaches included the analysis of building energy performance (heating and cooling loads) [HLK17, YM24, ALNK24], urban microclimates [HP21, DK21, MN23], performance evaluation and control of HVAC systems [SLS+20, ADMMV21, WLG+23, ZDS+23], thermal comfort requirements [GLH+22, LRW22, WLWZ23], indoor air quality [ADMMV21], but also the analysis of the building envelope (e.g., ventilated facades and roofs) [EAF17, DK21, THZS18, RHX+20].

Starting on a larger outdoor scale, [HP21] used BEPS results for initializing the CFD boundary conditions of outdoor air simulations for the analysis of urban microclimate and cooling system efficiency. [DK21, MN23] applied a sequential coupling in opposite direction, as they used OpenFOAM to pre-compute wind pressure coefficients (WPC) in outdoor environment simulations to replace the use of default WPCs in BEPS using EnergyPlus.

A broad range of studies focuses on the impact of outdoor airflow on natural ventilation of indoor spaces. [WW09] analyzed the accuracy of simulation results for different approaches of defining boundary conditions for natural ventilation, which revealed that the definition of pressure coefficients at the inlet resulted in more accurate solution than the definition of inlet velocities. [ZLYZ13] proposed an iterative coupling of EnergyPlus and the CFD software ANSYS Fluent to analyze its effect on natural ventilation and heat transfer coefficients compared to an uncoupled EnergyPlus simulation. In the coupling process, they used the intermediate software FlowPlus to extract temperature and velocity data from Fluent, before exchanging the data with EnergyPlus using the Building Controls Virtual Test Bed (BCVTB) [Wet11]. The BCVTB has been developed to support run-time data exchange for co-simulation of a variety of simulation tools. [HLK17] used EnergyPlus to calculate cooling energy consumption of a natural ventilated educational facility, applying a sequentially coupled CFD simulation using STAR-CCM+. The CFD analysis included heat gain through internal loads (electrical equipment and occupants) and solar radiation (obtained from EnergyPlus), but the study did not mention heat conduction and surface temperatures. The cooling energy consumption was decreased in two tested natural ventilation scenarios. [GLH+22] analyzed the efficiency of natural ventilation of a medium-sized gymnasium in subtropical regions, considering the adaptive PMV on the sports field and the spectator area to evaluate thermal comfort. They used surface temperatures and heat transfer coefficients from EnergyPlus as boundary conditions for CFD. [XC22] investigated the impact of street canyons on natural ventilation in buildings due to varying buoyancy effects during the day. They performed a simplified BEPS using EnergyPlus to define the surface temperatures as boundary conditions for an outdoor CFD and its impact on natural ventilated rooms. The effect of natural ventilation varied strongly during the day, but also for spaces on different storeys of the analyzed building.

Other studies applied the coupling of CFD and BEPS for indoor airflow simulations for mechanical ventilated buildings. [RWH17] applied a CFD study for two connected indoor spaces, using pre-calculated surfaces and heat fluxes to set the surface boundary conditions. [LRW22] evaluated the differences in thermal comfort (PPD) between the BEPS software IDA ICE and

the CFD software ANSYS CFX. They evaluated the PPD in rooms with a PPD greater than 10% in the occupancy section. They compared the PPD at the central point in the room, which resulted in higher PPD for IDA ICE compared to CFX in most analyzed rooms. [SLS+20] coupled a sub-zone BEPS of a large office space with CFD to optimize the HVAC control of this space with non-uniform heat gains and occupancy. The BEPS provided surface temperatures and supply airflow rates to the CFD simulation. A sub-zone control of thermostats showed a more even result for thermal comfort (PMV) than the single-setpoint thermostat control, which has been evaluated using the spatially high-resolved CFD results. [ADMMV21] coupled the calibrated BEPS of a university classroom with CFD in order to evaluate the optimization potentials of the HVAC setup in the room regarding energy and cost efficiency, thermal comfort, and indoor air quality in pandemic times.

In recent research, [ZDS+23] coupled surface temperatures from BEPS (EnergyPlus) with Ansys Fluent to successfully optimize the control of HVAC system for a the entertainment area with three subzones on a cruise ship. [WLWZ23] used the coupling to investigate three ventilation scenarios regarding thermal comfort and cooling energy consumption in the waiting hall of railway station in China. [WLG+23] applied external coupling of BEPS and CFD to analyze ventilation angles and air velocities in a small office room.

For more details on the coupling approaches of CFD and BEPS, data exchange, and their applications, [THZS18, RHX+20] provide in-depth reviews.

3.3.3 Preliminary Conclusion on Research Gap in IFC-based CFD

Related research shows that BEPS-CFD coupling has matured significantly over three decades of development and validation, but IFC-based CFD model setup has rarely been investigated. This leads to the following research gaps:

Research Gap 1: The setup of CFD models requires time-consuming manual effort for pre-processing. In cases where IFC-based (or other CAD-based) data exchange is available, model simplification and healing are the most common issues.

> *Explanation:* CFD models have the requirement of airtight sets of surface geometries, such that rooms do not have gaps to the rooms exterior spaces. Most architectural models, however, do not require airtight modeling, but provide high complex geometries (e.g., curved surfaces, door handles), e.g., for rendering purposes. The concept of IFC SBs defines a simplified set of geometry, which allows, depending on the implementation, the definition of a airtight set of boundary surfaces even for constructions that include gaps (cf. [Fic22]).

Research Gap 2: In related research, no studies outside the *bim2sim* project are available that use space boundary geometry to efficiently create CFD model setups based on IFC4 data. The existing studies generate suitable CFD geometry from scratch, leading to additional computational cost.

Explanation: The focus of related research on IFC-based CFD setup mainly addresses the optimization of generated meshes, while neglecting the existence of SBs. These approaches rather derive new bounding surfaces directly from IfcProducts, which unnecessarily increases the computational overhead, and requires further simplification and healing of gaps.

Research Gap 3: HVAC devices and furniture elements are either not available in IFC4 models, or not appropriately modeled for CFD purposes (i.e., too rough or too detailed) such that they cannot be automatically transformed to CFD input.

Explanation: CFD engineers claim that the manual model simplification is time consuming [MJvT+22]. However, for an accurate analysis of indoor air flow in CFD, details on the positions and shapes of furniture and HVAC elements are required [RLS+23]. HVAC devices (radiators, air terminals) need either replacement shapes or manual pre-processing for successful meshing and to define the exact inlet and flow direction.

Research Gap 4: The mapping of boundary conditions from IFC applications has not yet been studied for CFD model setup. This includes the mapping of boundary conditions generated from IFC-based BEPS, but also the further enrichment of CFD models with other IFC-based data (e.g., property sets on ventilation rates).

Explanation: The coupling of CFD and BEPS itself has been investigated for various indoor and outdoor airflow scenarios and thermal comfort applications, ranging from external static sequential coupling to full dynamic internal coupling. However, no studies have been found on the specifications of input data mapping from IFC-based BEPS with support of further IFC-based information, e.g., on furniture and HVAC setups.

3.3.4 Research Hypotheses

The four observed research gaps can be condensed into the following two research hypotheses, which correspond to the RQs defined in Section 1.3:

RH CFD 1: The IFC-based setup of CFD models utilizes the IFC definition of SBs to set up geometry combined with generated boundary conditions from IFC-based BEPS. This automated setup enhances accessibility of CFD simulations during the design phase by reducing manual effort for model pre-processing.

RH CFD 2: The transformation of existing IFC furniture and HVAC equipment into suitable geometry for CFD models enables the detailed evaluation of the characteristics of indoor air flow and temperature distribution. The parametric generation of missing IFC elements supports this evaluation for different usage scenarios of indoor spaces.

RH CFD 1 addresses RQ 1, as it proposes a methodology to support the IFC-based setup of CFD

models to enable the application in IFC-based BIM workflows. Reducing the manual effort for pre-processing additionally relates to the challenge of a seamless CFD workflow, defined in RQ 2. RH CFD 2 addresses the challenge of transforming and generating geometric data on HVAC design and space usage, which also relates to RQ 2. These RHs are addressed by the methodology, implementation, and evaluation presented in the following sections.

3.4 Methodology for Setting up an IFC-based CFD Model

The methodology for automatically generating input for the CFD kernel OpenFOAM consists of three major parts: (1) the generation of geometric input, (2) the setup of meshing, and (3) the setup of boundary conditions. In the center of Figure 3.7 these three steps are conceptually aligned after executing the *bim2sim* framework for IFC-based BEPS using EnergyPlus (Figure 3.7, left). The *bim2sim* pre-processing results in the supply of component data information, such as surface and equipment types, combined with the *GlobalId* from IFC, and the BEPS results. This component data includes both semantic and geometric information. For simplicity, the process in Figure 3.7 does not distinguish further between the data flows of semantic and geometric data. See [RvTF24] for further for details on these data flows. The data generated in the IFC-OpenFOAM transformation process is mapped to the OpenFOAM input data structure (Figure 3.7, right), as introduced in Figure 3.6.

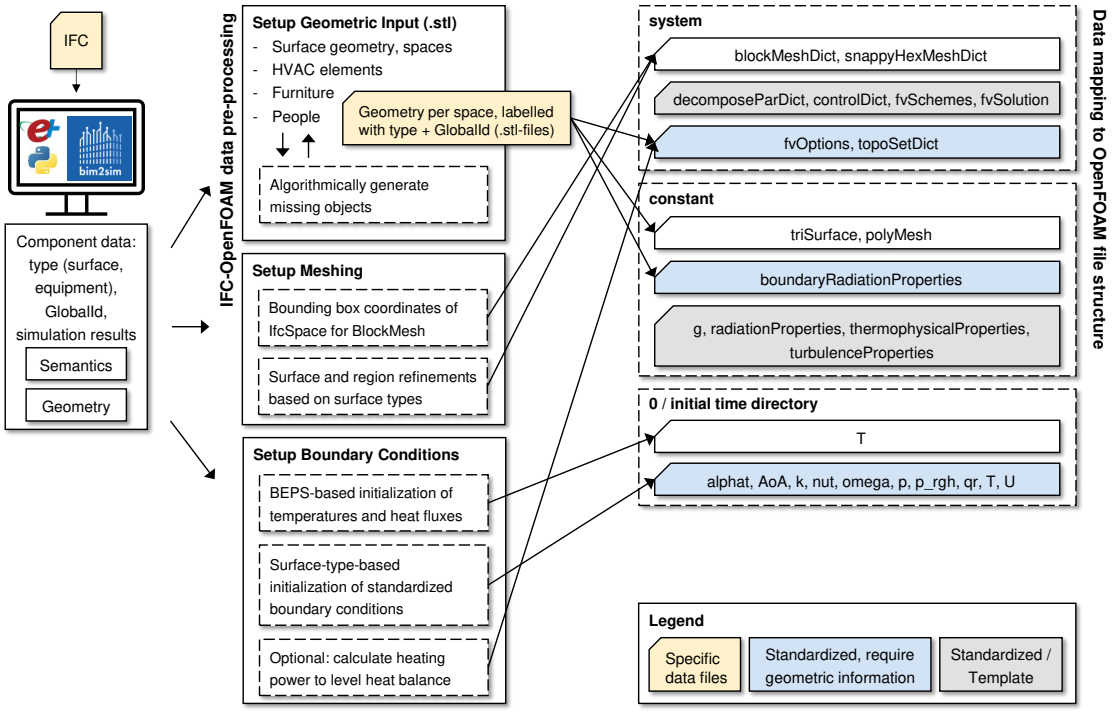

Figure 3.7: Pre-processing and data mapping for IFC-based generation of OpenFOAM input files.

This section starts with an introduction to the transformation of IFC to OpenFOAM, including the setup of the meshing process. This is followed by a brief description of the coupling of the BEPS results and the CFD input, as well as an introduction to the algorithms for the

parametric setup of CFD geometries. This section closes with an overview on the template-based enrichment of the OpenFOAM input data that can not be derived from IFC.

3.4.1 Transforming IFC to OpenFOAM Input Geometry

The transformation of IFC data to OpenFOAM input requires data pre-processing, as presented in the center of Figure 3.7. As introduced in Figure 3.5, OpenFOAM uses surface geometry mapped with boundary conditions to generate a computational mesh for simulation. To setup the input geometry for the simulation, the corresponding IFC data is identified, and, if needed, pre-processed or generated, before exporting the geometry to the desired input data format *.stl*, which stores the geometry in a triangulated form. The shapes of *IfcRelSpaceBoundary2ndLevel* form the basis of the surface geometries within the computational CFD domain.

Figure 3.8 displays the first triangulated surface within an example file. The stl file contains multiple solids for all SBs surrounding the computational domain. Each solid is uniquely named by the combination of the surface type (here: InnerWall), followed by the IFC *GlobalId*. For each analyzed space, an individual stl file is generated containing all relevant SBs. The space stl files are named using the related *GlobalId* of the *IfcSpace*. This ensures the unique mapping of IFC elements, BEPS results and CFD setup. The end of a solid is labeled with the same combination of surface type and *GlobalId*, before the next solid, i.e., next surface, starts.

```
solid InnerWall_3S62uZocO66ngdmMaRS2M9
facet normal 9.275 0.0 0.0
   outer loop
      vertex 3.8 9.7 2.5
      vertex 3.8 5.99 0.0
      vertex 3.8 9.7 0.0
   endloop
endfacet
facet normal 9.275 0.0 0.0
   outer loop
      vertex 3.8 9.7 2.5
      vertex 3.8 5.99 2.5
      vertex 3.8 5.99 0.0
   endloop
endfacet
endsolid InnerWall_3S62uZocO66ngdmMaRS2M9
solid Ceiling_14TeGe_aGDXLMTt8fX0vQP
facet normal 0.0 0.0 12.985001
   outer loop
      vertex 0.2999999 5.99 2.5
      vertex 3.8 9.7 2.5
```

Figure 3.8: Definition of triangulated surface geometry in .stl format.

If the set of SBs is defined correctly, these form an airtight set of space bounding surfaces. However, as described in Chapter 2, SBs are often erroneous, due to inaccurate modeling or even incorrect or incomplete implementation in the authoring tools. Before transforming space boundary shapes to CFD input, the airtightness needs to be evaluated and gaps should be filled with boundaries. In the *bim2sim* framework, these SBs are automatically generated for simplicity as adiabatic boundaries (i.e., type 2b), since 2b boundaries were missing systematically for IFC models exported from the ArchiCAD authoring tools (e.g., for open-source IFC4 models like the FZK Haus, cf. Figure 2.17). The surface geometry of HVAC equipment, furniture, and people, are exported to individual stl files to ensure optimal accessibility during the simulation setup and post-processing.

The HVAC setup can be generated depending on the available IFC data. In [RvTF24], a basic generative setup for heater positioning below windows and air terminal positioning on the ceiling is described. However, the presented algorithms are only applicable to small spaces, e.g., single offices, using a single set of air terminals and a single heater. IFC HVAC shapes are usually not directly suitable for use in CFD, as they are hard to mesh, not sufficiently modeled for fluid

flow (air terminals), or the air inflow points cannot be determined automatically. If available, the *IfcSpaceHeater* and *IfcAirTerminal* shapes can thus either be simplified or replaced with suitable CFD optimized objects at their positions in the space.

The proposed simplification process of *IfcSpaceHeaters* replaces the heater shape by the vertical surfaces of its bounding box. For air terminals, linear slot diffusers (german: Schlitzauslass) are replaced by its bounding box shape and an air inlet formed as a thin rectangular slot spanned over the longest axis at its lowest surface on the z-axis (=vertical axis). An example of an *IfcAirTerminal* is displayed in Figure 3.9.

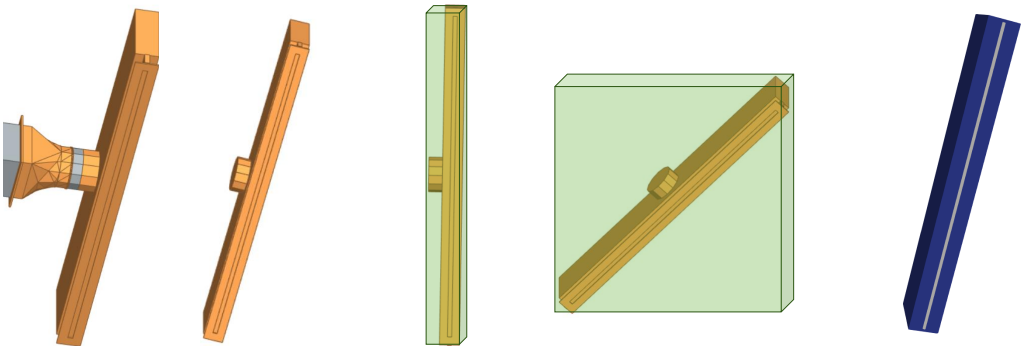

(a) IFC context (b) shape representation (c) bounding box (d) misaligned bounding box (e) replacement shape, bounding box (blue), inlet (grey)

Figure 3.9: Transformation of an *IfcAirTerminal* into a replacement shape for CFD.

The application of this approach is limited and requires more advanced features for automatic detection of slot orientation (facing down or to any side), and also the current bounding box approach is limited to HVAC that are aligned orthogonal to the global coordinate system axes (Figure 3.9c). If the air terminal is not oriented orthogonal to the axis, the generated bounding box is too large (Figure 3.9d), and the resulting replacement shape (Figure 3.9e) would be too large. The incorrect shape of the bounding box can be evaluated by comparing the air terminal shape volume and the bounding box volume. Tests for the illustrated type of slot diffuser have shown that if correctly oriented, the volume should not differ more than approximately 60%. This tolerance should be allowed due to the attached shape of the connection to the duct, which increases the size of the bounding box (cf. Figure 3.9c) but is only minorly reflected in the shape volume itself.

The proposed method can be improved by applying a local transformation of the shape to align with the global coordinate axes. The replacement of the inlet shape should be optimized by additional suitable diffuser shapes to adjust the inlet airflow direction. However, as this information is currently not provided in semantic IFC data, and geometric analysis and processing is computational expensive, for these unsupported cases the replacement of IFC shapes with suitable imported shapes from stl-files should be considered. These shapes could be provided in an open-source database, which could be set up in future research.

In case of replacement, suitable air terminal stl shapes should be pre-processed by defining

the diffuser shape combined with a dedicated air inlet position. The selected replacement diffuser should provide a matching size compared to the original IFC diffuser shape. The replacement diffuser is transformed to the position of the original IFC diffuser in space, where the lower center of the shape is a suitable position for aligning the shapes in the space setup (e.g., smoothely bounding with the ceiling), even if the heights of the diffuser box shapes may differ. The correct rotation of the replacement diffuser can be evaluated by comparing (A) the bounding box volumes of the replaced shape to (B) the bounding box shape of the original IFC shape, similar to the simplification process described before, cf. Figure 3.9.

3.4.2 IFC-based Parametric Geometric Enrichment

In some early-design cases, the space boundary geometry may be already modeled, but the positions of HVAC may not be fixed yet even if the total zone airflow may be defined, and the number and position of furniture and occupants are either not known or vary due to a flexible space usage.

For these cases, an IFC-based parametric geometric enrichment of these interior elements can be applied. A simplified setup for space heaters and air terminals has been introduced in [RvTF24], where a space heater was positioned underneath a window and the air terminals were placed attached to the ceiling. Since the exact HVAC setup usually should be defined at some point in the design phase, the following parametric setup of space interior focuses on the generative setup of furniture and occupants for different scenarios to consider flexible space usage.

The developed method for generative positioning of furniture and people starts with the definition of furniture positions. Based on the choice of available furniture setups (e.g., concert with chairs only, classroom with simple tables and chairs, office with an office desk and chair) and the required distances between furniture, a possible distribution of furniture elements in this room is computed. These positions are arranged on a rectangular grid, distinguishing between inter-object distances and the requested distance to the walls. The distance to the walls may result in a larger distance than requested, but the distances between furniture are restricted to the requested distance. The available furniture positions in the space are stored in a list. If the number of the available furniture positions is larger than the requested amount, only the requested furniture is placed in the space. If the requested number of furniture is larger than the available furniture positions, the maximum number is positioned.

The total number of people can either be manually assigned or defined according to the resulting occupant number from the schedules in the EnergyPlus simulation for the selected timestep. If the number of people is taken from EnergyPlus, it is rounded up to the next number, as partial persons cannot be properly represented in OpenFOAM. For the generative positioning of people in the room, choices of seated and standing people are provided. If the people are chosen to be seated, the maximum available number of people is limited by the available number of chairs. If the requested number of people is larger than the number of available chairs, the maximum

number of people is set to the number of available chairs. If the requested number of people is smaller than the available number of chairs, the people are distributed randomly over the available positions. For standing people, the requested number is also limited by the available number of positions in the room, determined by the choice of inter-person distances. Similarly to the distribution of furniture, standing people positions are also currently computed on a rectangular grid, which should be changed in further research, as people tend to not distribute evenly in rooms but interact with each other.

3.4.3 IFC-based Meshing Setup for OpenFOAM

Another major part of the transformation of IFC to OpenFOAM is the initialization of the meshing, including the definition of the *blockMeshDict* and the *snappyHexMeshDict*. For the definition of the blockMeshDict, the minimum and maximum coordinates of the *IfcSpace* shape's bounding box are calculated and used as required coordinates for defining the blockMesh. The meshing also requires the definition of the location point, which is defined at the center of the space. If people and furniture are included in the space, it is important for correct meshing to ensure that the location point is defined outside these shapes but inside the air volume of the space. For setting up the snappyHexMeshDict, surface-type-based surface refinements are applied. The refinements are chosen according to the expected surface granularity, i.e., air terminals are provided with a higher surface refinement required by detailed geometry to represent the air flow. Additionally, region refinements are defined for areas of expected higher turbulence and temperature differences, i.e., below air terminals and inside air heaters, where surface refinements are not sufficient to handle the complex flows inside whole regions. [HR24] proposed automated approaches for optimizing the refinements based on shape requirements and inter-object distances. This approach is prototypically implemented in the proposed *PlugInOpenFOAM* and allows to improve the general mesh quality while reducing computational time for simple spaces with a setup of heaters and air terminals. The implementation of their approach has been adapted to consider multiple heaters, air terminals, people, and furniture objects. However, this dissertation focuses more on the IFC-based transformation process and its application, so these mesh optimizations are not further discussed here. For the grid convergence tests, static mesh refinement levels are considered to ensure comparability between different block mesh sizes (cf. Table A.2 for exemplary mesh refinement levels and Table A.3 for refinement regions applied in the grid convergence tests in Section 3.6.1).

3.4.4 Coupling IFC-based BEPS and CFD for Boundary Conditions

To optimize the setup of boundary conditions within the IFC-based CFD process, the previously conducted IFC-based BEPS is coupled with the CFD setup to initialize the boundary conditions. This dissertation presents an IFC-based approach designed for simplified CFD analysis, e.g., in the detailed design stage, and is designed to be executed in steady cases and transient approaches with a small timeframe. Therefore, for the coupling itself, a simple one-way static

coupling (cf. Section 3.3.2) of BEPS and CFD is sufficient, i.e., the one-way export of temperature and heat flux boundary conditions from BEPS to CFD, which can also be considered as a sequential coupling for a single hourly BEPS timestep.

Within the coupled initialization of boundary conditions, parts are obtained from the IFC-based BEPS results, while other parameters are initialized by generalized assumptions. For quasi-steady-state simulations, which assume an approximately stationary behavior of a flow, the heat balance of the space-bounding surfaces and interior heat sources (i.e., people) is computed to define the resulting total heating or cooling load per space. The heat transfer calculated in BEPS through the boundaries is currently only considered using heat conduction, while solar radiation is not considered in the heat balance, and long-wave radiation is computed during runtime in OpenFOAM, but not transferred from BEPS as boundary condition. Other local heat sources than people (e.g., lighting, electrical equipment) are currently also not considered, such that the resulting heating or cooling power to level the heat balance may deviate from the required heating or cooling power calculated from the EnergyPlus simulation. The resulting deviation may be negligible in spaces with low internal heat gains (e.g., large single offices), but requires further evaluation particularly for spaces with high internal loads (e.g., kitchens, industry).

For all space-bounding surfaces, which are either converted from *IfcRelSpaceBoundary* entities or added to fill gaps to ensure airtightness of the space, the temperature initial conditions are set as *externalWallHeatFluxTemperature*. For SBs of type 2a, which are heat transferring surfaces, the surface inside face temperature is assigned as an initial uniform temperature, combined with a uniform surface heat flux, both generated from the EnergyPlus simulation. Adiabatic, i.e. 2b SBs, are defined to have no heat flux. Heater surfaces are initialized with the same temperature boundary condition type, but are assigned with the desired power to level the heat balance. The exact power per heater surface is defined by the ratio of assigned power on the heater surface and power in the porous medium (accounting for the heater's convective power) inside the heater. The latter is defined in the *fvOptions* dictionary as *scalarSemiImplicitSource*.

For cases which should not be heated or cooled by air conditioning, the air terminal inlet temperature is set to the fixed value of the resulting indoor air temperature obtained from the EnergyPlus simulation timestep, and set to zero gradient for outflows using OpenFOAMs *inletOutlet* boundary condition. If the air conditioning is used to cover cooling loads of the space, the required temperature difference for the inlet temperature is calculated using the volumetric flow rate per inlet.

To appropriately consider different heat flows throughout the body of simulated people, the heat flux and surface temperature is distinguished between body parts. For the simplest two-part subdivision of a person's body, the head is initialized with a higher surface temperature and higher relative power than the rest of the body. This two-part subdivision can be extrapolated to any number of body parts, considering the variety of clothing and activity options, which can be mapped to modeled or measured body part temperatures (e.g., MORPHEUS [Wöl17]) for profound analysis of thermal comfort. The temperature initial conditions of surfaces that

are passive to the system such as furniture and air terminal surfaces are declared to have a zero gradient temperature. The radiation of all surfaces is calculated during the CFD simulation.

The initial velocity boundary conditions are set to a fixed zero value for all surfaces except air inlets and outlets. Inlets are defined as *flowRateInletVelocity*, where the volumetric flow rate is defined as a constant value. This parameter can either be obtained from available IFC property sets, or generated based on space-type-based assumptions on occupancy and desired air quality. Air outlets are defined as OpenFOAM *inletOutlet*s to prevent reverse flow.

The other boundary conditions are initialized with standardized boundary conditions as these cannot be initialized from IFC or IFC-based pre-computations. *alphat* uses the compressible *alphatJayatillekeWallFunction*, *G* uses *MarshakRadiation*, *ILambda* uses *greyDiffusiveRadiation*, *k* uses the *kqRWallFunction*, and *nut* and *omega* use their respective wall functions as boundary condition for all surfaces. *p* and *qr* are set to be calculated during runtime. *p_rgh* is defined with a *fixedFluxPressure*. Apart from the temperature and velocities, the other initial values could also be defined collectively for all surfaces with the same initial conditions, which is not required since the computational cost for automatic IFC-based generation of boundary conditions for each surface individually is minimal and the individual surface representation provides more detail in case of debugging and enables quick individual modifications if required.

The *boundaryRadiationProperties* are also defined for each of the available OpenFOAM surfaces, but located in the *constant* directory instead of the initial time directory. They are defined with the type *lookup*, an emissivity and absorptivity of 0.9, and a transmissivity of 0. These properties are only required if radiation is applied, as well as the initial conditions for *qr*, *G*, and *ILambda*, which are additionally dependent on the choice of radiation model.

3.4.5 Template-based Enrichment of OpenFOAM Model

While standardized enriched boundary conditions have been introduced in previous sections and are individually defined for each surface, the general simulation control parameters and fundamental physical quantities can be defined purely template-based. This information is not provided in common IFC data files and thus requires enrichment. Physical properties, such as gravity *g*, *thermophysicalProperties*, and *turbulenceProperties* are stored in the *constant* directory and defined template-based independent of the actual building model. This is applicable as long as the general application of building indoor fluid simulations does not change, such that e.g., turbulence and radiation models, do not require modifications throughout different cases. Standardized settings are also provided in the constant directory for the choice of radiation models *P1* and *fvDOM*, which result in partially different input requirements for the initialization of the boundary conditions.

The solver settings *fvSolution*, the numerical schemes *fvSchemes*, and the general simulation control settings defined in the *controlDict* are set template-based depending on the choice between steady-state or transient simulation. The *decomposeParDict* requires information

on the available number of processors for parallel computation and the subdivision of the domain in x-y-z direction for distribution on the processors, which requires changes for cases with a modified number of processors, e.g., for using an increased number of processors for large computational domains (i.e., large and complex rooms), or for the evaluation of the computational performance.

3.5 *PluginOpenFOAM*: IFC-based CFD using OpenFOAM

The previously introduced methods for the transformation of IFC to OpenFOAM including the pre-computation of boundary conditions by IFC-based BEPS are implemented in the *bim2sim* tool as the *PluginOpenFOAM*. Figure 3.10 presents the general structure of the *PluginOpenFOAM* workflow. This new plugin incorporates the common and BEPS-specific pre-processing of the *bim2sim* tool (Figure 3.10, Steps (1) and (2)), as well as the methods implemented in the *PluginEnergyPlus* (Step (3)), which is used for the generation of the CFD boundary conditions. For a reference to the OpenFOAM file structure, see Figure 3.7.

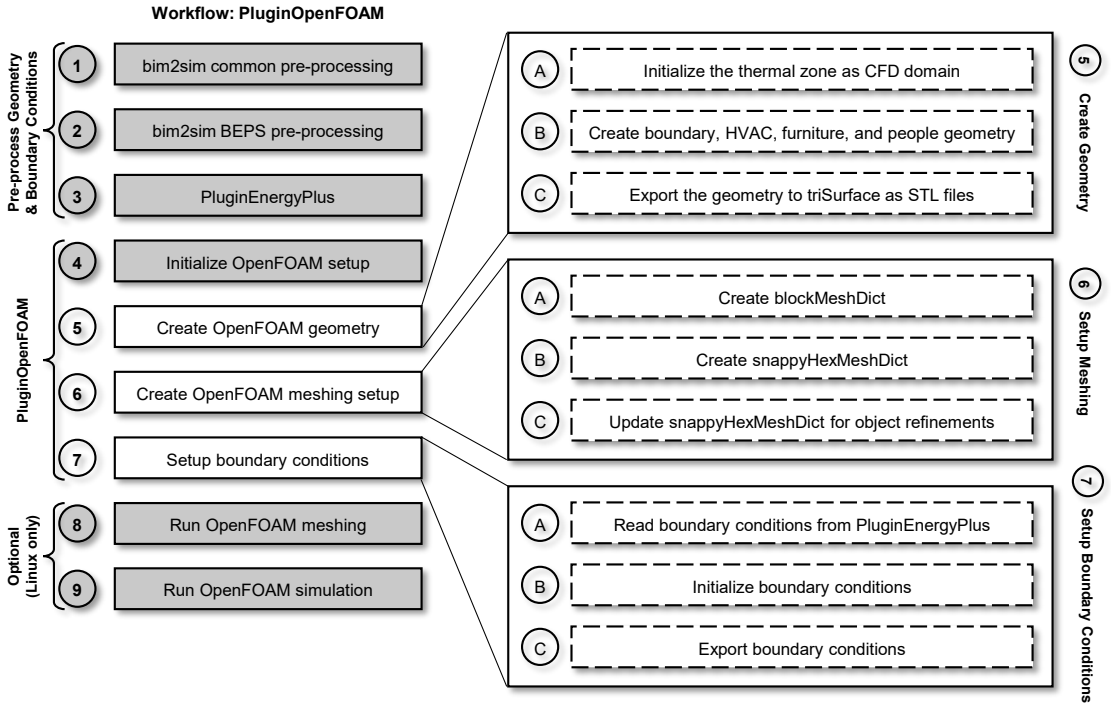

Figure 3.10: Workflow of the *PluginOpenFOAM* for IFC-based CFD in OpenFOAM.

The *PluginOpenFOAM* starts with the initialization of the OpenFOAM setup (Step (4)), including the setup of the directories *constant*, *system*, and *time series* directory (cf. Figure 3.6 and Figure 3.7). The initial setup also creates the standardized setup for physical properties in the *constant* directory, and simulation control settings and numerical schemes in the *system* directory.

After the OpenFOAM setup is initialized, in Step (5), the OpenFOAM geometry is generated.

First, the *IfcSpace*, which has been initialized in the previous *bim2sim* tasks as a thermal zone, is defined as the computational domain (A). This space is selected based on its IFC *GlobalId* in the *bim2sim sim_settings*. The space for detailed CFD analysis should be selected, for example, based on critical observed BEPS results (e.g., critical indoor temperatures), based on a complex HVAC setup that should be further evaluated, or based on requirements of high thermal comfort or a high level of indoor air quality. For this selected thermal zone, the related geometric shapes are transformed or generated (B). The bounding surfaces of the CFD domain are initialized, which have the same geometry as the BEPS model surfaces, as they both are created from the *IfcRelSpaceBoundary* entities in the *bim2sim* framework. The surface geometry in the *PluginOpenFOAM* uses unique keys for identification consisting of the surface type and the *GlobalId*. The *HVAC* setup is either simplified from provided IFC shapes, as presented in Section 3.4.1, or automatically generated as presented in [RvTF24]. For generation of furniture geometry, the shapes could also be adapted from *IfcFurniture* geometry, which is currently not implemented. For the positioning and shape generation of both furniture and people, the methods introduced in Section 3.4.2 are implemented. In the last step, the geometry is exported in the .stl-format (C) as introduced in Figure 3.8. The geometry is stored as individual stl-files in the *triSurface* directory within the *constant* directory, cf. Figure 3.7.

Step (6) in Figure 3.10 of the *PluginOpenFOAM* workflow addresses the meshing setup for the use in OpenFOAM based on the methodology introduced in Section 3.4.3. In this step, the dictionaries for the *blockMesh* and *snappyHexMesh* applications are generated. The *blockMeshDict* (A) is defined based on the *IfcSpace* shape and the grid size is defined in the *sim_settings*, which defaults to 0.1 m. The *snappyHexMeshDict* (B) is initialized with the boundary surface geometry, before the dictionary is updated with additional interior objects and their refinements (C). The snappyHexMesh algorithm requires the definition of the *locationInMesh* point. This point is placed at the center of the space but should be validated so that it does not lie in any other interior object to avoid false meshing. All interior objects are assigned with a range of applicable surface refinement levels. In order to both align with complex geometric shapes and varying blockMesh sizes, the range of the surface refinement levels are quite large, also to enable finer meshing for other close interior objects, and range from 2 to 3 for inner walls to 2 to 5 for detailed air terminal shapes (cf. Table A.2). Heaters and air terminals are provided with additional regional refinements to better resolve air turbulence due to forced or buoyant air flows (cf. Table A.3). Although the granularity of the resulting mesh is defined by the mesh refinements, other mesh control and quality settings should be evaluated related to the detail and size of the space geometry. If the number of *maxGlobalCells* in the snappyHexMeshDict is defined too small, the surface geometry cannot be refined as much as requested by the *refinementLevels*. Within this meshing setup, also the *topoSetDict* is created to add the geometry of the porous medium within the heater surfaces in the computational domain.

The setup of the meshing is followed by the BEPS-based setup of the boundary conditions of the CFD domain in Figure 3.10, Step (7). This step starts with reading the output boundary conditions from the *PluginEnergyPlus* simulation (A). From the large amount of data of typically

an annual hourly simulation, only one timestep is extracted (cf. Section 3.4.4) based on the selected date and time in the corresponding *sim_setting*. From this timestep, the relevant surface and zone temperatures and heat fluxes can be mapped onto the individual surfaces (B) to initialize their boundary conditions. For the heat flux, the conduction heat transfer is assigned as boundary condition. The surface temperatures are initialized with the surface inside face temperatures from the EnergyPlus output. The zone air is initialized with the calculated zone mean air temperature from EnergyPlus. The surfaces of the domain are assigned with either fixed temperatures or heat fluxes as boundary conditions in order to provide mathematically well-posed boundary conditions (cf. Section 3.1.3). The combination of fixed surface temperatures on inner walls, inner doors, and the floor is implemented as default, proving stable results for all radiation scenarios. These surfaces were chosen as they provide a sufficiently large surface area to maintain a constant temperature in the room, and the floor and inner vertical surfaces expected to have a rather stable and uniform temperature. Different combinations of surfaces with fixed temperatures were evaluated during the implementation, but the test results are not included in this work. In case solar radiation is integrated, the surface temperature of the floor should not be fixed to account for increased temperatures by incident solar radiation, which requires further tests on the overall convergence of the results (mainly temperature) in a quasi-steady state.

The required heating power for the heater is calculated based on the heat fluxes of the space bounding surfaces. This heating demand is reduced by the heating power emitted by the number of people positioned in this space such that the heat balance is leveled and can be simulated in a quasi-steady-state. If the evaluation of the heat balance reveals a resulting cooling load, the temperature difference, which is required to level this cooling load, is calculated to determine the required reduction of the inlet air temperature. If the heat balance should not be leveled for transient simulations, this can be set in a *sim_setting*. The type of radiators can be varied due to the ratio of heating power that is applied on the heating surface (defaults to 30% of total power) and the power on the porous medium inside the heater, imitating the purely convective part. Both, the ratio of power on the heater surface and the choice of radiation model can be defined in the *sim_settings*. The total airflow at the air inlets is calculated according to the requirements on air quality defined in [DIN16798-1], which is calculated based on the floor area and number of people and the desired air quality category (Category II is applied here per default for low-emission buildings). The total airflow is evenly distributed on the individual inlet air terminals. Once all surface boundaries are initialized with temperature and velocity boundary conditions, all boundary conditions can be exported (Figure 3.10, Step (7), (C)), which includes the surface-type-based export of standardized boundary conditions, cf. Section 3.4.4.

Since *PluginOpenFOAM* uses either the rounded-up results from the EnergyPlus simulation or user inputs from *sim_settings* to define the number of people in the space, the internal loads caused by people in the EnergyPlus simulation do not always match the *PluginOpenFOAM* conditions. Additionally, the volumetric flow rate is recomputed for the OpenFOAM simulation, based on the actual number of people used in CFD simulation, while the EnergyPlus simula-

tion only considers a fraction of a person to calculate the outdoor airflow. Additionally, the *PluginOpenFOAM* does not consider other template-based internal loads applied within the *PluginEnergyPlus* for electric equipment and lighting, which further limits the comparability of the plugins' implementations and results. The boundary surfaces in the OpenFOAM simulation are initialized with the surface heat conduction rate resulting from the EnergyPlus simulation. The impact of solar radiation is not considered in the OpenFOAM simulation, as the OpenFOAM solver (v2206) currently contains bugs in the implementation of solar load calculations using fvDOM radiation, resulting in the drastic reduction of surface temperatures (until freezing) at the location of incident solar radiation. As this dissertation focuses on the transformation of IFC-models into BEPS and CFD simulations, the correction and additional validation of the OpenFOAM solar radiation model is out of scope but should be addressed in further research. As the EnergyPlus simulation considers an exterior shading control of the windows for incident solar radiation higher than 150 W/m^2 according to [DIN4108-2], the impact of direct solar radiation for solar gains is already reduced in the *PluginEnergyPlus*.

The export of the boundary conditions (Figure 3.10, Step (7), (C)) concludes the export of the OpenFOAM input data files. Depending on the user's operating system, two additional optional steps can be applied on Linux distributions. These steps address the execution of the OpenFOAM meshing process with blockMesh and snappyHexMesh (Step (8)) and the execution of the OpenFOAM simulation (Step (9)) using buoyantSimpleFOAM (steady) or buoyantPimpleFOAM (transient). In any case, the meshing and simulation steps can be executed based on the exported OpenFOAM input files in the command line of other operating systems with a valid OpenFOAM installation (currently tested for OpenFOAM 2206) or on high performance clusters such as CLAIX-2023.[14]

3.6 Application and Testing of the *PluginOpenFOAM*

This section presents the testing of the proposed IFC-based CFD setup and demonstrates the application for an IFC model. For a detailed example on the fundamental setup of IFC-based generated floor heating, radiator, and air terminals, see [RvTF24]. The present tests, illustrated in Figure 3.11, analyze the impact of the grid size on the results (Test 1, Section 3.6.1), evaluate effect of the porous medium for three radiation settings on the heat distribution (Test 2, Section 3.6.2), and evaluate the air distribution of the transformed IFC-based slot diffuser (Test 3, Section 3.6.3). The HVAC setup in these examples is generated IFC-based and enriched with furniture settings and people.

To support the interpretation of the results, some visualizations use discrete colors representing isosurfaces with the same parameter values instead of continuous coloring, e.g., to highlight temperature stratification. Other visualizations use the Line Integral Convolution (LIC) method [CL93] for a non-directional visualization of the flow fields. The use cases in this section

[14] CLAIX High Performance Computing (HPC) System at RWTH Aachen University: https://www.hpc.itc.rwth-aachen.de/cms/hpc/Systeme-Services/~bcepsh/Systeme/lidx/1/, accessed on May 22, 2025.

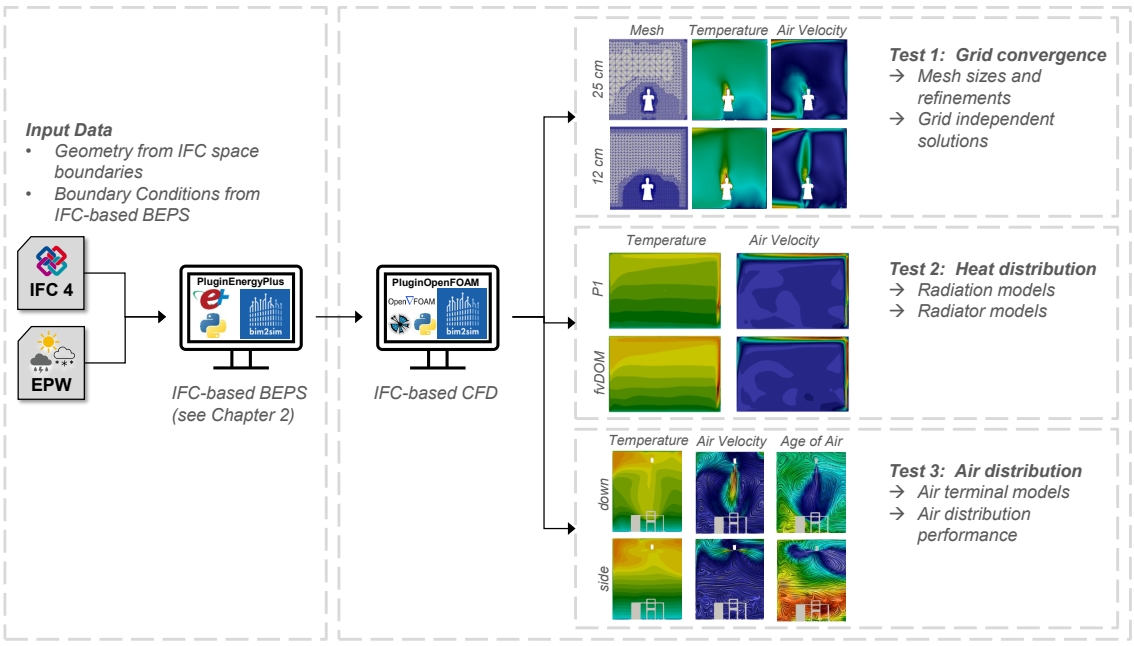

Figure 3.11: Overview on the test cases for IFC-based CFD using the *PluginOpenFOAM*.

evaluate the CFD results on a single room, conceptually visualized in Figure 1.4. All use cases in this section are simulated for the location of Aachen, using the Typical Meterological Year (TMYx) weather file provided by [LC22], based on historical weather data from 1931-2012. The simulations are applied for December 21, 11am, which represents the standard design day for the heating period as it is the solstice (i.e., shortest day of the year) [ASH17].

3.6.1 Test 1: Grid Convergence

For the evaluation of the grid independency of the simulation results, the simulation of a single office room was repeated for eight block mesh sizes between 5 and 25 cm. For a better comparison of the results, the refinement levels for surfaces and regions were kept the same over all block mesh sizes. This results in a better representation of surfaces in the cases with smaller block meshes. The boundary conditions are the same for all analyzed cases.

The office, visualized in Figure 3.12, is the test setup. It is equipped with two radiators located on the two external walls, an office desk setup with a seated person, a single air inlet and an outlet through overflow underneath the door. This grid testing includes a choice of features that were implemented IFC-based, such as the transformed space heaters, the modified slot diffusers, an overflow outlet underneath the door, and an occupied office desk setup. This space represents the *E01-*

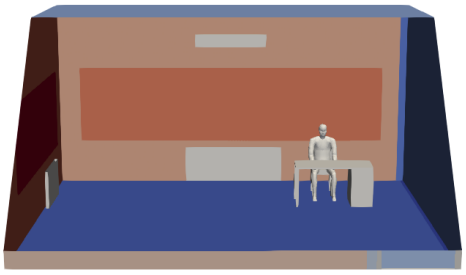

Figure 3.12: Single office with two external walls (left, back) with a radiator each, an air inlet (top), an overflow outlet underneath the door (front right), and an office desk; floor area: 37.5 m^2, height: 3.5 m^2.

13 Group office at the south-east corner on the top floor of the DigitalHub, cf. floor plan in Figure A.37. The full set for surface and region mesh refinement is listed in Appendix A.5.1, Table A.2 and Table A.3. The convergence is only tested for this relatively simple setup, as the tests are executed for block mesh sizes with a minimum of 5 cm, which results in a grid size of 1.56 mm for the fifth refinement level. This refinement level is defined as the maximum refinement level at the air terminals, listed in Table A.2. As a comparison, the fifth refinement level for a block mesh of 25 cm results in a grid size of 7.81 mm. Figure 3.13 shows the resulting meshes for the block mesh sizes of 0.07 m, 0.12 m, and 0.25 m. The area around the person (right) is highly refined due to the distance-based refinement of the objects, where the office setup was refined to level three within 0.03 m of the furniture surface, and refinement level two was applied for a distance of up to 0.60 m (cf. Table A.3). The latter large distance is an error in the automated setup, but it only affects the computational time and does not negatively affect the results. This error is fixed for further CFD setups to a default value of 0.06 m.

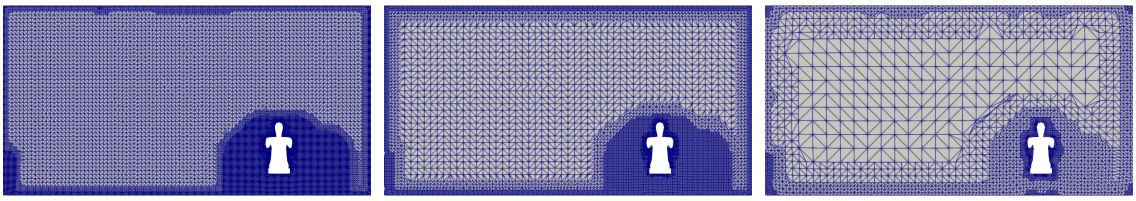

(a) Block mesh 0.07 m (b) Block mesh 0.12 m (c) Block mesh 0.25 m

Figure 3.13: Block meshes with a mesh size of 0.07 m, 0.12 m, 0.25 m.

This grid analysis presents a qualitative analysis of the simulation results to determine suitable grid sizes for the objectives of the CFD simulations in the IFC-based building design process. Figure 3.14 and Figure 3.15 display the air temperature and the air velocities, respectively, in a vertical slice through the computational domain, slicing through the head of the person sitting on the office desk (right). The slices of all cases show a heat plume above the head of the person, which appears to be larger for smaller block mesh sizes. The analysis has shown that the heat plume of block meshes larger 15 cm has not sufficiently been captured in the position of the slice, as the heat plume is rather released from the back of the head. All cases show areas of lower temperatures on the left and right lower corners of the slice. The left upper corner shows higher temperatures, as the heater is placed on the left side but is not cut by the analyzed slice.

The visualization of the air velocities in Figure 3.15 in the same position matches with the observed heat plumes caused by buoyancy forces. The observed air streams can be roughly clustered into two groups with similar characteristics, one consisting of the block mesh sizes 5, 8, 10, 12 cm and the other group consisting of 7, 15, 20, 25 cm. These differences in the results may result from the fact that these simulations only reached a quasi-steady state and that the domain still keeps fluctuating and thus switches between two states of air distribution. However, all cases show an increased air velocity at the floor and the ceiling, as well as a buoyancy force above the head, and some also capture the buoyancy of the heater.

Even if the air velocities caused by the persons body temperature cannot be evenly captured

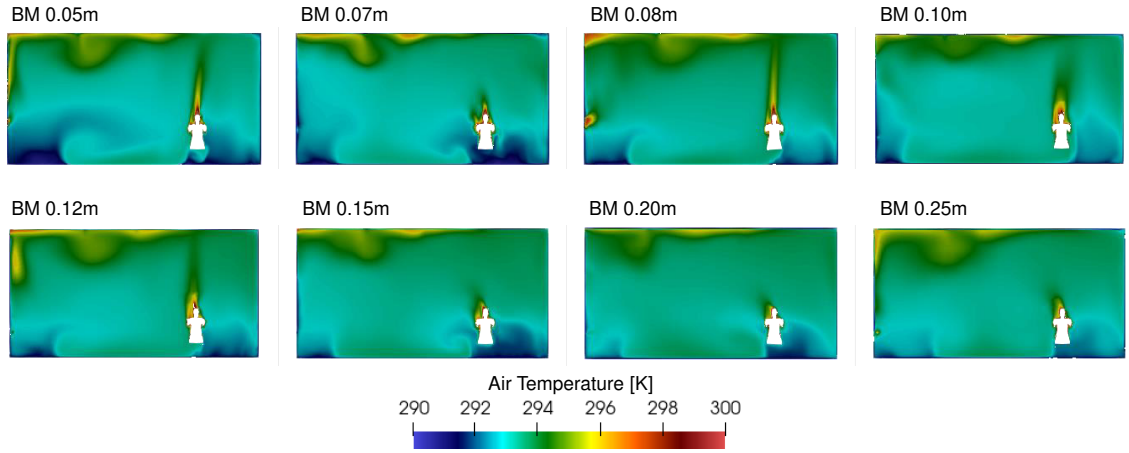

Figure 3.14: Air temperature for different block mesh sizes. Vertical slice through domain.

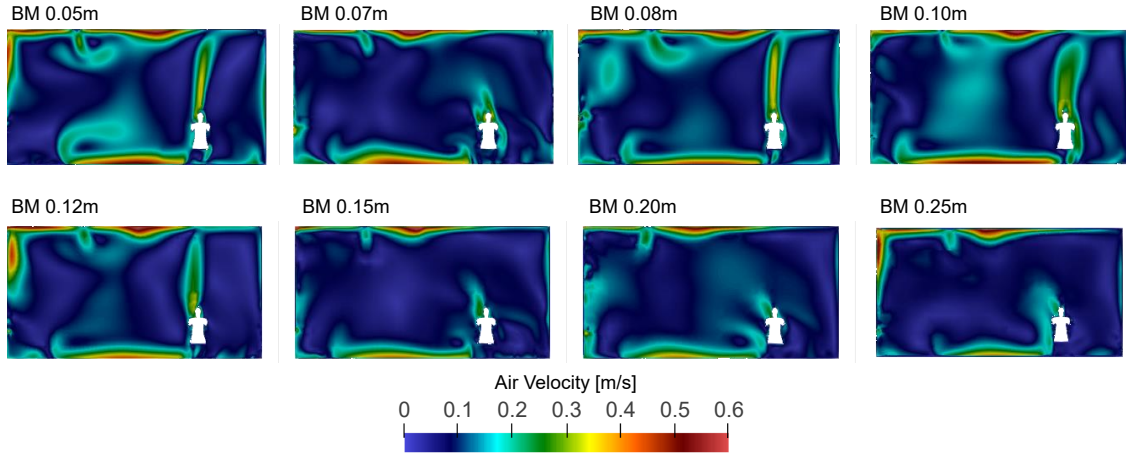

Figure 3.15: Air velocities for different block mesh sizes. Vertical slice through domain.

at all grid sizes, the air velocity of the inlet facing towards the floor results in similar results as presented in Figure 3.16. The airstream has similar velocity profiles for all cases with a block mesh size with a maximum of 12 cm. Larger grid sizes cannot resolve the high air velocities in the center of the stream due to the coarse grid cells.

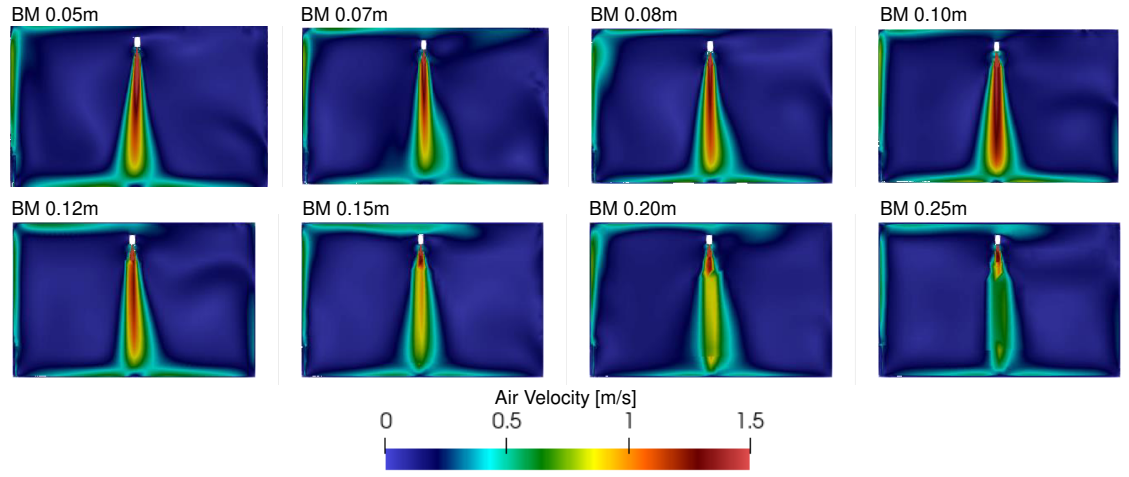

Figure 3.16: Air velocities for different block mesh sizes. Vertical slice through the air inlet.

The observed air temperatures and air velocities have shown similar qualitative profiles but did not exactly converge to an exact solution. This is caused by the quasi-steady simulations, and could be resolved by applying transient simulations. For the use in the design process of buildings, the general profile of air flows and temperatures are of interest, but minor reductions of accuracy can be neglected due to the uncertainties of the actual situation in the operational phase of the building. When considering the consistency of the results and the increased computational costs for a higher grid resolution, these grid tests have shown that block mesh sizes with a maximum of 12 cm are sufficient for the analyzed room to qualitatively capture the distribution of air temperature and air velocities throughout the computational domain to support design decisions in the design phase. These results may be limited to the analyzed room setup (i.e., geometric complexity, room size, HVAC setup) and require further investigation. Further research should also include additional qualitative evaluations of the grid independence, e.g., by evaluating the Grid Convergence Index (GCI) or other statistical analyses of the results.

3.6.2 Test 2: Heat Distribution

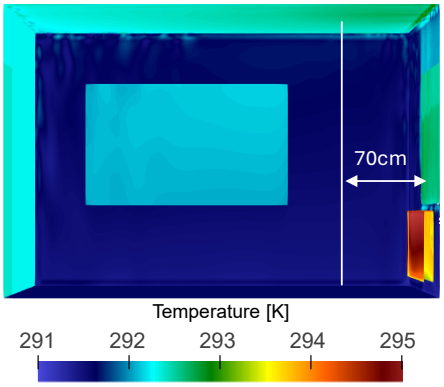

Figure 3.17: Surface temperatures for the P1 radiation model with 30% heat applied on the heater surface. Two external windows (right and back), and radiator (right). Vertical line indicates position of temperature evaluation (70 cm from wall).

In [RvTF24], the heating power of the heater was split up into a convective part that was assigned to a porous medium (70%) and a radiative part (30%), assigned on the heater surface and evaluated using the radiation model P1. For a better understanding of the impact of the power distribution combined with the choice of radiation model, additional tests study the impact of the proportion of heat on the heater surface and compare the results between the P1 and fvDOM radiation models and no radiation model. This test is applied for the *EG-02 Single office* (cf. Figure 2.17) in the FZK Haus, visualized with surface temperatures in Figure 3.17.

Figure 3.18 visualizes the distribution of the operative temperatures and Figure 3.19 the air velocity distribution in a vertical slice through the computational domain. All cases in this section were simulated using the same boundary conditions (December 21, 11am, TMYx (1931-2012) for Aachen [LC22], resulting in 265.16 W total heating power to balance heat loss through SBs) with the same settings for meshing (block mesh size: 10 cm, surface refinement level 2-3 for all surfaces, including radiator). All cases have a fixed surface temperature (i.e. Dirichlet boundary condition) for floor surfaces and inner vertical surfaces (walls, doors) obtained from the EnergyPlus simulation to ensure a converging solution of the domain. Ceiling, outer walls, and windows are defined by the calculated heat flux as Neumann boundary condition.

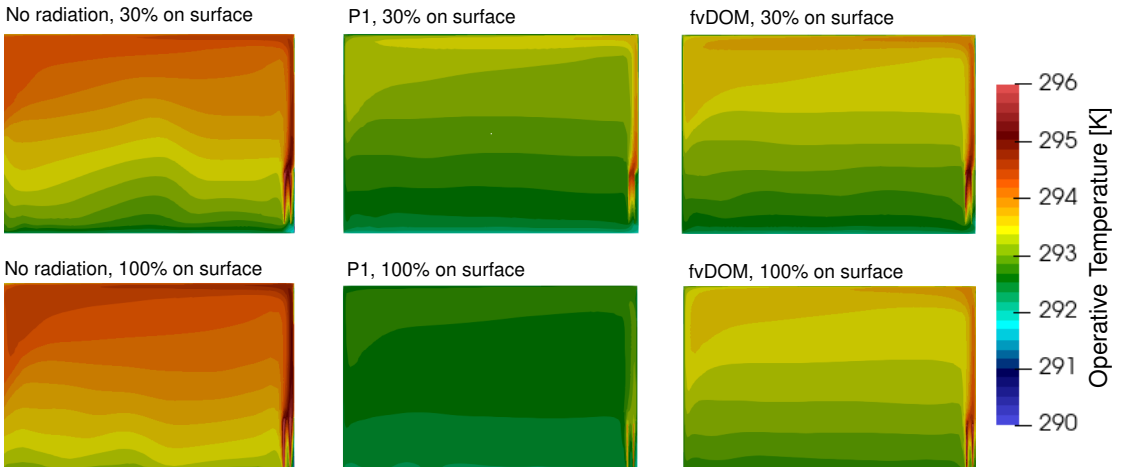

Figure 3.18: Comparison of the impact of heat on the porous medium (top) and heater surface (bottom) on the operative temperature distribution in space, compared for no radiation model (left), and the radiation models P1 (center) and fvDOM (right). Vertical slice through the domain, cutting the radiator.

The setup of Figure 3.18 and Figure 3.19 is similar, the left subfigures use no radiation model, the center subfigures show the results for the radiation model P1, and the right subfigures display the results for radiation model fvDOM. The upper subfigures have the setup used in [RvTF24] with 30% of the total heating power on the radiator surface and 70% of heating power on the porous medium inside the radiator. The lower subfigures have 100% of heating power applied on the heater surface, so the porous medium is neglected. The simulations were executed on 48 Cores of RWTH CLAIX-2023 (non-exclusive usage of the node). All results are visualized after executing 20 000 iterations. The evaluation of the residuals has shown that all cases have converged to a quasi-steady state by about 4000 to 5000 iterations.

The distribution of the operative temperature in Figure 3.18 shows a stronger temperature stratification within the domain for cases with a higher convective force, i.e., for cases using the porous medium approach. The stronger convective part is also visible in comparatively higher air velocities below the ceiling in the left subfigures of Figure 3.19. The operative temperature in the fvDOM case and the case without radiation model with total heating power on the heater surface still show the stratification effect, while the use of the P1 model for this case produces only a minor stratification. This is reasonable as the P1 uses a simplified radiation approach that smoothes the radiation throughout the space, while the fvDOM approach uses a detailed ray tracing approach, and the case without radiation does not release any heat through radiation and thus results in a pure convective heat transfer within the domain. The lower subfigures additionally show higher temperatures on the heater surface due to the higher power applied on the surface.

In the vertical slice representing the air velocities in Figure 3.19, the P1-case with full power on heater surface stands out (bottom center) with the lowest observed air velocities. In this case, the even temperature distribution in the space leads to small buoyancy forces resulting in smaller air velocities.

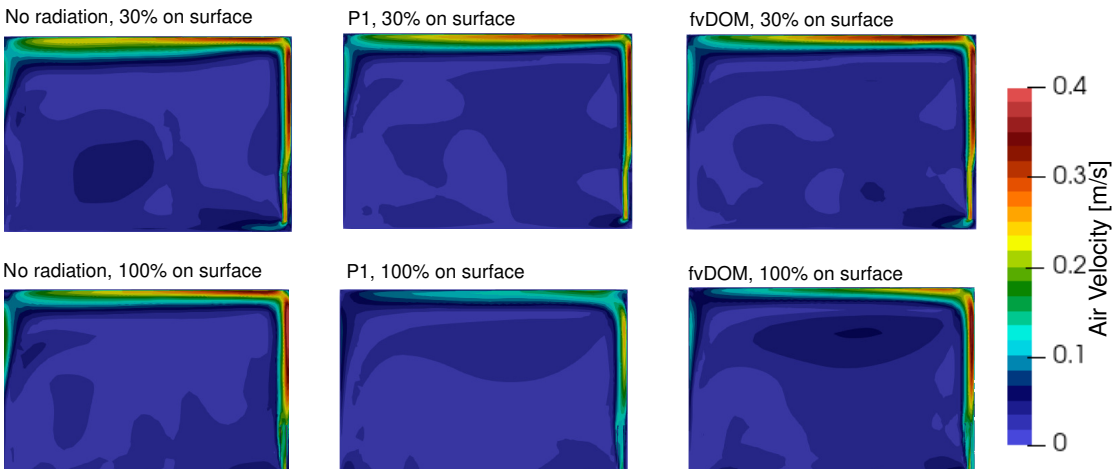

Figure 3.19: Comparison of the impact of heat on the porous medium (top) and heater surface (bottom) on the air velocity distribution in space, compared for no radiation model (left), and the radiation models P1 (center) and fvDOM (right). Vertical slice through the domain, cutting the radiator.

Figure 3.20 compares the vertical temperature lines for the central position in front of the radiator, located 70 cm from the wall with the radiator as illustrated in Figure 3.17. The operative temperature distribution in Figure 3.20a aligns with the distribution in the slices in Figure 3.18. For this location, the results of each case with 70% of power on porous medium results in lower operative temperatures than its related case with full power on the heater surface. The vertical operative temperature for the P1 model with 100% power on the surface is almost constant along the vertical line, which relates to the minimal temperature stratification observed in Figure 3.18, and also shows the lowest average operative temperature.

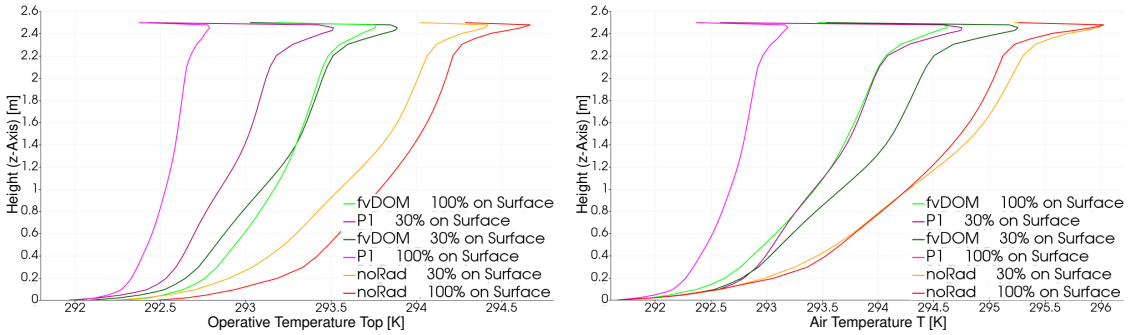

(a) Operative Temperature

(b) Air Temperature

Figure 3.20: Comparison of the vertical temperatures on a vertical line located 70 cm from the wall with the radiator.

The operative temperature lines of the fvDOM cases in Figure 3.20a are similar. The highest operative temperatures are observed for the cases without radiation model, which result from the missing capability of heat absorptance and emissions due to the lack of radiation model. The released heating power cannot be absorbed by materials and causes higher air temperatures. The air temperature distribution in Figure 3.20b shows a slightly different arrangement of temperature profiles among the radiation models and observed cases than for the operative

temperatures. While the P1 case with 100% heat on the surface has the lowest air temperature, the air temperature distribution of the P1 30% case shows a high similarity to the fvDOM 100% case, while the other fvDOM case shows higher temperatures. The air temperatures of the case without radiation model are similar show a slightly stronger vertical stratification than the operative temperature. Both operative and air temperature show an increased temperature below the ceiling, caused by the buoyancy effects of the radiator.

All cases were executed on RWTH HPC CLAIX23 in non-exclusive jobs with 48 cores, so the execution times should only be evaluated qualitatively. The simulation of the cases without radiation took between 1725 and 1830 s, the cases using P1 radiation between 1990 and 2500 s, and the fvDOM radiation cases took between 5570 and 7775 s, which is three to four times slower than P1. This ratio depends strongly on the geometric complexity of the computational domain.

The comparison of these four cases of radiator modeling and radiation models has shown that the correct choice of parameters critically affects the simulation results, especially when using the simplified radiation model P1. However, as a convective part of 70% power on the porous medium is supported by related research [RvTF24], and both radiation models P1 and fvDOM produce qualitatively similar results, the P1 model may be the choice for fast CFD analysis within the design stage due to smaller computational times. For complex room setups, including multiple furniture items and people, especially with the focus on local thermal comfort, the choice of radiation models should be evaluated again, unless the fvDOM radiation model is applied, which seems to provide the highest accuracy (but also the highest computational cost compared to the other evaluated radiation models).

3.6.3 Test 3: Air Distribution

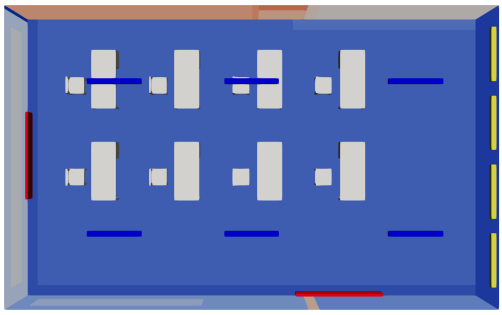

Figure 3.21: Room setup of the air distribution test case.

The IFC-based setup of CFD input files allows for an automated setup of models for comparing HVAC setups during the design phase. The implemented methods are evaluated on the *E00-11 Laboratory* (cf. floor plan in Figure A.37), at the ground floor of the DigitalHub, presented in Figure 3.21. The simulations are again executed for the TMYx weather file of Aachen [LC22], for December 21, 11am. The room is equipped with six slot diffusers as air inlets (blue) and four air outlets (yellow); the latter are located at the inner shorter wall (Figure 3.21, right) of the rectangular room. The room has two heaters (red), one located underneath the window at the shorter external wall (left), and the other heater is located at the other external wall (bottom). The HVAC components are modified from the original IFC shapes of these components. The setup has eight unoccupied office desks, which are automatically generated and positioned by the

PluginOpenFOAM.

The space has a floor area of 74.08 m^2, a height of 3.5 m and an air volume of 259.28 m^3. The lower surface of the air inlets and outlets are placed 3 m above the floor surface. In the unoccupied case, each of the air inlets has a flow rate of 88.90 m^3/h, resulting in a total volumetric flow of 533.78 m^3/h, such that the air is exchanged twice in the room per hour. This corresponds to the standard [DIN16798-1], Table B.6/B.7 for a building with high emissions and a resulting air quality of Category 1, which requires an air exchange of $2\,l/(s\,m^2)$. For this setup, the air distribution is compared for two outflow directions for all air terminals, (1) facing downwards and (2) facing sidewards.

Figure 3.22a displays the air temperature distribution within the space. The downward outflow leads to a uniform temperature distribution across the space height except for warmer air below the ceiling, which is observed above the suspended air terminals. The downward-facing airflow causes a locally warmer air stream below the inlets. The sidewards-facing inlets produce a higher vertical temperature stratification. Both phenomena can be explained with the air velocity distribution in Figure 3.22b, where the sidewards inlets produce air streams that do not reach the lower parts of the room. The better mixture of air can also be seen in the representation of the Age of Air (AoA) in Figure 3.22c. The AoA visualizes the time of the air inside the room in seconds, where the downward-facing air inlets produce a much better mixture of the air in the room. However, even for the downward facing air flow and well-mixed air in the room, the area underneath the outlets has a larger AoA, where the short distance between air inlet and outlet causes a short circuit of the air streams.

The simulation is repeated for the same furniture setup, where each desk is occupied, such that an additional 7 l/s/person are added for eight people (air quality of Category 2 [DIN16798-1]), resulting in a new total volumetric flow rate of 734.98 m^3/h, 122.47 m^3/h per air inlet and an air exchange rate of factor 2.83 h^{-1}. This case is evaluated for the sidewards outflow. Figure 3.23 displays the air velocity, air temperature and AoA of the occupied space with sidewards outflow direction. The air velocity profile is dominated by the buoyancy air stream above the people's head. The space has a lower vertical temperature stratification and a slightly better mixture of air, resulting in an overall lower AoA caused by the higher air exchange rate compared to the unoccupied cases. However, even with this higher air exchange rate, the front office desks still are likely to have a worse air quality compared to the office desks in the back of the space. In consequence, the function of the air inlets was verified; they are correctly meshed and release an airstream to the space (cf. Figure A.5), such that this phenomenon does not result from errors in the CFD setup. The air distribution system requires an optimization of the inlets, e.g., by adjusting the outflow direction, to provide an even air distribution throughout the space. For a better evaluation of the air quality, the indoor air quality could be evaluated by measures such as CO_2, which requires an estimation of the released CO_2 by the people.

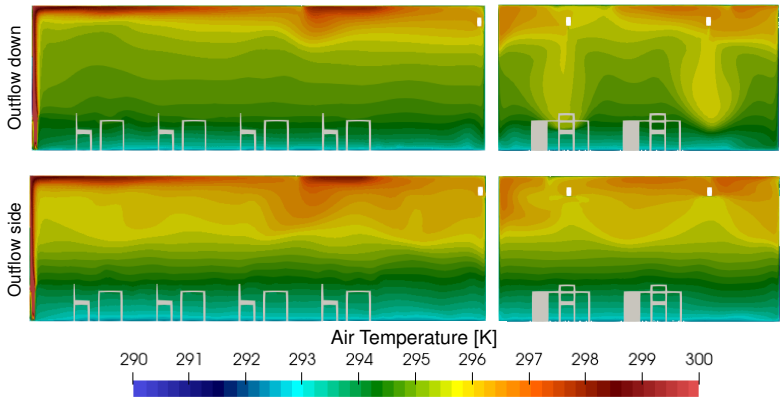

(a) Air Temperature

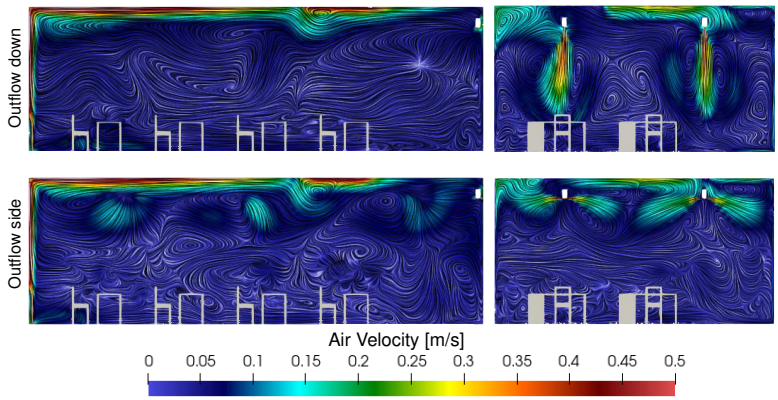

(b) Air Velocity using LIC representation

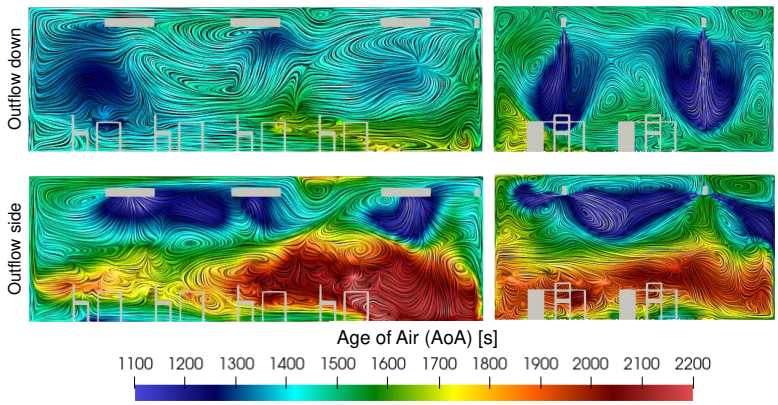

(c) Age of Air (AoA) using LIC representation

Figure 3.22: Comparison of temperature, velocity, and age of air distribution for downwards (top) and sidewards (bottom) outflow direction for slot diffusers. Vertical slices through the domain.

Evaluate Air Distribution using Air Streams

The actual air streams can be analyzed and visualized using stream tracers in ParaView, which is tested on the use case of the *E01-13 Group office* at the first floor of the DigitalHub, i.e., the same office as in the grid convergence test in Section 3.6.1, with only a single air inlet. In this

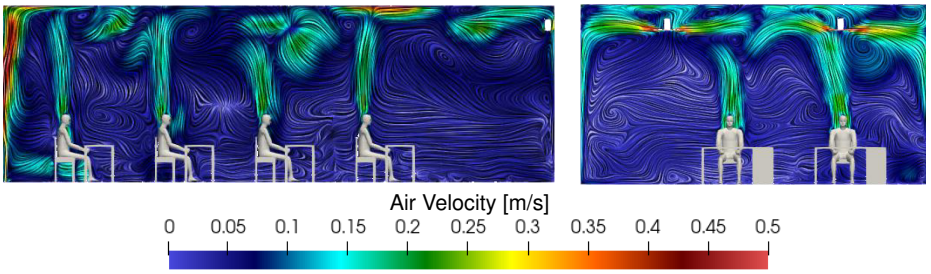

(a) Air velocity, LIC representation

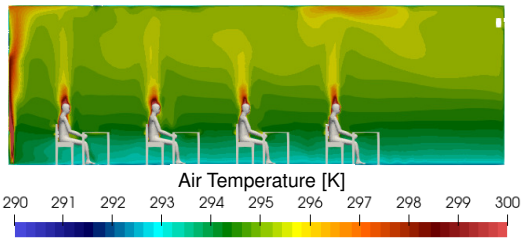

(b) Air temperature

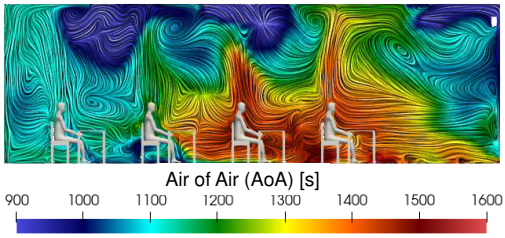

(c) Age of Air (AoA), LIC representation

Figure 3.23: Air velocity, temperature, and age of air distribution for sidewards outflow direction of slot diffusers in an occupied space. Vertical slices through the domain.

case, a cutout below the door is inserted for the return air. This case includes four occupied office desks. The office has a floor area of 37.48 m^2 and a room height of 3.5 m. The air inlet has a volumetric flow rate of 370.66 m^3/h, which results in an air exchange rate of 2.83 h^{-1}.

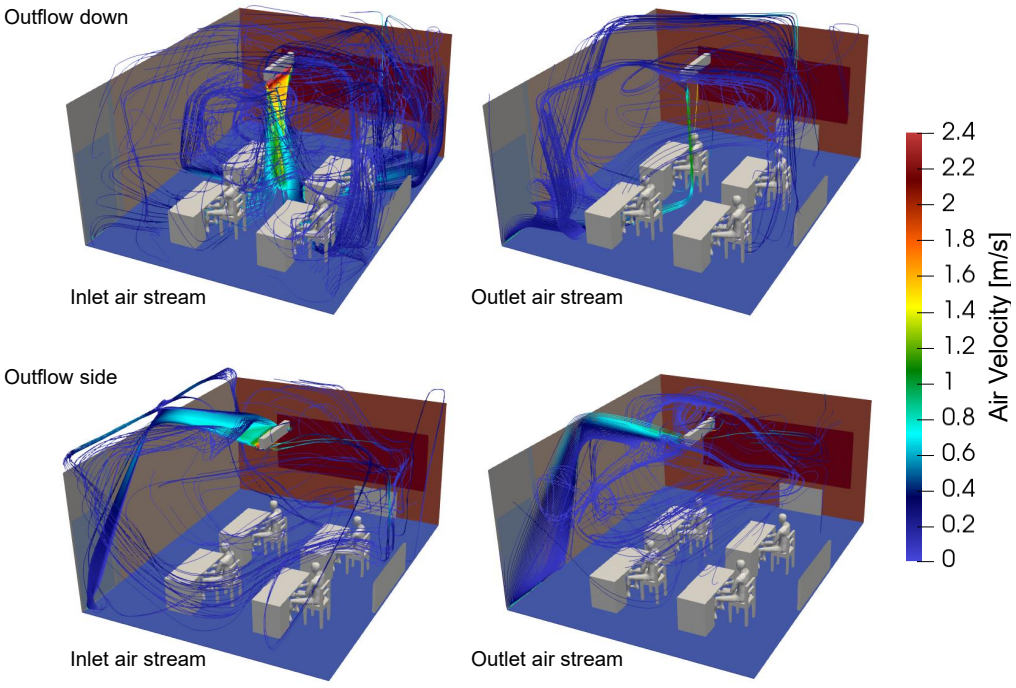

Figure 3.24: Inlet and outlet air streams, for outflow directions downwards (top) and sidewards (bottom).

The door with the cutout at the bottom edge is located in the left corner of the subfigures presenting the air streams in Figure 3.24. In this figure, the air streams are traced from the

inlet (left) and from the outlet (right) for both downwards facing outflow direction of the slot diffuser (top) and sidewards facing outflow (bottom). The downward-facing outflow results in better airflow distribution inside the room, as seen by the spread of both the inlet and outlet streamlines across the entire space. The sidewards facing outflow is only partially distributed in the room, but flows mostly directly to the air outlet below the door. This method of stream tracing is a suitable method for detecting airflow short circuits in spaces to ensure a high indoor air quality.

3.7 Evaluation and Summary of the Research Hypotheses

This section evaluates the outcome of this chapter under the scope of the RHs defined in Section 3.3.4 and the RQs defined in Section 1.3. The relation between the RHs and RQs is visualized in Figure A.1. RH CFD 1 states that the IFC-based setup of CFD using BEPS-based boundary conditions enhances the accessability of CFD within the design process of buildings. Therefore, a method for an automated IFC-based setup of CFD model was proposed using pre-computed boundary conditions from IFC-based BEPS. The full process of setting up surface geometry, HVAC systems, furniture, and people was prototypically implemented and tested for different spaces in an IFC4 building. Surface geometry can be generated by the use of SBs, which can be directly parametrized with boundary conditions from BEPS, as they have the IFC as common origin of data. The meshing process was automated using surface-type-based refinements. This verifies RH CFD 1, which addresses the RQ 1 with its automated setup of IFC-based CFD models, but also addresses the challenge of high manual effort for model setup related to RQ 2.

However, the presented approach requires further development and validation. The grid convergence test was only evaluated qualitatively, but no quantitative analysis, e.g., by evaluating the GCI, was performed. The evaluation of computational performance for different grid sizes also requires further research. This includes a scalability analysis of the parallelization of the OpenFOAM simulations in general and for different space sizes, interior designs, occupancy setups, and mesh refinement choices. The evaluation of the grid convergence revealed that block mesh sizes up to 0.12 m have shown plausible results for temperature and velocity distribution. Thus, a block mesh size of 0.12 m is used as standard for further CFD simulations in this work, as the geometric complexity of those use cases is similar (i.e., cuboid, small to medium-sized office rooms). In addition, a suitable number of maximum cells in meshing control is required, combined with suitable mesh refinement levels, to avoid failure in the CFD computation due to meshing errors on inlets and outlets. If outlets are not correctly meshed and thus missing in the resulting mesh, but inlets provide a supply of air, the balancing equations cannot be solved by OpenFOAM, and the simulation crashes.

The simulation setup was designed to reach a quasi-steady state, which revealed a switching behavior between two flow patterns. To fully capture the dynamic effects within the domain, transient simulations are required. Due to their high computational cost, transient simulations

should be preferably restricted in the design phase to cases with imbalanced heat fluxes, e.g., simulating overheating of indoor spaces over time.

The proposed methods do not include solar radiation, due to errors in the implementation of the solar calculation used for the radiation model fvDOM within OpenFOAM. The results may additionally differ between BEPS and CFD due to the missing internal heat sources in CFD, which have to be considered in further development and research. The current implementation is limited to floorheating (tested in [RvTF24]) and radiators, and cooling using air terminals (applied in Section 4.7 and Section 5.4). In future research, other HVAC devices should be tested, e.g., radiant cooling, heating using air terminals, or even a combination of radiators and heated air. Further research should include the release of CO_2 by occupants as an additional measure for indoor air quality, as AoA does not provide insight into the actual distribution of contaminants. The tests of the implementation were not compared to the BEPS results, which provided the boundary conditions for the CFD setup. Furthermore, no cooling use case was evaluated in this chapter but only heating cases were considered. Evaluations on both, CFD to BEPS comparison and cooling use cases, are provided in Section 4.7, where air temperature and thermal comfort measures are compared for BEPS and CFD, and also the cooling of the space is evaluated in CFD.

RH CFD 2 states that either existing IFC furniture and HVAC equipment or parametrically generated geometries can be used for the setup of IFC-based CFD models. The automated transformation of IFC HVAC elements into geometric shapes suitable for CFD applications was developed for slot diffusers, an overflow outlet, and space heaters. The modification of slot diffusers relies on simplified assumptions that require further testing and further advances in robustness, e.g., for alignment and outflow direction. As the sideward-facing air terminal partially produced a poor mixture of air, and the downward-facing air terminal produced high air velocities in the occupied zone, additional simplifications of the IFC-based air terminals and the approximation of their outflow characteristics and direction should be designed and evaluated for their performance. The results of these simplifications should be compared to suitable replacement models from proprietary air terminals in further research. For cases where only a single air inlet is available from IFC, but no air outlet is provided in the space, the assumption is made that the return air is considered as an overflow outlet located underneath the door. Further implementations require an analysis of doors that can actually be used for overflow. The neighboring spaces, which are connected through the space of interest using this door, require an analysis on the existence of respective air outlets such that the overflow can be realized. The space heater is modeled using a combination of the heater surface and a porous media to enhance the convective performance of the space heater. While this setup is evaluated for three radiation cases (i.e., None, P1, fvDOM), it requires further validation using reference cases from related research. Furniture was not available in the evaluated IFC files, which was compensated by an algorithm to generate furniture setups with and without occupancy. These setups were prototypically implemented as *PluginOpenFOAM* and tested within the *bim2sim* framework. The successful transformation of IFC objects and generation of missing objects

supports the RH 2 and addresses the challenge of missing data along with RQ 2.

However, this current implementation of the interior setup for furniture, occupants, and HVAC, should only be considered as a prototypical state with a limited applicability for IFC data from other authoring tools than tested or for different space setups. As no furniture is available from the evaluated IFC data, the automatic transformation of furniture elements was not tested but can be added using the proposed methods for geometric processing of IFC elements. The furniture shapes may not even require further simplifications unless they are used as heating or cooling devices (e.g., for personalized comfort systems), such that a simple triangulation of the IFC shape would be sufficient for further use within OpenFOAM.

The presented CFD setup includes algorithms for the algorithmic distribution of furniture and occupants in the indoor space based on user inputs. The current implementation includes concert, office, and classroom setups, where the furniture is positioned on a rectangular grid. In future developments, the furniture arrangements should be improved regarding their orientation in space and further account for different office settings such as single, double, group, or even open-plan workspaces. While the interior design in office spaces is expected to remain constant over longer time periods, the arrangement of multi-purpose spaces may vary from day to day. To prevent local discomfort resulting from the HVAC operation and to reduce the risk of low indoor air quality, these spaces should be evaluated during the design phase for multiple usage scenarios. These scenarios could not only assist in evaluating the indoor air quality and local thermal comfort in steady conditions but also in optimizing the operation of HVAC at peak loads using transient simulations.

The modeling and simulation of air inlets from IFC is based on simplifications, which have the risk for inaccurately modeling the air distribution in the space. A solution for this potential uncertainty is the setup of a database with suitable CFD geometries for air terminals, which could be used as replacement geometries of available IFC air terminal representations. In cases, where no air terminals are available from IFC, the air terminals can be automatically positioned in space, similar to the positioning of furniture. While this procedure implies a high risk of uncertainty for the actual air distribution, this approach can be used to evaluate different air distribution scenarios in the conceptual design phase, where only the total air exchange for the space has been defined, but not yet the actual distribution system. However, this approach requires further development to comply with design practices for air distribution systems. Regardless of the availability of air terminals from IFC, the implementation of the air distribution system for CFD assumes an optimal air supply for each air terminal. Imbalances between the air terminals, caused by imbalances in pressure losses in the distribution systems due to inefficient design or variable flow control, are not included in the setup. The CFD analysis of the air distribution system itself is expected to generate a large computational overhead and thus seems unreasonable for the scope of the presented indoor CFD analysis. However, the air distribution system's expected pressure conditions could be pre-calculated using standardized static approaches and further be added as boundary conditions to the individual air inlets to account for a potential uneven distribution of supply air across the air terminals within a space.

The computational performance of the simulation of air terminals could further be improved, as they require a high level of mesh refinement to mesh the air diffusers accurately with their curved surfaces and tiny gaps. The flow profiles of the air terminals can be evaluated regarding their potential for pre-computation, such that the final simulation includes these flow profiles mapped to a flat surface. This approach is expected to reduce the total number of cells required for mesh refinements of air terminals within a space and thus increase the computational performance in large spaces with a large amount of same-type air terminals.

Overall, the presented approaches proved both RHs defined for the IFC-based CFD setup. For a generalized application on IFC data, the current methods require additional tests on robustness, for additional building use cases, and especially for larger rooms.

4 IFC-based Thermal Comfort Analysis

Thermal comfort of humans is determined by the body's heat balance, which relates to personal parameters (activity and clothing), and environmental parameters (air and radiant temperatures, air velocity, and humidity) [ISO7730]. As the environmental parameters can be determined by BEPS and/or CFD, which can be setup using an IFC-based approach as demonstrated in Chapter 2 and Chapter 3, the prediction of thermal comfort mainly requires the personal parameters as additional input. Once the personal parameters are determined, thermal comfort can be predicted in IFC-based workflows on a zonal scale using BEPS, or on a high-resolved scale using CFD. In this chapter, a method for IFC-based thermal comfort simulations using BEPS and CFD is proposed, which requires the automated enrichment of personal parameters as extension to the archetypal zones provided by the TEASER templates used in the *PluginEnergyPlus* in Chapter 2.

Section 4.1 starts with a brief introduction into thermal comfort metrics, the required input data, and standards. In Section 4.2, the related research is analyzed to elaborate the research gap, which leads to the definition of the research hypotheses (cf. Section 4.2.2). Section 4.3 describes the requirements and extension of the archetypal TEASER data set for the use in thermal comfort in order to automate the enrichment process of personal comfort data. Section 4.4 proposes the methodology for both BEPS- and CFD-based comfort analysis that builds upon the template-based enrichment using archetypal TEASER data. Using these methods, Section 4.5 describes the implementation as *PluginComfort* and Section 4.6 the extension to the *PluginOpenFOAM*. The developed approaches are tested in Section 4.7, and evaluated for the RHs in Section 4.8.

4.1 Fundamentals of Thermal Comfort

This section provides a short introduction to the fundamentals of thermal comfort, including comfort metrics and their input requirements, as well as regulations and building certifications on thermal comfort.

4.1.1 Thermal Comfort Metrics

Thermal comfort metrics have been developed to determine general comfort conditions for static environment conditions, but also to consider adaptive behavior with respect to environmental conditions. These models are available to predict comfort either by modeling generalized or detailed physiological processes. These comfort metrics have different requirements for input parameters and their spatial resolution. Parts of this fundamentals section have been

adapted from [RLS+23].

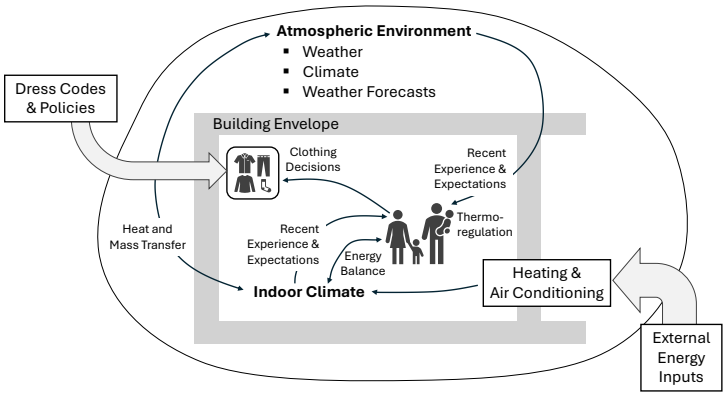

Figure 4.1: Interaction between outdoor weather conditions, the indoor environment, and a person's clothing. Adapted from [MDD03].

The general interaction between outdoor weather conditions, the indoor environment, and a person's clothing is described by [MDD03] as presented in Figure 4.1. Thermal comfort of a human body results from its interaction with its surrounding environment. While the indoor climate affects the energy balance of the body with its thermoregulatory mechanisms, the indoor climate is impacted by the outdoor environment by heat and mass transfer through the building envelope, but it may also be controlled by heating and air conditioning. The condition of the outdoor environment further affects the person's expectations of indoor conditions. The clothing choices are not only affected by the person's own choices but also by dress codes and policies.

[Fan70] developed an approach to determine thermal comfort based on the balance of human heat, based on four environmental parameters (air and radiative temperature, air velocity, humidity) and two personal parameters (clothing and activity). He defines measures of thermal comfort, which express the imbalance of human heat balance on a seven-point scale in terms of the Predicted Mean Vote (PMV) from -3 (very cold) to 3 (very warm), and the Predicted Percentage of Dissatisfied (PPD) from 5 to 100%, respectively. This approach is adapted within major international standards [ISO7730, ASH55]. Studies have shown that the prediction of comfort using PMV and PPD is limited in real buildings, where even simplified measures could provide better results [CSP+19]. As the PMV is only applicable for mechanically ventilated buildings, adapted PMV measures have been proposed, whose prediction accuracy varies in different climate zones [LHW+25]. A higher prediction accuracy of thermal comfort using adaptive measures supports the reduction of energy consumption in buildings [LCK+24]. Despite the criticism about the static calculation, which neglects changing outdoor environmental conditions and adaptive user behavior, Fanger's comfort metrics are still commonly applied [ZLL21].

[AHA+19] compared the input requirements of the comfort metrics [Fan70], [ASH55], [ISO7730], which is presented as an updated version in Table 4.1. These metrics share Fanger's input requirements on environmental and personal parameters, while the standardized approaches in [ISO7730] and [ASH55] require additional input parameters on surface, air, and radiative temperatures to predict local comfort in terms of the Percentage Dissatisfied (PD) due to temperature differences and radiant asymmetry, as well as the Draught Risk (DR). Fanger's input parameters and the outdoor air temperature are the most commonly used inputs in thermal

comfort studies [MHMA22].

Table 4.1: Data requirements for IFC-based thermal comfort analysis, adapted from [AHA+19, RLS+23].

Parameter	Unit	Fanger	ASHRAE 55	ISO 7730
Air temperature	°C	x	x	x
Air velocity	m/s	x	x	x
Clothing insulation	clo	x	x	x
Relative humidity / Partial water vapor pressure	% / Pa	x	x	x
Mean radiant temperature	°C	x	x	x
Metabolic rate	met	x	x	x
Running mean outdoor air temperature	°C		x	
Operative temperature	°C		x	
Radiant Asymmetry	°C		x	x
Floor temperature	°C		x	x
Mean monthly outdoor temperature	°C		x	
Vertical Air Temperature difference	°C		x	x

[ASH55] includes adaptive thermal comfort metrics for naturally conditioned spaces by defining an 80% acceptability range of thermal comfort based on the arithmetic or weighted mean daily outdoor air temperatures of the previous seven to 30 days. A similar adaptive approach that considers the outdoor mean temperature is provided in [DIN16798-1], which defines up to four comfort categories, where categories I to III match with the definitions of Category A, B, and C described in [ISO7730], and Category IV is defined as an additional category representing the worst indoor conditions. [DIN16798-1], (German) National Appendix (NA) defines the comfort categories for mechanically conditioned buildings as follows:

Category I: PPD < 6%, -0.2 < PMV < 0.2
Category II: PPD < 10%, -0.5 < PMV < 0.5
Category III: PPD < 15%, -0.7 < PMV < 0.7
Category IV: PPD < 25%, -1.0 < PMV < 1.0

According to Category II, which is recommended by [DIN16798-1], NA for design unless specified otherwise, the difference in the radiant temperature $\Delta\theta_{rad}$ must not exceed 5 K for warm ceilings, 14 K for cool ceilings, 10 K for cool walls, and 23 K for warm walls. The surface temperature of the floor must be between 19 and 29 °C. The vertical air temperature difference between head (height=1.1 m) and feet (height=0.1 m) should not exceed 3 K to accomplish Category II of the NA. Category II further requires a DR below 15%, and maximum air velocities of 0.13 m/s and 0.20 m/s in winter and summer, respectively.

These static and adaptive comfort measures are mainly applicable to predict thermal comfort on a zonal level for a group of people, while only providing limited capability to estimate comfort for individuals. Although [DIN16798-1] and [ASH55] provide simplified local discomfort measures to evaluate temperature differences, e.g., between head and feet, the comfort analysis for individual body parts is not supported and cannot capture detailed asymmetric effects on body parts, e.g., through radiation. The review by [AMSW22] revealed an improved prediction accuracy of thermal comfort for applications that include physiological parameters, such as

skin temperature, additionally to environmental parameters.

Several thermo-physiological models have been developed to consider individual physiological processes as individual computational nodes for the body core, muscles, fat, and skin, while segmenting the body into a single or multiple parts. These approaches are analyzed in a comprehensive review of [KLZ16]. Fanger's comfort model can be categorized as a one-node single segment model [Fan70], while [GSN71] presented a two-node single-segment model, which provides a computational node for the core and the skin of a human body. The first multi-node multi-segment model has been introduced by [Sto71] as a 25-node system, which considers six body segments (head, trunk, arms, hands, legs, feet) of four layers each (core, muscles, fat, skin), connected to a central blood system. Examples of further developments on multi-node multi-segment approaches are [FLS99, TKN$^+$02, Zha03b, Str11, Wöl17, dPR24].

[AMSW22] claims the lack of diversity in the evaluation of personal comfort models based on their systematic literature review. This is addressed by [RM22], who evaluated differences in thermo-physiological responses regarding age, Body Mass Index (BMI), and gender using the multi-node model by [Str11]. The results revealed significant higher core temperatures and resulting lower temperatures at the extremities for females. For candidates with a high BMI (>25 kg/m^2), lower skin temperatures were observed due to higher insulation from fat mass, and higher temperatures at hands and feet. Younger candidates perceived lower temperatures as colder than older candidates, who were more comfortable. Thus, the thermo-physiological responses vary with multiple factors of the human conditions. As a result, the presented standardized models for static (PMV, PPD) and adaptive approaches should be considered as standardized approaches for a standardized group of people. The detailed prediction of (local) thermal comfort requires a deeper analysis for the effects on a more diverse population.

4.1.2 Regulations and Certifications for Thermal Comfort

As introduced in the previous section, [ASH55, ISO7730] provide metrics adapted from [Fan70] to predict thermal comfort based on static PMV and PPD calculations. Adaptive approaches are standardized in [ASH55, DIN16798-1]. According to the NA to [DIN16798-1], further referred to as NA, the thermal comfort Category II should be considered in building design and refurbishment, which is reached as long as not more than 1% of the occupied time exceeds the acceptable limits. However, the proposed limits for adaptive temperature in the NA differ from the general limits presented in [DIN16798-1]. Annex H in [ISO17772-2] of the international standard [ISO17772-1] for indoor environmental input parameters for design and energy performance assessment of buildings states similar comfort categories as the [DIN16798-1] for the long-term assessment of indoor comfort, but additionally suggests a PPD-weighting of the observed PMV.

Additional requirements on thermal comfort are defined in [DIN4108-2], which defines a limit of maximum excess degree-hours of 1200 Kh/a for residential and 500 Kh/a for non-residential buildings. The operative temperature limit for excess temperatures is distinguished for the three summer climate regions A, B, and C, and defined as 25, 26, and 27 °C, respectively. This standard

further defines standardized boundary conditions for BEPS regarding occupancy, internal loads, infiltration, heating set-points, and window shading, to enhance the comparability of the results.

The German guideline [ASR35] provides minimum requirements for the air temperature in workplaces, depending on the activity degree during work (e.g., between 20 and 26 °C for light seated activity), which can be compensated by a local conditioning of work places, or organizational and personal interventions such as clothing adaptations.

Besides incorporation in regulations and standards, thermal comfort is also considered in national and international building certifications, where its impact on the overall result differs between the certifications. In the certification of DGNB for non-residential buildings [DGNB23], thermal comfort represents between 3.8% (health care buildings) and 5.6% (supermarkets) of the total rating of the building, and refers to [DIN16798-1, ISO7730, DIN4108-2, ASR35] to estimate thermal comfort. Bonus points can be reached by proving thermal comfort resilient to climate change using future TRY weather data. The LEED certification for new constructions [LEEDv5] refers to the latest [ASH55] for comfort assessment but considers only one out of 110 total points for environmental thermal comfort.

4.2 Related Research on IFC-based Thermal Comfort Analysis

After the introduction to the fundamentals of thermal comfort metrics, this section addresses related research on the application of these metrics within IFC-based approaches for thermal comfort analysis. Parts of this review of related research have been adapted from [RLS+23].

Stationary and adaptive thermal comfort approaches require both environmental and personal parameters. The four environmental parameters required by [Fan70] are standard output parameters of BEPS and/or CFD, for which the automated IFC-based setup has already been proven in related research (cf. Table 2.4) and by the development of the *PluginEnergyPlus* and *PluginOpenFOAM* presented in Chapter 2 and Chapter 3, respectively. The outdoor temperature, which is required for adaptive approaches, is determined by the weather file used as input for the IFC-based BEPS and is directly related to the four indoor environmental parameters, i.e., air and radiant temperatures, air velocity, and humidity. The two personal parameters, activity degree and clothing level, still need to be defined as additional inputs, as they cannot be obtained from simulation outputs.

Related research on IFC-based Thermal Comfort analysis is sparse. [AKO17] defined a subset of input requirements for thermal comfort simulation based on the IFC4 standard aiming to define an MVD for CFD simulations. In [AKPO17], they included this subset of requirements in an MVD for IFC-based thermal comfort analysis using BEPS, referring to the available entities within the IFC4 standard. [AHA+19] defined input requirements for thermal comfort analysis for the application in an early design stage. As personal parameters are not provided in the IFC standard, they proposed an extension of comfort-related IFC property sets, but these

were not included in the latest IFC schema.[1] Within the *bim2sim* tool, missing parameters for the usage of thermal zones are automatically enriched using archetypal templates [MJvT+22]. However, these parameters do not provide clothing parameters, and even though activity levels are provided, their standardized values do not reflect realistic activities within these spaces and are thus not applicable to predict reliable thermal comfort [RSFvT23].

No other studies have been found that address IFC-based thermal comfort. From related research, input requirements for the IFC-based application of thermal comfort have been defined, but these have neither been incorporated in the latest IFC standard nor have they been implemented in automated IFC-based BEPS or CFD approaches to predict thermal comfort. As this research gap is evident, additional related research is considered to gain insights that can be transferred to the application in an IFC-based model setup. This additional research focuses on simulation approaches and their input parameters to predict thermal comfort and supports the elaboration of limitations of further developments using automated IFC-based setups for thermal comfort.

[DK21] analyze the influence of external wind pressure coefficients (WPC) on the thermal comfort in indoor spaces, remarking that the spatial variations of indoor wind speeds cannot be represented by the simplified calculation of indoor air velocities for just a single computational node per space in BEPS. They suggest a spatially high-resolved analysis of thermal comfort in later design stages. Since BEPS is insufficient to provide these spatially high-resolved comfort results, CFD analysis provides suitable spatially high-resolved results.

The research of [DCOZZ07] discovered that the choice of clothing correlates to the outdoor air temperature at 6 am, which was selected as reference time for clothing choices before leaving the house in the morning. For air-conditioned buildings, the clothing varies during the day, regardless of the outdoor temperature, of about 0.2 clo, which relates to the clo value of a jacket. For natural ventilated buildings, the clothing value varies about 0.27 clo for outdoor air temperatures (6 am) around 0 °C, while the variation during the day decreases for increasing outdoor temperatures in the morning. When comparing the clothing changes related to the indoor temperatures, males have shown significant clothing changes, while women kept their clothing almost constant. The authors denoted that major parts of the data set originate from Pakistan, which underlines the impact of cultural clothing restrictions on clothing assumptions, as these women may not have been able to adapt their clothing.

[SL13] discovered that even in cold climates in Michigan and Canada, the average winter clothing values are smaller (i.e., 0.7 clo and 0.8 clo, respectively) than those from international standards (1.0 clo). They also concluded that the choice of clothing at 6 am correlates with the outdoor air temperature and the indoor operative temperature, while the air velocity and metabolic rate have a smaller impact on the choice of clothing. [YLYT16] evaluates the impact of manikin simplification. [RBMV22b, RBMV22a] introduce a data set of standing male and female manikins representing the US population's distribution of BMI, which also includes

[1] buildingSMART, IFC4x3 schema: https://standards.buildingsmart.org/IFC/RELEASE/IFC4_3/, accessed on June 11, 2025.

overweight manikins.

[JCM+21] proposed a method to simulate the range of thermal comfort for the whole population in terms of the nine-step thermal sensation, ranging from -4 (very cold) to +4 (very hot) according to [Zha03b]. The application of the standard manikin failed to detect uncomfortable warm situations for 16%, and uncomfortable cold situations for 31% of the population [JCM+21]. This approach relies on the methods presented in [JCG20], where they proposed approaches for thermal comfort evaluation from preliminary to detailed design stage. Here, they proposed a web-tool for early design studies and a CFD integration of thermal comfort into ANSYS CFX 2018, which applied a 65-node physiological model developed by [TKN+02]. This approach was evaluated in a case study analyzing the thermal comfort of passengers on their typical path through an airport. Their analysis resulted in adjusted temperature setpoints which increase the energy efficiency while ensuring thermal comfort.

Considering the overall applicability of thermal comfort metrics in built environments, [MLL+23] claim a lack of scalability of current thermal comfort models developed in laboratory environments to real-world scenarios, e.g., for office environments. They also claim the lack of individual occupant thermal comfort assessed in studies on offices. Further research on office field studies may provide assistance for reliable design decisions supporting occupant thermal comfort in non-residential environments.

4.2.1 Preliminary Conclusion on Research Gap in IFC-based Thermal Comfort Analysis

A broad range of thermal comfort metrics has been developed over the last five decades, applying both static and adaptive comfort measures. The models range from average global thermal comfort metrics to physiological models simulating the layers of skin and core of the body while segmenting the body surface into multiple parts. It has been discovered that the use of standard male manikins fails to estimate the comfort state for the whole population, which has been addressed by the proposal of a detailed data set for the US population, including overweight people.

All of these approaches can be applied to improve the accuracy of thermal comfort predictions. However, it has also been shown that the IFC standard does not yet provide standardized parameter sets for thermal comfort, and archetypal templates do not include standardized data sets for automated enrichment of thermal comfort parameters. Thus, thermal comfort cannot even be automatically estimated with standardized measures in the design process of buildings, but is often neglected. From this, the following research gaps can be concluded:

Research Gap 1: No IFC-based thermal comfort simulation approach has been found in related research, neither for BEPS nor for CFD.

> *Explanation:* The input requirements for thermal comfort analysis have been analyzed and defined as a proposal for an extension of the IFC schema, which is not yet included in the schema. However, even using an extended IFC schema, a

methodology for the automated IFC-based setup of thermal comfort simulations is yet to be defined.

Research Gap 2: Personal comfort parameters (activity, clothing) are not provided by the latest IFC4 schema. These parameters are also not sufficiently provided in archetypal templates to enrich use conditions in thermal zones.

Explanation: As thermal comfort parameters are not included in standardized property sets in the IFC4 schema, these parameters can only be provided by custom property sets. The use of customized parameter sets does not support the automated setup of IFC-based simulation models due to the lack of standardization. While the general setup of IFC-based BEPS has successfully been supported by template-based enrichment of missing data, this option is currently not applicable to thermal comfort analysis, as personal comfort parameters are not provided in these templates. However, template-based enrichment could enhance an automated parametrization of these parameters, as it aligns with currently used enrichment processes within the IFC-based setup of BEPS.

These identified research gaps only address the setup of simplified thermal comfort models, as this dissertation focuses on the automation of comfort analysis within IFC-based simulations during the design phase. Other remaining research issues, such as extending the applicability of comfort predictions to a diverse population, are out of the scope of this work, as this dissertation does not focus on developing new comfort metrics. Advances in thermal comfort metrics can be incorporated to the IFC-based methods in future research.

4.2.2 Research Hypotheses

The following two RHs on IFC-based Thermal Comfort (TC) are concluded from the identified research gaps in response to the RQs defined in Section 1.3, visualized in Figure A.1:

RH TC 1: The IFC-based BEPS simulations enhance a simplified thermal comfort analysis for a building on a zone level; detailed results are obtained by a high spatial resolution simulation using CFD.

RH TC 2: The template-based enrichment for archetypal zone usage replaces missing data in the design process to facilitate the impact evaluation of design on thermal comfort through IFC-based simulations from early design stage.

RH TC 1 is derived from the lack of available IFC-based thermal comfort simulations, which has been elaborated in the first research gap. The RH TC 1 addresses RQ 1, as it proposes the usage of IFC-based BEPS and CFD simulations for comfort predictions for use cases with different requirements regarding the spatial resolution. This RH further addresses RQ 3 by proposing a combination of simplified BEPS and detailed CFD for different spatio-temporal resolutions of comfort predictions, which allows avoiding the computational overhead of computationally expensive CFD simulations. RH TC 2 directly refers to RQ 2, as it addresses the challenge of miss-

ing parameters for thermal comfort analysis by template-based data enrichment. These RHs are addressed by the extension of archetypal templates, the methodology and implementation of IFC-based thermal comfort, and the evaluation presented in the following sections.

4.3 Methodology for Input Parameter Enrichment for IFC-based Thermal Comfort Analysis

This section addresses the availability and enrichment of required input parameters for thermal comfort analysis. In the first subsection, the requirements and applicable data sources within the IFC-based process are derived. In the second subsection, the extension of the archetypal templates within *bim2sim* is presented. The third and final subsection briefly presents an approach to determine the applicable simulation approaches based on data availability.

4.3.1 Input Parameters for Thermal Comfort Analysis

Parts of this section have been adapted from [RLS+23]. As the review of related research revealed, the required parameters for thermal comfort analysis are only partially available from the IFC schema and IFC-based BEPS and CFD simulations. Therefore, the input data requirements presented in Table 4.1 are further analyzed regarding data availability within IFC-based simulation processes. An analysis of the input data requirements is presented in Table 4.2 for the thermal comfort metrics defined in [ISO7730].

Table 4.2: Parameters for thermal comfort metrics according to [ISO7730], limits are stated if applicable. 1 clo = 0.155 m^2 K/W, 1 met = 58.2 W/m^2, E = Environmental parameters, P = Personal parameters, PD = Percentage Dissatisfied, adapted from [RLS+23].

			Data source				Applicability according to ISO 7730				
	Parameter	Unit	derived (runtime)	IFC	Template (average)	default	PMV, PPD	DR	PD Vertical Temperature	PD Floor temperature	PD radiation asymmetry
E	Air temperature	°C	x				10…30	20…26			
E	Air velocity	m/s	x				0…1	0…0.5			
E	Mean radiant temperature	°C	x				10…40				
E	Partial water vapour pressure	Pa	x				0…2700				
E	Radiant Asymmetry	°C	x								-15…+23/35
E	Floor temperature	°C	x							x	
E	Local Turbulence intensity	%	x			x		10…60 (default = 40)			
E	Vertical Air Temperature difference (head and feet)	°C	x						<8		
P	Clothing insulation	clo		x	x		0…2				
P	Metabolic rate	met		x	x		0.8…4				

Table 4.2, adapted from [RLS+23], lists options for the data source of the required input parameters (center), as well as the applicable data ranges for the measures. As most of the parameters are environmental (E) parameters, these can be calculated from IFC-based simulations during runtime, as long as applicable boundary conditions (outdoor conditions, constructions, internal loads, setpoint temperatures, ...) for the domain are stated. Personal (P) parameters (i.e.., met and clo) can either be defined from applicable standards (e.g., clothing: 0.5/1.0 clo

(summer/winter), activity: 1.2 met [DIN16798-1]), from custom property sets in IFC [AHA+19], or enriched by templates for archetypal zone usage [MJvT+22]. The local turbulence intensity can also be defined by its default value of 40% if it cannot be derived at runtime. If other environmental parameters are unknown when calculating comfort measures, suitable values within the applicable limits could be manually selected by the designer to obtain an initial estimate. The error in this estimate can be further evaluated using a sensitivity analysis. However, this approach is not recommended due to the inherent uncertainty in the resulting prediction.

To provide guidance on the selection of input data sources based on their availability, a hierarchical approach is proposed in [RLS+23], which is briefly described here. This approach evaluates the availability of input requirements by subsequential checks, starting with an evaluation of the availability in the provided IFC using IDS, followed by an evaluation of [VDI6070] room book data, if this is provided. If none of these data sources provide the requested data, template-based archetypal enrichment can be applied if the space usage is known, or a default value can be specified otherwise.

While the previous input parameters are required for the application of both BEPS and CFD, the high spatial resolution of CFD simulations requires additional input regarding the interior space to provide accurate results. As BEPS simulations use a single computational node per air volume, it is considered as a uniform well-mixed environment, neglecting the exact location of HVAC systems. Internal loads are considered to be evenly distributed, and furniture can only be considered as thermal mass, which does not disturb the airflow. For the setup of CFD simulations, the location and geometry of these objects are crucial to obtain reliable results. Thus, the position and geometry of heaters, air terminals, furniture, and occupants are additional input requirements for the setup of CFD models. The setup of these additional parameters has been described in the previous Chapter 3 for the implementation of the *PluginOpenFOAM* in Section 3.5.

4.3.2 Enrichment of Thermal Comfort Parameters for Archetypal Zone Usage

While environmental parameters for thermal comfort analysis can be derived using BEPS and CFD and their presented IFC-based setups (cf. Chapter 2 and Chapter 3), personal parameters have to be provided from additional resources as presented in Table 4.2, as these are not included in the latest IFC standard. Standardized parameters from applicable standards (e.g., [DIN16798-1]) could be applied, but these do not consider differences in personal parameters due to the zone usage or requirements. Furthermore, research has found that the observed winter clothing was less than these standardized clothing level [SL13].

Archetypal zone templates have been used for the automatic enrichment of use conditions in IFC-based simulations [MJvT+22]. As the use conditions between these zonal archetypes vary according to the zone usage, the activity degree and the clothing level, representing the personal parameters, also vary according to the space usage. To enhance an automated enrichment of personal parameters using archetypal zonal templates, these templates have to be extended

accordingly. The following subsections describe the expansion and refinement of the TEASER templates (cf. Section 2.2.3) based on established standards for use in thermal comfort applications. This extension has been initially presented in [RSFvT23]. The following subsections present adapted excerpts of this publication.

Enrichment of Activity Degree Parameters for Archetypal Zone Usage

This subsection presents an adapted excerpt of [RSFvT23]. The existing TEASER templates already include archetypal data for different usage of thermal zones, including occupant activity degree data and occupant heat flow in W/person. These parameters are derived from values provided by the Swiss standard [SIA2024], which provides data to calculate the energy demand of buildings in early building design stages. However, these available activity degrees are standardized (mostly either 1.2 met or 2.0 met) and do not reflect the expected variations in activity due to the individual conditions within the archetypal zones. Therefore, these parameters are unsuitable for evaluating zone-usage-based thermal comfort, as an initial comparison of the existing TEASER activity data with standards for thermal comfort analysis [ISO7730, ASH17] has shown [RSFvT23].

There are several national and international standards for defining the activity degree of occupants. [DIN8996] provides data to accurately determine the metabolic rate in working environments. This standard also provides calculation methods to determine the metabolic rates for various activities, taking into account human conditions such as gender, age, and body weight. However, aiming to extend a template-based approach that provides approximate data to enrich archetypal zone setups, more generalized metabolic data is required at this stage. For this purpose, [DIN8996] categorizes metabolic rates in its Annex A, ranging from (0) Resting (100 – 125 W/person) to (4) Very high metabolic rate (> 465 W/person). As these categories are broad, each covering a range of metabolic rates of about 100 W/person, the extension of the archetypal zone templates is founded on other international standards and guidelines (i.e., [ISO7730, ASH17]) for more specific metabolic data related to particular activities.

[ISO7730] provides metabolic rates and heat flows for different activities in its Table A.5 and Table B.1. [ASH17] give a detailed introduction to thermal comfort analysis in its Chapter 9, providing typical metabolic rates for an average adult person (person's body surface area A = 1.8 m^2) in its Table 4. These tables from the standards are explicitly stated as a reference within the derived parameter sets in Table 4.3 and in Appendix, Table A.5.

Table 4.3 displays an excerpt of the activity values for the archetypal room types in a residential setting from the existing TEASER template (cf. Appendix, Table A.5 for full set of parameters for all zone types), along with the corresponding derived activity values obtained from [ISO7730] and [ASH17]. To make the data derivation process transparent, the activity types are listed as mapping to each room type from both sources (columns (4) and (5)) and their related individual metabolic rates. The metabolic rates from [ISO7730] and [ASH17] show only minor deviations (mostly 0 – 0.2 met), although the matched activities vary due to differences in specifications.

The newly derived (and combined) activity degree is calculated as the mean of columns (6) and (7), rounded up to the nearest decimal place. This value is rounded up because a higher activity degree results in higher cooling loads and an increased risk of occupant overheating during summer. On the basis of this combined activity degree, the heat flow (W/person) is displayed in column (10), calculated with 1 met = 58.1 W/m^2 and the average adult surface area of $A = 1.8\,\mathrm{m}^2$ [ASH17].

Table 4.3: Deriving activity parameters for archetypal enrichment of thermal zones based on ASHRAE Fundamentals and ISO 7730, including a comparison to existing TEASER template values. Columns: (1) Room type according to TEASER templates, (2) Activity degree from TEASER templates (met), (3) Heat flow from TEASER templates (W/person), (4) Chosen activity type according to ASHRAE Fundamentals, Chapter 9 Table 4, (5) Chosen activity type according to ISO 7730, Table A.5 and B.1, (6) ASHRAE activity degree (met), (7) ISO 7730 activity degree (met), (8) Resulting combined activity degree (met), (9) Absolute deviation from TEASER activity degree (met), (10) Resulting heat flow (W/person), (11) Absolute deviation from TEASER heat flow (W/person). Initially presented in [RSFvT23].

(1) Room type	(2)	(3)	(4) ASHRAE Fundamentals	(5) ISO 7730	(6)	(7)	(8) Activity Degree (met)	(9)	(10) Heat flow (W/person)	(11)
Single office	1.2	70	Office, Typing	A.5, Single office	1.1	1.2	1.2	0.0	125	55
Bed room	1.2	70	Resting, Sleeping	B.1, Reclining	0.7	0.8	0.8	0.4	84	14
Kitchen in non-residential buildings	1.2	70	Cooking	B.1, Standing, medium activity	1.8	2	1.9	0.7	199	129
WC and sanitary rooms in non-residential buildings	1.2	70	Resting, Seated, quiet	B.1, Seated, relaxed	1	1	1	0.2	105	35
Traffic area	1.2	70	Office Walking	B.1, Walking, 2 km/h	1.7	1.9	1.8	0.6	188	118
Living	1.2	70	Resting, Seated, quiet	B.1, Sedentary activity	1	1.2	1.1	0.1	115	45

Columns (9) and (11) show the absolute difference to the original activity parameters from the TEASER Templates given in columns (2) and (3), respectively. While some of the metabolic rates correspond to the previous TEASER values, the new values for the heat flow per person greatly exceed the previous values (mostly between 79 and 169%, referring to the full parameter set in Appendix, Table A.5).

Updating the activity data in the TEASER Templates is necessary for thermal comfort analysis, as they show high deviations from the metabolic rates reported in existing thermal comfort standards. Since the activity values provided in [ASH17] and [ISO7730] show only small deviations, the derived combined values give a reasonable estimate for these corrected parameter values.

Enrichment of Clothing Insulation Parameters for Archetypal Zone Usage

This subsection presents an adapted excerpt of [RSFvT23]. Contrary to the derivation of activity parameters, the TEASER templates do not provide pre-existing values for clothing insulation parameters. Thus, these values have to be derived from scratch. These values could be derived from the detailed clothing combinations in the international standard [DIN9920], which focuses on detailed descriptions of clothing settings. However, similar to the [DIN8996] standard for activity degrees, the [DIN9920] describes the clothing insulation with such high detail that it is not easily applicable for deriving standardized clothing insulation settings for extending the pre-existing templates. It is likely that these more detailed clothing parameters would only increase

the accuracy of the simulation results if a massive study on average clothing in buildings were performed, which is out of the scope of this dissertation.

Similar to the previous section, [ISO7730], Table C.1 and the [ASH17], Chapter 9, Table 7 provide data for predefined clothing sets. Opposite to activity degrees, clothing parameters may vary with the seasons. [ISO7730] states operative temperatures for summer and winter, referring to a general clothing value of 0.5 clo (summer) and 1.0 clo (winter). However, as for the individual archetypal room settings (e.g., offices), specific clothing standards may apply that do not vary with the seasons. This initial version of the data set only provides a single clothing parameter since the setpoint cooling and heating temperatures also do not vary with the seasons in the TEASER templates.

The calculation of the complete clothing insulation I_T consists of multiple parts, e.g., base insulation (clothing insulation I_{cl}), air insulation I_a, and clothing area factor f_{cl} [DIN9920]. The position of the human body (e.g., seated, standing) and the surroundings (e.g., chair if seated, bed if sleeping) also affect the person's insulation. [ASH17, ISO7730] state that a factor of up to 0.15 clo should be added to the clo value caused by clothing when a person is seated on a chair. Nevertheless, clothing insulation and air insulation can technically not simply be added, as the clothing affects the air layers [DIN9920]. The surrounding insulation also significantly affects the effectiveness of a person's insulation in bedding systems. However, aiming to propose a new set of generalized templates for archetypal zone usage that is used for simple estimation of thermal comfort in the design phase, the clothing insulation values are added as additional insulation factors, such as chairs (when seated) or beds (when sleeping). The reduced accuracy of the clothing insulation is negligable, considering the general assumption of an estimation of an average/standard setup (of person, clothing, and activity degrees) per archetypal zone usage, which already includes a high uncertainty on predicting thermal comfort.

Table 4.4: Deriving clothing parameters for archetypal enrichment of thermal zones based on ASHRAE Fundamentals and ISO 7730. Columns: (1) Room type according to TEASER templates, (2) Chosen clothing type according to ASHRAE Fundamentals, Chapter 9 Table 7, (3) Chosen clothing type according to ISO 7730, (4) ASHRAE clothing (clo), (5) ISO 7730 clothing (clo), (6) Resulting combined clothing parameter (clo), (7) Chosen surrounding insulation type, (8) Surrounding insulation (clo). Initially presented in [RSFvT23].

(1) Room type	(2) ASHRAE Fundamentals	(3) ISO 7730	(4)	(5)	(6) Clothing insulation (clo)	(7) Surrounding insulation description	(8) Surrounding insulation (clo)
Single office	Trousers, long-sleeved shirt	Underwear, shirt, trousers, socks, shoes	0.61	0.7	0.66	ISO 7730, C.3 Executive chair	0.15
Bed room	Walking shorts, short-sleeved shirt	Panties, T-shirt, shorts, light socks, sandals	0.36	0.3	0.33	Average based on Zhang, N. et al. (2023)	2
Kitchen in non-residential buildings	Long-sleeved overalls, T-Shirt	Underpants, shirt, trousers, smock, socks, shoes	0.72	0.9	0.81	None	
WC and sanitary rooms in non-residential buildings	Trousers, long-sleeved shirt	Underwear, shirt, trousers, socks, shoes	0.61	0.7	0.66	None	
Traffic area	Trousers, long-sleeved shirt	Underwear, shirt, trousers, socks, shoes	0.61	0.7	0.66	None	
Living	Trousers, long-sleeved shirt	Underwear, shirt, trousers, socks, shoes	0.61	0.7	0.66	ISO 7730, C.3 Executive chair	0.15

In the proposed template (see Table 4.4 for an excerpt and cf. Appendix, Table A.6 for the full parameter set), the insulation parameter is split into two parts: clothing insulation and surrounding insulation. By splitting these parameters, the transparency of assumptions is ensured and can be adapted if required for specific use cases. The sum of these two parameters is considered in the further thermal comfort analysis of this dissertation.

Depending on climate zones as well as culture, bedding systems vary with regard to insulation, materials, and general configuration. However, as [ZCZ23] describe, the filling of the bedding materials has a minor effect on the resulting insulation of the bedding system. Still, it highly depends on the weight per unit area of the bedding system. Thus, even a study on Chinese bedding systems can be considered for Western Europe if the weight of the bedding system is chosen appropriately. [ZCZ23] measured bedding system insulation between 1.53 and 4.89 clo depending on the percentage of body coverage and system. Aiming for a surrounding insulation factor that can be added to the clothing insulation, the additional surrounding insulation factor is estimated as 2.0 clo. This surrounding insulation factor for bedding already incorporates a reduction of the combined clothing and surrounding insulation value. It has to be noted that this surrounding insulation factor highly depends on the bedding system weight (that may be changed due to weather conditions), body coverage, and even sleeping posture. Further research should include statistics for average sleep parameters. For PMV calculations in [ISO7730], the maximum clo value is limited to 2.0 clo, which the proposed combinations of clothing and additional insulation may exceed. Thus, the applicability of the [ISO7730] needs to be tested further.

As the effect of surrounding insulation is rather small (e.g., for wooden stools), these parameters can be considered optional and used for the fine-tuning of models (e.g., in classroom or meeting room settings, where all people are expected to be seated on a chair). The additional insulation of the bedding systems is expected to be crucial for thermal comfort, while office chairs are negligible. However, the impact of clothing and surrounding insulation factors on the general thermal comfort within a space, also considering different activity levels, should be elaborated in more detailed case studies.

4.3.3 Model Maturity Stages in the Design Process

The choice of simulative approaches for thermal comfort analysis not only depends on the desired spatial resolution of results but also on the availability of the required IFC data for automated setup of simulations. In [RLS+23], the applicability of BEPS and CFD for thermal comfort analysis has been mapped to the available IFC data by introducing six maturity stages. While simplified PMV and PPD predictions could already be derived from archetypal simulations and reduced-order approaches for BEPS using TEASER, additional predictions on local discomfort (e.g., DR, radiant asymmetry) require knowledge on individual surface temperatures as provided by BEPS using EnergyPlus. The spatial resolution of BEPS thermal comfort analysis depends on the zoning strategy but can only provide an average thermal comfort prediction per space. The

spatial resolution can be increased using CFD-based comfort predictions, which additionally require detailed HVAC, furniture, and occupant geometry, positions, and semantic parameters to define the boundary conditions of the computational domain correctly. For further details on the IFC input data requirements for the derived IFC maturity levels and their application in thermal comfort, see [RLS+23].

4.4 Methodology for Setting Up an IFC-based Thermal Comfort Analysis

Considering the scope of this dissertation, the available thermal comfort metrics need to be evaluated for their applicability within the IFC-based design process using the automated setup of BEPS and CFD models. Fanger's PMV and PPD [Fan70, ISO7730, ASH55] and adaptive approaches [ASH55, DIN16798-1] are designed to predict thermal comfort for a group of people inside a uniform environment, which aligns with the single-node calculation within the IFC-based BEPS, as implemented in the *PluginEnergyPlus*. As an extension to this presented implementation, these comfort approaches require information on the personal comfort parameters as inputs, which have been derived in the previous section as an extension of the archetypal templates. This allows the prediction of thermal comfort within annual IFC-based BEPS. The single-node BEPS simulation further enhances a limited analysis of local thermal comfort by analyzing radiant asymmetry and surface temperatures according to the standards [ISO7730, DIN16798-1, ASH55].

A detailed local thermal comfort of occupants, considering temperature differences at specific heights (ankle and head), cannot be determined from a single-node BEPS. Here, IFC-based CFD allows a high-resolved spatial analysis of thermal comfort within a space. However, while general local thermal comfort analysis according to [ASH55, DIN16798-1] does not require additional input parameters compared to IFC-based BEPS, the setup of CFD environments requires the definition of furniture and occupant positions. Once occupants are defined, these can be modeled using multi-node segmented thermo-physiological models that directly interact with the spatially high-resolved environmental parameters calculated by CFD. On a temporal scale, the IFC-based CFD is applicable for a short time period and for a selection of spaces, considering the high computational cost of these spatially high-resolved simulations.

This section starts with the general methodology to setup an IFC-based thermal comfort analysis based on IFC-based BEPS as introduced in Chapter 2, before extending this approach for the requirements for IFC-based CFD as introduced in Chapter 3.

4.4.1 BEPS-based Analysis

For the BEPS-based comfort analysis, extended archetypal templates are used to enrich personal comfort parameters within the general enrichment of use conditions of the *bim2sim* preprocessing. The resulting IFC-based BEPS simulation allows the direct calculation of PMV and PPD using these inputs. Additionally, by evaluating the surface temperatures within the space,

a limited local thermal comfort prediction can be applied that includes radiant asymmetry and the evaluation of floor surface temperatures [vTr10]. The NA to the [DIN16798-1] refers to comfort Category II as the standard category for indoor environments in design decisions, which is the basis for further comfort evaluation within this dissertation.

For the limited evaluation of local thermal comfort, the surface θ_{surf} and air temperatures θ_{air} from the EnergyPlus-based BEPS results can be used to calculate radiant asymmetry using $\Delta\theta_{rad} = \text{abs}(\theta_{surf} - \theta_{air})$ for walls and ceiling, and by directly evaluating the surface temperature of the floor (cf. Section 4.1.1 for applicable limits). The DR and vertical temperature difference between the head and feet are not evaluated within this dissertation using BEPS, as the temperature stratification is unknown and estimates of the resulting indoor air velocity would be uncertain. These evaluations are performed using CFD, which follows the suggestion from [vTr10].

To evaluate adaptive comfort within BEPS, in [RSFvT23], the adaptive comfort has been evaluated based on the international comfort categories defined in [DIN16798-1]. Here, the comfort indoor operative temperature θ_{op} is defined by the running mean outdoor temperature θ_{rm} in the range of [10, 30]°C, using $\theta_{op} = 0.33\,\theta_{rm} + 18.8\,°\text{C}$. The upper and lower limits for each category are defined relative to the comfort temperature within the following bounds: Cat I, +2/−3 K; Cat II, +3/−4 K; Cat III, +4/−5 K.

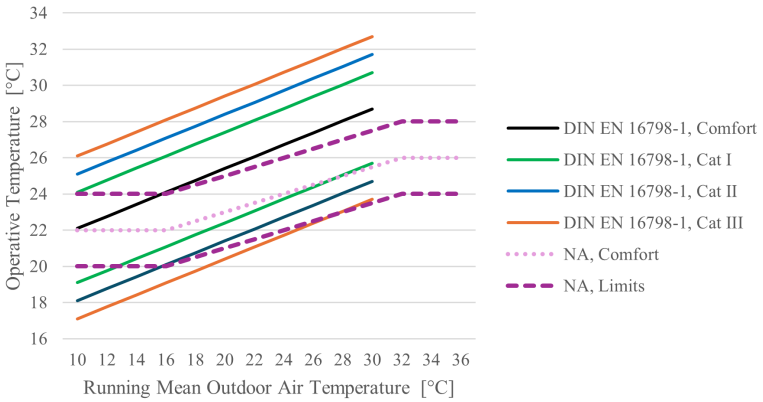

Figure 4.2: Comparison of the thermal comfort categories and their temperature limits defined in [DIN16798-1] and its German National Appendix (NA).

However, as illustrated in Figure 4.2, the [DIN16798-1], NA uses a different comfort temperature calculation, which appears to be common, given the variety of overheating criteria defined in regional standards [TMP+23]. The comparability of findings is limited by inconsistencies in determining the reference outdoor air temperature (e.g., mean or weighted over various time ranges) in related research and between applicable standards [DDWAZ25].

In the NA of [DIN16798-1], the hourly average outdoor temperature θ_{out} in the range of [16, 32]°C is used to calculate the comfort temperature $\theta_{op} = 18\,°\text{C} + 0.25\,\theta_{out}$, with limits of ±2 K. Outside of the defined range, the comfort temperature is defined as 20 °C and 26 °C for lower and larger outdoor temperatures, respectively, while maintaining the ±2 K range around the comfort temperature as an acceptable range. This temperature range within the NA refers

to the design objective of reaching a Category II state. The temperature limits must not be exceeded for more than 1% of the occupied hours and up to ±2 K while exceeding each bound has to be stated separately, which is evaluated by the annual excess temperature hours and degree-hours (cf. Section 4.1.1). These limits are stated for a medium sedentary activity in residential houses or offices with an activity degree of 1.2 met and a clothing level of 0.5 clo (summer) and 1.0 clo (winter) and may be adjusted for deviations in the personal parameters [DIN16798-1]. According to [DIN16798-1], NA, the observed high indoor air temperatures (> 26 °C) can be corrected if occupant-controlled ventilation systems are available, depending on the resulting mean air velocity at office desk level (1.2 K for $v_{air} = 0.6\,\mathrm{m/s}$, 1.8 K for $v_{air} = 0.9\,\mathrm{m/s}$, 2.2 K for $v_{air} = 1.2\,\mathrm{m/s}$). Local ventilation systems are currently not considered in the implementation, but could be added in further research.

To compensate the reduced indoor air temperatures during heating setbacks at night and the resulting high discomfort caused by low temperatures in thermal zones with a persistent minimum occupancy (e.g., living room), an occupancy-weighted evaluation of the adaptive comfort is proposed, where the time exceeding the thresholds is normalized by the percentage of full occupancy. The effect of this occupancy weighting is further evaluated and tested in the use cases. An evaluation of the PPD-weighted PMV as defined in [ISO17772-1] is not applied in this dissertation, as it is not referenced in the applicable German standard [DIN16798-1].

To mitigate overheating, the simplified approach of natural ventilation used in Section 2.7.1 has been adapted according to the requirements defined in [DIN4108-2]. For residential homes, this standard defines a baseline air exchange rate of $n = 0.5\,\mathrm{h}^{-1}$. This baseline air exchange rate can be increased if the indoor air temperature exceeds 23 °C to up to $3\,\mathrm{h}^{-1}$ to mitigate overheating during the occupied hours from 6 am to 11 pm, and to up to $2\,\mathrm{h}^{-1}$ during unoccupied hours at night. For non-residential buildings, the baseline air exchange rate during occupied hours (7 am to 6 pm) is empirically defined as $n = 4\frac{A_{floor}}{V_{space}}\mathrm{h}^{-1}$ using the floor area A_{floor} and the volume of the space V_{space}. Here, the air exchange rate is reduced to $n = 0.24\,\mathrm{h}^{-1}$ during unoccupied hours. For non-residential buildings the same increased ventilation rates can be applied as for residential buildings within their (un-)occupied times.

4.4.2 CFD-based Analysis

The high spatial resolution of CFD results enhances the full analysis of local thermal comfort according to [DIN16798-1]. According to the standard, the operative temperature should be evaluated at the height of 0.6 m for spaces with a temperature stratification. Since the results in the IFC-based CFD analysis have shown a temperature stratification, cf. Section 3.6, the operative temperature for adaptive thermal comfort should be evaluated at this height of 0.6 m. The high resolution of the CFD analysis allows for the evaluation of the vertical air temperature difference between head (height = 1.1 m) and feet (height = 0.1 m) level. The DR is implemented in OpenFOAM according to its definition in [ISO7730], which predicts the PD towards draught for seated people at their neck, while it may overestimate the predicted draught rate at arms

and legs [ISO7730]. Thus, within this dissertation, the DR is evaluated at head level (i.e., 1.1 m). [DIN16798-3] provides a definition for the occupied zone with a height of 0.05-1.80 m above floor level, 0.5 m from walls, and 1.0 m from external doors and windows, which can be applied for evaluations of the domain that actually affects the thermal comfort conditions of occupants. Due to the high computational cost of CFD, the local thermal comfort can only be evaluated for a specific time of the year, not in an annual simulation.

Enhancing an accurate prediction of the airflow within the computational domain, occupants and furniture are positioned as described in Section 3.4. For the representation of occupants, the posture of a RAMSIS[2] manikin, originally used in research on vehicle indoor comfort for visualization purposes [Wöl17], is modified using the software Blender[3] for the use in building indoor environments (i.e., modified the manikin's posture for sitting on a chair). To test the capability of future coupling of thermo-physiological models, the shape of this manikin is split into 19 body parts, referring to the subdivision presented of MORPHEUS [Wöl17], leading to the body parts and surface areas presented in Table 4.5. In Figure 4.3, the resulting body surface areas are compared to FIALA-FE and MORPHEUS as an extension of the comparison in [Wöl17]. The legs and arms are considered as single body parts in this comparison according to FIALA-FE, instead of the subdivision in upper and lower parts in [Wöl17], which is also used in this dissertation.

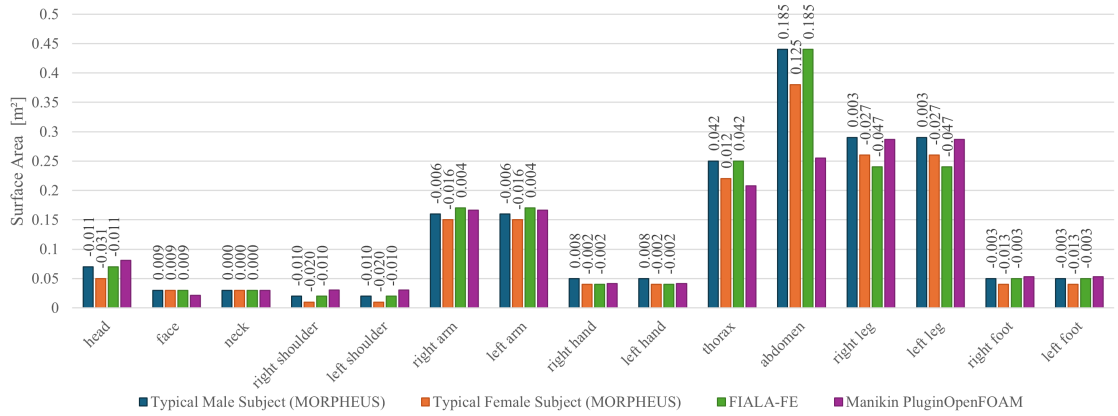

Figure 4.3: Comparison of the surface areas per body part between FIALA-FE (1.86 m^2) and the typical male (1.96 m^2) and female (1.71 m^2) subjects of MORPHEUS presented in [Wöl17], and the body surface areas (1.75 m^2) of the manikin used for comfort evaluation in this dissertation within the *PluginOpenFOAM*. The annotations denote the absolute deviations in the body surface area compared to the manikin used in the *PluginOpenFOAM*.

The surface areas for the manikin used in this dissertation show smaller surface areas for the abdomen and thorax, which result from differences in the subdivisions, resulting in larger surface areas in the neighboring parts of the shoulders, arms, and legs. Similarly, the back of the head shows a larger surface area, which is compromised by a smaller face area than in the other models. The total surface area of the surface model in this dissertation is smaller

[2] Rechnergestütztes Anthropometrisch-Mathematisches System zur Insassen-Simulation (RAMSIS), a computational model for vehicle passengers, introduced by [GKS95, KSS97].
[3] Blender, open-source 3D creation suite: https://www.blender.org/, accessed on June 03, 2025.

than the presented male models from [FLS99] and [Wöl17]. As this dissertation focuses on the general proof of automated transformation, these deviations do not limit the applicability of automated IFC-based CFD setups. When eventually coupling thermo-physiological models in future research, the subdivision of body parts should be adapted to improve the reliability of results, e.g., by using a broader range of RAMSIS models for the representation of diverse manikins.

The integration of thermo-physiological models commonly results in the prediction of skin temperatures, which would require an additional transformation to account for resulting clothing surface temperatures as boundaries for CFD. Therefore, the surface boundary conditions of the individual body parts in the proposed CFD model are prototypically defined by clothing surface temperatures from literature. For clothing/skin temperatures and radiation and convection heat transfer coefficients $h_r + h_c$, the third use case by [YYN23] has been selected, as it provides a similar ventilation setting as the use cases in this dissertation. The face temperature has been derived from [ZKOS07]. The resulting parameters for this dissertation are presented in Table 4.5, stating the exemplary heat flux and power per body part for an operative temperature of 21 °C leading to a total heating power induced by the person of 98.32 W.

Table 4.5: Resulting body parts and parameters: surface area, clothing/skin surface temperatures, heat transfer coefficients, and power based on an operative temperature of 21 °C.

	Area m^2	Temperature °C	$h_r + h_c$ $W/(m^2 K)$	Heat flux W/m^2	Power W
Abdomen	0.255	27.25	7.81	48.81	12.46
Head	0.081	32.43	9.89	113.04	9.19
Face	0.021	35.90	9.92	147.81	3.13
Left foot	0.053	29.33	20.62	171.72	9.07
Left hand	0.042	32.00	8.20	90.20	3.76
Left lower arm	0.075	26.23	7.82	40.83	3.05
Left lower leg	0.096	25.21	14.32	60.29	5.77
Left shoulder	0.030	25.87	8.35	40.62	1.22
Left upper arm	0.092	26.23	7.82	40.83	3.74
Left upper leg	0.191	26.20	4.06	21.09	4.04
Neck	0.030	31.25	9.27	95.02	2.86
Right foot	0.053	29.33	20.62	171.72	9.07
Right hand	0.042	32.00	8.20	90.20	3.76
Right lower arm	0.075	26.23	7.82	40.83	3.05
Right lower leg	0.096	25.21	14.32	60.29	5.77
Right shoulder	0.030	25.87	8.35	40.62	1.22
Right upper arm	0.092	26.23	7.82	40.83	3.74
Right upper leg	0.191	26.20	4.06	21.09	4.04
Thorax	0.208	26.65	7.99	45.08	9.37
Total	1.752				98.32

These mapped clothing surface temperatures are considered as a preliminary method within the prototypical implementation of the IFC-based approach. In future research, these parameters should be upgraded by integrating the calculation of clothing temperatures from skin temperatures using thermo-physiological models into the IFC-based CFD setup, along with clothing values per body part. The current implementation is further limited since changes in

the environmental conditions are not reflected in changes in the body surface temperatures and resulting heat fluxes.

4.5 *PluginComfort*: IFC-based BEPS for Thermal Comfort Analysis

Main parts of this section are an excerpt from [RSFvT23], unless otherwise specified. The proposed *PluginComfort* is an extension of the *bim2sim PluginEnergyPlus* (cf. Figure 2.5). This new plugin requires comfort parameters for each thermal zone, introduced as simplified usage-based parameters in Section 4.3.2.

Figure 4.4 visualizes the structure of the proposed thermal comfort plugin. This plugin builds upon the existing implementation of the *PluginEnergyPlus* within the *bim2sim* framework, as described in Figure 2.5. While the general tasks like loading IFC data and general element setup from IFC are the same as for all other plugins within the *bim2sim* environment, additional template-based data are loaded within the enrichment process of the thermal zones, adding personal comfort parameters for activity and clothing. If these data were available from the given IFC data, these personal parameters could also be loaded directly from the IFC. However, since IFC does not yet provide standardized property sets for these personal parameters, the current implementation only considers a template-based enrichment for personal parameters.

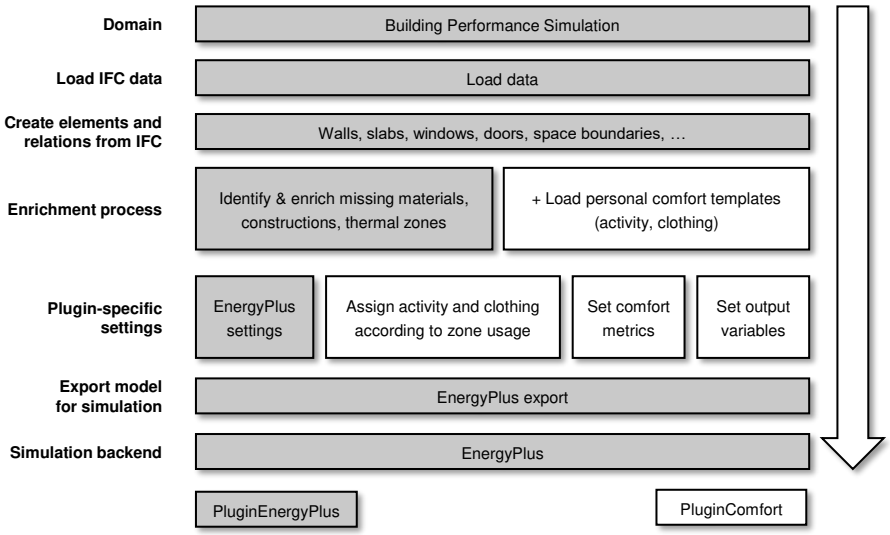

Figure 4.4: Simplified representation of the workflow of the *bim2sim*-based thermal comfort plugin *PluginComfort*; the new plugin builds upon the existing parts of the *PluginEnergyPlus* (gray) by loading additional data in the enrichment process and comfort-related settings in the plugin-specific settings (white). Adapted from [RSFvT23].

Within the plugin-specific settings, the implementation of the *PluginEnergyPlus* is extended by the additional settings in the *PluginComfort*, which adds the personal comfort parameters for activity and clothing to the individual thermal zones according to their zone usage. Furthermore, the applicable comfort metrics are selected, and the related output variables are set. The export of the EnergyPlus simulation model is the same as for the *PluginEnergyPlus*. The simulation

results of the *PluginComfort* can be evaluated with suitable visualizations to support design decisions within the individual design stages of the building.

With this IFC-based thermal comfort plugin, BEPS models for design variants can quickly be created, minimizing the manual effort to remodel the geometry. The presented setup enhances evaluating the thermal resilience of the design variants by applying future weather data to consider climate change. In this dissertation, thermal resilience is considered as the building's ability to maintain an adequate indoor thermal comfort even under extreme weather conditions in future climates [HMK+23]. Other studies focus on the thermal resilience of indoor environments during power outages or failures of HVAC systems [SOT+23], which is not addressed here. For evaluating thermal resilience in this dissertation, the heating and cooling loads can be related to the resulting thermal comfort of the building. Apart from evaluating thermal resilience, the modular structure of the *bim2sim* framework also supports the analysis of the embodied carbon of the design variants, which can be easily added to further support design decisions by extending the existing implementation of the LCA Plugin *PluginLCA* [MJvT+22].

As initially discussed in [RLS+23], the derived template values for the clothing parameters are static throughout the whole year as a simplification for template-based model enrichment. In further research, the dynamic clothing model of [ASH55] could be evaluated in comparison to the presented static template-based clothing parameter set. [ASH55] enables dynamic clothing based on outdoor air temperatures. This may not be applicable to office and other formal situations (e.g., in formal office or meeting situations, or due to specific cultural requirements [DCOZZ07]), so zone-usage-based clothing may be more applicable in these cases. [RLS+23]

For the implementation of the comfort evaluation in EnergyPlus, several inbuilt comfort parameters are available in EnergyPlus. These include static measures, such as Fanger's PMV, and PPD, but also adaptive approaches. For the adaptive approaches, a method for the [ASH55] is provided, which is the applicable standard for use in the United States of America. For use in Europe, the now outdated [DIN15251] is included, which differs from the currently valid international version of the [DIN16798-1]. The resulting differences are discussed in Appendix A.6. The evaluation of the adaptive comfort thus requires a re-implementation, which is included within the *PluginComfort* for both the international [DIN16798-1] and the NA within the post-processing of the EnergyPlus results. In this dissertation, only the NA is applied and evaluated. For the application of the international version of [DIN16798-1], see [RSFvT23].

While the presented implementation of the *PluginEnergyPlus* includes the control of the air temperature per default (Section 2.5), the adaptive comfort measures in [DIN16798-1] and [ASH55] define acceptability ranges for operative temperatures in indoor environments. Thus, to obtain acceptable thermal comfort results in further analysis, the implementation of the *PluginEnergyPlus* is extended by an additional option for operative room temperature control, which can be activated by a *sim_setting*. This extension is added to the *PluginEnergyPlus* instead of the *PluginComfort*, as the control of the operative temperature could also be used for energy efficiency analyses of buildings that do not explicitly focus on thermal comfort.

Similarly, the natural ventilation to mitigate overheating is also adjusted within the *PluginEnergyPlus*, where the choice of residential or non-residential ventilation can be made using a *sim_setting*. Since heat mitigation ventilation is controlled by the minimum indoor air temperatures and space temperatures are controlled by operative temperatures, there is a risk of excessive heat loss during the winter when indoor air temperatures often exceed operative temperatures by more than 2 K, cf. Figure 4.21. To avoid these excessive heat losses, the implementation of the heat mitigation ventilation considers the outdoor air temperature as an additional threshold. For indoor air temperatures between 23 °C and 26 °C, the heat mitigation ventilation is only applied if the outdoor air temperature exceeds 12 °C (occupied hours) and 15 °C (unoccupied hours). For higher indoor air temperatures, heat mitigation ventilation is applied regardless of the outdoor air temperature. This temperature bandwidth has been successfully tested during implementation to prevent overheating in winter, but should still be further validated. Another option could be to restrict the heat mitigation ventilation to the summer period, which has not been considered in this dissertation, as it would not allow heat mitigation ventilation for overheated spaces caused by internal loads in winter (e.g., in the kitchen).

As a prerequisite for later analysis of the future weather impact on thermal comfort, the maximum heating and cooling capacity within the BEPS simulation can be fixed to a specific maximum power per space, instead of relying on EnergyPlus-internal autosizing. Per default, the heating capacity is unlimited, and the cooling capacity limit is autosized for a typical design day. Therefore, two additional *sim_settings* are introduced in the *PluginEnergyPlus*, which allow either enforcing the sizing of the maximum heating and cooling capacities to the choice of design period (typical or extreme design day) within the same weather file, or using another weather file to precompute the maximum applicable system sizings. This allows comparing the performance of defined HVAC systems under different weather conditions.

The application of the *PluginComfort* and the evaluation of standardized comfort measures such as [DIN16798-1] requires well-defined occupancy patterns that match the actual heating and cooling schedule of the analyzed spaces. As an example, when applying a heating set back at night for all indoor spaces (e.g., from 21 °C to 18 °C), in spaces where the occupancy schedule predicts occupancy with a small probability for the night time (e.g., in the living room, cf. Figure A.34), this night-occupancy affects the overall thermal comfort rating of the space. Considering [DIN16798-1] and its NA, these temperature hours that exceed both thresholds of the acceptability range are accounted for all occupied hours and, thus, also for the small probability of occupancy during night set-back. This issue is addressed by the implementation of an additional weighting of the exceeded temperature hours by the percentage of the actual occupancy, resulting in reduced weights for these low occupancy probabilities at night. Considering occupant user behavior, these low temperatures are likely to be compensated by short-time additional clothing, which the standardized simulation setup in this dissertation cannot cover.

4.6 Extension of *bim2sim PluginOpenFOAM* by including *PluginComfort*

The implementation of thermal comfort within the IFC-based CFD simulation using OpenFOAM is not a separate plugin, but an extension of the *PluginOpenFOAM*. As the *PluginOpenFOAM* includes a detailed interior setup, including HVAC systems, furniture, and people as presented in Chapter 3, only minor modifications are required to incorporate thermal comfort in *OpenFOAM*. The extension of the *PluginOpenFOAM* for thermal comfort relies on the thermal comfort enrichment from the *PluginComfort* used in BEPS, which uses the template-based enrichment of clothing parameters and activity degrees based on the archetypal zone usage. These parameters are inserted in the additional OpenFOAM input files for thermal comfort, using the provided OpenFOAM comfort calculations of PMV, PPD, DR, and T_{op}.

Thermal zones for an in-depth spatially high-resolved thermal comfort analysis using CFD can either be selected manually for a time and date of interest, or by evaluation of the BEPS-based comfort results from the *PluginComfort*. Based on these BEPS results, thermal zones exceeding the desired [DIN16798-1] categories (either international version or NA) regarding the adaptive temperature limits or the limited local discomfort analysis can be selected for further analysis. As an example from related research, [LRW19] introduced a measure to compare overall comfort within spaces, which is defined by the product of the PPD, the occupied volume of the space, and the occupancy time in this space. Only PPD values with an average greater than 10% are considered in their evaluation, as this exceeds the general acceptable conditions (i.e., PPD <10%, -0.5 < PMV < 0.5) defined by [ASH55].

Using this presented coupling of BEPS and CFD analysis for thermal comfort, the computational cost of simulations can be drastically reduced compared to a full CFD analysis for the whole building. This is achieved by identification of thermally critical zones using BEPS and applying selective CFD analysis in high-risk zones of thermal comfort in order to determine compensative approaches for a more resilient design and operation of the building.

4.7 Application and Testing of the IFC-based Comfort Applications

The proposed methodology for IFC-based thermal comfort assessment is evaluated for both BEPS and CFD, and builds upon the evaluation of the already evaluated approaches from Chapters 2 and 3. The structure of the evaluation is illustrated in Figure 4.5.

Use Cases 1 and 2 evaluate the methods of BEPS-based thermal comfort on the use case buildings of the FZK-Haus (heated, naturally ventilated) and DigitalHub (heated and cooled, mechanically ventilated), to evaluate the annual performance of the static and adaptive thermal comfort measures, as well as the overheating risk. Use Cases 3 and 4 apply a steady-state CFD-based thermal comfort analysis using the *PluginOpenFOAM*, providing thermal comfort results with a high spatial resolution. Use Case 3 evaluates the impact of two sets of construction types on the local thermal comfort in winter, while Use Case 4 evaluates the impact of HVAC system

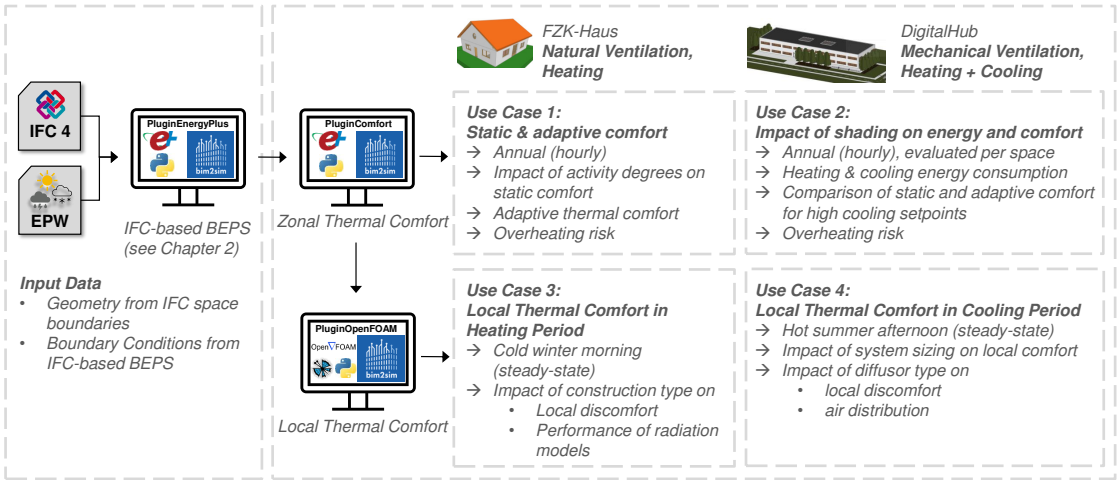

Figure 4.5: Overview on the use cases for IFC-based thermal comfort analysis using *PluginComfort* and *PluginOpenFOAM*.

sizing and diffusor types on local thermal comfort for a hot summer day.

The evaluation of thermal comfort in indoor environments requires an appropriate choice of evaluation measures. While static thermal comfort measures such as Fanger's PMV and PPD are designed for mechanically conditioned spaces and consider personal parameters for clothing and activity levels, adaptive measures such as [DIN16798-1] are applicable for naturally ventilated spaces. The normative bounds of the adaptive measures in [DIN16798-1] refer to activities with 1.2 met and clothing of 0.5 clo and 1.0 clo in summer and winter, respectively, and may require adjustments for other use conditions. This dissertation evaluates the adaptive comfort without adaptations, such that the proposed template-based personal comfort parameters are only applied when evaluating PMV and PPD in BEPS and CFD. All simulations within this section use the TMYx historical weather data from 2007 to 2021 for the location of the Cologne/Bonn Airport, which is further referenced as TMYx in this section. The weather data is provided by [LC22].

4.7.1 Use Case 1: Natural Ventilation using *PluginComfort*

For the following analysis of thermal comfort, the use case of the FZK-Haus (cf. Section 2.7.1) was adapted regarding construction materials, ventilation, and thermal comfort parameters, while the building geometry and other use conditions remain unchanged. An overview on the applied use conditions and schedules is given in Appendix A.10.1. A comparative overview on the simulation parameters and results of the FZK-Haus use cases is presented in Table A.9. The building is ventilated using natural ventilation according to [DIN4108-2] and only heated, but not cooled. The heating capacity is not limited, so all heating demands can be covered as requested. The construction is template-based enriched and complies with the KfW 40 requirements [KfW20, GEG24], resulting in U-values of 0.134 W/(m^2 K) for outer walls, 0.192 W/(m^2 K) for the ground floor, 0.095 W/(m^2 K) for roofs, 0.703 W/(m^2 K) for inner walls, 0.534 W/(m^2 K) for

inner floors, and 0.799 W/(m^2 K) for windows, 1.291 W/(m^2 K) for outer doors and 1.157 W/(m^2 K) for inner doors. These U-values include the EnergyPlus calculation of heat transfer coefficient which results in slightly different results than applying the common German coefficients for heat transfer. Compared to the use case in Section 2.7.1, the heating setpoint temperature of the *Bathroom* is reduced to 22 °C during occupied hours (cf. Figure A.32), to not exceed the adaptive comfort limits according to [DIN16798-1], NA. The indoor temperatures are controlled for operative temperatures as opposed to the use case in Section 2.7.1, where the indoor air temperatures were controlled. The night setback in the spaces with usage *Living* is postponed by one hour to provide comfort within the high occupied times. The exterior shadings are activated above a solar radiation of 150 W/m^2 as a simplification of the requirements defined in [DIN4108-2], in cases where the indoor air temperature exceeds the setpoint of the operative temperatures by 2 K. This combination of setpoints is applied to reduce the heating loads in winter when the indoor air temperature exceeds the operative temperature.

This setup is simulated for an annual timeframe in hourly timesteps and results in an annual total energy consumption of 52.77 kWh/(m^{2}a), consisting of 34.89 kWh/(m^{2}a) for heating energy and 17.88 kWh/(m^{2}a) for electricity. The energy efficiency rating of this building meets the requirements of efficiency class A (≤ 50 kWh/(m^{2}a)) [GEG24], which could be further reduced by considering a mechanical ventilation system using a heat recovery unit.

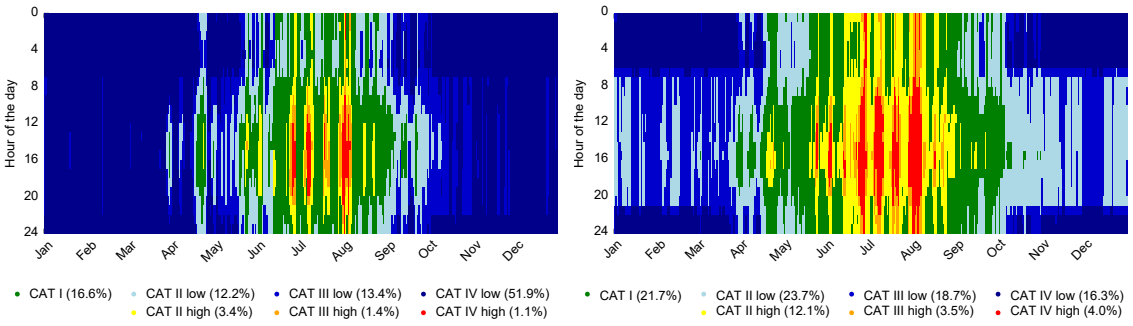

(a) Living, activity 115 W (=1.1 met)

(b) Single office, activity 125 W (=1.2 met)

Figure 4.6: Heatmap of hourly PMV categories according to [DIN16798-1], NA, both with an operative temperature of T_{op} = 21 °C, between 7 am and 10 pm (office) / 11 pm (living) and setback to 18 °C otherwise, and a combined clothing value of 0.81 clo. The legend states the relative amount of hours per category.

Figure 4.6 displays the heatmap of the annual PMV categories (cf. Section 4.1.1) according to [DIN16798-1], NA, for the spaces *EG-05 Living* and *EG-02 Single office* , which are both located on the ground floor level of the building (see floor plan in Figure 2.17). The legend of this heatmap states the fraction of annual time within the respective categories, where the fractions within the upper and lower bounds of the categories are stated separately. These fractions include all hours of the year and do not distinguish between occupied and unoccupied hours. This representation of the comfort categories in an annual hourly heatmap is an adaptation of the calendar heatmaps used in [RSFvT23], which displayed the daily mean PMV index of spaces in six steps from -3 to +3. This previous simplified visualization is applicable to estimate the

effects of climate change, but does not reflect the hourly effects of weather, occupancy, internal gains, and heating setback, which are required for an in-depth evaluation of thermal comfort performance according to standards like [DIN16798-1].

The comfort categories in the presented heatmap underline the limited applicability of the PMV metric as measure for thermal comfort in indoor environments without cooling. For the *Living* space in Figure 4.6a, categories I and II are only reached in 32.2% of the annual time, while 33.3% are affected by the night setback of the heating. In the *Single office* space, categories I and II are reached in 57.5% while 37.5% of the annual time is affected by night setback. These differences in the reached comfort categories result from the differences in occupant activity levels, which lead to a higher required indoor temperature to maintain thermal comfort in the *Living* space. The *Single office* space shows longer periods of overheating in summer, which are caused by the higher internal gains due to electric equipment. These internal gains cannot be fully compensated by natural ventilation in summer, as the natural ventilation is additionally limited to cases where the outdoor air temperature is below the indoor air temperature.

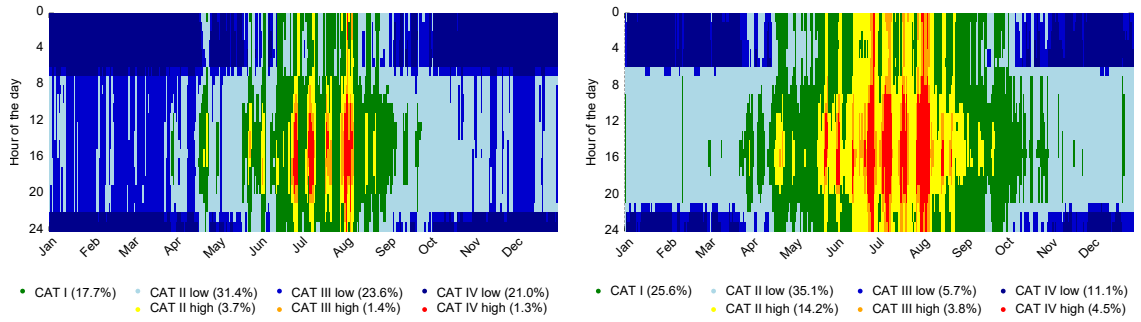

(a) Living, activity 115 W (=1.1 met)

(b) Single office, activity 125 W (=1.2 met)

Figure 4.7: Heatmap of hourly PMV categories according to [DIN16798-1], NA, with an increased operative temperature of $T_{op} = 22\,°C$ between 7 am and 10 pm and setback to 18 °C otherwise, and a combined clothing value of 0.81 clo. The legend states the relative amount of hours per category.

Figure 4.7 displays the heatmap for an increased operative temperature setpoint of 22 °C during the occupied hours. This increased setpoint is applied to the *Single office* space (EG-02) and the two *Living* rooms (EG-05, OG-07), cf. Figure 2.17. The total annual energy consumption of the building is increased to 57.12 kWh/(m^{2}a), caused by the increase of the heating energy consumption by 4.34 kWh/(m^{2}a) to 39.23 kWh/(m^{2}a). As a result, the comfort categories I and II are now reached in 52.8% and 74.9% of the annual time in the *Living* and *Single office* space, respectively. However, to limit the heating energy consumption, the further analysis of the results is proceeded using a heating setpoint of 21 °C.

As the PMV index has limited applicability in these spaces without mechanical ventilation, the thermal comfort is evaluated in terms of the overheating risk using the adaptive comfort limits according to [DIN16798-1], NA. The results for the two selected spaces are displayed in Figure 4.8, showing the operative temperatures during the occupied hours (see Figure A.8 for the full year including unoccupied hours). The orange lines display the 2 K acceptability range

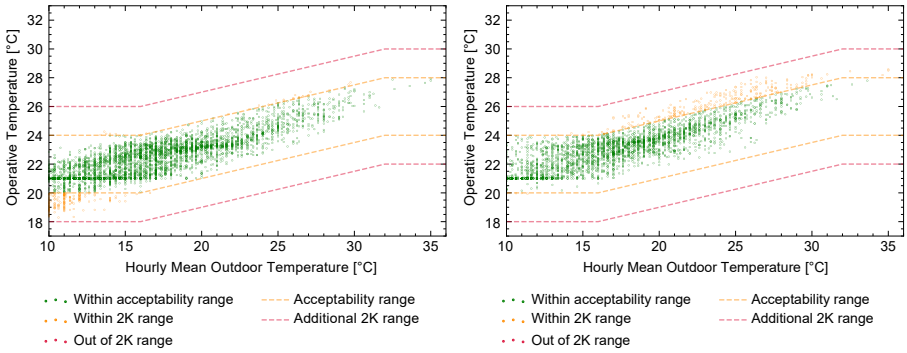

(a) Living (occupied) (b) Single office (occupied)

Figure 4.8: Evaluation of adaptive thermal comfort according to DIN EN 16798-1, NA, for the *Living* space and the *Single office*. Results are displayed for operative temperatures during the occupied hours.

around the comfort temperature defined in [DIN16798-1], NA, extended by an additional tolerance 2 K range, limited by red lines. As opposed to the international version of the [DIN16798-1], the mean hourly outdoor air temperature is used as reference instead of the running mean outdoor air temperature. Also, differences in the acceptance ranges apply (cf. Figure 4.2). While the *Living* space shows multiple timesteps where the operative temperature is below the comfort temperature acceptability range, the *Single office* shows more timesteps exceeding the upper comfort limit. For the *Living* space, the low temperatures are caused by the night setback and the occupancy during the night.

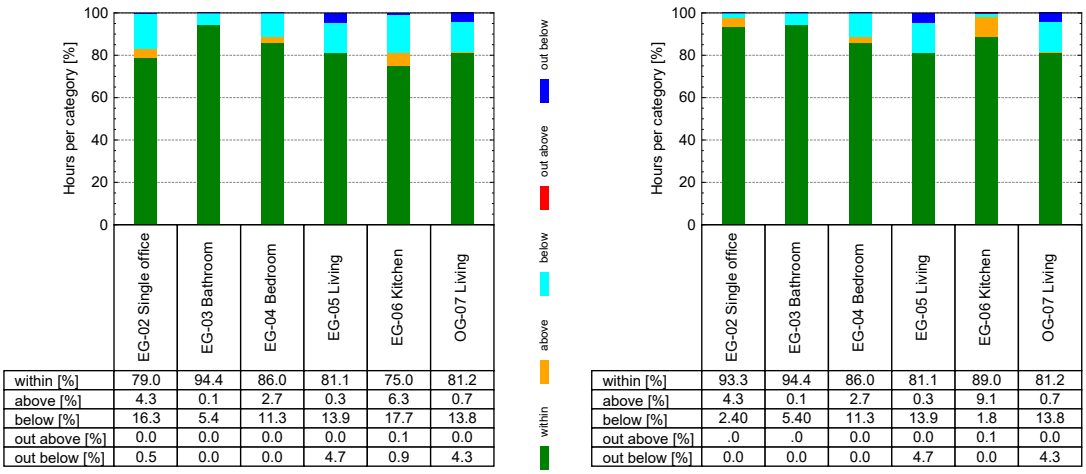

	EG-02 Single office	EG-03 Bathroom	EG-04 Bedroom	EG-05 Living	EG-06 Kitchen	OG-07 Living
within [%]	79.0	94.4	86.0	81.1	75.0	81.2
above [%]	4.3	0.1	2.7	0.3	6.3	0.7
below [%]	16.3	5.4	11.3	13.9	17.7	13.8
out above [%]	0.0	0.0	0.0	0.0	0.1	0.0
out below [%]	0.5	0.0	0.0	4.7	0.9	4.3

(a) Total

	EG-02 Single office	EG-03 Bathroom	EG-04 Bedroom	EG-05 Living	EG-06 Kitchen	OG-07 Living
within [%]	93.3	94.4	86.0	81.1	89.0	81.2
above [%]	4.3	0.1	2.7	0.3	9.1	0.7
below [%]	2.40	5.40	11.3	13.9	1.8	13.8
out above [%]	.0	.0	0.0	0.0	0.1	0.0
out below [%]	0.0	0.0	0.0	4.7	0.0	4.3

(b) Occupied

Figure 4.9: Evaluation of adaptive thermal comfort according to DIN EN 16798-1, NA. Operative temperatures are evaluated within the temperature limits for the full year (left) and the occupied hours (right).

Figure 4.9 displays the analysis of the operative temperatures within the bounds of the NA for the full year (Figure 4.9a) and the occupied hours (Figure 4.9b) for all conditioned zones, i.e., the corridor is neglected due to a low daily heating setpoint of 18 °C. While the constant (though limited) occupation of the *Living* and *Bathroom* spaces do not result in any differences between

these plots, the *Kitchen* and *Single office* spaces show a reduction of hours below the acceptable limits in the occupied case, since these spaces are not occupied during night-setback.

However, the evaluation of adaptive comfort does not solely rely on the number of hours that exceed the acceptable temperature range but rather requires an evaluation of the degree-hours within these hours. Figure 4.10a displays the excess hours evaluated as degree-hours. As already derived from Figure 4.8, the *Living* spaces show a high occurrence of hours during occupancy that are below the thresholds of acceptability, caused by the night-setback. Using this evaluation, the degree-hour limits are only met for the *Bathroom* and *Single office* (i.e., below 1% of the 2 K degree-hours).

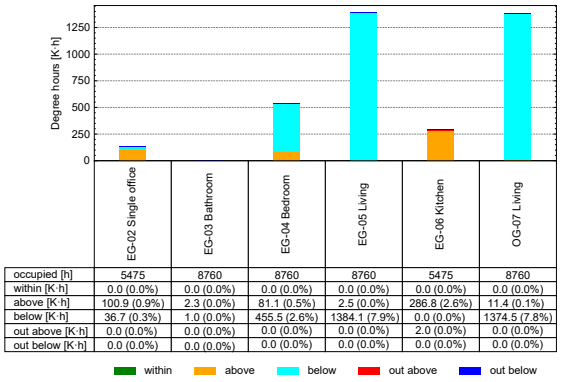

	EG-02 Single office	EG-03 Bathroom	EG-04 Bedroom	EG-05 Living	EG-06 Kitchen	OG-07 Living
occupied [h]	5475	8760	8760	8760	5475	8760
within [K·h]	0.0 (0.0%)	0.0 (0.0%)	0.0 (0.0%)	0.0 (0.0%)	0.0 (0.0%)	0.0 (0.0%)
above [K·h]	100.9 (0.9%)	2.3 (0.0%)	81.1 (0.5%)	2.5 (0.0%)	286.8 (2.6%)	11.4 (0.1%)
below [K·h]	36.7 (0.3%)	1.0 (0.0%)	455.5 (2.6%)	1384.1 (7.9%)	0.0 (0.0%)	1374.5 (7.8%)
out above [K·h]	0.0 (0.0%)	0.0 (0.0%)	0.0 (0.0%)	0.0 (0.0%)	2.0 (0.0%)	0.0 (0.0%)
out below [K·h]	0.0 (0.0%)	0.0 (0.0%)	0.0 (0.0%)	0.0 (0.0%)	0.0 (0.0%)	0.0 (0.0%)

(a) Excess degree-hours

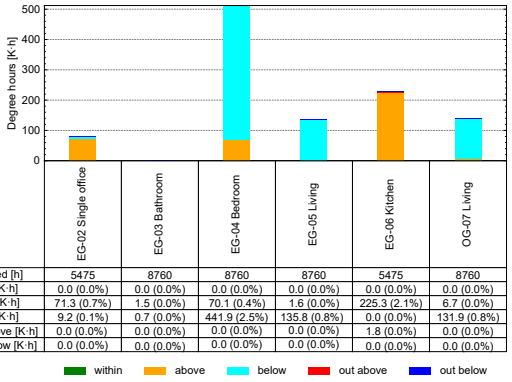

	EG-02 Single office	EG-03 Bathroom	EG-04 Bedroom	EG-05 Living	EG-06 Kitchen	OG-07 Living
occupied [h]	5475	8760	8760	8760	5475	8760
within [K·h]	0.0 (0.0%)	0.0 (0.0%)	0.0 (0.0%)	0.0 (0.0%)	0.0 (0.0%)	0.0 (0.0%)
above [K·h]	71.3 (0.7%)	1.5 (0.0%)	70.1 (0.4%)	1.6 (0.0%)	225.3 (2.1%)	6.7 (0.0%)
below [K·h]	9.2 (0.1%)	0.7 (0.0%)	441.9 (2.5%)	135.8 (0.8%)	0.0 (0.0%)	131.9 (0.8%)
out above [K·h]	0.0 (0.0%)	0.0 (0.0%)	0.0 (0.0%)	0.0 (0.0%)	1.8 (0.0%)	0.0 (0.0%)
out below [K·h]	0.0 (0.0%)	0.0 (0.0%)	0.0 (0.0%)	0.0 (0.0%)	0.0 (0.0%)	0.0 (0.0%)

(b) Occupancy-weighted degree-hours

Figure 4.10: Evaluation of adaptive thermal comfort according to DIN EN 16798-1, NA. Operative temperatures are evaluated within the occupied hours regarding the excess degree-hours (left) and the occupancy-weighted excess degree-hours (right).

To avoid these low operative temperatures during occupancy, either the occupancy during the night setback could be set to zero, or the space could be heated without night setback. As the latter option would drastically increase the heating demand and the modification of occupancy schedules is out of scope for this dissertation, a weighting factor is introduced. As a result, times with a small scheduled occupancy are compromised with this weighting factor that normalizes the degree-hours by the occupancy-rate compared to maximum occupancy in this zone during those hours. The adapted results are displayed in Figure 4.10b, resulting in acceptable degree-hours below 1% for all spaces except for the kitchen. The occupancy-weighting has only minor effect on the degree-hour results of the kitchen, as the *Kitchen* is commonly occupied during the day, when the overheating risk is high especially in the summer due to the combination of high internal loads and outdoor air conditions. Regardless of the occupancy weighting, all spaces fulfill the requirements of [DIN4108-2] of a maximum of 1200 Kh excess degree-hours based on a reference of 26 °C for residential houses, which applies as reference temperature for the location of the weather file at Cologne/Bonn Airport.

In addition to the evaluation of PMV, adaptive comfort, and overheating, the limited local comfort analysis was applied as described in Section 4.4.1. This limited local analysis evaluated the temperature differences between surface and air temperature and surface temperatures itself. The observed results complied with the limits stated in [DIN16798-1], NA, except for four

and eleven hours of the year for the *Living* spaces, respectively. These spaces have shown a surface temperature of the floor below the minimum threshold of 19 °C, which were observed in the simulation results for 4am and 5am during the night setback, where the occupancy probability in the *Living* spaces is low.

4.7.2 Use Case 2: Mechanical Ventilation using *PluginComfort*

The IFC-based thermal comfort methods are further evaluated for a three-storey office building with a full mechanical air conditioning named DigitalHub, displayed in Figure 4.11. The original IFC4 model of the DigitalHub[4] was enriched with *IfcRelSpaceBoundary2ndLevel* using the *IFC2SB*[5] tool. This improved set of space boundaries allows the automated generation of two different EnergyPlus input files using the *bim2sim* toolchain: (1) using the internal space boundaries, resulting in a simplified IDF displayed in Figure 4.11b, and (2) additionally using the external space boundaries to generate shading elements, displayed in Figure 4.11c. The external space boundaries, which are used for the automated generation of the shading elements, are part of the IFC4 schema but have not yet been seen to be generated by commercial authoring software, but only by research tools such as IFC2SB,[5] which limits the applicability of the presented approach in industry. Therefore, the following analysis of IFC-based thermal comfort starts with the investigations of the IDF model without such external shading elements. All use cases still use external window shading, implemented and controlled like in the previous use case on thermal comfort.

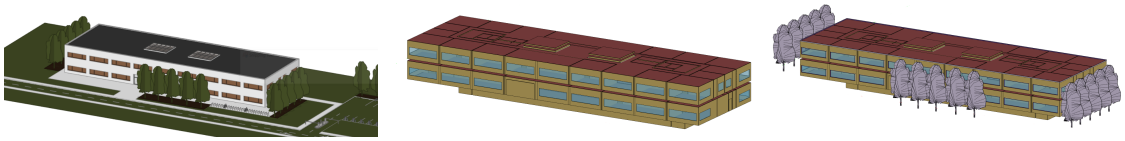

(a) IFC4 (b) IDF (c) IDF with external shadings

Figure 4.11: DigitalHub, IFC4 in BIMVision and EnergyPlus IDF in OpenStudio.

The mechanical cooling is implemented in EnergyPlus using an *IdealLoadsAirSystem* that uses an outdoor air economizer to reduce cooling loads in cases where these can be covered by outdoor air. In this mechanically conditioned building, for energy efficiency reasons, the heating setpoint is set to an operative temperature of 21 °C for occupied hours in office spaces with a heating setback to 18 °C at night. The cooling setpoint is set to an operative temperature of 26 °C in summer, and to 36 °C at unoccupied times to prevent cooling at night. An overview on the floor plans, use conditions, and schedules is given in Appendix A.10.2. The construction materials are chosen according to the KfW40 standard, as applied for the FZK-Haus in the previous use case in Section 4.7.1, resulting in the same U-values. For the unshaded building (Figure 4.11b), an annual heating energy consumption of 29.93 kWh/(m^{2}a) and a cooling energy consumption of 3.02 kWh/(m^{2}a) was simulated, using an unlimited heating capacity and an autosized cooling

[4] DigitalHub IFC4 model: https://github.com/RWTH-E3D/DigitalHub, accessed on June 11, 2025.
[5] IFC2SB Space Boundary Generation Tool: https://github.com/RWTH-E3D/IFC2SB., accessed on June 11, 2025.

capacity limit based on the *TypicalSummer* days provided in the TMYx weather file. For a comparison between the system sizing options and the impact on the simulation results, see Appendix A.8.1, and for a full set of BEPS results for the DigitalHub using extreme day system sizing, see Appendix A.8.3. The total energy demand for this setup is 61.61 kWh/(m^{2}a), including additional electric energy, 9.63 kWh/(m^{2}a) for lighting and 19.03 kWh/(m^{2}a) for electric equipment.

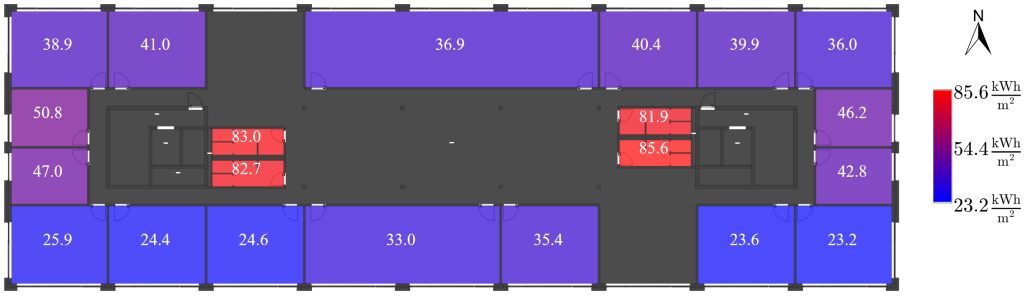

(a) Heating energy in kWh/(m^2 a)

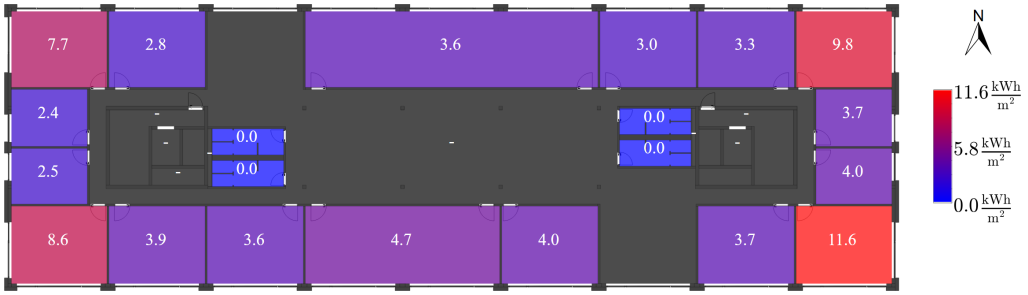

(b) Cooling energy in kWh/(m^2 a)

Figure 4.12: Heating and cooling energy consumption on the top floor, no external shadings. Operative temperature setpoints of 21 °C/26 °C during the occupied hours, and 18 °C/36 °C otherwise, for heating/cooling, respectively.

The resulting heating and cooling energy demand for individual spaces is displayed in Figure 4.12 for the top floor of the building, which mainly includes (group and open-plan) offices and meeting rooms. The spaces facing south show the lowest heating energy consumption, as they are heated by the incident solar radiation in winter. The spaces at the west and east side of the building have an increased heating load, as those meeting rooms require an increased demand of outdoor air. The spaces with the high heating loads in the east and west center of the building are the bathrooms. These high heating loads result from their surrounding mainly unconditioned traffic areas (i.e., heating setpoint 15 °C).

Figure 4.13 displays the annual mean PMV within the occupied hours per space. According to the comfort categories for PMV defined in DIN EN 16798-1, these annual mean PMV value are mainly within the Category II ($-0.5 < PMV < 0.5$) lower bounds, as they range from -0.4 to -0.5 in the spaces at the north side of the building, and result in a slightly warmer PMV prediction between -0.3 to -0.4 at the south side. The group offices at the south corners show the highest average PMV of -0.3, caused by the high solar gains during the day. This also leads to the highest cooling loads of the building, observed on the south-east corner (cf. Figure 4.12b).

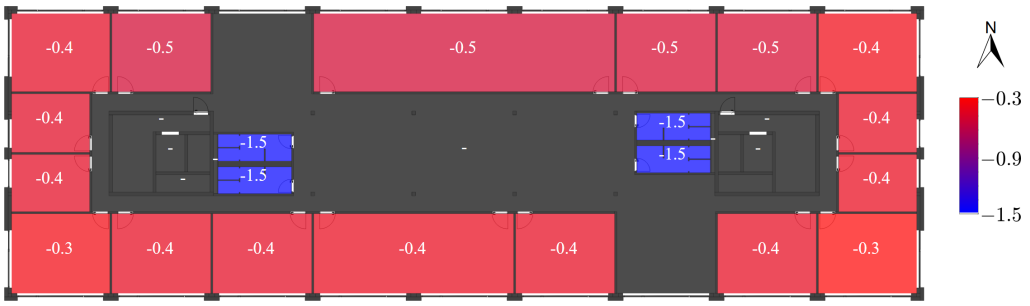

Figure 4.13: PMV mean (occupied hours) top floor, no external shadings. Operative temperature setpoints of 21 °C/26 °C during occupied hours for heating/cooling, respectively.

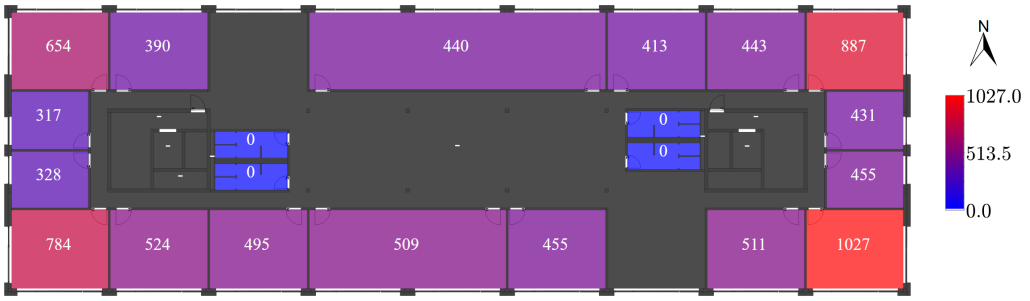

(a) Number of hours for $PMV > 0.5$.

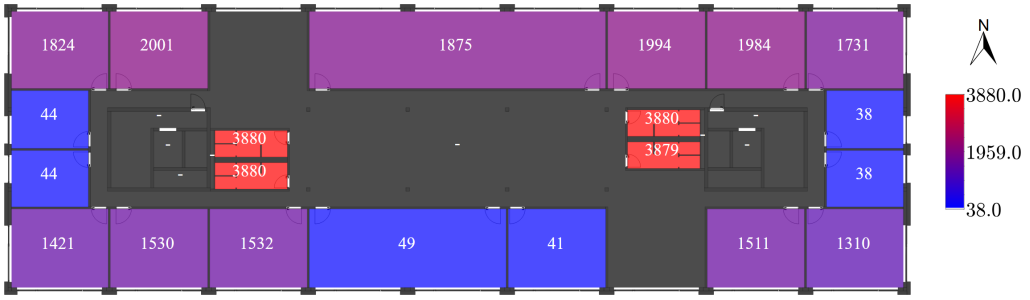

(b) Number of hours for $PMV < -0.5$.

Figure 4.14: Number of hours above and below Category II ($-0.5 < PMV < 0.5$) for the occupied hours on the top floor, without external shading.

However, even if the annual mean PMV values promise an all-year round thermally comfortable indoor climate for the office spaces, a detailed analysis of the actual hourly PMV values reveals a high number of hours exceeding the Category II comfort limits for the PMV, which are visualized in Figure 4.14. This figure displays the number of occupied hours above (Figure 4.14a) and below (Figure 4.14b) the acceptability limits of Category II. This analysis reveals, that a great number of hours per year the PMV is below the Category II limit, which is up to half of the occupied annual time for the north spaces, and about a third of the occupied hours in the south spaces. The number of hours exceeding the upper Category II limit is only about 8 to 13% of the occupied times, except for the spaces at corners of the building, ranging from 16 to 26%.

As the group office at the south-east corner of the building (i.e., *E01-13 Group Office*, cf. floor plan in Figure A.37) shows the highest number of hours with a PMV above the Category II limits, this space is additionally analyzed using a CFD-based thermal local thermal comfort

analysis for a hot summer day in Section 4.7.4 and in Appendix A.8.5. The annual heatmap of PMV categories for this space is displayed in Figure 4.15a. While the evaluation of Fanger's non-adaptive PMV and PPD metrics are in general designed for fully air-conditioned buildings like in this use case, the heating and cooling setpoints within this analyzed use case are too broad to be applicable for PMV analysis. This is derived from the hourly PMV heatmap of a typical group office, where the comfort categories I and II are only reached in a limited time of the year, even during occupancy. Narrowing the heating and cooling setpoints (e.g., 22 °C for heating and 23 °C for cooling) is expected to show a better performance with respect to the PMV categories. The evaluation of the adaptive comfort measures allows slightly better compliance with [DIN16798-1], as displayed in Figure 4.15b. This representation reveals that even in adaptive comfort, a large number of hours during the year exceed the upper comfort limit of the acceptable temperature range defined in [DIN16798-1], NA. Some of these observed operative temperatures exceed the operative cooling setpoint of 26 °C, which is caused by the limited cooling capability in this space, as the cooling capacity was sized for a typical summer day. In this space, an adaptive control of cooling would increase the time within the adaptive comfort bandwidth.

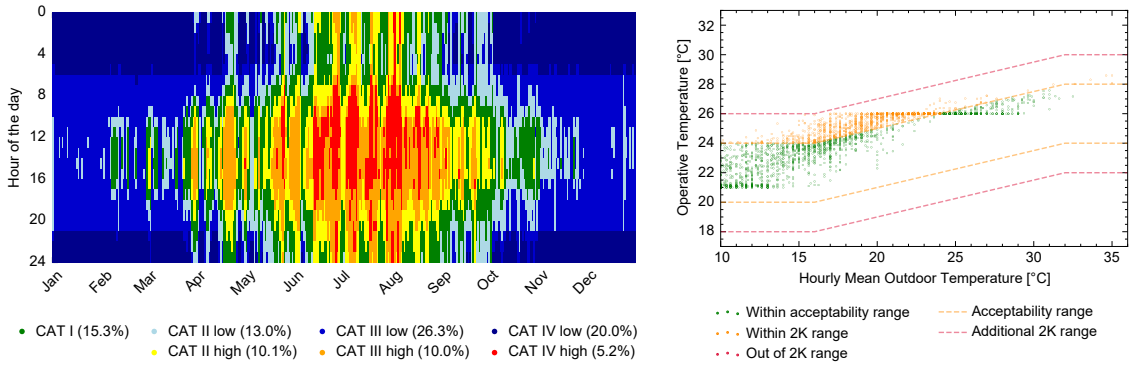

(a) Heatmap with PMV Categories.

(b) Adaptive thermal comfort.

Figure 4.15: Group office top floor, south-east corner according to [DIN16798-1], NA.

As displayed in Figure 4.16, the analysis of adaptive comfort of this *E01-13 Group Office* results in 564 Kh of unweighted temperature excess, which are 7% of the 2 K degree-hours instead of the acceptable 1% for the occupied time (cf. Section 4.4.1 and [DIN16798-1]). This evaluation of the excess hours further reveals that four other group offices (i.e., E00-10, E01-04, E01-10, E01-20) also exceed the acceptability limit of 1% excess degree-hours according to [DIN16798-1]. This south-east corner office (E01-13) even exceeds the threshold defined in [DIN4108-2] for non-residential buildings of 500 Kh per year for excess degree-hours. In Appendix A.8.5, the local thermal comfort for this office is evaluated using the *PluginOpenFOAM*, using the same typical day system sizing as applied here, while Use Case 4 (Section 4.7.4) provides a local thermal comfort analysis using improved extreme day system sizing for this office space.

Previous results were generated without considering external shading elements from external space boundaries, as those external space boundaries have only been observed as output from research tools. However, the following results include these external shadings generated from

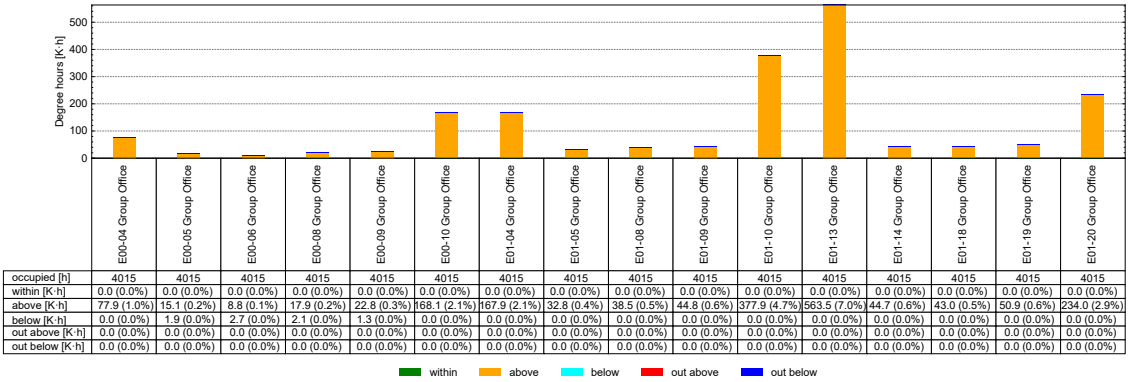

	E00-04 Group Office	E00-05 Group Office	E00-06 Group Office	E00-08 Group Office	E00-09 Group Office	E00-10 Group Office	E01-04 Group Office	E01-05 Group Office	E01-08 Group Office	E01-09 Group Office	E01-10 Group Office	E01-13 Group Office	E01-14 Group Office	E01-18 Group Office	E01-19 Group Office	E01-20 Group Office
occupied [h]	4015	4015	4015	4015	4015	4015	4015	4015	4015	4015	4015	4015	4015	4015	4015	4015
within [K·h]	0.0 (0.0%)	0.0 (0.0%)	0.0 (0.0%)	0.0 (0.0%)	0.0 (0.0%)	0.0 (0.0%)	0.0 (0.0%)	0.0 (0.0%)	0.0 (0.0%)	0.0 (0.0%)	0.0 (0.0%)	0.0 (0.0%)	0.0 (0.0%)	0.0 (0.0%)	0.0 (0.0%)	0.0 (0.0%)
above [K·h]	77.9 (1.0%)	15.1 (0.2%)	8.8 (0.1%)	17.9 (0.2%)	22.8 (0.3%)	168.1 (2.1%)	167.9 (2.1%)	32.8 (0.4%)	38.5 (0.5%)	44.8 (0.6%)	377.9 (4.7%)	563.5 (7.0%)	44.7 (0.6%)	43.0 (0.5%)	50.9 (0.6%)	234.0 (2.9%)
below [K·h]	0.0 (0.0%)	1.9 (0.0%)	2.7 (0.0%)	2.1 (0.0%)	1.3 (0.0%)	0.0 (0.0%)	0.0 (0.0%)	0.0 (0.0%)	0.0 (0.0%)	0.0 (0.0%)	0.0 (0.0%)	0.0 (0.0%)	0.0 (0.0%)	0.0 (0.0%)	0.0 (0.0%)	0.0 (0.0%)
out above [K·h]	0.0 (0.0%)	0.0 (0.0%)	0.0 (0.0%)	0.0 (0.0%)	0.0 (0.0%)	0.0 (0.0%)	0.0 (0.0%)	0.0 (0.0%)	0.0 (0.0%)	0.0 (0.0%)	0.0 (0.0%)	0.0 (0.0%)	0.0 (0.0%)	0.0 (0.0%)	0.0 (0.0%)	0.0 (0.0%)
out below [K·h]	0.0 (0.0%)	0.0 (0.0%)	0.0 (0.0%)	0.0 (0.0%)	0.0 (0.0%)	0.0 (0.0%)	0.0 (0.0%)	0.0 (0.0%)	0.0 (0.0%)	0.0 (0.0%)	0.0 (0.0%)	0.0 (0.0%)	0.0 (0.0%)	0.0 (0.0%)	0.0 (0.0%)	0.0 (0.0%)

Figure 4.16: Adaptive excess degree-hours for all group offices in the DigitalHub.

external space boundaries, representing the shading of the window by its surrounding walls and the trees, resulting in the tree-shading of the west windows, as well as of parts of the south and east windows, visualized in Figure 4.11c. Figure 4.17 exemplary shows the shading for the south-east group office on the top floor, which has now a shaded east facade. Considering the partial shading of the building, the energy consumption is now increased by 3.16 kWh/(m^{2}a) (10.56%) to 33.09 kWh/(m^{2}a) for heating and slightly decreased by 0.66 kWh/(m^{2}a) (−21.85%) to 2.36 kWh/(m^{2}a) for cooling.

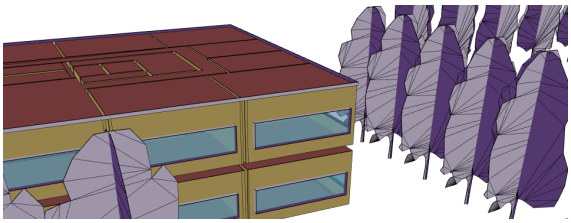

Figure 4.17: External Shadings for the group office at the south-east corner of the DigitalHub.

Looking at the number of hours exceeding the Category II limits for the PMV, the number of hours below the limit increases compared to the unshaded results in Figure 4.14, especially for the shaded building parts, while the number of hours above these limits drastically decrease (cf. Figure 4.18). As the group office at the north-east corner of the building is not directly surrounded by trees, it shows the lowest reduction of excess hours.

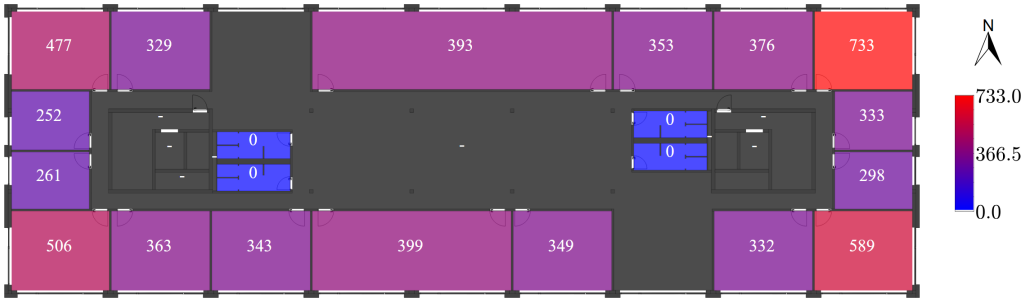

Figure 4.18: Number of hours with PMV above 0.5, CAT II (occupied hours) top floor, with external shadings.

This reduction of hours with high PMV is also reflected in the resulting hourly heatmap for the

south-east group office in Figure 4.19a. The evaluation of the operative temperatures within the adaptive comfort limits in Figure 4.19b reveals a drastic reduction of excess hours.

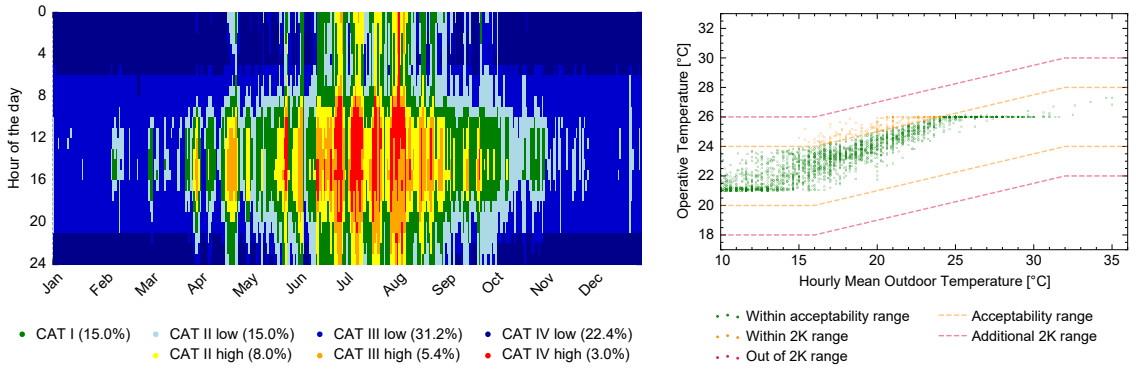

(a) Heatmap with PMV Categories

(b) Adaptive thermal comfort

Figure 4.19: Group office top floor, south-east corner according to [DIN16798-1], NA, with external shadings.

Considering the external shadings, this group office only shows 64.7 Kh excess degree-hours (0.8%, i.e., reduction of 6.2% compared to case without external shadings) and is thus within the 1% limit of acceptability. In this use case with external shadings, only one other office space remains that exceeds the temperature limits in adaptive comfort according to [DIN16798-1], NA, as displayed in Figure 4.20. The north-east corner *E01-10 Group Office*, which has the least shaded facade, now shows the highest excess degree-hours of 208.1 Kh (1.6% above the acceptability limit). The threshold of 500 Kh excess according to [DIN4108-2] is not exceeded in this shaded use case.

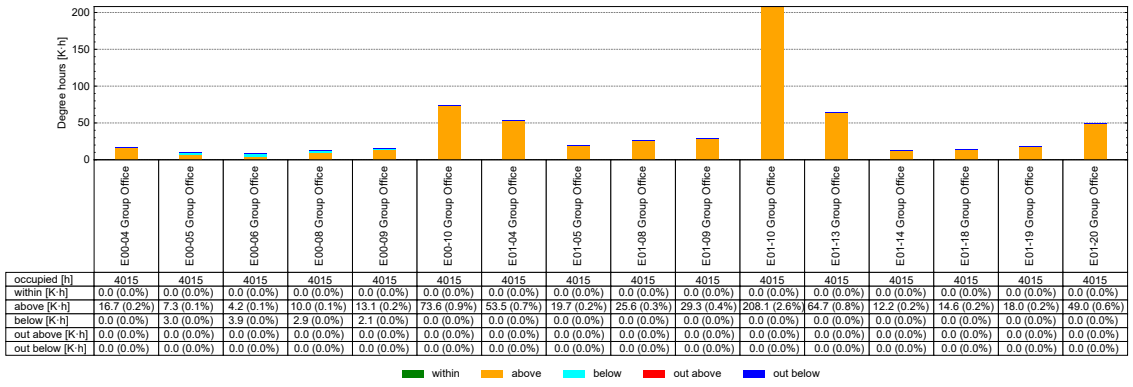

	E00-04 Group Office	E00-05 Group Office	E00-06 Group Office	E00-08 Group Office	E00-09 Group Office	E00-10 Group Office	E01-04 Group Office	E01-05 Group Office	E01-08 Group Office	E01-09 Group Office	E01-10 Group Office	E01-13 Group Office	E01-14 Group Office	E01-18 Group Office	E01-19 Group Office	E01-20 Group Office
occupied [h]	4015	4015	4015	4015	4015	4015	4015	4015	4015	4015	4015	4015	4015	4015	4015	4015
within [K·h]	0.0 (0.0%)	0.0 (0.0%)	0.0 (0.0%)	0.0 (0.0%)	0.0 (0.0%)	0.0 (0.0%)	0.0 (0.0%)	0.0 (0.0%)	0.0 (0.0%)	0.0 (0.0%)	0.0 (0.0%)	0.0 (0.0%)	0.0 (0.0%)	0.0 (0.0%)	0.0 (0.0%)	0.0 (0.0%)
above [K·h]	16.7 (0.2%)	7.3 (0.1%)	4.2 (0.1%)	10.0 (0.1%)	13.1 (0.2%)	73.6 (0.9%)	53.5 (0.7%)	19.7 (0.2%)	25.6 (0.3%)	29.3 (0.4%)	208.1 (2.6%)	64.7 (0.8%)	12.2 (0.2%)	14.6 (0.2%)	18.0 (0.2%)	49.0 (0.6%)
below [K·h]	0.0 (0.0%)	3.0 (0.0%)	3.9 (0.0%)	2.9 (0.0%)	2.1 (0.0%)	0.0 (0.0%)	0.0 (0.0%)	0.0 (0.0%)	0.0 (0.0%)	0.0 (0.0%)	0.0 (0.0%)	0.0 (0.0%)	0.0 (0.0%)	0.0 (0.0%)	0.0 (0.0%)	0.0 (0.0%)
out above [K·h]	0.0 (0.0%)	0.0 (0.0%)	0.0 (0.0%)	0.0 (0.0%)	0.0 (0.0%)	0.0 (0.0%)	0.0 (0.0%)	0.0 (0.0%)	0.0 (0.0%)	0.0 (0.0%)	0.0 (0.0%)	0.0 (0.0%)	0.0 (0.0%)	0.0 (0.0%)	0.0 (0.0%)	0.0 (0.0%)
out below [K·h]	0.0 (0.0%)	0.0 (0.0%)	0.0 (0.0%)	0.0 (0.0%)	0.0 (0.0%)	0.0 (0.0%)	0.0 (0.0%)	0.0 (0.0%)	0.0 (0.0%)	0.0 (0.0%)	0.0 (0.0%)	0.0 (0.0%)	0.0 (0.0%)	0.0 (0.0%)	0.0 (0.0%)	0.0 (0.0%)

Figure 4.20: Adaptive excess degree-hours for all group offices in the DigitalHub.

The limited local discomfort checks passed in all cases, for both the unshaded and the shaded building. The implementation of BEPS-based local discomfort according to [DIN16798-1] is designed to detect significant differences between indoor air and surface temperatures that cause local discomfort. However, as the analyzed building is well-insulated and provides low U-values according to the KfW 40 standard, the changes in outdoor air temperature have only a minor effect on the surface temperatures, preventing drastic changes in indoor air temperature. The simulation of buildings with lower insulation standards results in higher local discomfort,

which is caused by a stronger decrease of surface temperatures during heating setbacks at night and a stronger impact of solar radiation on the surface temperature increase on hot summer days. This effect is further analyzed in the following Section 4.7.3.

This thermal comfort analysis for a mechanically ventilated building using IFC-based BEPS was executed on an hourly annual basis for the individual thermal zones of the buildings. The implemented IFC-based methods for thermal comfort analysis provide quick insights into the impact of model changes on thermal comfort. The presented comfort analysis underlines the importance of correctly modeling external shadings to increase the reliability of simulation results. The heating and cooling setpoints were chosen to comply with typical design parameters used in Germany. However, the difference between heating and cooling setpoints of 5 K may be too large to comply with the defined thresholds for the non-adaptive comfort metric PMV according to [DIN16798-1] and would require an increase of the heating setpoint and a decrease of the cooling setpoint to comply with the PMV requirements of Category II. The evaluation of adaptive comfort metrics shows better applicability for this range of setpoints.

4.7.3 Use Case 3: Local Thermal Comfort in Heating Period using OpenFOAM

The local discomfort of the winter case is evaluated for the FZK Haus, using the Cologne/Bonn TMYx (2007-2021) weather. The *EG-02 Single office* space, located in north-west corner of the ground floor of the FZK Haus (cf. Figure 2.17) is evaluated on January 17, 8am, as this has shown one of the lowest PMV values of the year. The space temperature is controlled for operative temperature of 21 °C in the BEPS simulation. The resulting local thermal comfort is simulated and compared for the KfW40 construction setup (KfW case) with triple-glazing windows, as well as with IWU heavy construction for the year 1960 (IWU case) (cf. Section 2.7.1), with double-glazing and wooden frames. Those envelope parameter sets are selected to compare the impact of low U-values on local discomfort, since an increased local discomfort is expected for buildings with lower insulation standards. An overview on the applied use conditions and schedules is given in Appendix A.10.1, which are applied as use conditions for both construction variants. The resulting U-values and BEPS-based annual energy consumptions are presented in Table A.9.

The indoor and outdoor temperatures simulated using the *PluginEnergyPlus* are displayed in Figure 4.21 for both construction sets. Both cases are simulated for the selected space and time using the *PluginOpenFOAM* with P1 and fvDOM radiation model with 30% radiation on the radiator surface, 70% on the porous medium. The BEPS results in Figure 4.21 show a high indoor air temperature of 24.59 °C for the IWU case, caused by the high U-values for these constructions (e.g., 1.27 W/(m^{2}K) for external walls, 2.17 W/(m^{2}K) for the roof, 2.7 W/(m^{2}K) for windows) resulting in high heat losses and low surface temperatures, which are compensated in the operative room temperature control. Due to this compensation in the operative temperature by increasing the indoor air temperature, the resulting PMV only slightly differs between these cases.

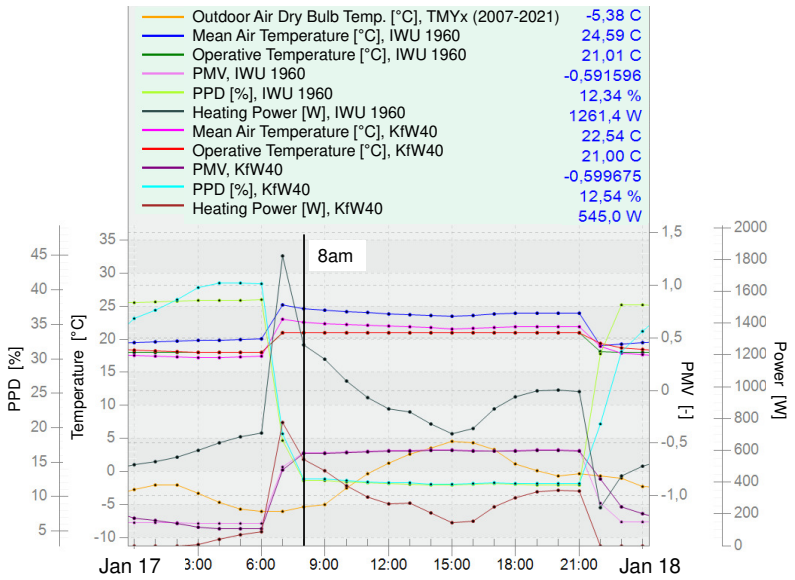

Figure 4.21: Outdoor air temperature, zone air and operative temperature, PMV, PPD in the FZK Haus office, using IWU 1960 and KfW40 constructions, simulated in EnergyPlus for the TMYx (2007-2021) weather data for Cologne/Bonn Airport, January 17, 8am. Visualization adapted from DesignBuilder Results Viewer.[6]

This operative temperature control may lead to very high air temperatures in some extreme winter cases, as visualized for the *EG-05 Living* room (ground floor) in Figure A.12, showing an air temperature of 25.7 °C. These high air temperatures in the BEPS results lead to high radiation asymmetry on 32 days in this *EG-05 Living* room, as the mean air temperature shows large differences from the wall surface temperatures (> 10 K, Category II limit [DIN16798-1]) in the morning after heating up the space after night setback. This occurs at 6am at all of these days, and additionally at 7am at two of these days. The *OG-07 Living* room on the first floor shows a radiant asymmetry on more than fifty days, which result from large temperature differences between mean air temperature and wall surface temperatures as observed on the ground floor, but also in additional six cases, a local asymmetry is caused by large differences between air temperature and ceiling temperature (> 14 K, Category II limit [DIN16798-1]). Even more significant for the local discomfort in the IWU 1960 building are the low floor surface temperatures below the Category II limit of 19 °C, which are observed in all spaces, e.g., for up to 86% of the occupied time in both living rooms. This includes the time during night setback. Thus, this IWU 1960 case shows a significantly worse local thermal comfort than the KfW40 case of the FZK Haus (cf. Section 4.7.1), which was expected due to the poor U-values of the IWU case (cf. Table A.9).

The CFD simulation for the *EG-02 Single office* space at the north-west corner of the FZK Haus was executed for 20 000 iterations in a steady-state using the *buoyantSimpleFOAM* solver. The quasi-steady state was reached after approximately 3500 iterations in all cases. The OpenFOAM setup did not include ventilation and thus represents the simplified case of an airtight building

[6] DesignBuilder Results Viewer, Version 4.1, https://designbuilder.co.uk/download/previous-versions, accessed on June 05, 2025.

without infiltration and natural ventilation. The simulations were executed on 48 CPUs on a non-exclusive node on CLAIX23, such that the resulting execution times may include disturbances from other simulations. The execution times for 20 000 steady state iterations were measured for the fvDOM cases 3089.69 s (IWU) and 2787.53 s (KfW), and for the P1 cases 1409.83 s (IWU) and 1307.48 s (KfW). Both KfW cases required less computational time for the requested number of iterations, which can be caused by the lower temperature differences within the domain due to the high insulation rate.

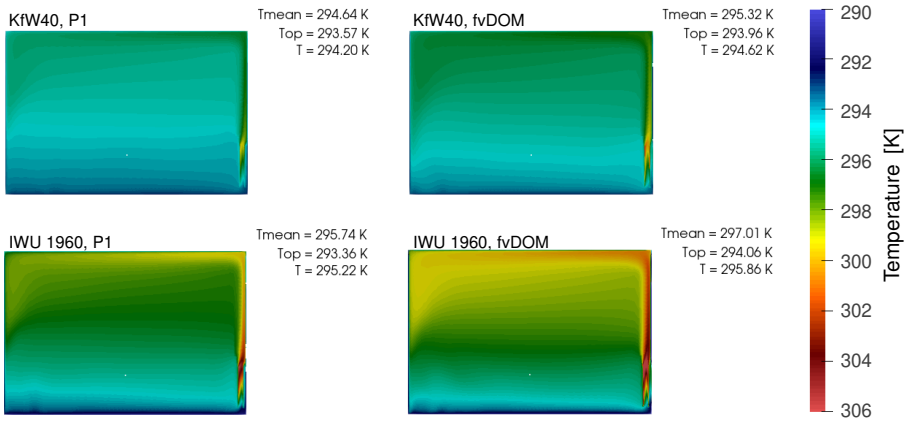

Figure 4.22: Air temperature, mean air temperature over slice, and air and operative temperature at z=0.6 m above floor level in the FZK Haus office on January 17, 8am.

Figure 4.22 displays the mean air temperature at a vertical slice through the radiator. The high heating loads in the IWU case result in a high temperature stratification caused by the radiator. The stratification is stronger for cases simulated with the radiation model fvDOM than in cases with the P1 model. These differences in stratification result from the simplified radiation calculation in the P1 radiation model, as opposed to the ray-tracing approach applied in the fvDOM approach. The temperature stratification of the KfW40 case is smaller due to the lower heating demand, and thus lower heating power of the radiator. Additionally to the mean air temperature, the air and operative temperatures are stated in Figure 4.22 at the center of the slice for a height of $z = 0.6$ m above floor level, which is the required location according to [DIN16798-1] for the measurement of operative temperatures in spaces with temperature stratification. For the P1 radiation model, the operative air temperatures deviate 0.58 K (KfW) and 0.79 K (IWU) from the EnergyPlus operative temperature of 21 °C = 294.15 K. For the fvDOM radiation, these differences are lower, i.e. 0.19 K (KfW) and 0.09 K (IWU). The mean air temperatures show larger deviations. The EnergyPlus simulation of the KfW40 case resulted in a mean air temperature of 22.54 °C (=295.69 K), which is a difference of 1.05 K (P1) and 0.37 K (fvDOM). The mean air temperature of the IWU case was simulated in EnergyPlus as 24.59 °C (=297.74 K). The resulting mean air temperature differences are 2.0 K (P1) and 0.74 K (fvDOM). Here, the fvDOM model again outperforms the P1 model, as it better captures the differences of operative and air temperatures, and thus promises more accurate results for local thermal comfort evaluations.

These differences in the temperature stratification are also measured in the evaluation of the

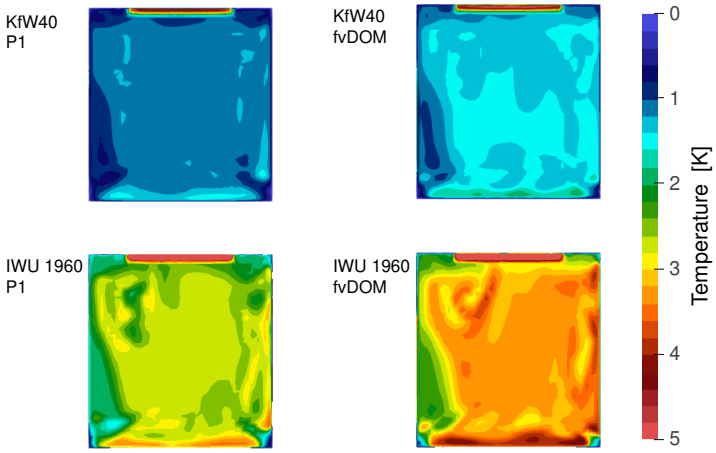

Figure 4.23: Vertical air temperature difference between a height of 0.1 m (foot level) and 1.1 m (head level) on January 17, 8am.

local thermal discomfort caused by vertical temperature differences between head (1.1 m) and feet (0.1 m) level, displayed in Figure 4.23. While the KfW case presents acceptable vertical air temperature differences in the occupied zone between 1 and 1.4 K (P1) and 1.2 and 1.6 K (fvDOM), the IWU case partially exceeds the Category II threshold of 3 K. While for the P1 radiation model, the vertical temperature difference ranges from 2.4 to 3.0 K, for the fvDOM model it exceeds the 3 K limit in most of the occupied space. For the further evaluation on vertical temperature differences, the fvDOM model should be applied as it provides better results, while the P1 model tends to result in lower stratification due to its simplified radiation model. The use of the fvDOM model is particularly important for use cases with high heating and cooling loads, resulting in high air temperature stratification. This effect may be amplified for cases with furniture and people, as these require a more detailed modeling of radiation.

The observed DR at head height (1.1 m) is below 5% in all simulated cases, and meets the requirement of comfort Category I according to [DIN16798-1] (cf. Figure A.13). The air velocity threshold for Category II is defined as 0.13 m/s. As visualized in Figure A.14, all areas exceeding this threshold are located at the ceiling, caused by the heater's buoyancy, and in the corners of the space, and thus do not affect the occupied space.

The evaluation of the local thermal comfort for non-ventilated, unoccupied cases using IFC-based OpenFOAM revealed an increased risk of local discomfort in buildings with low insulation standards, as demonstrated for the IWU 1960 use case. The use case with the KfW40 constructions provided a high local thermal comfort, due to the low heating loads and moderate surface temperatures.

As the IWU 1960 case included larger local discomfort, this case is further analyzed for the impact of furniture and people on the evaluation of local thermal comfort. The heating power of the radiator is diminished by the heat released by the occupant. Figure 4.24 displays the air temperatures for this case (cf. Figure 4.22 without furniture). Here, the mean air temperature shows a similar deviation from the EnergyPlus results of 1.97 K for the P1 radiation model, and a

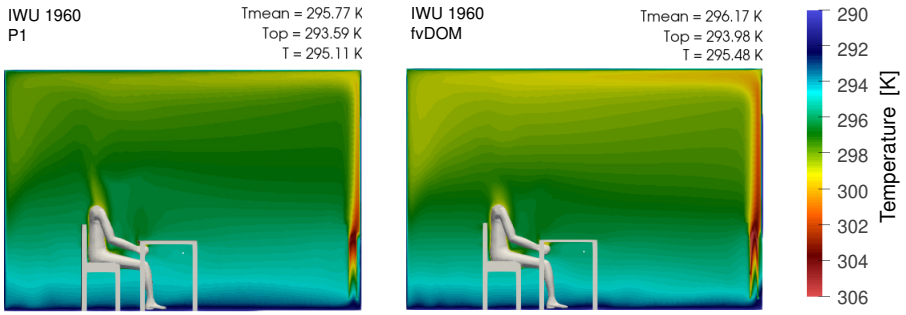

Figure 4.24: Air temperatures, mean air temperature over slice, and air and operative temperature at z=0.6 m above floor level on January 17, 8am.

larger error of 1.57 K for the fvDOM model compared to the empty space. This larger error may result from disturbed radiative heat transfer caused by interior elements (furniture, occupants) in the fvDOM case, compared to the simplified radiation calculations in EnergyPlus, which do not account for the geometry of internal elements. The operative temperature is similar to the case without furniture; however, here, the measurement position for evaluation (i.e., at center of space, 60 cm above floor) is located right underneath the table, which may impact the result. The vertical air temperature differences between head and feet level in Figure 4.25 show similar differences and patterns as those in the case without furniture in Figure 4.23.

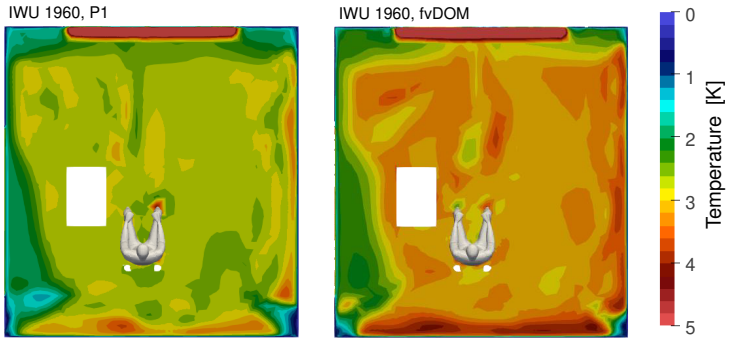

Figure 4.25: Vertical air temperature difference between a height of 0.1 m (foot level) and 1.1 m (head level) on January 17, 8am.

Figure 4.26a visualizes the DR at head level, which is slightly increased around the persons head, while the overall flow pattern remain, compared to the previous empty space displayed in Figure A.13. The visualization of the air velocities exceeding 0.13 m/s, displayed in Figure 4.26b allow a more detailed analysis of discomfort risk with a high spatial resolution. The increased air velocity above the person's head result from the buoyancy forces caused by the assumed skin temperatures. A coupled thermo-physiological model, such as MORPHEUS [Wöl17] (cf. Section 4.1), would increase the reliability of these results.

The additional evaluation of the space including furniture revealed that the temperature distribution in the space is only minorly affected by the chosen occupied office desk setting. The vertical air temperature evaluation revealed similar results. The local evaluations that are predominately affected by air velocities, such as DR and air velocity magnitude, increase the spatial accuracy of the results, as they can capture airflow and resulting turbulence around interior

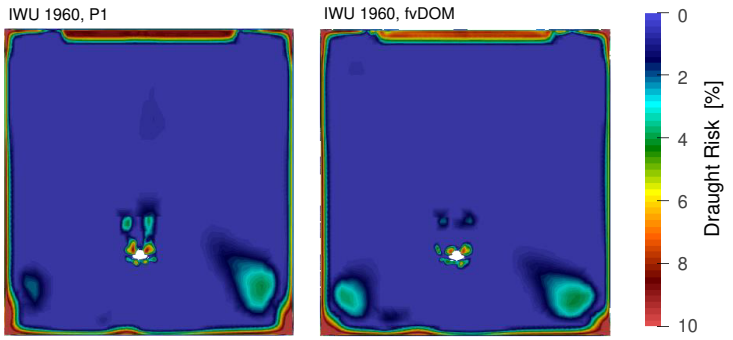

(a) DR at 1.1 m (head level)

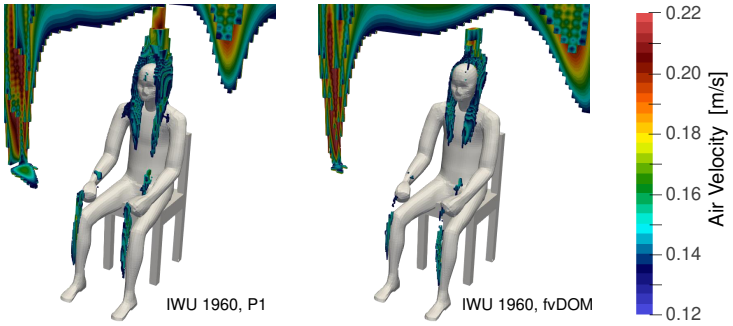

(b) Air velocities larger than 0.13 m/s

Figure 4.26: Draught risk and air velocity evaluation for the occupied FZK Haus on on January 17, 8am.

elements and occupants. These findings may be limited to cases without ventilation that just consider buoyancy forces.

4.7.4 Use Case 4: Local Thermal Comfort in Cooling Period

While the previous Use Case 3 evaluated CFD-based local thermal comfort during the heating period in a simplified occupied *Single office* setting without ventilation, Use Case 4 addresses the evaluation of local thermal comfort during the cooling period, including two occupied office desk setups. An overview on the applied use conditions and schedules is given in Appendix A.10.2. The evaluation focuses on the use case of the KfW40 DigitalHub office building without external shading elements. The *E01-13 Group office* space on the south-east corner of the building is simulated for the ventilation scenarios of down- and sidewards outflow of the air inlet, including an overflow through a cutout underneath the door, cf. Figure 3.12. The two ventilation scenarios are analyzed for a day with high cooling demands on August 2, 4pm, using the TMYx (2007-2021) historic weather data for Cologne/Bonn Airport [LC22].

The use of system sizing for a typical summer day (cf. annual BEPS analysis in Section 4.7.2) results in exceeded cooling capacity limits for the analyzed hot summer day. As visualized in Figure A.15, the EnergyPlus simulation results an operative temperature of 28.59 °C and a mean air temperature of 27.67 °C. The cooling system, sized for the typical summer day, reaches its maximum cooling capacity from 9am to 6pm on August 2. As this system sizing for a typical

summer day results in exceeded cooling setpoints by 2.59 K, this use case is not suitable as a baseline scenario for further analysis of local thermal comfort using future extreme weather scenarios in the following Chapter 5. Thus, the local comfort results using the typical system sizing are included in Appendix A.8.5 for further reference, while the further local comfort analysis in this section uses the extreme day system sizing for defining the maximum cooling capacities. An analysis of the annual BEPS results using the extreme-day-sized capacities is presented in Appendix A.8.3. The differences in the annual energy demand and in local comfort are small compared to the typical day results from Section 4.7.2, but show a significant effect on hot summer days, as visualized in Figure A.7. A full overview on the BEPS results of the DigitalHub is presented in Table A.10.

To provide a basis for further evaluation of predefined cooling capacity limits using future weather scenarios, the system sizing for the TMYx is repeated for the extreme winter and summer days (cf. Appendix A.8.3 for annual BEPS results). This scenario has an annual heating demand of 27.88 kWh/(m^{2}a) and a cooling demand of 1.81 kWh/(m^{2}a). Considering the electric energy use for lighting 9.63 kWh/(m^{2}a) and electric equipment 19.03 kWh/(m^{2}a), the building has a total energy consumption of 58.35 kWh/(m^{2}a).

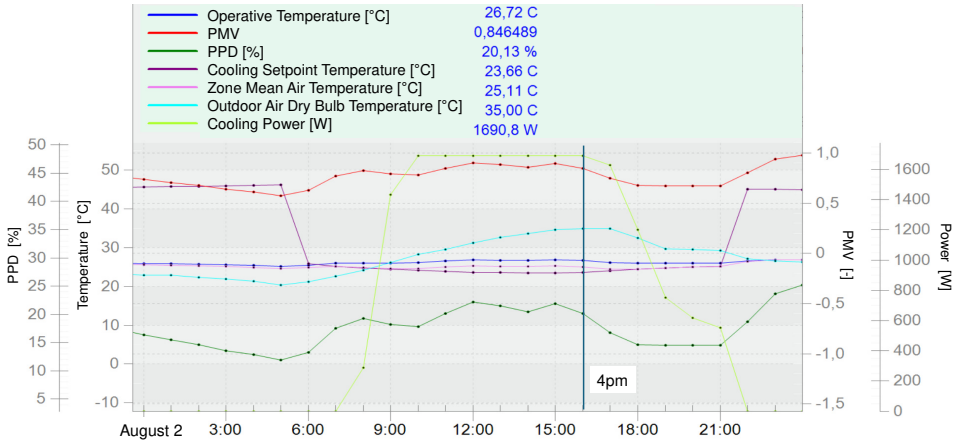

Figure 4.27: EnergyPlus results for the south-east office space on August 2, 4pm. T_{op} = 299.87 K, T_{mean} = 298.26 K, $T_{set,cool}$ = 296.81 K, sized and simulated using extreme summer day of TMYx (2007-2021) weather data for Cologne/Bonn Airport.

The BEPS results for August 2 are displayed in Figure 4.27. The maximum cooling power is fixed to 1690.8 W, which corresponds to the maximum peak cooling load on the extreme summer design day of the TMYx historic weather file. Based on these BEPS results, the CFD model was parametrized using the *PluginOpenFOAM*. Figure 4.28a displays the air temperature distribution at a vertical slice through the center of the domain. The downward outflow produces a higher temperature stratification than the sidewards outflow. Both types of air inlet results show similar results ($\Delta T_{mean,slice}$ = 0.37 K, $\Delta T_{op,0.6m}$ = 0.14 K). The comparison of these temperatures to the BEPS results reveals slightly larger deviations, ΔT_{mean} = 1.43/1.05K (outflow down/side) and ΔT_{op} = 0.32/0.46K (down/side).

Figure 4.28b verifies these differences in temperature stratification by displaying the air temperature difference between (1.1 m) and feet (0.1 m) level of the space. The vertical difference is

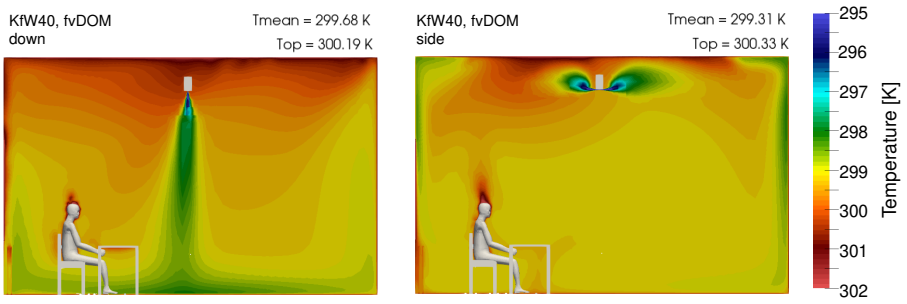

(a) Vertical temperature distribution

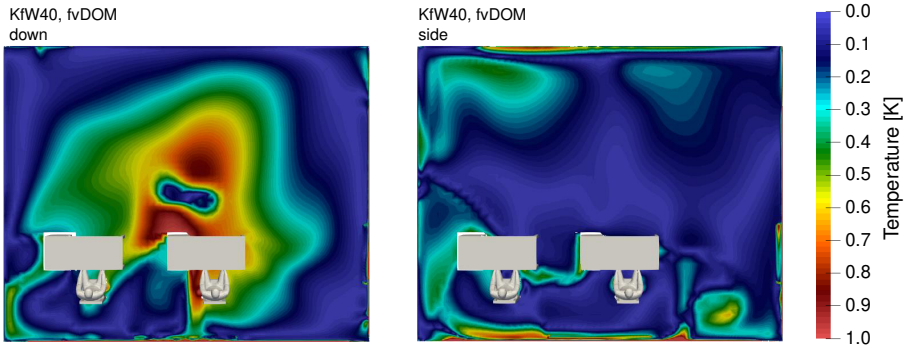

(b) Vertical temperature difference between head (1.1 m) and feet (0.1 m) level.

Figure 4.28: Vertical temperature distribution and difference in the south-east office space for down- and sidewards outflow direction. Simulated for August 2, 4pm, sized and simulated using extreme summer day of TMYx (2007-2021) weather data for Cologne/Bonn Airport.

below the threshold for Category I [DIN16798-1] (=2 K). However, the downward-facing airflow results in an uneven temperature distribution in space. The observed air velocity exceeding the Category II limit of 0.2 m/s in summer is displayed in Figure 4.29. The downward-facing inlet leads to exceeded air velocity limits at the floor level, also affecting the office desk settings, which is also reflected in the DR in Appendix A.8.6, Figure A.20a. The sideward-facing outflow results in increased air velocity at the ceiling and the walls, as well as at the upper body and head of the person sitting on the right-hand side in Figure 4.29. This does not affect the DR for this person (cf. Figure A.20a).

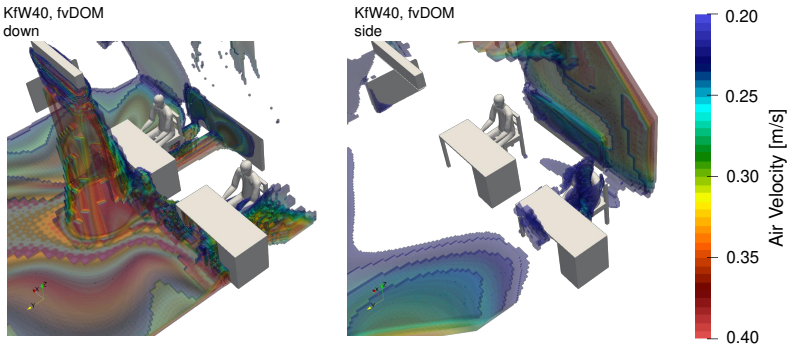

Figure 4.29: Air velocity above the Category II threshold (0.2 m/s in summer) defined in [DIN16798-1], NA, in the south-east office space for down- and sidewards outflow direction. Simulated for August 2, 4pm, sized and simulated using extreme summer day of TMYx (2007-2021) weather data for Cologne/Bonn Airport.

Figure 4.30 displays the comfort measures PMV, PPD, DR, but also the AoA on the vertical slice. Both outflow directions result in a mean PMV of 1.02, which is 0.17 larger than the BEPS results for this timestep on August 2, 4pm. The resulting PPD from the CFD analysis is also about 7% higher than the BEPS result. The mean DR at head level is between 4-5%, and thus within the acceptable limits of [DIN16798-1]. The downward-facing outflow, however, exceeds the Category II limit for DR (15%) below the inlet. The two outflow directions of the inlet result in differences in the air mixture of the room, resulting in a higher AoA for the sideward-facing outflow, which is also visible in the vertical slice in Figure A.20b.

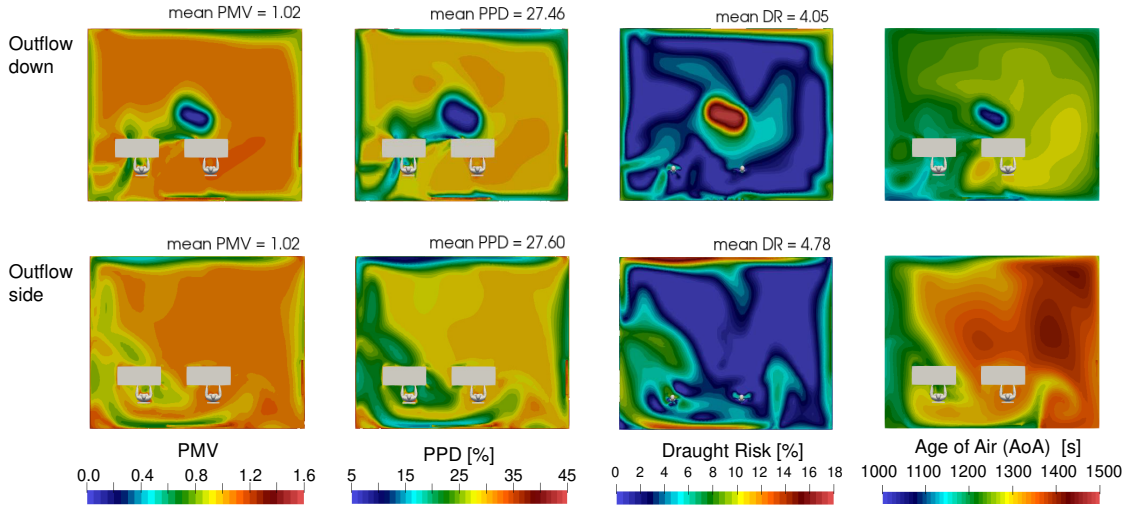

Figure 4.30: PMV, PPD, and Age of Air at a height of 0.6 m and draught risk at a height of 1.1 m in the south-east office space for down- (top) and sidewards (bottom) outflow direction. Simulated for August 2, 4pm, sized and simulated using extreme summer day of TMYx (2007-2021) weather data for Cologne/Bonn Airport.

The observed high operative temperatures in space, exceeding the 26 °C threshold for Category II ([DIN16798-1], NA) by more than 1 K in both airflow cases, could be compensated using occupant-controlled local ventilation, i.e., induced by a local fan (cf. Section 4.4.1), which allows the increase of operative air temperatures in the space by 1.2 K even for low air velocities of 0.6 m/s on office desk level.

4.8 Evaluation and Summary of the Research Hypotheses

This section evaluates the RHs on IFC-based thermal comfort analysis defined in Section 4.2.2 under the scope of the RQs in Section 1.3. The proposed methodology for an IFC-based thermal comfort setup using BEPS and CFD simulations was successfully implemented, evaluated, and validated for plausibility to prove RH TC 1 within the scope of RQ 1. The results were validated for plausibility due to the lack of suitable sets of IFC and monitoring data for the purpose of IFC-based thermal comfort analysis. The evaluation of the results has shown that the IFC-based BEPS analysis provides insight into the annual hourly thermal comfort performance at the zonal level (RH TC 1, Part 1). This BEPS-based assessment allows the identification of indoor

spaces with the highest risk of thermal discomfort using available international thermal comfort metrics. The annual hourly analysis enables the detection of periods with a high risk of low indoor air temperatures or overheating. The use of external shading elements (here, trees from IFC data transformed to space boundaries by the IFC2SB tool) results in a significant reduction of summerly overheating. The annual BEPS results further support a simplified local discomfort detection by analyzing radiant asymmetry and exceeded floor temperatures.

These identified discomfortable spaces, as well as those spaces with high heating or cooling demands due to either external or internal loads, can be selected for a further detailed CFD-based local thermal comfort analysis. This CFD-based analysis allows the spatially high-resolved analysis of thermal comfort within individual thermal zones, including the analysis of the effectiveness of the air distribution considering interior elements and occupants (RH TC 1, Part 2). This CFD analysis is applied to only a single timestep (steady-state), which could also be executed as a transient simulation to simulate the dynamic effects within spaces (e.g., changes in internal loads due to occupancy, external loads, or changes in HVAC setpoints). Further evaluations are required on the impact of radiation models on fully air-conditioned spaces in both heating and cooling scenarios, as the radiation models were only evaluated for cases without ventilation for a heating case. Further research should provide an analysis for the occupied zone according to [DIN16798-3], cf. Section 4.4.2, as the occupied zone was only evaluated by visual analysis of vertical and horizontal slices through the domain, but not for the occupied space volume as whole.

Within the thermal comfort evaluation, the operative temperature is controlled as setpoint temperature to provide better compliance with thermal comfort standards even for buildings with low thermal insulation, resulting in high deviations between indoor air and operative temperatures. This operative temperature control may not be feasible in real-world scenarios as it requires measurement devices with a higher complexity (i.e., a globe thermometer), resulting in higher costs compared to measuring air temperature.

Since CFD simulations are computationally expensive and should only be run for specific time frames, the combination of BEPS and CFD-based thermal comfort analysis provides a sound basis for efficient building evaluation, which was tested in the use cases. Using IFC as a common data source, these simulation approaches are thus accessible within open-BIM design workflows. The proposed methods for the IFC-based approaches for BEPS- and CFD-based thermal comfort analysis have thus not only proven the scope of RH TC 1 as part of RQ 1. This work also proposed combining these methods for building thermal performance assessment to minimize computational effort in a sustainable design process, which addresses RQ 3. Within the efforts on combining the BEPS- and CFD-based approaches, the appropriate sizing of HVAC systems and capacities is crucial. While the analysis of annual BEPS results only reveals differences between the sizing options for typical and extreme days, the evaluation of single extreme days underlines the failures of incorrectly sized systems. This outcome is crucial for the further evaluation of the impact of climate change on indoor thermal comfort.

Despite the analysis of thermal comfort, the indoor air quality should be evaluated to optimize

the general energy consumption to maintain a comfortable indoor climate. Considering the current implementation of the IFC-based BEPS setup, it uses an ideal loads air system in EnergyPlus, using an outdoor air economizer to reduce the cooling loads. The resulting reduced cooling loads may reflect similarities towards mixed-mode operation of buildings, even if natural ventilation by opening windows is not considered. Here, further validation of the ventilation operation is required to quantify the actual impact of the outdoor air economizer on the cooling load.

The personal parameters (activity level and clothing), which are required for the application of common thermal comfort metrics, are currently not available as standardized property sets in the IFC schema, and thus are not applicable for the automated IFC-based thermal comfort simulation setup. Therefore, for the integration of thermal comfort analysis in IFC-based BEPS and CFD simulations, an extension of the existing templates for zone-usage-based enrichment was required, which was defined in RH TC 2, addressing RQ 2. The parameter set was developed as an extension of the TEASER templates and was successfully applied in the automated parameter enrichment in the evaluated thermal comfort use cases. The validation of these parameter sets requires either further studies on clothing and activity statistics within these defined space usage scenarios or validation on real use cases. Some of these parameters, e.g., the additional surrounding clothing for bedding, result in a total clothing combination that falls out of the bounds of the PMV applicability and requires further testing and validation. These personal parameters were developed based on international standards for Western European clothing standards for different space usages and do not distinguish between sex, gender, age, cultural background, seasons, weather, and other influences that affect clothing and activity degree. The activity levels also do not reflect mixed activities that include changes throughout the day. However, the extension of the existing parameter set facilitates the assessment of thermal comfort in the design phase of buildings. In this phase, the availability of occupant data may be limited, but template-based comfort assessment can support design decisions in the IFC-based design process. For use in the operational phase, the presented input parameters should be evaluated on their applicability in the specific use case (which is also true for all other template-based enrichment choices) and adjusted to reflect the case-specific requirements.

In the proposed methods, static (PMV, PPD) and adaptive comfort measures are included and evaluated, which are developed for comfort predictions on large groups of people and are criticized for failing thermal comfort predictions for individuals due to neglecting the diversity of humans conditions. The static measures are developed for mechanically conditioned spaces, requiring a small bandwidth of indoor environmental conditions to provide comfort within the acceptable range of Category II ($-0.5 < PMV < 0.5$) defined by [DIN16798-1]. The results in Section 4.7.2 revealed that by using the wide bandwidth of heating and cooling setpoints, resulting from cooling setpoints defined as 26 °C according to [DIN16798-1], Category II, these results do not meet the acceptable range of the static comfort measures. The resulting indoor air temperatures rather comply with the requirements of adaptive thermal comfort, which is applicable for naturally ventilated buildings where occupants can adjust the ventilation using

operable windows, but not for fully mechanically conditioned buildings such as the DigitalHub.

[PDB20] found that the adaptive comfort metrics also apply to mixed-mode ventilated buildings, as they show a stronger correlation between indoor and outdoor temperatures compared to fully mechanically conditioned buildings, where the indoor air temperatures are considered to be independent of the outdoor conditions and observed all-year-round setpoint temperatures of 22 °C. [PDB20] claim that the analyzed ASHRAE Global Thermal Comfort Database II [FLCZ+18] does not include fully air conditioned buildings with adaptive heating and cooling setpoints, such that an adaptation to indoor air temperatures in fully conditioned buildings cannot be evaluated. However, the authors [PDB20] suggest a deeper analysis of adaptive control strategies in mechanically conditioned buildings, as it is promising for increasing indoor thermal comfort while reducing costs. They expect the occupant to adapt to the indoor air temperature regardless of the ventilation system. [GSA09] suggested adjusting the cooling setpoints in office buildings to 23.33 °C to 25.56 °C, as they claim that they observed indoor air temperatures falling out of the comfortable range from 23.33 °C to 27.78 °C in the cooling period, leading to a thermal dissatisfaction of up to 60%. The observed cooling setpoints for mechanically ventilated buildings (i.e., all-year-round 22 °C) in the database analyzed by [PDB20] do not comply with the cooling setpoints implemented according to [DIN16798-1] in this dissertation, where indoor air temperatures of up to 26 °C are acceptable. The setpoints in this dissertation rather align with the recommendations by [GSA09] and should be further evaluated and validated in further research, especially regarding the applicability of adaptive comfort metrics.

The CFD-based analysis of thermal comfort included a simplified thermal manikin, enhancing a future integration of thermo-physiological models. While the manikin is partitioned into the same body parts as MORPHEUS [Wöl17], the partitions require adjustments to fully comply with the respective MORPHEUS partition surface areas. The first step of the integration in future research is the replacement of the current static clothing surface temperatures from related research by calculating temperatures based on the skin temperatures and body-part-specific clothing values. This would support the prediction of the individual occupant's thermal comfort, as the current implementation only allows comfort evaluations in proximity to the manikin, but not at the surface, where standard PMV and PPD measures are not applicable.

To conclude, both RH are supported by the proposed methods and evaluations, which provide the automated filling of missing personal comfort data, and allow for the evaluation of thermal comfort on different spatio-temporal scales. The automated data enrichment requires a critical evaluation for the specific use cases; also, the applicable comfort metrics have to be selected according to project-specific requirements. The presented algorithms have to be evaluated and tested regarding their applicability in real-world scenarios, but are prepared for adaptations in related fields, e.g., for adopting thermo-physiological models.

5 Evaluating the Climate Impact on Indoor Thermal Comfort using IFC-based Simulations

Global warming affects the indoor environment of buildings, leading to shifts in energy consumption for heating and cooling and an increasing risk of overheating. The proposed IFC-based methods for BEPS and CFD enhance the automated simulation model generation during the design process of buildings but can also be applied during the operation for optimizations or refurbishments of buildings. With the use of these proposed methods while considering future weather scenarios, the building design can be further improved for thermal resilience and energy efficiency while maintaining thermal comfort.

Section 5.1 starts with a brief introduction to climate change scenarios and methods to generate future weather data from climate models. Section 5.2 provides a review on related research for the identification of research gaps, on which basis two RHs are defined (cf. Section 5.2.3). Section 5.3 defines a methodology for the analysis of the impact of climate change in response to the RHs, including the process of generating future weather data. Section 5.4 provides the application of the presented method, starting with an analysis of the characteristics of the weather data before analyzing the effects on the IFC-based simulations.

5.1 Fundamentals of Future Weather Scenarios for the Use in Building Performance Simulation

The IPCC defined five Shared Socio-economic Pathways (SSPs) to illustrate possible climate response scenarios covering the range of possible changes in industrial and social developments. These scenarios are labeled in the format SSPx-y, where the 'x' declares the socio-economic trend, and the 'y' describes the level of radiative forcing in W/m^2 that is prognosed for the year 2100. The scenarios SSP1-1.9 and SSP1-2.6 represent scenarios with low GHG emissions that are reduced to net-zero by 2050 and 2070. The SSP2-4.5 represents a scenario with intermediate GHG emissions, which are kept on current level for the following two to three decades. The high GHG scenarios SSP3-7.0 and SSP5-8.5 represent scenarios that double the GHG emissions until 2100 and 2050, respectively. Representative Concentration Pathways (RCPs) have been defined additionally in the format RCPy, where the 'y' again defines the radiative forcing in W/m^2. When comparing RCP and SSP scenarios with the same 'y', for the SSPs the resulting effective radiative forcing tends to be higher. The SSP scenarios allow estimates for the global warming for the year 2081-2100 of [1.0, 1.8]°C (SSP1-1.9) to [3.3, 5.7]°C for SSP5-8.5. [IPCC23]

The following paragraph is an adapted and extended excerpt from [RSFvT23]. To consider these

future weather scenarios in building simulations, suitable future weather data needs to be generated from the proposed climate models using applicable methods. General Circulation Models (GCMs) are downscaled from their worldwide scale of typically 1 – 5° latitude and longitude [JJBB13] (i.e., about 111 – 555 km) to regional scale high-resolved Regional Climate Models (RCMs) with a resolution of 4 km or less [TNM+20]. Four statistical downscaling approaches were introduced by [WW97]: regression, weather pattern approaches, stochastic weather generators, and limited-area climate models. [BHP05] further refined these approaches to dynamical downscaling, stochastic weather generation, interpolation, and introduced morphing. Each approach has disadvantages: Dynamical downscaling is computationally expensive, stochastic weather generation requires large input data sets, and interpolation may lead to biased resulting data. The proposed morphing technique has low computational cost and builds upon real climate data [BHP05]. Morphing methods, however, are criticized in related research for its limitations to predict variability in future weather scenarios [ZKT+23], leading to an overestimation of cooling loads and prediction of thermal discomfort [FL23].

5.2 Related Research on Future Weather for BEPS and Thermal Comfort Analysis

This section includes an analysis of related research for the application of future weather scenarios and the required data generation, as well as for their application in IFC-based approaches. From the analyzed research, two research hypotheses are derived.

5.2.1 Related Research

Parts of this section have been initially presented in [RSFvT23] and are adapted and extended. [ZKT+23] present a recent critical review on the generation approaches of future weather data for building performance simulation, giving advice for the choice of future weather files according to the application (i.e., energy analysis, thermal resilience, HVAC design, utility analysis). For the analysis of thermal resilience, they recommend the use of future extreme weather data instead of typical year weather data. However, morphed weather data, criticized for being unable to reflect the actual future weather variability, was still used in related research [ZKT+23].

While [ZKT+23] focused on the methods for generating future weather data for the use in specific applications, [NK21] presented a review on the use of future climate models in existing BEPS research. They discovered that more than half of their 47 analyzed studies (2015 and newer) used the outdated weather data of the Coupled Model Intercomparison Project (CMIP) 3,[1] partially due to the availability through the *CCWorldWeatherGen* Tool [JJBB13] that easily generates EnergyPlus weather files. Only five out of the analyzed studies underlined why they chose the selected climate model even though the resulting weather files show high variance and may lead to an erroneous interpretation of the simulation results. The ways to deal with solar radiation

[1] CMIP3: Phase 3 of the Coupled Model Intercomparison Project (CMIP), supporting the fourth assessment report of the Intergovernmental Panel on Climate Change (IPCC) based on weather data mostly generated in 2005 and 2006: https://pcmdi.github.io/mips/cmip3/, accessed on June 10, 2025.

data for BEPS are manifold in related research, as global horizontal irradiance from GCM and RCM have to be converted to direct normal irradiance and diffuse horizontal irradiance for the use in BEPS [NK21]. However, some research [PU19] even neglects the changes in solar irradiance and cloud cover and keeps these parameters unchanged. This is critical, as the level of solar irradiance has increased in recent historical weather data [PPCL24] and may reduce the accuracy of the BEPS results. [NK21] published the results of their study on a continuously updated webpage,[2] including data from 88 studies and a total of 216 locations (status as of May 2024). [RSFvT23]

To enhance the accessibility to future weather data, [RFC23] propose an open-source morphing tool for future weather data, as the existing tools (*CCWorldWeatherGen* [JJBB13], *Weather Morph* [JLCZ19], *WeatherShift*[3]) have limited accessibility (i.e., not open-source), rely on outdated data models, or are not free to use and, thus, may not be accessible for researchers with limited funding. [RSFvT23]

The systematic review by [DDWAZ25] analyses the benefits and limitations of individual future weather generation methods and available tools and supports the presented open-source framework by [RFC23], as it allows the use of up-to-date climate models.

Within the collaboration of International Energy Agency (IEA) EBC Annex 80,[4] [MSPT+24] proposed new typical and extreme weather data sets for use in building simulation resulting from the international collaboration within the IEA EBC Annex 80. This study includes a data set[5] containing weather data for 15 locations across the globe, including two data sets for climate zone 5A (Toronto, Copenhagen), which is the climate zone that is also assigned to large parts of Germany, as well as Aachen [ASH169]. This data set relies on the outdated RCP climate scenarios of CMIP5 [MSPT+24], which, nevertheless, provide a higher spatial resolution and more output parameters than the previous CMIP3 scenarios [TSM12]. Another data set of future Typical Meterological Year (TMY) (fTMY) for the United States of America was proposed by [BNRK22] for the application in BEPS. This data set is based on the latest climate model CMIP6.

While previously named studies mainly focused on the generation of future weather files for the use in BEPS, the following studies give a brief introduction to the impact of climate change on the built environment, supporting the further evaluation of future weather impact on the IFC-based simulations in this dissertation.

[HMK+23] discuss ten questions on building's and occupants adaptation to climate changes. Considering changes in the outdoor environment and their impact on the buildings, they list general climate trends and local weather conditions, urban micro-climate and heat island effects, and hazards as influential on the thermal resilience of buildings. [RSFvT23]

[2] FutureWeatherBPS: www.futureweatherbps.com, accessed on May 19, 2024.
[3] WeatherShift: https://weathershift.com/, accessed on June 04, 2025.
[4] IEA Energy in Buildings and Communities Programme (EBC) Annex 80: Resilient Cooling of Buildings, https://annex80.iea-ebc.org/, accessed on June 04, 2025.
[5] WDC Climate, IEA EBC Annex 80 data set: https://www.wdc-climate.de/ui/q?hierarchy_steps_ss=WDTF_Annex80_build_v1.0&entry_type_s=Dataset, accessed June 04, 2025.

[TMP+23] analyze the risk of residential overheating with a focus on Central and Northern Europe. They also state the impact on overheating of Urban Heat Island (UHI) and local microclimates around buildings, which are often not considered for the design of residential buildings. The effect of individual outdoor and indoor conditions (e.g., solar heat gains, heat conduction, ventilation, internal gains) on overheating is also influenced by the building construction, materials, and the building's location. Heavy constructions with a high thermal mass reduce the impact of air temperature peaks, external shading reduces solar heat gains, and nightly increased ventilation assists in reducing indoor temperatures, while large south-oriented glazings and uninsulated roofs increase the overheating risks [TMP+23]. The model-based prediction of overheating risks requires a use-case-specific choice of input parameters. The simulation of transient effects using dynamic simulations is significant for highly-insulated low-energy houses with large glazings. As shadings and nightly ventilation require occupant actions combined with technological prerequisites, they claim overheating is a sociotechnical problem. Thus, mitigation of climate impact additionally needs a better understanding from the occupants apart from technical solutions. [TMP+23]

A systematic review on the challenges in predicting the climate change impact on buildings is provided by [DDWAZ25]. They focus on the BEPS-based assessment of climate change impact on thermal building performance. Besides analyzing the methods for generating future weather files, they analyze the applied performance metrics in related research and claim limited comparability between studies caused by the use of inconsistent measures. While the future energy demand is commonly assessed using kWh/(m^{2}a), the related energy use predictions may use different conversion factors for primary energy demand and different underlying floor area measures (gross area vs. conditioned area). [DDWAZ25] additionally highlight the differences between national adaptive comfort metrics, which have also been elaborated by [TMP+23]. To address these inconsistencies in evaluating climate change impact, [DDWAZ25] proposed a six-step framework for assessing the impact of future climate on building thermal performance.

To state quantification of the climate change impact on building energy demand in Europe, [DPE+22] evaluate the impact of future climate on the design and performance of nearly zero energy buildings (NZEB) for eight locations across Europe. They detect a significant decrease in the heating demand for up to 50% in colder regions, while the cooling demands double in warmer regions. They emphasize the increasing demand to reduce summerly overheating in buildings.

Regarding the IFC-based simulation of climate change impact, the available research is sparse. [CHM15] proposed an IFC-based extension to a low-energy building design software and evaluated the design of a certified Passivhaus[6] in Wales with respect to its resilience to future climate scenarios. The IFC-based building simulation using future weather scenarios revealed that the Passivhaus requirement for an annual heat demand of 15 kWh/(m^{2}a) will still be met, while 1) the low U-values lead to an even lower heating demand, and 2) the south-facing windows

[6] Passivhaus Certification: https://passivehouse.com/03_certification/03_certification.htm, accessed on June 04, 2025.

could be increased in their size. The research presented in [RvTF24], which includes parts of the works presented in this dissertation, evaluated the effect of climate change scenarios in the IFC-based setup of thermal comfort simulations, daily mean PMV predictions represented in calendar plots and adaptive comfort evaluations according to [DIN16798-1, DIN15251].

5.2.2 Preliminary Conclusion on Research Gap

The application and generation of future weather data in BEPS simulations has been discussed in related research. The IEA EBC Annex 80 on resilient cooling of buildings even presented a new data set for building simulations. The choice of generation methods for future weather data is an ongoing topic in related research, but shows a positive trend regarding the use of current climate models by proposing open-source frameworks [RFC23] for weather file generation [DDWAZ25]. Related research on the general climate change impact on the built environment has only briefly been analyzed in this dissertation, but the studies [HMK$^+$23, TMP$^+$23, DDWAZ25] provide in-depth reviews. However, studies considering future weather scenarios in IFC-based design processes are rare.

Research Gap 1: The impact of climate change is not yet automatically analyzed in IFC-based simulations.

> *Explanation:* While the impact of future weather on buildings has been evaluated in related research, this has not yet been included as a common approach in the IFC-based design process of buildings. [TMP$^+$23] emphasize the importance of dynamic simulations to assess transient effects in buildings to prevent overheating. While an early approach by [CHM15] includes the evaluation of future weather into their IFC-based extension of low-energy building design software, other related IFC-based studies have not been found. Apart from tools for generating future weather files, no open-source tools are available in research for integrating future weather analysis into the design process, neither for BEPS nor for CFD.

5.2.3 Research Hypotheses

The following two RHs for the IFC-based analysis on the impact of Climate Change (CC) impact are concluded from the identified research gaps in response to the RQs defined in Section 1.3:

RH CC 1: The application of future weather data on IFC-based BEPS enables the assessment of climate change effects on energy efficiency and thermal comfort on a zonal scale.

RH CC 2: The IFC-based CFD analysis of spaces with critical thermal comfort from IFC-based BEPS analysis enables a deeper understanding of the impact of future climate on thermal comfort in indoor spaces.

These RHs are defined based on the identified gaps in related research and built upon the tested and evaluated methods from the previous sections. The first RH CC 1 addresses the

analysis of climate change impact on indoor environments on a zonal scale, which was already demonstrated in the previous Section 4.7 for the use on thermal comfort, but is now extended for the evaluation of climate change impacts. While RH CC 1 addresses the zonal scale, RH CC 2 aims to analyze the detailed spatial evaluation of the impact of future weather on thermal comfort using CFD. This CFD analysis does not only provide insights into local thermal comfort but also into the effectiveness of HVAC systems under future weather conditions. Both RHs address RQ 3, as the BEPS and CFD approaches are not only individually applied to evaluate a building's performance but also combined, as already demonstrated in Section 4.7.

5.3 Methodology for Assessing the Impact of Climate Change on Building Thermal Performance

[DDWAZ25] claim the inconsistencies in the evaluation of climate change impact and propose a six-step procedure for the evaluation of building thermal performance in future climate scenarios. These steps include (1) defining the research scope and goal, (2) selecting a future climate scenario, (3) generating future weather data, (4) modeling the construction and use of future buildings, (5) choosing the building performance assessment approach, and (6) evaluating the results. The evaluation of the climate change impact on the IFC-based simulations in this dissertation follows this procedure introduced by [DDWAZ25] and is applied as follows:

The research goal and scope (1) of the climate change impact analysis is defined for the same location as applied in the previous Section 4.7, which is chosen to be a location with the climate of the Cologne/Bonn Airport. The evaluation is applied on a building scale, as the input data is obtained from IFC and focuses on the evaluation of indoor spaces. Both residential and non-residential buildings are studied in the evaluation, as the IFC-based methods require thorough testing through simulations and evaluation for plausibility, and no real-world use case is available for validation. The scope of the evaluation is the energy consumption, as well as the thermal comfort assessment.

The future climate scenario (2) is initially compared from two sources to evaluate the uncertainties in evaluation: The BBSR predictions for future climate for 2045[7] derived from the CMIP5 climate scenarios RCP4.5 and RCP8.5 [DWD17], and the SSP scenarios based on the EC-Earth3 [EC19] model from the latest IPCC CMIP6.

For the definition of future weather files (3), the BBSR weather for 2045 predictions are converted to the EnergyPlus epw format using the *CCMEditor*.[8] The Test Reference Year (TRY) (1995-2012) weather data provided by BBSR is used as a historical reference and also converted to epw. The SSP climate scenario data requires a downscaling and transformation to a regional level

[7] Bundesinstitut für Bau-, Stadt- und Raumforschung, engl.: Federal Institute for Research on Building, Urban Affairs, and Spatial Development (BBSR) weather data for 2045: https://www.bbsr.bund.de/BBSR/DE/forschung/programme/zb/Auftragsforschung/5EnergieKlimaBauen/2013/testreferenzjahre/01-start.html, accessed on June 04, 2025.

[8] CCMEditor, IBK Dresden: https://www.bauklimatik-dresden.de/ccmeditor/help/de/index.html, (added a COMMENT 2 in resulting epw-file to make it work in EnergyPlus.), accessed on June 04, 2025.

and a conversion to the epw format. Here, the *Future Weather Generator* (v1.1.1) [RFC23] has been used as described in [RvTF24] to generate future weather data for the IPCC SSP scenarios based on the EC-Earth from the IPCC CMIP6 and a recent set of historical weather data (TMYx, 2007-2021). While this weather generator still requires further validation of the accuracy and reliability of the resulting morphed weather files, it is recommended for use in BEPS due to the availability of recent climate models and the open-source implementation [DDWAZ25]. As the BBSR weather predictions are available for the year 2045, these are compared to the SSP5-8.5 weather prediction for 2050, but for completeness, also the SSP5-8.5 2080 weather is compared in the initial evaluation of the weather data. As this dissertation focuses on the IFC-based setup and evaluation of BEPS and CFD, a further detailed analysis of extreme weather events and urban heat islands is considered for further research.

The building use case chosen as simulation objective (4) is generated using the IFC-based setup described in the previous sections. The dynamic effects of climate change are considered using static and adaptive thermal comfort limits according to [DIN16798-1], while the location, construction materials and occupancy schedules remain unchanged compared to the thermal comfort use cases in Section 4.7.

The building energy performance (5) is predicted using a dynamic building simulation using BEPS (EnergyPlus), with a coupled detailed analysis of local thermal comfort using CFD (OpenFOAM). Since no real-world use case is available for calibration and validation of these scenarios, the resulting energy demands of the use cases for historical weather in Section 4.7 were set up according to national and international standards and the energy consumption was rated according to energy efficiency standards, while all historic and future case results are additionally evaluated for plausibility.

To interpret the simulated results (6), standardized measures (e.g., energy consumption, degree-hours, thermal comfort) are evaluated for both historic and future weather data to assess the impact of climate change.

5.4 Evaluation of Energy-Efficiency and Thermal Comfort in Future Weather Scenarios

Different climate change scenarios have been evaluated for the Cologne/Bonn Airport. The generation of the weather files is described in Section 5.3. The analyzed weather files include the TMYx from 2007-2021, the TRY 2015 based on the years (1995-2012), the BBSR predictions for an average, hot, and cold climate in 2045 (based on predictions for 2031-2060 using RCP-4.5 und RCP-8.5), and the weather prediction for the SSP5-8.5 scenario for the years 2050 and 2080. A statistical overview of the annual weather data is provided in Appendix A.12. The weather data set provided by [MSPT+24] is not used, as it is not available for the analyzed position at Cologne/Bonn Airport and refers to the outdated CMIP5 weather scenario. From this data set, weather data for the same climate zone as Cologne/Bonn (ASHRAE 5A) are only available for

Copenhagen and Toronto, and thus not further considered for evaluation.

Figure 5.1 displays the monthly outdoor air drybulb temperature distribution for these weather files. As the BBSR TRY 2015 weather data refer to a time frame ending in 2012, this weather data shows the least effect of global warming and climate change, resulting in the lowest temperatures throughout the year, but similar to the cold winter scenario prediction for 2045. The most recent historical weather data set, TMYx (2007-2021), shows a quantitative similarity to the BBSR TRY 2045 weather file predictions. However, the historical TMYx weather data shows even warmer temperatures in the spring and summer. The prediction for a 2045 hot summer year shows a prediction of slightly higher temperatures from May through December compared to the TMYx historic data. The SSP5-8.5 weather data predictions for 2050 and 2080 show the highest temperatures throughout the year.

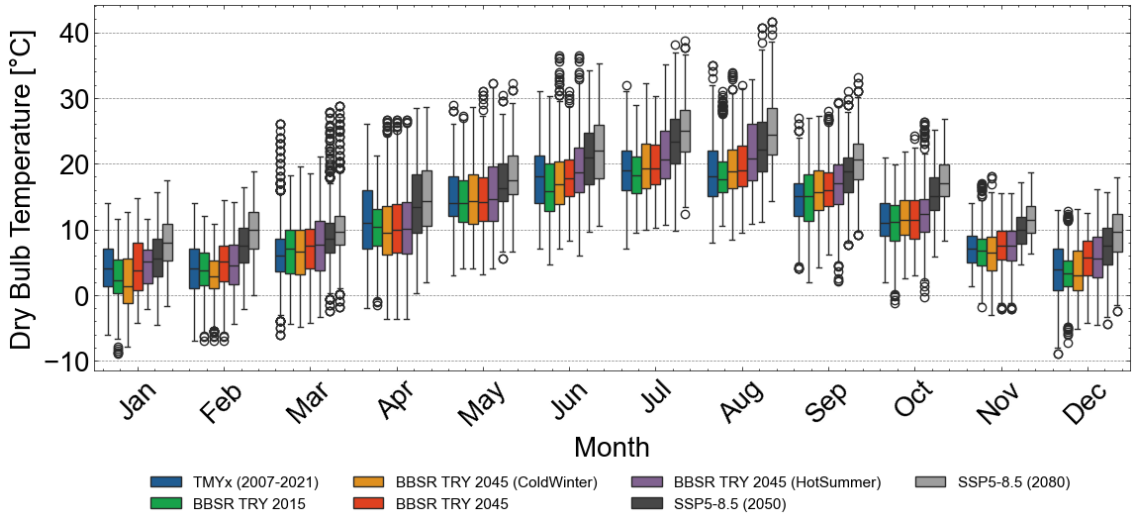

Figure 5.1: Boxplots of monthly outdoor air dry bulb temperature distribution for historical and future weather scenarios for the Cologne/Bonn Airport.

Figure 5.2 displays the direct normal radiation distribution per month, using the daily maximum value per weather scenario for a reduction of the data bandwidth. The comparison of the daily maximum direct normal radiation per month results in similar ranges from February through October for all data sets except for the SSP5-8.5 scenarios, which show maximum radiations that are twice as high, which even exceed the maximum possible radiation defined by the solar constant.[9] The scenario of the cold winter (2045) shows comparably high solar radiation in winter, as cold temperatures in winter often result from a dry weather with low sky cover caused by clouds.

Table 5.1 states the annual mean values for the data displayed in Figure 5.1 and Figure 5.2. The annual mean radiation of the TRY 2045 Hot Summer prediction only slightly deviates from the

[9]The solar constant defines the solar radiation at the upper atmospheric boundary of the earth, considering the mean distance between earth and sun. The mean value of about 1367 W/m^2 was defined by the World Radiation Center based on measurements. The observed solar radiation fluctuates annually by about ±3.3%, i.e., a variation between 1321 W/m^2 (summer) and 1415 W/m^2 (winter), caused by the elliptic path of the earth around the sun, which affects the sun-earth distance. [DB13]

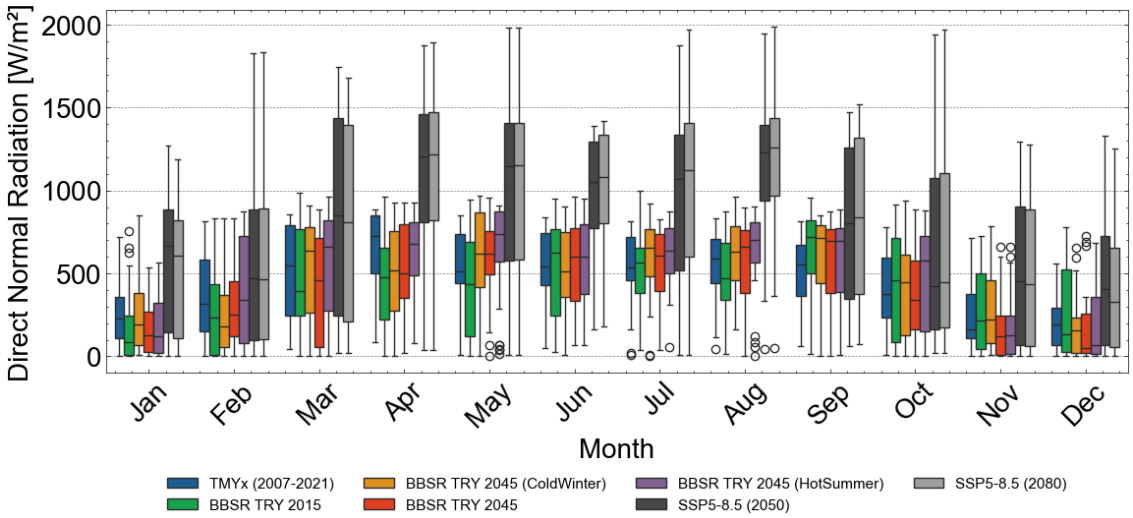

Figure 5.2: Boxplots of maximum daily direct normal radiation in a monthly distribution for historical and future weather scenarios for the Cologne/Bonn Airport.

historical TMYx (2007-2021) data set, such that the hot summer prediction for 2045 represents already a present scenario in terms of the radiation. This supports the importance of the re-evaluation of current weather trends and the requirement of continuous calculation of future weather scenarios. For an additional evaluation of the annual characteristics of the outdoor air temperatures and the direct normal radiation, Figure A.43 provides a violin plot illustration.

Table 5.1: Annual mean dry bulb temperatures and mean direct normal radiation for the historical and future weather scenarios for the Cologne/Bonn Airport.

	DryBulb Temperature [°C]	Direct Normal Radiation [W/m^2]
TMYx (2007-2021)	11.16	140.49
BBSR TRY 2015	10.62	99.84
BBSR TRY 2045 (Cold Winter)	10.95	117.11
BBSR TRY 2045	11.72	105.79
BBSR TRY 2045 (Hot Summer)	12.34	139.68
SSP5-8.5 (2050)	14.32	158.34
SSP5-8.5 (2080)	16.02	163.15

Since the maximum direct normal radiation values in the SSP5-8.5 cases exceed the solar constant, but their annual mean values in Table 5.1 do not provide insights in the causes of these errors, the daily radiation characteristics require further evaluation. For this purpose, Figure 5.3 displays the direct normal radiation of the historic TMYx and three future weather files (i.e., BBSR TRY 2045, and both SSP5-8.5 cases) for four days in July. In this figure, the generated SSP5-8.5 weather files exhibit high peaks at 5 am (i.e., 1878 W/m^2 and 1970 W/m^2 on July 19 for SSP5-8.5 in 2050 and 2080, respectively) which is not realistic for the Cologne/Bonn airport location in terms of both, absolute radiation value and hour of the day. Thus, transforming the TMYx data in the *Future Weather Generator* must have caused this error, as the TMYx data itself does not show any peaks early in the morning. Since, apart from these peaks, the daily course of the radiation and the annual mean radiation in Table 5.1 seem reasonable, the SSP5-8.5 weather

scenarios are considered for the further evaluation in this dissertation.

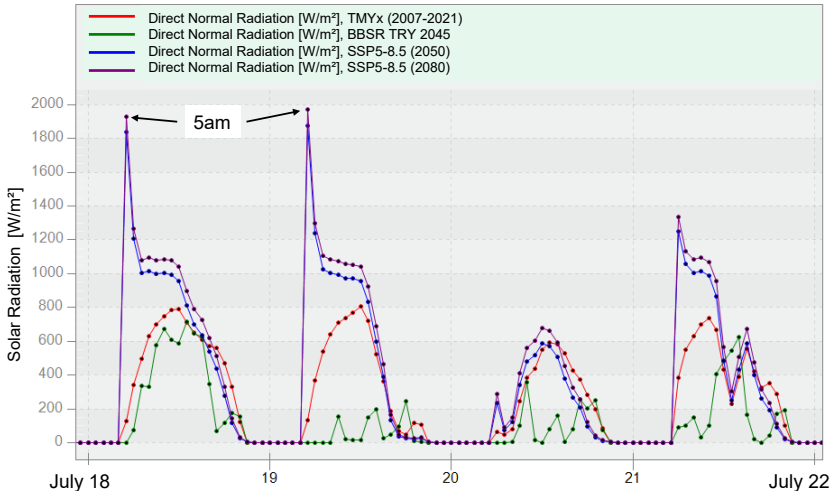

Figure 5.3: Comparison of direct normal radiation for historic and future weather data for Cologne/Bonn Airport.

This dissertation provides methods to automatically set up simulation models based on IFC4 data to enhance model-based evaluation of the impact of design decisions regarding energy efficiency and thermal comfort in current and future climates. To further prove the capabilities of the proposed methods in this dissertation, the further exemplary evaluation of the climate change impact uses the worst-case SSP5-8.5 scenario for 2050 in comparison to the TMYx (2007-2021) historical weather data. The evaluation process, visualized in Figure 5.4, starts in Use Case 1 with the analysis of the impact of climate change on the naturally ventilated FZK-Haus, which includes the BEPS-based evaluation of energy consumption and overheating risk. This first use case relates to the use case presented in Section 4.7.1. Use Case 2 evaluates the impact of future weather on the mechanically ventilated non-residential building DigitalHub using an annual BEPS, which relates to the use case evaluated in Section 4.7.2. Use Case 3 evaluates the impact of future weather on local thermal comfort, which relates to the use case described in Section 4.7.4.

5.4.1 Use Case 1: FZK-Haus - Impact of Climate Change on Residential Houses

When applying the SSP5-8.5 weather scenario prediction for the year 2050 on the same model setup as described in Section 4.7.1 (i.e., FZK-Haus, KfW40, TMYx (2007-2021)), the heating energy consumption (unlimited heating capacity) reduces to 23.29 kWh/(m^{2}a) annually, which is a reduction of 33.25%. The heating energy consumption is further reduced when applying the SSP5-8.5 (2080) weather data to 17.85 kWh/(m^{2}a), which is stated here as reference but not further analyzed in this dissertation.

Figure 5.5 displays the percentage of occupied hours related to the adaptive comfort categories and the occupancy-weighted excess degree-hours for the SSP5-8.5 scenario in 2050 for the Cologne/Bonn Airport. The related results for the historical TMYx (2007-2021) weather file are

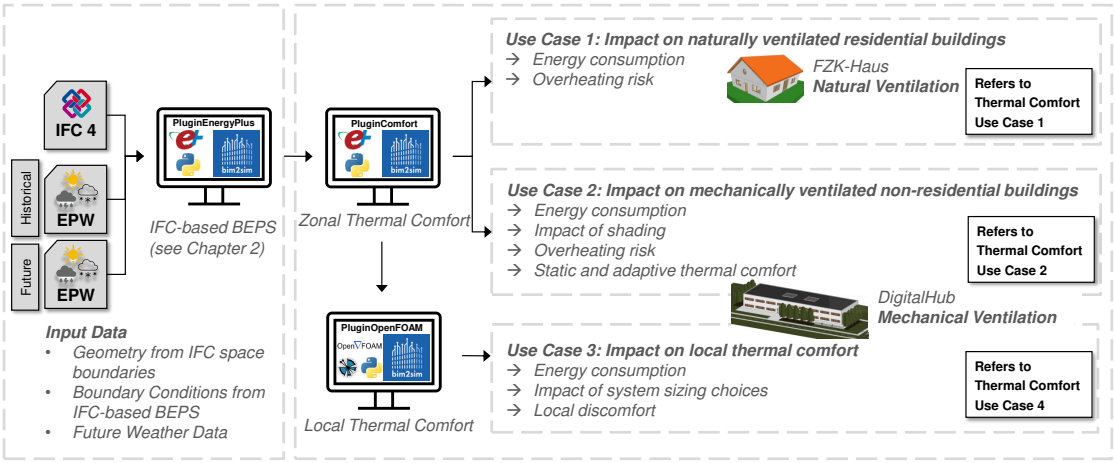

Figure 5.4: Overview on the use cases for IFC-based Thermal Comfort analysis in future weather scenarios using *PluginComfort* and *PluginOpenFOAM*.

displayed in Figure 4.9b and Figure 4.10b. The living spaces in the TMYx case showed 0.8% degree-hours below the comfort limit (cf. Figure 4.10b), which reduces to 0.6% in Figure 5.5b in the current SSP5-8.5 (2050) scenario. However, the application of the SSP5-8.5 (2050) scenario here results in a drastic exceeding of temperature limits in all spaces: the scenario exceeds the upper threshold of 1% for the 2 K degree-hours (Figure 5.5b, *above*) and also shows timesteps that exceed this additional 2 K limit (i.e., *out above*) in all spaces.

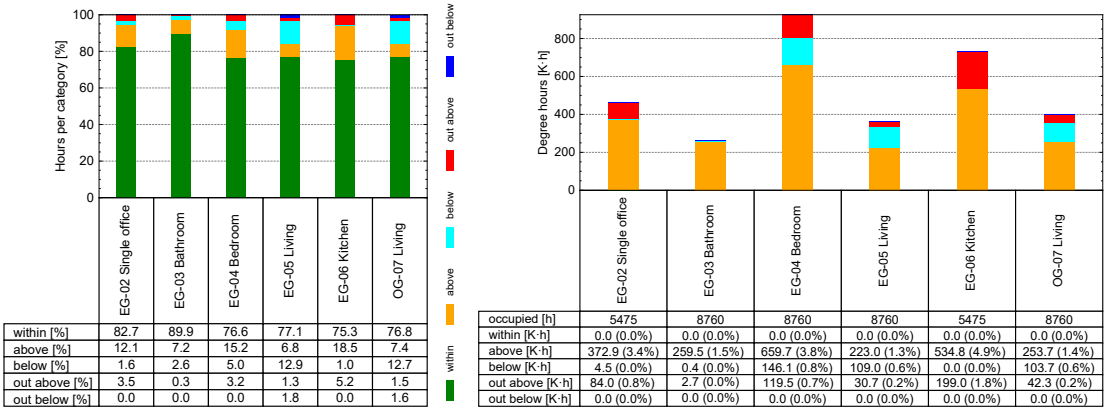

	EG-02 Single office	EG-03 Bathroom	EG-04 Bedroom	EG-05 Living	EG-06 Kitchen	OG-07 Living
within [%]	82.7	89.9	76.6	77.1	75.3	76.8
above [%]	12.1	7.2	15.2	6.8	18.5	7.4
below [%]	1.6	2.6	5.0	12.9	1.0	12.7
out above [%]	3.5	0.3	3.2	1.3	5.2	1.5
out below [%]	0.0	0.0	0.0	1.8	0.0	1.6

(a) Excess hours (occupied, no weights)

	EG-02 Single office	EG-03 Bathroom	EG-04 Bedroom	EG-05 Living	EG-06 Kitchen	OG-07 Living
occupied [h]	5475	8760	8760	8760	5475	8760
within [K·h]	0.0 (0.0%)	0.0 (0.0%)	0.0 (0.0%)	0.0 (0.0%)	0.0 (0.0%)	0.0 (0.0%)
above [K·h]	372.9 (3.4%)	259.5 (1.5%)	659.7 (3.8%)	223.0 (1.3%)	534.8 (4.9%)	253.7 (1.4%)
below [K·h]	4.5 (0.0%)	0.4 (0.0%)	146.1 (0.8%)	109.0 (0.6%)	0.0 (0.0%)	103.7 (0.6%)
out above [K·h]	84.0 (0.8%)	2.7 (0.0%)	119.5 (0.7%)	30.7 (0.2%)	199.0 (1.8%)	42.3 (0.2%)
out below [K·h]	0.0 (0.0%)	0.0 (0.0%)	0.0 (0.0%)	0.0 (0.0%)	0.0 (0.0%)	0.0 (0.0%)

(b) Degree-hours (occupancy-weighted)

Figure 5.5: Evaluation of adaptive thermal comfort according to DIN EN 16798-1, NA. Operative temperatures are evaluated within the occupied hours regarding the excess occurrence (left) and the resulting occupancy-weighted degree-hours (right) for the SSP5-8.5 scenario in 2050.

The evaluation of the BEPS-based limited local discomfort revealed an increase of the floor temperature to more than 29 °C in up to 132 h of the simulated annual timeframe, mainly observed at the beginning of August. This is caused by persistent high indoor air temperatures that cannot be reduced using natural ventilation, due to the high outdoor air temperatures.

This reduced ability to use natural ventilation to prevent overheating in the SSP5-8.5 weather scenario is displayed in Figure 5.6, where the day ventilation is reduced to the baseline of 0.5 h^{-1}

due to the increased outdoor air temperature as opposed to the TMYx case, where the heat mitigation ventilation is applied. This may result in reduced indoor air quality in times of high occupancy, as no mechanical ventilation is available.

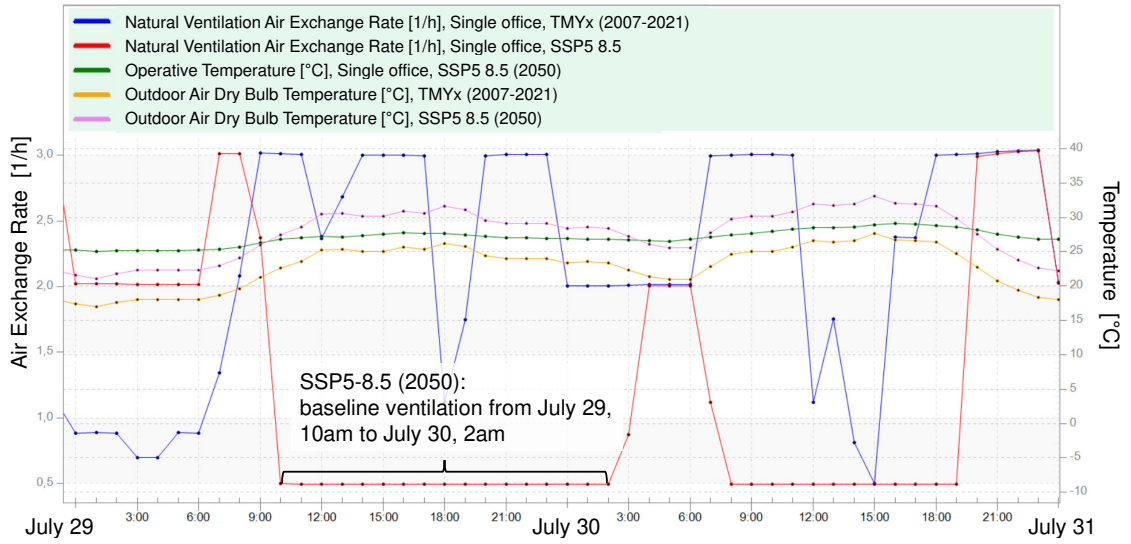

Figure 5.6: Reduced natural ventilation due to high outdoor air temperature.

The application of the SSP5-8.5 weather prediction for 2050 to the automatically generated IFC-based BEPS model underlines the upcoming overheating risks for naturally ventilated buildings caused by the changing climate. Using this automated model setup, each design attempt towards a more resilient building can quickly be analyzed. Even if the template-based enrichment may not reflect the exact building usage (e.g., in terms of occupancy profiles) of the future operated building, the template-based enrichment assists in comparing the impact of design decisions. In addition, these design decisions can be compared using the same template-based enrichment under current weather conditions (cf. Section 4.7.1), which allows for validation of the building performance with historic data, e.g., by applying model calibration or comparison with statistical data.

5.4.2 Use Case 2: DigitalHub - Impact of Climate Change on Non-Residential Office Buildings

The use case of the unshaded mechanically ventilated DigitalHub model, as described in Section 4.7.2, is simulated and sized for typical summer and winter days of the SSP5-8.5 (2050) future weather file. This sizing choice, using the future weather file for system sizing, leads to an increased cooling capacity on hot summer days (Figure A.26) compared to the sizing for typical days of the TMYx weather data (Figure A.15). Compared to the simulation with the TMYx weather data, this leads to a reduction of the annual heating energy consumption from 29.93 kWh/(m^{2}a) to 20.84 kWh/(m^{2}a) and an increase of the cooling energy consumption from 3.02 kWh/(m^{2}a) to 11.67 kWh/(m^{2}a), such that the total energy consumption (i.e., heating and cooling energy combined) only slightly reduces by 0.44 kWh/(m^{2}a) due to the shift of heating demand towards cooling demand. See Table A.10 for an overview on all BEPS results of the

DigitalHub.

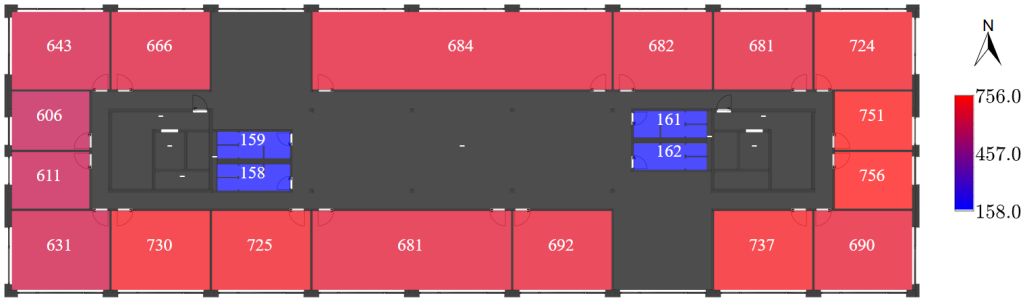

(a) Difference in number of hours for $PMV > 0.5$.

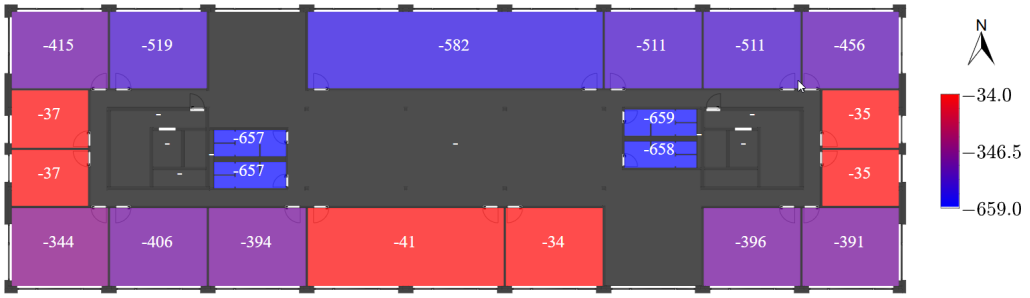

(b) Difference in number of hours for $PMV < -0.5$.

Figure 5.7: Difference in number of hours above and below Category II ($-0.5 < PMV < 0.5$) for the occupied hours on the top floor, without external shading, for the SSP5-8.5 (2050) climate scenario, compared to the simulation based on historic weather data TMYx (2007-2021).

While the mean PMV during the occupied times is now slightly increased and ranges between -0.3 and -0.1 in the top floor, the number of hours with a PMV > 0.5 is increased by between 606 to 756 hours in the offices and meeting rooms (Figure 5.7a), while the number of hours with a PMV < -0.5 decreases by between 34 to 582 hours (Figure 5.7b). For the *E01-13 Group office* in the south-east corner of the building, the PMV exceeds the 0.5 threshold in a total of 1717 hours, compared to 1027 hours in the TMYx case (cf. Figure A.21). This dramatic increase of discomfort is additionally highlighted in Figure 5.8, which displays the heatmap with PMV categories and adaptive temperature bounds (cf. Figure 4.15 for TMYx results). During the occupied time, the indoor operative temperatures are 31.4% of the time above the adaptive 2 K threshold (=758.5 Kh, i.e. 9.4% instead of acceptable 1%, cf. Figure A.22). In 15 out of 16 group offices in this building, the 1% degree-hour limit of [DIN16798-1] is exceeded. In the remaining space, the limit of 1% degree-hours is reached, but not exceeded. Two offices (north-east and south-east) exceed the threshold of 500 Kh for non-residential buildings defined in [DIN4108-2]. The analysis of the BEPS-based limited local discomfort showed an exceeded ceiling temperature ($\Delta T_{max} = 5$ K between indoor air and ceiling) in two offices for up to 23 h/a per space. The number of hours with observed local discomfort is lower than for the FZK-Haus use case, as mechanical ventilation allows effective cooling of the indoor air, resulting in lower local heating of surfaces in this south-east corner office.

However, as also the TMYx case (cf. Section 4.7.2) resulted in 26.9% (=563.5 Kh, i.e. 7%) of the occupied time above the adaptive comfort threshold, this high discomfort is not only caused by

the extreme weather scenario but also by the missing shading.

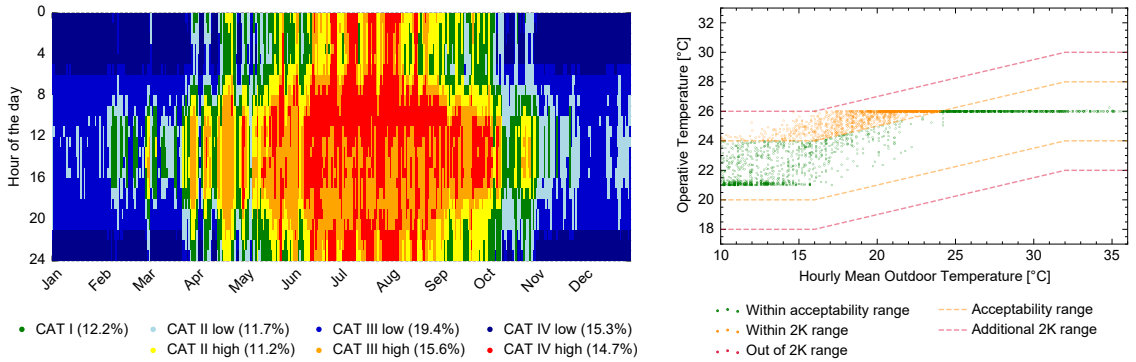

(a) Heatmap with PMV categories.

(b) Adaptive thermal comfort.

Figure 5.8: Group office top floor, south-east corner according to [DIN16798-1], NA, SSP5-8.5 (2050), without external shadings.

For the case with external shadings, the cooling energy is increased from 2.36 kWh/(m^{2}a) to 10.0 kWh/(m^{2}a) and the heating energy reduced from 33.09 kWh/(m^{2}a) to 23.07 kWh/(m^{2}a), which is a reduction of the total building energy consumption (i.e., heating and cooling combined) of 2.38 kWh/(m^{2}a) compared to the case with external shadings described in Section 4.7.2. The mean annual PMV on the top floor ranges from -0.3 to -0.2, which is slightly less than for the unshaded case, however, the number of overheated hours increased, as visualized in Figure A.23.

Compared to the case with external shadings in Section 4.7.2, the number of occupied hours above the acceptability range for the south-east corner *E01-13 Group office* is increased from 4.8% to 11.0% (=158.8 Kh, i.e. 2.0% instead of acceptable 1%, cf. Figure A.24). The overheated occupied hours for the north-east *E01-10 Group office* increased from 12.0% to 20.1% (=397.2 Kh, i.e. 4.9% instead of acceptable 1%, cf. Figure A.24) of the occupied time. In the SSP5-8.5 case with external shadings, out of the 16 group offices, three offices are below the 1% degree-hour acceptability limit, two group offices reach the limit of 1%, and eleven group offices exceed this acceptability limit. None of the offices exceed the threshold of 500 Kh for non-residential buildings defined in [DIN4108-2]. This improved performance of the building with external shadings, compared to the unshaded SSP case, is also visualized in the detailed heatmaps of the south-east corner group office in Figure A.25.

Applying the SSP5-8.5 weather scenario for 2050 to the IFC-based BEPS model of the DigitalHub further supports the importance of correctly considering the external shading elements for BEPS, as it highly affects the resulting heating and cooling loads. In current design practices, heating and cooling systems are mainly designed and evaluated using standardized static calculations, e.g., [DIN12831-1, DIN4108-2]. These static calculations cannot capture the transient effects [TMP+23] of physical responses, operation, and occupancy of the building, resulting in an increased risk of inefficiently sized heating and cooling systems. This effect is further increased in these times of a changing climate, where even historical weather data for building simulations requires recent updates, as the differences between the weather files for TRY 2015 and TMYx (2007-2021) (cf. Figures 5.1 and 5.2) have shown. While BEPS can simply use more recent

weather files to obtain more accurate results, and even use future weather predictions, the outdoor air design temperatures for specific regions within the standards cannot reflect these dynamics upon the next release of the standard.

5.4.3 Use Case 3: Impact of Climate Change on Local Thermal Comfort

The BEPS-based analysis of energy efficiency and thermal comfort in the previous section applied the system sizing for typical summer and winter days of the respective applied future weather scenario. The related results for the local thermal comfort analysis are presented in Appendix A.9.2 for the DigitalHub without external shading elements generated from space boundaries (cf. Figure 4.11b). These results revealed an overall acceptable thermal comfort for the south-east office on August 2, 4pm, since the system sizing using a typical summer day of the SSP5-8.5 weather file allowed a maximum cooling capacity for this space of 2400 W (Figure A.26). This is twice the cooling capacity limit resulting from the typical day system sizing for the TMYx (2007-2021) use case (cf. Appendix A.8.5, Figure A.15). These results highlight the drastic increase of cooling demand to provide thermally comfortable indoor environments in future, resulting in a high energy use for cooling supply.

While the aspect of estimating future cooling capacity requirements is crucial for the long-term sizing of cooling plants, this evaluation of future weather impact on buildings further focuses on the prediction of future indoor comfort, where the existing cooling capacities are exceeded. Therefore, for further analysis of the future weather impact on design decisions, the heating and cooling systems of the building are sized for an extreme summer day of the TMYx historic weather (see performance of these extreme-day-sized systems under historic TMYx conditions in Appendix A.8.3), but the BEPS simulation itself uses the future SSP5-8.5 scenario for 2050. The typical-day-sizing used in Section 4.7.2 is not used as baseline scenario for system sizing here, as it already revealed a high local discomfort on hot summer days using historic TMYx weather data (cf. Appendix A.8.5) due to insufficient typical day system sizing, which would be further amplified using future weather.

This simulation of the SSP5-8.5 case with TMYx-extreme-day-sized cooling capacities predicted an annual heating demand of 19.67 kWh/(m^{2}a) and cooling demand of 8.89 kWh/(m^{2}a), which is a decrease of the heating demand by 29.45%, and the cooling demand is almost four times larger than while using the TMYx weather data (cf. Appendix A.8.3). The electricity demand for lighting and electric equipment remained constant so that the reduction of heating demand is almost fully shifted to the cooling demand, resulting in the reduction of the total energy demand of only 1.13 kWh/(m^{2}a).

In Figure 5.9, the results for the limited cooling capacity applied on the SSP5-8.5 scenario are compared to the sizing scenario of TMYx. While both cases have the same cooling capacity limit of 1690.8 W, the prevailing outdoor air temperature in the SSP case of 40.7 °C leads to an indoor operative temperature in this case of 29.46 °C. While both cases have a higher cooling demand than available (cf. Figure 5.9), the TMYx case only reaches the cooling capacity limit from 10am

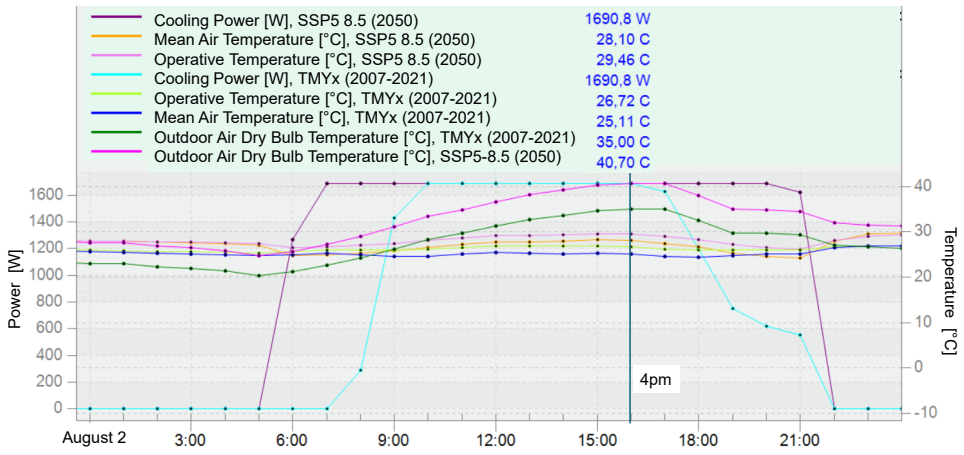

Figure 5.9: Comparison of the EnergyPlus results for the south-east office space on August 2, 4pm in the TMYx (2007-2021) and SSP5-8.5 (2050) scenarios. The cooling capacity is sized in both cases for an extreme summer day in the TMYx (2007-2021). Results for Cologne/Bonn Airport.

to 4pm (=6 hours), while the SSP case reaches the capacity limit from 7am to 8pm (=13 hours).

Figure 5.10 visualizes the resulting zonal parameters simulated in BEPS for the given timestep that is further analyzed in CFD using the *PluginOpenFOAM*. The BEPS results reveal an increase of the dissatisfaction PPD of 30% and an increase of the PMV of 0.65, compared to the results using recent TMYx weather in Figure 4.27.

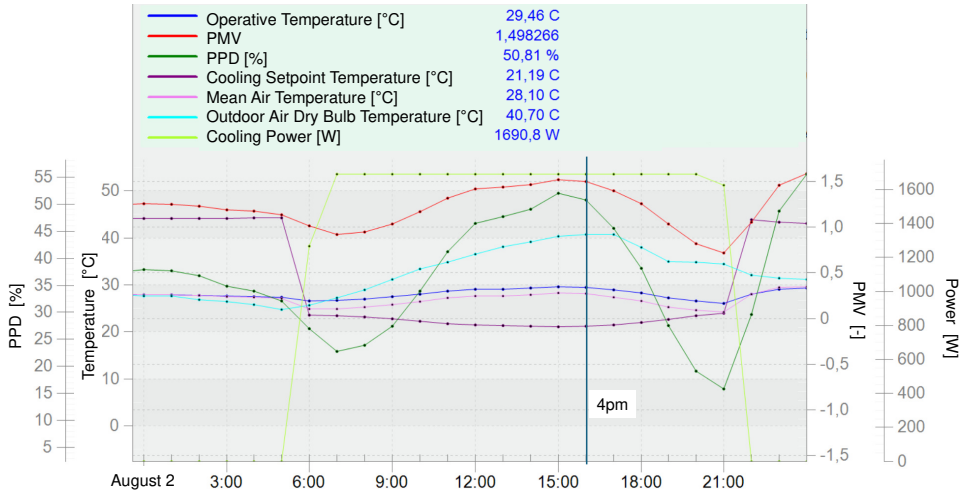

Figure 5.10: EnergyPlus results for the south-east office space on August 2, 4pm. T_{op} = 302.61 K, T_{mean} = 301.25 K, $T_{set,cool}$ = 294.34 K in SSP5-8.5 (2050) scenario for Cologne/Bonn Airport, maximum cooling capacity is sized using extreme summer day of TMYx (2007-2021).

The CFD analysis in Figure 5.11 for August 2, 4pm shows small deviations between to the BEPS results (ΔT_{op} = 0.21/0.31K (outflow down/side), ΔT_{mean} = 0.85/0.5K (down/side)). The temperature stratification is still stronger for the downward-facing outflow than for the sideward-facing outflow, as displayed in Figure 5.11a, similar to the stratification patterns observed for the TMYx case in Figure 4.28a. However, a layer of warm air is observed underneath the ceiling for both outflow directions. The vertical temperature difference between head and feet level is even further reduced compared to the TMYx results in Figure 4.28b, and thus within the acceptable

limits stated in [DIN16798-1].

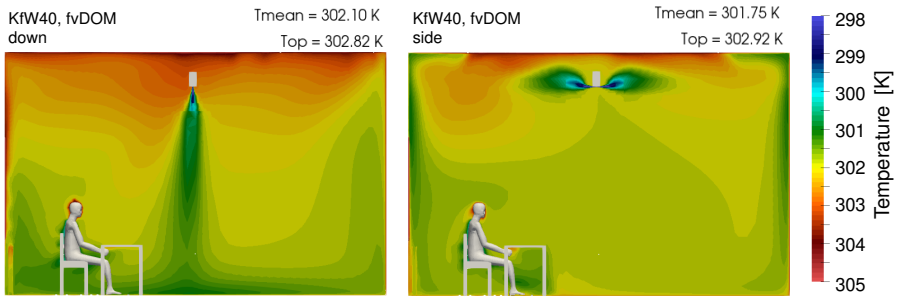

(a) Vertical temperature distribution.

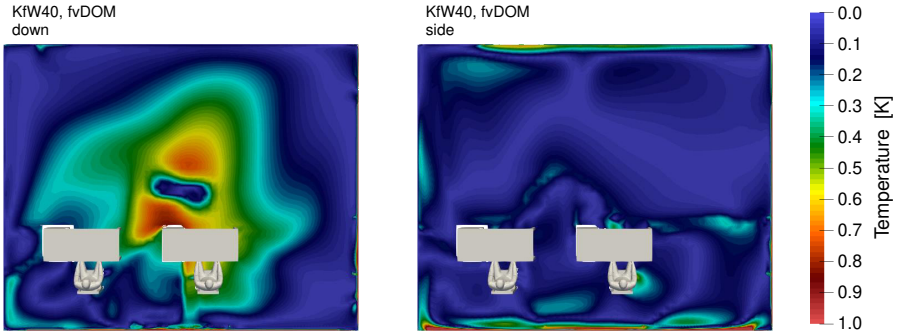

(b) Vertical temperature difference between head (1.1 m) and feet (0.1 m) level.

Figure 5.11: Vertical temperature distribution and difference in the south-east office space for down- and sidewards outflow direction. Simulated for August 2, 4pm, sized using extreme summer day of TMYx (2007-2021), simulated for SSP5-8.5 (2050) for Cologne/Bonn Airport.

While the air velocities in Figure 5.12 show a slight increase in some areas of the floor for the sidewards outflow, they show a reduction of the air velocity around the right occupant (cf. Figure 4.29). The resulting draught risk has decreased as visualized in Figure A.31 (cf. Figure A.20a for DR in TMYx (2007-2021) case), caused by an increased acceptability towards high air velocities with increased indoor temperatures (cf. Section 4.4.1 and [DIN16798-1]).

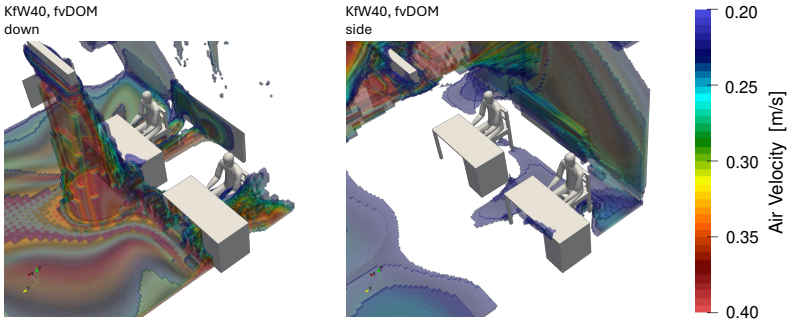

Figure 5.12: Air velocity above the Category II threshold (0.2 m/s in summer) defined in [DIN16798-1], NA, in the south-east office space for down- and sidewards outflow direction. Simulated for August 2, 4pm, sized using extreme summer day of TMYx (2007-2021), simulated for SSP5-8.5 (2050) for Cologne/Bonn Airport.

Figure 5.13 displays the results of the comfort metrics PMV, PPD, and DR, as well as the AoA. The resulting PMV is about 0.18 higher resulting from CFD compared to the BEPS result. The

application of the future weather resulted in an increase of the PMV of 0.66 and in an increase of the PPD of about 33%, compared to the TMYx case. The mean DR at head level is reduced by 1.5-2%. The AoA increased in the SSP5-8.5 case, which might be caused by the lower mixture of air due to a lower air temperature stratification.

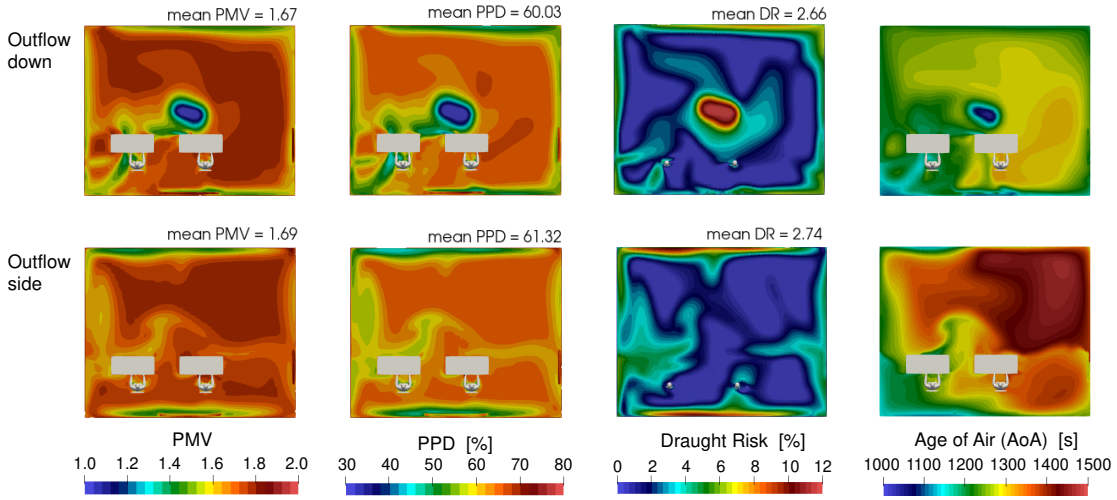

Figure 5.13: PMV, PPD, and Age of Air at a height of 0.6 m and draught risk at a height of 1.1 m in the south-east office space for down- (top) and sidewards (bottom) outflow direction. Simulated for August 2, 4pm, sized using extreme summer day of TMYx (2007-2021), simulated for SSP5-8.5 (2050) for Cologne/Bonn Airport.

The evaluation of the local thermal comfort revealed 37 hours annually of exceeded floor temperature (Category II limit: 29 °C) in the north-east *E01-10 Group office*, and six hours above this threshold for the south-east *E01-13 Group office*, which was the subject of the current analysis. For the analyzed timestep on August 2, 4pm, the BEPS results predicted a floor temperature of 29.45 °C, which has been set as boundary condition for OpenFOAM simulation. This floor temperature is only partially visible in Figure 5.11b for the sidewards outflow, as the downward outflow reduces the air temperature above the floor, such that the floor temperature itself is not visible in the slice.

5.5 Evaluation and Summary of the Research Hypotheses

This section evaluates the RHs on the assessment of the impact of climate change using IFC-based simulations as stated in Section 5.2.3, relating to RQ 3 defined in Section 1.3. The developed methods for IFC-based BEPS, CFD, and their application in thermal comfort analysis were successfully evaluated on the impact of climate change. The analysis of the BEPS results provided insights on energy consumption and thermal comfort on a zonal scale, which supports RH CC 1. While the annual evaluation of the BEPS results predicts future changes to the energy consumption and the required heating and cooling capacities, the evaluation of hourly BEPS results reveals cooling demands that may be affected by capacity limits, resulting in increased indoor temperatures, which again affect the indoor thermal comfort. The evaluation of the BEPS results revealed that the use of natural ventilation is limited in future climate scenarios

due to longer periods of high outdoor air temperatures. An additional evaluation of IFC-based CFD of spaces with critical BEPS results allows for a local thermal comfort analysis. This local analysis was applied to evaluate the effectiveness of the mechanical HVAC system under these extreme conditions, which supports RH CC 2. To maintain thermal comfort under increased cooling loads, the air exchange rate at the air terminals has to be increased (not evaluated in this work), or the supply air temperature has to be further decreased, which may cause unacceptably high air velocities or local air temperature differences, leading to draft risk or other forms of thermal discomfort. The evaluation of the impact of climate change on indoor environments is limited to cases with or without mechanical ventilation, as natural ventilation is not in the scope of the CFD analysis of this dissertation. Further research is required for CFD analysis on natural ventilation, as well as for other cooling systems, e.g., radiant cooling.

This combination of the applied BEPS and CFD-based analysis of thermal comfort provides a grasp on the impacts of climate change on all building spatio-temporal scales, starting from the annual building evaluation, over the hourly analysis on a zonal scale, to a high-resolved spatial scale for a single timestep (or short timeframe, if transient CFD would be applied) for a single zone of interest. This combination of the proposed methods of this dissertation was demonstrated in response to RQ 3.

While the RHs and RQs were addressed, some additional remarks have to be considered for the application of the proposed methods. For the evaluation of future local thermal comfort, the choice of system sizing is critical. Both evaluated scenarios, (1) the comparison of the typical-day-sized systems (unlimited heating, autosized cooling capacity) using the same weather data for sizing and simulation (TMYx and SSP5-8.5), and (2) the comparison of the TMYx-extreme-day-sized simulations (limited heating and cooling capacity) for TMYx and SSP5-8.5, lead to a heating reduction of about 30% and a cooling energy increase of almost 400%. However, the comparison of the typical-day-sized systems (1) revealed an undersized cooling capacity of 1200 W in the TMYx case, incapable of providing thermal comfort during TMYx hot summer days, while the SSP5-8.5 typical day sizing revealed a sufficiently sized cooling capacity of 2400 W, providing better thermal comfort for the evaluated hot summer day. Thus, the typical day sizing resulted in better performance when applied on future weather data. This may be caused by the general conditions for typical days in the respective weather files, as the TMYx file only includes two days per year with temperatures exceeding 32 °C, while the SSP5-8.5 data includes 19 days annually exceeding this threshold. While the results of Scenario (1) provided a prediction of future required cooling capacities, Scenario (2) evaluated the performance of systems sized under current conditions under the impact of future weather scenarios. The analysis revealed a drastic reduction of thermal comfort in future climates, leading to a PMV of 1.5 (BEPS) and 1.7 (CFD) and a resulting PPD of 50% (BEPS) to 60% (CFD).

Besides the correct choice of the sizing approaches related to the individual use case, some limitations of the current methods have to be considered. The evaluation of the impact of future weather on local thermal comfort currently neglects direct solar radiation and considers only surface temperatures and conductive heat fluxes from BEPS and calculates long-wave radiation

in OpenFOAM during runtime. Adding solar radiation to the representation of the simulated space in CFD would not only require the use of a corrected solver for the solar load (e.g., a corrected version of the solar load calculation in the radiation model fvDOM) but also requires the definition of shading elements (e.g., controllable external shadings), which are not included in the available use case IFC file. Considering external shading elements in the IFC-based OpenFOAM setup that are generated from external space boundaries (cf. Figure 4.11c) could be a first step in further research to consider shading elements in IFC-based CFD. However, even if these IFC- and OpenFOAM-related issues are solved, the reliability of solar radiation data in future weather files remains a source of significant uncertainty on the predicted results, since the methods to transform global horizontal irradiance to direct normal and diffuse horizontal irradiance vary [NK21], or future predictions on irradiance are even neglected [PU19]. The analysis of the SSP5-8.5 weather files generated using the *Future Weather Generator* revealed high peaks of direct normal radiation (cf. Figure 5.3) that exceeded the solar constant, which requires further investigation. In addition, the analysis in this dissertation revealed that the hot summer prediction of the BBSR 2045 scenario shows an increase of 40% on its baseline scenario TRY 2015 (1995-2012), but results in an even slightly lower average direct normal irradiance as the historical TMYx weather data (cf. Table 5.1). This underlines the importance of using up-to-date weather files (i.e., TRY data based on recent recordings) for further generation of future weather files. While the uncertainty of solar radiation parameters in the weather data is currently only directly affecting the BEPS results, the resulting effect of the error propagation would be increased if solar radiation was included in CFD, and would further increase the uncertainties in the local thermal comfort predictions.

Overall, the proposed IFC-based approach allows an automated setup of BEPS and CFD models that can be evaluated on different climate change scenarios. This allows the assessment of the dynamic performance of the building on all spatio-temporal scales considering transient effects, which cannot be assessed by static simulations. Using the automated setup of IFC-based simulation models, design changes can quickly be analyzed on their impact on energy efficiency and thermal comfort to enhance thermal resilience even in future climates. However, the comparison of the available weather files for historical and future weather scenarios revealed that the choice of weather file has a significant impact on the simulation results. Even if IFC-based simulations are applied, these should be evaluated for uncertainties causing a performance gap, which results from choices on the construction, occupancy, and operation, but also from uncertainties in the choice of weather data.

6 Discussion and Limitations

This dissertation presents a methodology for the IFC-based setup of BEPS and CFD, including a further extension of these approaches to evaluate thermal comfort. These approaches are tested and evaluated individually and combined to assess the thermal performance of buildings and to further predict the impact of climate change on buildings. In this section, all proposed methods are discussed within the scope of the Research Questions (RQs) defined in Section 1.3.

Research Question 1:

> "How can both, BEPS and CFD simulations, be integrated into an IFC-based BIM-workflow to increase the accessibility to dynamic building analysis for energy efficiency and thermal comfort?"

In related research, the lack of interoperability between BIM tools and simulation tools, which leads to to significant efforts for model setup, is one of the most common issues for the poor accessibility of simulations in BIM workflows (cf. Section 2.3.2 and Section 3.3.1).

To overcome these accessibility issues, this dissertation proposed an IFC-based concept for the integration of BEPS and CFD simulations in the multi-domain open-source simulation framework *bim2sim*. Using open-source simulation kernels (i.e., EnergyPlus for BEPS and OpenFOAM for CFD) provides the advantages of an architecture that is free of charge and allows for code insights and necessary modifications. Combined with the use of the open data exchange format IFC, the presented framework is accessible for all IFC-based BIM-workflows, and allows dynamic building analysis in research and industry without additional license cost.

For the integration of the simulations into IFC-based BIM workflows, the input requirements for simulation model requirements were identified and analyzed. All discussed simulation approaches have the common requirement of a suitable representation of surface geometry, which is further defined by applicable boundary conditions. For the geometric representation in the simulation model, second-level space boundaries were identified from related research as a suitable representation in the IFC schema, which are linked in the IFC to spaces, building elements, and their respective property sets. The *GlobalId* is identified as a suitable common IFC-based identifier for building elements, spaces, and space boundaries to enhance a seamless integration of all simulation results into the IFC-based BIM process. For an improved applicability of the approaches within the BIM workflows, the need for automation of model setup processes was identified.

Based on these identified fundamental concepts for the IFC-based setup of simulation models,

three main approaches for the integration of (1) BEPS, (2) CFD, and (3) thermal comfort into the BIM workflow were proposed in this dissertation. An automated (1) IFC-based BEPS setup (Chapter 2) uses the geometric and semantic representation of space boundaries combined with the template-based enrichment of building constructions to setup a BEM for the simulation with the open-source kernel EnergyPlus. This setup allows for the automatic setup for external shadings from external space boundaries (cf. Section 4.7.2 and Figure 4.11c). The (2) IFC-based setup of CFD models for the simulation with the open-source kernel OpenFOAM (cf. Chapter 3) uses the same set of space boundaries as the geometric basis for the surface geometry of the space, such that the surface temperatures and heat fluxes calculated in the IFC-based BEPS are applied as boundary conditions for CFD. Besides this definition and parametrization of the boundaries of the computational CFD domain, HVAC systems are derived from available IFC elements or parametrically generated. Parametric generation is also applied to the positions of furniture and occupants. The setup of (3) IFC-based thermal comfort analysis (cf. Chapter 4) includes methods for both the BEPS and CFD scale of the building and individual zones. The proposed setup includes the template-based enrichment of personal comfort parameters, as these are not yet available in the IFC standard. The approach additionally included the integration of a manikin with segmented body parts, which are adapted from the thermo-physiological human model MORPHEUS [Wöl17]. This segmented manikin allows for a body-part-specific assignment of local boundary conditions.

As defined in RQ 1, the IFC-based simulations are requested to be used for dynamic building analysis to evaluate energy efficiency and thermal comfort, which were addressed by the selection of applicable measures throughout the evaluations of this work. The evaluation in Section 2.7.3 addresses the energy efficiency assessment by analyzing the annual heating energy consumption of the total building, the peak heating power demands per space, and the indoor surface temperatures in a space. Radiators were evaluated in Section 3.6.2, comparing radiation models and radiator models. The air distribution in the space was evaluated in Section 3.6.3 using the prototypical implementation of the downward- and sideward-facing slot diffusers regarding temperature distribution, air velocities, and resulting AoA. This evaluation of HVAC systems is a basis for the optimization of HVAC design, balancing operational cost and indoor environmental quality. The evaluation of thermal comfort simulations in Section 4.7 supported the annual BEPS-based evaluation of static and adaptive thermal comfort on space level to identify spaces with high risk of discomfort and summerly overheating, as well as a limited local thermal comfort analysis based on surface temperatures. The evaluation of thermal comfort in Section 4.7.2 demonstrates a reduction of the unacceptable overheating in office spaces where external spatial elements are considered while the heating demand increases.

The proposed automated IFC-based simulation approaches successfully addressed the significant efforts for model setup by providing automated model setup processes and thus drastically decreased the required modeling time. This is achieved by the fully automated processes for algorithmically setting up model geometry and boundary conditions, such that only general simulation settings require a manual setup. This includes the setup of CFD models, where

the mesh refinement based on IFC objects supported a fully automated meshing process that did not require any manual rework in the evaluated use case. The simulation of BEPS and BEPS-based thermal comfort can be automatically executed and provides an automated representation of the results in diagrams and a floorplan representation, which assists in decision making within BIM-workflows. The evaluation of the energy efficiency and thermal comfort results used applicable measures on different spatial and temporal scales, providing a profound overview of the building's thermal performance. The structure of the model setup allows for an adaptation of the output variables according to the specific project needs. Using the *GlobalId* from IFC elements as a global identifier was successfully applied to transfer the simulation results from BEPS to the setup of boundary conditions in CFD. The plugin-based structure of the *bim2sim* framework allows for an easy integration of further plugins or adaptations of existing workflows.

However, the outlined framework still has its limitations. The proposed framework is limited by the quality of the available IFC data on space boundaries, constructions, materials, and HVAC devices. The second research question addresses these challenges on model quality in the model setup in detail. The evaluation of results underlined the importance of external shading elements to produce accurate predictions of indoor conditions. The required external space boundaries can be generated from space boundary algorithms in research [Fic22], but have not been found in IFC exported by commercial BIM authoring tools; thus, this approach has limited applicability outside of research. Transforming IFC-based HVAC systems for the use in CFD is currently limited to typical radiators and slot diffusers, and was not compared to flow profiles from research or industry, but only evaluated for plausibility. In general, the underlying physical models for CFD simulations (e.g., for turbulence and radiation) are pre-selected within the prototypical implementation but should be verified by experienced engineers for the applicability in the respective use case. The integration of the manikin with segmented body parts adapted from MORPHEUS [MJvT+22] is prototypically implemented using skin temperatures and heat fluxes from related research. Extending this approach to coupling the full thermo-physiological MORPHEUS model would allow for comfort predictions for each body part, enhancing the use of personalized comfort systems within IFC-based CFD simulations or even in operated buildings coupled to an IFC model.

Despite of the model quality, the implementation of the framework may be limited to small to medium-sized IFC files, as it has not been evaluated for computational efficiency on large scale IFC models. In related research, no suitable case studies have been found for a validation that provided both a suitable IFC4 model and applicable simulation results. Thus, all of these IFC-based methods for setting up simulation models have been tested and evaluated, but mainly validated by comparing simulation variants or tested for plausibility, which should be elaborated when applying these approaches to other projects. The simulation kernels EnergyPlus and OpenFOAM itself are validated and do not require further validation in this dissertation. The resulting building geometry in the IDF model used for BEPS, which has the same geometric basis as the CFD model, is validated to match with the input IFC geometry using the proposed

IFC2IDFValidationTool (cf. Section 2.6). Thus, for the accuracy of the results, the template-based enrichment of materials, constructions, and usages provides the highest risk of uncertainty for the BEPS simulation, which can be assessed using sensitivity and uncertainty analysis in future research. While this uncertainty is propagated to the boundary conditions of the CFD model, the CFD setup itself provides additional uncertainties. These include neglecting solar radiation, the simplified static definition of occupant clothing surface temperatures, the lack of additional local heat sources representing technical equipment and lighting, the simplification of air inlets, the generative positions of furniture and occupants, and the application of quasi-steady-state instead of transient simulations. The presented IFC-based thermal comfort analysis further propagates the errors of the BEPS and CFD setups. The applied thermal comfort measures (PMV, PPD, local comfort, adaptive comfort) are designed for the prediction of thermal performance for large groups of people and often fail to estimate the individual thermal comfort, lacking to reflect the diversity of human conditions. As the presented methods allow for a quick IFC-based setup of even high-resolved CFD models, the proposed methods are expected to enhance the required validation of (local) thermal comfort in field studies on real-world scenarios in residential and non-residential buildings. Each of these uncertainties requires validation or quantification in further research.

Additionally, the framework was not evaluated within the BIM workflow of a building design process in industry, as no suitable industry project has been available within the scope of this dissertation to share applicable IFC data. Thus, even though the proposed IFC-based approaches provide methods for evaluating energy efficiency and thermal comfort, the integration into design processes outside of research has not yet been verified and tested. The data transfer of simulation results throughout the IFC-based design process remains an open question, but should be based on the IFC *GlobalId*. The proposed workflow is not designed to provide bi-directional feedback to the IFC-model, such that the simulation results are not automatically fed back into the IFC model. Including the simulation results would drastically increase the size of the IFC file if hourly BEPS results were added component-wise as *IfcTable*s, while adding CFD exceeds the known technical capabilities of the latest IFC4 standards. Bi-directional data transfer has also been discussed within the scope of the working group on guideline VDI 2552 Part 11.9 on BIM-based data transfer for building physics and has quickly been disregarded for these reasons. Another issue with bi-directional simulation data transfer is the liability for the results. If design changes are applied to the building facade, e.g., by the architect, the simulation results in the model may become inaccurate, which may remain unnoticed and cause further errors in the building design.

Overall, the proposed methods form a suitable framework in response to RQ 1, which enhances the automated generation of IFC-based simulation models requiring a minimum manual rework. The applicability of the framework is limited by the quality of the underlying IFC data, which is partially mitigated by the enrichment and correction processes developed in response to RQ 2.

Research Question 2:

> "How can current challenges in the simulation model setup (i.e., manual effort, availability and quality of data) be addressed to enhance seamless automated integration of IFC-based simulations?"

This second research question addresses the current challenges within the IFC-based model setup that hinder the seamless automated IFC-based integration of simulations into the BIM workflow. The prevailing challenges are elaborated based on related research and are addressed by applicable strategies to overcome these challenges. As elaborated in the discussion of RQ 1, the lack of interoperability between architectural and simulation software partially results from the quality of the available IFC data, which hinders the use of dynamic simulations in the design process. The IFC-based framework for BEPS and CFD using automated model setup needs to provide robustness towards poor IFC quality, which can be achieved by integrating applicable validation, correction, and enrichment approaches for the required IFC data.

For the seamless integration of the IFC-based simulations, this dissertation proposes pre-processing steps for the IFC, workflow-integrated corrections, and a model validation as a post-processing of the BEPS model setup. For the pre-processing of the IFC-based BEPS process, the *IFC2IDFValidationTool* was introduced in Section 2.6, which provides a visual and algorithmic analysis to resolve IFC space boundary errors prior to the *bim2sim* workflow to reduce computational overhead in repeated simulations. The validation tool provides a subset of validation rules available in related research, which addresses the validation requirements based on the IFC files used in this dissertation. Similarly, this tool is used for post-processing, where the surface transformations between the IFC and the output EnergyPlus IDF are validated, which has not yet been observed in related research. The IFC-based setup of BEPS models (cf. Section 2.5) addresses the syntactic, semantic, geometric, and consistency errors observed in the space boundary geometry, which is the basis for the setup of geometry in all simulation approaches of this dissertation. The space boundary algorithms implemented in the *bim2sim* tool include workflow-integrated corrections for vertex- and surface normal errors, and derive missing data, e.g., relations between corresponding boundaries and parent-child relationships between walls and windows.

For missing construction, material, or space usage data, the *bim2sim* framework includes a data-enrichment framework, which was developed prior to this dissertation (cf. Section 2.2.3). This dissertation includes an extension of the existing enrichment framework for enriching personal comfort data (i.e., activity level and clothing), as this data is not available in the latest IFC schema. The extension of personal comfort data aims to distinguish between the clothing and activity levels based on the different usage of spaces, as opposed to the general standardized definition of clothing (0.5/1.0 clo for summer/winter) and an activity level of 1.2 met for all space settings. While the presented parameters are derived based on clothing and activity parameters from international standards, the underlying choices for the activities and clothing rely on assumptions, which is a limitation upon further validation of these assumptions.

The setup of CFD models using IFC benefits from the aforementioned validation and correction algorithms developed for the BEPS setup, as the CFD setup builds upon the corrected space boundary data, using both geometry and simulated temperature and heat fluxes to define the boundary conditions. Apart from the building geometry, the IFC-based CFD setup requires suitable HVAC geometry, which can be used as heat sources, inlets, and outlets, but also requires an appropriate representation of the indoor environment, using furniture. This raises the challenge of transforming existing IFC elements into suitable CFD geometry, which is addressed by algorithmic transformations triggered by applicable user-defined simulation settings. Transformed or generated air inlets are currently assumed to show homogeneous inlet pressure over multiple air inlets within the same space, which may result in inaccurate flow patterns. If furniture geometry is not available or subject to daily changes, e.g., in multi-purpose spaces, this dissertation provides prototypical approaches for the generation of such objects.

The proposed methods were successfully applied to address the identified challenges in automatically generating applicable simulation models for BEPS, CFD, and thermal comfort from the evaluated IFC data. All validations, corrections, and enrichment processes comply with the identified need for automated processes from RQ 1. The automated integration of correction algorithms provides the risk of unwanted changes when applying the algorithms to new IFC models, e.g., resulting in surface geometry errors caused by errors in vertex correction algorithms for complex geometry. Therefore, the validation of the resulting simulation model and results by an experienced engineer is crucial in such fully automated processes that combine automated model setup, simulation execution, and post-processing of results.

However, the list of identified challenges from related research that are addressed in this dissertation should be considered as non-exclusive and requires further research. The presented approaches may be limited to the challenges and errors observed in the evaluated IFC data, which provide a comparatively high data quality, as these were designed for research purposes. Resulting from the tested IFC data, minimum IFC requirements have been defined. All proposed methods have the definition of space boundaries as a minimum requirement, but also have minimum quality requirements. Even though the set of space boundaries is allowed to show gaps, the space boundaries should not overlap. Also, each space boundary must provide a semantic relation to its related building element and the relating space.

Thus, the presented algorithms are expected to be limited in their robustness in real-world use cases. Here, the proposed validation and correction algorithms require generalization and extensions to cover the variety of errors that may arise from different modeling practices and IFC exports of IFC authoring tools. For the generation of HVAC elements and furniture for CFD, the algorithms require further testing regarding handling diffuser and radiator types, as well as transforming furniture into suitable CFD geometry.

To conclude for RQ 2, common challenges in the IFC-based simulation setup can be addressed by applicable algorithms to enhance the seamless automated integration in BIM workflows. The proposed methods in this dissertation have shown that the issues can be resolved algorithmically and thus allow for automation within the BIM setup. However, the heterogeneity of IFC data

quality that arises from IFC models in industry projects requires additional algorithms to ensure the required robustness for fully automated model transformations.

Research Question 3:

> "How can IFC-based BEPS and CFD approaches be computationally efficiently combined to evaluate the energy efficiency and thermal comfort of buildings, especially related to climate change?"

The third research question requires an evaluation of the computationally efficient combination of IFC-based BEPS and CFD simulations to be applied for simulative evaluations. Therefore, the energy efficiency and thermal comfort in residential and non-residential buildings (cf. Chapter 4) and the impact of climate change on these buildings (cf. Chapter 5) were evaluated using a combination of BEPS and CFD to assess the thermal performance of the building. Using the large-scale BEPS-based thermal performance of the building, the annual energy consumption and hourly thermal performance of the building can be evaluated on global and zonal levels. The floor plan representation of the building allows the identification of zones with heating and cooling demands, as well as spaces with high occurrences of overheating or other discomfort. While this BEPS-based analysis is available at low computational cost, it allows a profound identification of times and spaces within the annual hourly simulation of the whole building that require a more detailed local comfort analysis using CFD. Thus, the computationally expensive CFD simulations are performed for only selected timesteps. With the current setup, the CFD simulations require the use of high-performance computing environments, choosing an appropriate number of cores depending on the size of the simulated room, to produce CFD results in a reasonable time, and are therefore not executable on lower-performance office computers.

This combination of BEPS and CFD presents an approach to select spaces with a high risk of local discomfort but does not identify spaces with dysfunctional HVAC systems, high local internal loads, or complex interior design, which may result in an incomplete mixture of air, high differences in local air temperature, or poor indoor air quality. Thus, the selection of spaces for an in-depth CFD analysis should not only be selected based on the BEPS results but also from additional use-case-specific knowledge on critical spaces.

Using these combined approaches further allows for the detailed assessment of limited heating and cooling capacities under different climate scenarios. The choice of system-sizing strategy depends on the choice of heating and cooling systems to optimize the efficiency of these systems during operations. For heat pumps, it may be useful to risk a slight undersizing of the system (e.g., using typical days) to operate the system in optimum efficiency for larger parts of the year, while additional heating or cooling power on extreme days may be provided by an additional electric source.

Within the combination of the IFC-based setup of BEPS, CFD, and thermal comfort, an ad-

ditional validation is required that aligns with further validation needs discussed for RQ 1. Additional validation is required to evaluate the impact of future climate scenarios. The validation of global climate models is out of scope for this dissertation. However, the downscaling methods for generating local weather scenarios for use in BEPS require validation to estimate the uncertainties caused by the choice of the downscaling approach. For this downscaling, the latest available climate models should be used, as the evaluation in Section 5.3 has shown the large deviations between historic weather files and future weather predictions.

Overall, for RQ 3, the proposed combination of IFC-based BEPS and CFD approaches supports the simulation-informed selection of spaces and timesteps with a high risk of thermal discomfort. This informed choice of CFD simulation objectives reduces the risk of increased computational cost through repeated simulations. The combination of BEPS and CFD is not only applicable to current weather scenarios, but can be similarly applied to evaluate the increased risk of overheating in future weather scenarios. Using BEPS to define the boundary conditions for CFD also allows for the detailed evaluation of changes in the required heating and cooling capacities under changing environmental conditions.

7 Conclusion

The mitigation of the impact of climate change on ecosystems and the human population requires a reduction of greenhouse gas emissions to reduce the effect of further global warming [IPCC23]. As more than 30% of the German energy consumption results from the energy consumed by HVAC systems [AGEB24], the optimization of energy-efficient building design and operation is crucial to no longer exceed the national limits within the path of reducing greenhouse gas emissions [Ago25, KSG24].

To improve the assessment of a building's thermal performance, this dissertation presented approaches for the BIM-based setup of simulation models using the open data exchange format IFC. The IFC-based setup of BEPS for the simulation in EnergyPlus uses the concept of space boundaries to set up the BEM as a digital representation of the building physics and usage. Within this setup process, challenges on the input data quality are addressed by applying proposed algorithms to correct, enrich, and validate the available input data. For the coupled setup of IFC-based CFD simulations using OpenFOAM, the BEPS results for surface heat flux and temperature are used as boundary conditions for the CFD domain. The setup of the indoor environment for the CFD simulation, including the setup of HVAC systems, furniture, and occupants, is generated using available IFC data, geometric simplifications, and parametric enrichment. For the IFC-based assessment of thermal comfort, personal comfort parameters are derived as an extension of zone-usage-specific templates, which were originally created for the parametrization of the reduced-order building simulation approach TEASER. These personal parameters are used for the assessment of indoor thermal comfort in an annual hourly evaluation at building and zone level using BEPS, as well as for the analysis of local thermal comfort within a single space using CFD.

The use of a combination of the presented IFC-based setup for BEPS, CFD, and thermal comfort enhances the evaluation of the thermal performance of a building on multiple scales. The evaluation of the BEPS results identifies spaces with a high risk of thermal discomfort, which are further evaluated for local thermal comfort using CFD. The combined evaluation of BEPS and CFD further enhances the evaluation of limited heating and cooling capacities caused by system sizing choices. These limited capacities can also reflect changes in outdoor conditions to predict the impact of climate change on the indoor environment.

The proposed methods were evaluated for the building thermal performance using recent historical TMYx weather data for the years 2007-2021 and future weather derived from the SSP5-8.5 future climate scenario for the year 2050. A comparison of two building constructions with low and high U-values demonstrated the differences in local thermal comfort. The results also highlighted the importance of accurately modeling external shading elements, such as trees and

surrounding buildings, as reducing solar gains reduces the inacceptable overheating of spaces while it leads to increasing heating energy consumption. The comparison of building performance using historical and future weather data revealed that the simulated non-residential office building using a KfW40 construction shows a decrease of 30% in energy demand, while the cooling demand increases by 400%.

The presented work demonstrated the chances of a future integration of the automated IFC-based assessment of building thermal performance impacted by a changing climate into BIM-based design workflows. With appropriate validation in field studies in future research, the IFC-based assessment of the building's energy efficiency and comfort will enhance the simulation-based support of decision-making within BIM workflows, leading to an optimized design and operation of current and future buildings.

8 Outlook

The evaluation of the methodology presented in this dissertation revealed issues requiring further research, which can be grouped into two categories: (1) Further testing, robustness improvements, and validation of the presented approaches, and (2) propagation, adaptation, and integration of the presented approaches to other research areas.

8.1 Future Developments and Validation of the Proposed Methods

While all presented approaches were implemented and evaluated for plausibility, future research should include a deeper validation of the presented methods. For the optimization of HVAC system sizing, the evaluation of the impact of typical-day and extreme-day sizing requires further analysis. For the field of CFD, further validation should include additional tests for the *PluginOpenFOAM* regarding the computational evaluation of grid independence, e.g., using statistical results or the Grid Convergence Index (GCI). Considering the computational performance of the CFD, a scalability analysis should be applied regarding parallelization performance for the resulting mesh sizes. These grid and performance tests should be applied to spaces with different complexities, interior designs, and occupancies. The generation of HVAC systems from IFC models for CFD simulations requires an extension to additional components and validation with heat and airflow distribution profiles from related research or industry. Future research should also address improvements of the computational performance of CFD simulations, e.g, by simplifying repetitive mesh patterns like air inlets and outlets and map their flow profiles to surfaces.

To fully comply with BEPS and CFD simulations and their boundary conditions, the solar radiation in the OpenFOAM kernel should be debugged in further research, such that solar radiation can be integrated into the *PluginOpenFOAM*. A preliminary result using a modified version of the OpenFOAM kernel of the resulting surface temperatures in a single office with furniture is visualized in Figure 8.1 and requires further validation. Here, further research is required on the automated integration of external shadings into CFD from space boundaries and surrounding buildings.

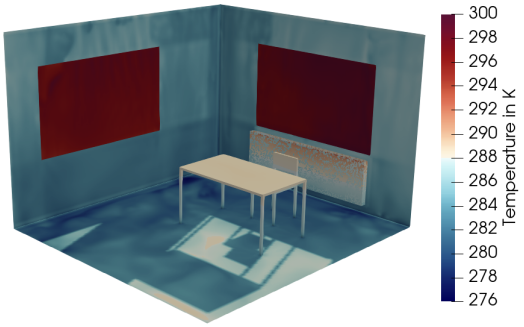

Figure 8.1: Preliminary surface temperature results on solar radiation in single office.

For an in-depth validation of the presented approaches, further research is required to validate

the simulation results on real-world use cases, also including model calibration. As this dissertation evaluated the methods on high-quality IFC4 models from research, the application on real-world scenarios may require further improvements on the robustness of the algorithms, including additional algorithms for model healing, such as corrections for missing or incorrect IFC data.

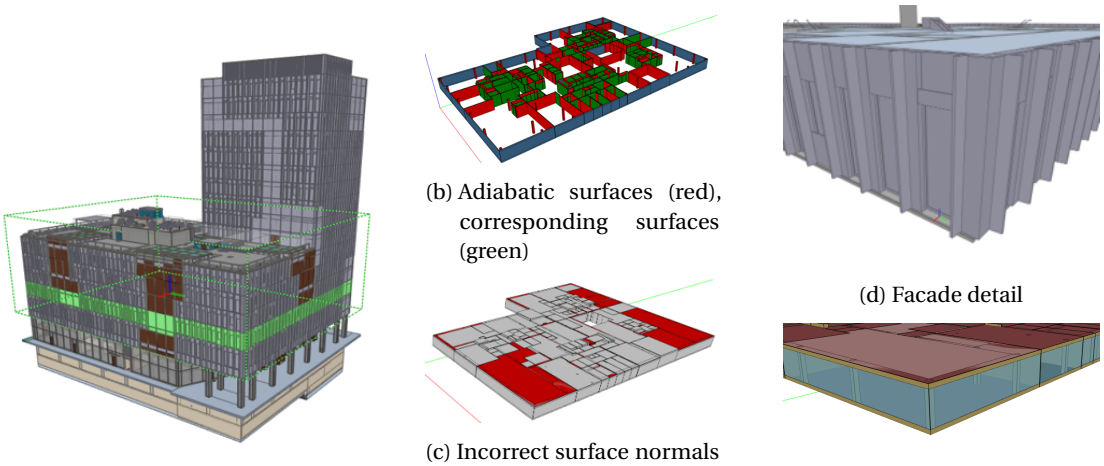

(a) Selected storey

(b) Adiabatic surfaces (red), corresponding surfaces (green)

(c) Incorrect surface normals (red)

(d) Facade detail

(e) Simplification of facade

Figure 8.2: Outlook on the Real-world use case building EDGE from BIM2Praxis project.

Initial tests on the real-world use case of the EDGE building within the BIM2Praxis-Project,[1] visualized in Figure 8.2, revealed a large number of missing relations of space boundaries to building elements, resulting in a mismatch of corresponding boundaries between spaces. Initial tests on a single storey (Figure 8.2a) resolve errors from mismatching inner boundaries by setting them to adiabatic (Figure 8.2b) but require additional efforts to correct surface normals (Figure 8.2c). Missing relations to facade elements (Figure 8.2d) are prototypically algorithmically resolved, combined with inserting openings based on manual input for window-to-wall ratio (Figure 8.2e). Future research has to include the algorithmic generation of external shading elements for these generated windows. These methods outlined for this real-world use case show the potential for a drastic speedup of the simulation model setup process, along with the ongoing need for identifying IFC model quality issues. While additional algorithmic corrections are under development, future research could include artificial intelligence for spatial reasoning for model corrections, validation, and corrections. The validation of the simulation results in future research should not solely focus on evaluating the result itself, but also on quantifying the errors arising from additional model simplifications and assumptions, which are used to fill in missing, incomplete, or incorrect data. These errors can either be determined from comparisons between (simplified) simulations or from calibrated models of as-is buildings.

Additionally, future research should include an evaluation of the usability of the approaches within the design process of buildings. The IFC-based setup of BEPS and CFD enhances the

[1] BIM2Praxis Project, funded by the Federal Ministry for Economic Affairs and Climate Action, grant number 3EN1050A.

estimation of thermal building performance within the BIM-based design of buildings. The presented approaches thus support the recent research efforts on enhancing design decisions towards energy efficiency and thermal resilience in future climates. However, the usability of the methods in the design process depends on integrating these simulations into the decision-making processes in projects. Here, further research is needed to identify the design-decision milestones with the most significant impact on the energy efficiency and thermal comfort of buildings, which the IFC-based simulations should support. With further validation of the proposed approaches, the presented workflows can be integrated into established software products to make dynamic simulations accessible to design engineers within their BIM workflows with minimal additional effort. The simulations could be integrated as an additional approach to the state-of-the-art static calculations for heating and cooling demands. These dynamic simulations could be applied to evaluate the static system sizing under dynamic conditions under current and future climate conditions to facilitate an optimized system design.

8.2 Extrapolation of Proposed Methods to Other Research Areas

All presented methods in this dissertation are integrated into the open-source *bim2sim* framework, which allows for adoption and extrapolation into related research fields by any researcher. The plugin-based structure of the *bim2sim* tool allows for fast adaptations into related fields according to the specific needs of further projects in research and industry. The thermal comfort evaluations using BEPS and CFD can be extended for indoor air quality simulations, e.g., to evaluate the concentration of CO_2 depending on mechanical and natural ventilation. To consider the impact of breathing of occupants on indoor air quality, a further subdivision of the manikin's head surface should be considered to represent mouth and nose as a combined inlet and outlet. Additionally, this approach could be further extended by integrating pre-computed pressure conditions at air inlets to evaluate the performance of mechanical ventilation systems in a room with higher accuracy. These approaches should also consider transient approaches in CFD, which were excluded from this dissertation due to computational resources. The *PluginOpenFOAM* could be modified to support smoke control simulations [Klo16], a typical application within the field of CFD in indoor environments [MJvT+22]. To verify concepts on natural smoke venting [KK17], the wind-dependent airflow surrounding the building is crucial, which requires knowledge of the outdoor environmental conditions and the building surroundings [MJvT+22]. In future research, the IFC-based simulations could be integrated into their urban environment, represented by a city model in the CityGML format. This integration would not only support smoke control simulations but also general natural ventilation analysis for indoor environments. If the IFC-based simulation is integrated at the building level into an urban energy modeling approach, urban heat islands may be detected and evaluated on their impact on the indoor environmental conditions inside the building, e.g., on natural ventilation. Another approach could be the integration of an IFC-based building simulation into an urban energy model to evaluate the building's interaction with a grid of renewable energy supply. The integration of the city model could also be used to generate external shading elements in both BEPS and

OpenFOAM simulations.

The proposed methods further support the assessment of the building performance in an operational stage, representing the first stage towards a calibrated model, which allows for optimizing energy efficiency and operational cost within the scope of an overall reduction of greenhouse gas emissions. The presented IFC-based methods further enhance the integration of the predicted building thermal performance into a digital twin of the building, which could assist in maintaining the optimal building performance, even under the impact of climate change.

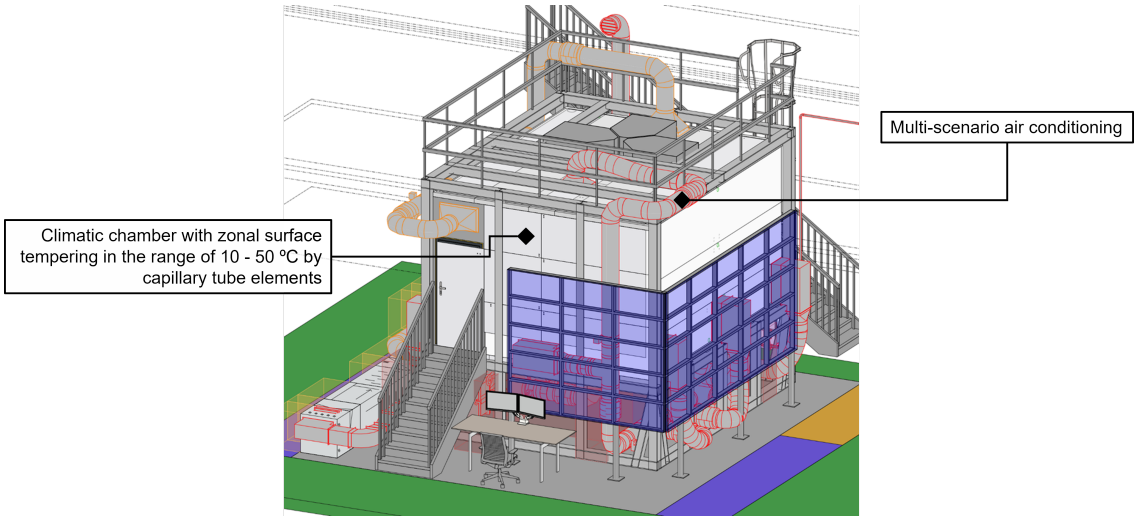

Figure 8.3: iCare laboratory: Individual Comfort in Augmented Reality Environments.

The methods proposed in this dissertation not only allow for adaptations for further simulation approaches or operational optimizations but also for integration into laboratory facilities. The results from BEPS can be utilized to condition the surface temperatures and indoor air conditions of laboratory environments, such as the iCare laboratory,[2] visualized in Figure 8.3. The iCare laboratory combines a climatic chamber with an immersive augmented reality environment. This laboratory setup can be used for studies on experiencing future climate scenarios in different augmented environments and support further evaluations on the effects of future weather conditions on human well-being and productivity in work environments. These studies can also be extended to experiencing the impact of unmet heating or cooling setpoint, e.g., caused by slightly undersized heat pumps to operate in optimum efficiency for large parts of the year. This setup can also be used to validate the CFD results for extreme outdoor conditions. Further research could also couple a thermo-physiological manikin in the laboratory to the virtual manikin adapted from MORPHEUS [Wöl17] in the *bim2sim PluginOpenFOAM* to enhance the validation of the CFD simulations regarding impact on occupants.

[2] iCare Laboratory: Individual Comfort in Augmented Reality Environments, funded by DFG (Deutsche Forschungsgemeinschaft, engl.: German Research Foundation), located at RWTH Aachen University, Institute for Energy Efficient and Sustainable Building (E3D), https://www.e3d.rwth-aachen.de/cms/e3d/forschung/projekte/laufende-projekte/~riyqi/icare-individual-comfort-in-augmented/, accessed on May 10, 2025.

Bibliography

[ACT+21] D. Aviv, K. W. Chen, E. Teitelbaum, D. Sheppard, J. Pantelic, A. Rysanek, and F. Meggers. A fresh (air) look at ventilation for COVID-19: Estimating the global energy savings potential of coupling natural ventilation with novel radiant cooling strategies. *Applied Energy*, 292:116848, June 2021. doi:10.1016/j.apenergy.2021.116848.

[ADMMV21] F. Ascione, R. F. De Masi, M. Mastellone, and G. P. Vanoli. The design of safe classrooms of educational buildings for facing contagions and transmission of diseases: A novel approach combining audits, calibrated energy models, building performance (BPS) and computational fluid dynamic (CFD) simulations. *Energy and Buildings*, 230:110533, Jan. 2021. doi:10.1016/j.enbuild.2020.110533.

[AGEB24] AG Energiebilanzen e.V. (AGEB). Anwendungsbilanzen zur Energiebilanz Deutschland. Endenergieverbrauch nach Energieträgern und Anwendungszwecken. Technical report, Oct. 2024.

[Ago25] Agora Energiewende. Die Energiewende in Deutschland: Stand der Dinge 2024. Rückblick auf die wesentlichen Entwicklungen sowie Ausblick auf 2025. Technical report, Berlin, 2025.

[AHA+19] F. Alshehri, C. Hoare, U. Ali, M. Shamsi, P. Kenny, and J. O'Donnell. Extending IFC to support thermal comfort prediction during design. In *Proceedings of the 2019 European Conference on Computing in Construction*, Computing in Construction, pages 284–293. University College Dublin, Jan. 2019. doi:10.35490/EC3.2019.203.

[AKO17] F. Alshehri, P. Kenny, and J. O'Donnell. Requirements for BIM-based Thermal Comfort Analysis. In *Proceedings of the 2017 Symposium on Simulation for Architecture and Urban Design (SimAUD 2017)*. Society for Modeling and Simulation International (SCS), Jan. 2017. doi:10.22360/SimAUD.2017.SimAUD.002.

[AKPO17] F. Alshehri, P. Kenny, S. Pinheiro, and J. O'Donnell. Model View Definition (MVD) for Thermal Comfort Simulation in Conventional BEPS tools. In *PLEA Proceedings*. Jan. 2017.

[ALES21] A. Alonso, J. Llanos, R. Escandón, and J. J. Sendra. Effects of the COVID-19 Pandemic on Indoor Air Quality and Thermal Comfort of Primary Schools in Winter in a Mediterranean Climate. *Sustainability*, 13(5):2699, Mar. 2021. doi:10.3390/su13052699.

[ALNK24] G. Abhijeet Ganesh, S. Lata Sinha, T. Nath Verma, and S. Kumar Dewangan. Energy consumption and thermal comfort assessment using CFD in a naturally ventilated indoor environment under different ventilations. *Thermal Science and Engineering Progress*, 50:102557, May 2024. doi:10.1016/j.tsep.2024.102557.

[AM02] N. Ashgriz and J. Mostaghimi. An Introduction to Computational Fluid Dynamics. In *Fluid Flow Handbook*, McGraw-Hill Handbooks. McGraw-Hill, New York, 2002.

[AMSW22] L. Arakawa Martins, V. Soebarto, and T. Williamson. A systematic review of personal thermal comfort models. *Building and Environment*, 207:108502, Jan. 2022. doi:10.1016/j.buildenv.2021.108502.

[ARHZ15] E. E. Asmi, S. Robert, B. Haas, and K. Zreik. A standardized approach to BIM and energy simulation connection. *International Journal of Design Sciences and Technology*, 21(1):59–82, Jan. 2015.

[ASH140] ANSI/ASHRAE Standard 140-2020: Method of test for evaluating building performance simulation software. American Society of Heating, Refrigerating and Air-Conditioning Engineers (ASHRAE). ASHRAE Special Publications, 2020.

[ASH169] ANSI/ASHRAE Addendum a to ANSI/ASHRAE Standard 169-2013: Climatic Data for Building Design Standards. ASHRAE. 2020.

[ASH17] *2017 ASHRAE Handbook: Fundamentals*. ASHRAE, Atlanta, Georgia, SI edition, Jan. 2017. ISBN: 978-1-5231-1351-4.

[ASH55] ANSI/ASHRAE Standard 55: Thermal Environmental Conditions for Human Occupancy. ASHRAE Special Publications, Jan. 2017.

[ASK18] A. Andriamamonjy, D. Saelens, and R. Klein. An automated IFC-based workflow for building energy performance simulation with Modelica. *Automation in Construction*, 91:166–181, Jan. 2018. doi:10.1016/j.autcon.2018.03.019.

[ASR35] Technische Regeln für Arbeitsstätten: Raumtemperatur. Bundesanstalt für Arbeitsschutz und Arbeitsmedizin (BAuA). 2022.

[Baz08] V. Bazjanac. IFC BIM-Based Methodology for Semi-Automated Building Energy Performance Simulation. Technical report, Berkeley, CA (United States), Jan. 2008.

[Baz09] V. Bazjanac. Implementation of semi-automated energy performance simulation: Building geometry. In A. Dikbas, E. Ergen, and H. Giritli, editors, *Managing IT in Construction/Managing Construction for Tomorrow*, pages 595–602, Boca Raton, Jan. 2009. Chapman and Hall/CRC.

[Baz10] V. Bazjanac. Space Boundary Requirements for Modeling of Building Geometry for Energy and Other Performance Simulation. In International Council for Research and Innovation in Building and Construction, editor, *Proceedings of the CIB W78 2010: 27th International Conference –Cairo, Egypt, 16-18 November*. Jan. 2010.

[Bea00] I. Beausoleil-Morrison. *The Adaptive Coupling of Heat and Air Flow Modelling within Dynamic Whole-Building Simulation*. PhD thesis, University of Strathclyde, 2000. doi:10.48730/ZV50-8Q07.

[BHM+20] E. Brembilla, C. J. Hopfe, J. Mardaljevic, A. Mylona, and E. Mantesi. Balancing daylight and overheating in low-energy design using CIBSE improved weather files. *Building Services Engineering Research and Technology*, 41(2):210–224, Mar. 2020. doi:10.1177/0143624419889057.

[BHP05] S. E. Belcher, J. N. Hacker, and D. S. Powell. Constructing design weather data for future climates. *Building Services Engineering Research and Technology*, 26(1):49–61, Jan. 2005. doi:10.1191/0143624405bt112oa.

[Bjö92] B.-C. Björk. A conceptual model of spaces, space boundaries and enclosing structures. *Automation in Construction*, 1(3):193–214, Dec. 1992. doi:10.1016/0926-5805(92)90013-A.

[BKKB18] A. Borrmann, M. König, C. Koch, and J. Beetz, editors. *Building Information Modeling*. Springer International Publishing, Cham, Jan. 2018. doi:10.1007/978-3-319-92862-3.

[BNRK22] B. Bass, J. New, D. Rastogi, and S.-C. Kao. Future Typical Meteorological Year (fTMY) US Weather Files for Building Simulation, July 2022. doi:10.5281/ZENODO.6939749.

[BPDSFB21] G. Bastos Porsani, K. Del Valle de Lersundi, A. Sánchez-Ostiz Gutiérrez, and C. Fernández Bandera. Interoperability between Building Information Modelling (BIM) and Building Energy Model (BEM). *Applied Sciences*, 11(5):2167, Jan. 2021. doi:10.3390/app11052167.

[BS20] T. Bloch and R. Sacks. Clustering Information Types for Semantic Enrichment of Building Information Models to Support Automated Code Compliance Checking. *Journal of Computing in Civil Engineering*, 34(6):04020040, Jan. 2020. doi:10.1061/(ASCE)CP.1943-5487.0000922.

[bui23] buildingSMART. Information Delivery Specification standard (IDS). https://github.com/buildingSMART/IDS, Jan. 2023.

[Cao18] J. Cao. *SimModel Transformation Middleware for Modelica-based Building Energy Modeling and Simulation*. PhD thesis, RWTH Aachen University, Aachen, Jan. 2018.

[CDCC23] Z. Chen, Z. Deng, A. Chong, and Y. Chen. AutoBPS-BIM: A toolkit to transfer BIM to BEM for load calculation and chiller design optimization. *Building Simulation*, Jan. 2023. doi:10.1007/s12273-023-1006-4.

[CDGC21] W. Chen, M. Das, V. J. L. Gan, and J. C. P. Cheng. *Integrated Data Model and Mapping for Interoperable Information Exchange Between BIM and Energy Simulation Tools*, volume 98 of *Springer eBook Collection*, pages 496–506. Springer International Publishing; Imprint Springer, Cham, 1st ed. 2021 edition, Jan. 2021. doi:10.1007/978-3-030-51295-8_35.

[CHM15] A. Cemesova, C. J. Hopfe, and R. S. Mcleod. PassivBIM: Enhancing interoperability between BIM and low energy design software. *Automation in Construction*, 57:17–32, Jan. 2015. doi:10.1016/j.autcon.2015.04.014.

[CL93] B. Cabral and L. C. Leedom. Imaging vector fields using line integral convolution. In *Proceedings of the 20th Annual Conference on Computer Graphics and Interactive Techniques*, pages 263–270, Anaheim CA, Sept. 1993. ACM. doi:10.1145/166117.166151.

[Cla01] J. A. Clarke. *Energy Simulation in Building Design*. Butterworth-Heinemann, Oxford, 2nd edition, Jan. 2001.

[CLW+01] D. B. Crawley, L. K. Lawrie, F. C. Winkelmann, W. F. Buhl, Y. Huang, C. O.

Pedersen, R. K. Strand, R. J. Liesen, D. E. Fisher, M. J. Witte, and J. Glazer. EnergyPlus: Creating a new-generation building energy simulation program. *Energy and Buildings*, 33(4):319–331, Jan. 2001. doi:10.1016/S0378-7788(00)00114-6.

[CSP+19] T. Cheung, S. Schiavon, T. Parkinson, P. Li, and G. Brager. Analysis of the accuracy on PMV – PPD model using the ASHRAE Global Thermal Comfort Database II. *Building and Environment*, 153:205–217, Apr. 2019. doi:10.1016/j.buildenv.2019.01.055.

[dB98] R. J. de Dear and G. S. Brager. Developing an Adaptive Model of Thermal Comfort and Preference. *ASHRAE Transactions*, 104, 1998.

[DB13] J. A. Duffie and W. A. Beckman. *Solar Engineering of Thermal Processes*. Wiley, Hoboken, New Jersey, 4th edition, Apr. 2013. doi:10.1002/9781118671603.

[DBCD+22] C. Di Biccari, F. Calcerano, F. D'Uffizi, A. Esposito, M. Campari, and E. Gigliarelli. Building information modeling and building performance simulation interoperability: State-of-the-art and trends in current literature. *Advanced Engineering Informatics*, 54:101753, Jan. 2022. doi:10.1016/j.aei.2022.101753.

[DCOZZ07] M. De Carli, B. W. Olesen, A. Zarrella, and R. Zecchin. People's clothing behaviour according to external weather and indoor environment. *Building and Environment*, 42(12):3965–3973, Dec. 2007. doi:10.1016/j.buildenv.2006.06.038.

[DDWAZ25] Z. Duan, P. De Wilde, S. Attia, and J. Zuo. Challenges in predicting the impact of climate change on thermal building performance through simulation: A systematic review. *Applied Energy*, 382:125331, Mar. 2025. doi:10.1016/j.apenergy.2025.125331.

[dena23] S. Becker, J. Hagen, S. Joshi, R. Krüger, and S. de la Serna. dena-Gebäudereport 2024. Zahlen, Daten, Fakten zum Klimaschutz im Gebäudebestand. Technical report, Berlin, Nov. 2023.

[dena24] Deutsche Energie-Agentur GmbH (dena). Leitfaden Energetische Gebäudebilanzierung nach DIN V 18599. Technical report, Berlin, Aug. 2023.

[DGNB23] DGNB System: Kriterienkatalog Gebäude Neubau. Deutsche Gesellschaft für Nachhaltiges Bauen (DGNB). Stuttgart, 2023.

[DIN12831-1] DIN EN 12831-1: Energy performance of buildings – Method for calculation of the design heat load – Part 1: Space heating load. Deutsches Institut für Normung (DIN). Beuth Verlag GmbH, Berlin, Feb. 2017. doi:10.31030/2571775.

[DIN15251] DIN EN 15251: Indoor environmental input parameters for design and assessment of energy performance of buildings addressing indoor air quality, thermal environment, lighting and acoustics, German version. Deutsches Institut für Normung (DIN). Beuth Verlag GmbH, Berlin, Dec. 2012. doi:10.31030/1912934.

[DIN16739] DIN EN ISO 16739-1, Industry Foundation Classes (IFC) für den Datenaustausch in der Bauwirtschaft und im Anlagenmanagement –Teil 1: Datenschema (ISO 16739-1:2024); Englische Fassung EN ISO 16739-1:2024. DIN.

Sept. 2024.

[DIN16798-1] DIN EN 16798-1:2022-03: Energy performance of buildings – ventilation for buildings – part 1: Indoor environmental input parameters for design and assessment of energy performance of buildings addressing indoor air quality, thermal environment, lighting and acoustics. Deutsches Institut für Normung (DIN). Beuth Verlag GmbH, Berlin, Mar. 2022. doi:10.31030/3327351.

[DIN16798-3] DIN EN 16798-3:2022-12, Energetische Bewertung von Gebäuden - Lüftung von Gebäuden - Teil 3: Lüftung von Nichtwohngebäuden - Leistungsanforderungen an Lüftungs- und Klimaanlagen und Raumkühlsysteme (Module M5-1, M5-4); Deutsche und Englische Fassung prEN 16798-3:2022. DIN Media GmbH. doi:10.31030/3344998.

[DIN17423] DIN EN 17423: Energy performance of buildings – Determination and reporting of Primary Energy Factors (PEF) and CO2 emission coefficient – General Principles. Deutsches Institut für Normung (DIN). Beuth Verlag GmbH, Berlin, Feb. 2021. doi:10.31030/3187565.

[DIN4108-2] DIN 4108-2: Thermal protection and energy economy in buildings Part 2: Minimum requirements to thermal insulation. Deutsches Institut für Normung (DIN). Beuth Verlag GmbH, Berlin, Feb. 2013. doi:10.31030/1929159.

[DIN52000-1] DIN EN ISO 52000-1: Energy performance of buildings – Overarching EPB assessment – Part 1: General framework and procedures. Deutsches Institut für Normung (DIN). Beuth Verlag GmbH, Berlin, Mar. 2018. doi:10.31030/2577378.

[DIN52003-1] DIN EN ISO 52003-1: Energy performance of buildings – Indicators, requirements, ratings and certificates – Part 1: General aspects and application to the overall energy performance. Deutsches Institut für Normung (DIN). Beuth Verlag GmbH, Berlin, Mar. 2018. doi:10.31030/2560187.

[DIN52010-1] DIN EN ISO 52010-1: Energy performance of buildings – External climatic conditions – Part 1: Conversion of climatic data for energy calculations. Deutsches Institut für Normung (DIN). Beuth Verlag GmbH, Berlin, Mar. 2018. doi:10.31030/2569185.

[DIN52016-1] DIN EN ISO 52016-1: Energy performance of buildings – Energy needs for heating and cooling, internal temperatures and sensible and latent heat loads – Part 1: Calculation procedures. Deutsches Institut für Normung (DIN). Beuth Verlag GmbH, Apr. 2018. doi:10.31030/2577376.

[DIN52017-1] DIN EN ISO 52017-1: Energy performance of buildings – Overarching EPB assessment – Part 1: General framework and procedures. Deutsches Institut für Normung (DIN). Beuth Verlag GmbH, Berlin, Mar. 2018. doi:10.31030/2563574.

[DIN52018-1] DIN EN ISO 52018-1: Energy performance of buildings – Indicators for partial EPB requirements related to thermal energy balance and fabric features – Part 1: Overview of options. Deutsches Institut für Normung (DIN). Beuth Verlag GmbH, Berlin, Oct. 2020. doi:10.31030/3139520.

[DIN6946] DIN EN ISO 6946:2018-03, Bauteile - Wärmedurchlasswiderstand und Wärmedurchgangskoeffizient - Berechnungsverfahren (ISO 6946:2017); Deutsche

Fassung EN ISO 6946:2017. DIN Media GmbH. doi:10.31030/2518301.

[DIN8996] DIN EN ISO 8996:2022-10: Ergonomics of the thermal environment - Determination of metabolic rate (ISO 8996:2021); German version. Deutsches Institut für Normung (DIN). Beuth Verlag GmbH, Berlin, Oct. 2022. doi:10.31030/9567844.

[DIN9920] DIN EN ISO 9920:2009-10: Ergonomics of the thermal environment - Estimation of thermal insulation and water vapour resistance of a clothing ensemble (ISO 9920:2007, Corrected version 2008-11-01); German version. Deutsches Institut für Normung (DIN). Beuth Verlag GmbH, Berlin, Oct. 2009. doi:10.31030/1532005.

[DINV18599-10] DIN V 18599-10: Energy efficiency of buildings - Calculation of the net, final and primary energy demand for heating, cooling, ventilation, domestic hot water and lighting - Part 10: Boundary conditions of use, climatic data. Deutsches Institut für Normung (DIN). Beuth Verlag GmbH, Berlin, Sept. 2018. doi:10.31030/2874436.

[DINV18599-1] DIN V 18599-1: Energy efficiency of buildings - Calculation of the net, final and primary energy demand for heating, cooling, ventilation, domestic hot water and lighting - Part 1: General balancing procedures, terms and definitions, zoning and evaluation of energy sources. Deutsches Institut für Normung (DIN). Beuth Verlag GmbH, Berlin, Sept. 2018. doi:10.31030/2874317.

[Dju05] E. E. Djunaedy. *External Coupling between Building Energy Simulation and Computational Fluid Dynamics*. PhD thesis, Technische Universiteit Eindhoven, 2005.

[DK21] T. Dogan and P. Kastner. Streamlined CFD simulation framework to generate wind-pressure coefficients on building facades for airflow network simulations. *Building Simulation*, 14(4):1189–1200, Aug. 2021. doi:10.1007/s12273-020-0727-x.

[DPE+22] D. D'Agostino, D. Parker, I. Epifani, D. Crawley, and L. Lawrie. How will future climate impact the design and performance of nearly zero energy buildings (NZEBs)? *Energy*, 240:122479, Feb. 2022. doi:10.1016/j.energy.2021.122479.

[dPR24] F. R. d'Ambrosio Alfano, B. I. Palella, and G. Riccio. THERMODE 2023: Formulation and Validation of a new Thermo-physiological Model for Moderate Environments. *Building and Environment*, 252:111272, Mar. 2024. doi:10.1016/j.buildenv.2024.111272.

[DSFvT23] L. Drexler, M. Shamovich, J. Frisch, and C. van Treeck. Low-order building model for district energy simulations in Matlab. In *Tagungsband 34. Forum Bauinformatik 2023*, pages 306 KB, 8 pages, Bochum, 2023. Ruhr-Universität Bochum. doi:10.13154/294-10095.

[DWD17] Deutscher Wetterdienst. Ortsgenaue Testreferenzjahre von Deutschland für mittlere und extreme Witterungsverhältnisse: Projektbericht. Technical report, Offenbach, Germany, Jan. 2017.

[EAF17] S. El Ahmar and A. Fioravanti. Evaluating the capability of EnergyPlus in simulating geometrically complex Double-Skin Facades through CFD modelling. In *eCAADe 2017 : ShoCK! – Sharing of Computable Knowledge!*, pages 757–764,

Rome, Italy, 2017. doi:10.52842/conf.ecaade.2017.1.757.

[EC19] EC-Earth Consortium. EC-Earth-Consortium EC-Earth3 model output prepared for CMIP6 CMIP. Technical report, Jan. 2019. doi:10.22033/ESGF/CMIP6.181.

[EEG23] Gesetz für den Ausbau erneuerbarer Energien (Erneuerbare-Energien-Gesetz - EEG 2023), 2024.

[EnEfG23] Gesetz zur Steigerung der Energieeffizienz in Deutschland (energieeffizienzgesetz - EnEfG), 2023.

[EnSikuMaV] Verordnung zur Sicherung der Energieversorgung über kurzfristig wirksame Maßnahmen (Kurzfristenergieversorgungssicherungsmaßnahmenverordnung - EnSikuMaV), 2022.

[EnSimiMaV] Verordnung zur Sicherung der Energieversorgung über mittelfristig wirksame Maßnahmen (Mittelfristenergieversorgungssicherungsmaßnahmenverordnung - EnSimiMaV), 2022.

[EUECL] Regulation (EU) 2021/1119 of the European Parliament and of the Council of 30 June 2021 establishing the framework for achieving climate neutrality and amending Regulations (EC) No 401/2009 and (EU) 2018/1999 ('European Climate Law'), 2021.

[EUEE] Directive (EU) 2023/1791 of the European Parliament and of the Council of 13 September 2023 on energy efficiency and amending Regulation (EU) 2023/955 (recast), 2023.

[EUEPBD] Directive (EU) 2024/1275 of the European Parliament and of the Council of 24 April 2024 on the energy performance of buildings (recast) (Text with EEA relevance), 2024.

[Eur21] European Commission. Directorate General for Communication. Making our homes and buildings fit for a greener future. Technical report, LU, 2021.

[Fan70] P. Fanger. *Thermal Comfort: Analysis and Applications in Environmental Engineering*. Danish Technical Press, Copenhagen, 1970.

[Fic22] E. Fichter. *Automatisierte Erzeugung Geometrischer Modellefür Die BIM-basierte Gebäudesimulation*. PhD thesis, RWTH Aachen University, Jan. 2022. doi:10.18154/RWTH-2022-11049.

[FL23] Z. Fu and C. Liu. Investigation into the use of statistically and dynamically downscaled future climate datasets in assessing building performance. In *2023 Building Simulation Conference*, Sept. 2023. doi:10.26868/25222708.2023.1596.

[FLCZ+18] V. Földváry Ličina, T. Cheung, H. Zhang, R. De Dear, T. Parkinson, E. Arens, C. Chun, S. Schiavon, M. Luo, G. Brager, P. Li, S. Kaam, M. A. Adebamowo, M. M. Andamon, F. Babich, C. Bouden, H. Bukovianska, C. Candido, B. Cao, S. Carlucci, D. K. Cheong, J.-H. Choi, M. Cook, P. Cropper, M. Deuble, S. Heidari, M. Indraganti, Q. Jin, H. Kim, J. Kim, K. Konis, M. K. Singh, A. Kwok, R. Lamberts, D. Loveday, J. Langevin, S. Manu, C. Moosmann, F. Nicol, R. Ooka, N. A. Oseland, L. Pagliano, D. Petráš, R. Rawal, R. Romero, H. B. Rijal, C. Sekhar, M. Schweiker, F. Tartarini, S.-i. Tanabe, K. W. Tham, D. Teli, J. Toftum, L. Toledo,

K. Tsuzuki, R. De Vecchi, A. Wagner, Z. Wang, H. Wallbaum, L. Webb, L. Yang, Y. Zhu, Y. Zhai, Y. Zhang, and X. Zhou. Development of the ASHRAE Global Thermal Comfort Database II. *Building and Environment*, 142:502–512, Sept. 2018. doi:10.1016/j.buildenv.2018.06.022.

[FLS99] D. Fiala, K. J. Lomas, and M. Stohrer. A computer model of human thermoregulation for a wide range of environmental conditions: The passive system. *Journal of Applied Physiology*, 87(5):1957–1972, Nov. 1999. doi: 10.1152/jappl.1999.87.5.1957.

[FPS20] J. H. Ferziger, M. Perić, and R. L. Street. *Computational Methods for Fluid Dynamics*. Springer Nature, Cham, 2020. doi:10.1007/978-3-319-99693-6.

[FRFvT21] E. Fichter, V. Richter, J. Frisch, and C. van Treeck. Automatic generation of second level space boundary geometry from IFC models. In *Proceedings of Building Simulation 2021: 17th Conference of IBPSA*, Building Simulation Conference Proceedings. KU Leuven, Jan. 2021. doi:10.26868/25222708.2021.30156.

[GEG24] Gesetz zur Einsparung von Energie und zur Nutzung erneuerbarer Energien zur Wärme- und Kälteerzeugung in Gebäuden (Gebäudeenergiegesetz - GEG), Oct. 2024.

[Gha23] K. Ghaib. *Introduction to Computational Fluid Dynamics*. Essentials. Springer Fachmedien Wiesbaden, Wiesbaden, 2023. doi:10.1007/978-3-658-37619-2.

[GKLR19] G. I. Giannakis, K. I. Katsigarakis, G. N. Lilis, and D. V. Rovas. A Workflow for Automated Building Energy Performance Model Generation Using BIM. In V. Corrado, editor, *Proceedings of Building Simulation 2019: 16th IBPSA International Conference and Exhibition, 2-4 Sept., Rome*, volume Vol. 16 of *Building Simulation Conference Proceedings*. International Building Performance Simulation Association, Rome, Jan. 2019.

[GKS95] H. Geuss, R. Krist, and A. Seidl. RAMSIS: ein System zur Erhebung und Vermessung dreidimensionaler Körperhaltungen von Menschen zur ergonomischen Auslegung von Bedien- und Sitzplätzen im Auto. In *RAMSIS ein System zur Erhebung und Vermessung dreidimensionaler Körperhaltungen von Menschen zur ergonomischen Auslegung von Bedien- und Sitzplätzen im Auto*, number 123 in FAT-Schriftenreihe. FAT, Frankfurt am Main, Germany, 1995.

[GLG+15] G. I. Giannakis, G. N. Lilis, M. A. Garcia, G. Kontes, C. Valmaseda, and D. V. Rovas. A methodology to automatically generate geometry inputs for energy performance simulation from ifc bim models. In J. Mathur and V. Garg, editors, *Building Simulation 2015: 14th International Conference of IBPSA, December 7-9, 2015, Hyderabad, India : Conference Proceedings*. BS Publications, Hyderabad, Jan. 2015.

[GLH+22] W. Guo, S. Liang, Y. He, W. Li, B. Xiong, and H. Wen. Combining EnergyPlus and CFD to predict and optimize the passive ventilation mode of medium-sized gymnasium in subtropical regions. *Building and Environment*, 207:108420, Jan. 2022. doi:10.1016/j.buildenv.2021.108420.

[GNH+22] J. Grunewald, A. Nicolai, S. Hirth, D. Weiß, C. Treeck, J. Frisch, A. Nouri, C. Emunds, M. Madjidi, J. Agudelo, I. Reichenbach, R. Rolffs, R. Strobel, R. Tang, and

F. Höppchen. SimQualitiy; ENOB: SimQuality - Entwicklung von Qualitätsstandards für die energetische Gebäude- und Quartierssimulation als Planungswerkzeug; Akronym: SimQuality : Schlussbericht : Laufzeit: 01.08.2018 bis 31.01.2022, Laufzeitverlängerung: 31.12.2020. Technical report, 2022. doi:10.2314/KXP:1859246915.

[GSA09] GSA Public Building Service. Energy Savings and Performance Gains in GSA Buildings: Seven Cost-Effective Strategies. Technical report, Washington, D.C., USA, 2009.

[GSN71] A. P. Gagge, J. A. J. Stolwijk, and Y. Nishi. An Effective Temperature Scale Based on a Simple Model of Human Physiological Regulatiry Response. In *ASHRAE Transactions*, Philadelphia, USA, 1971.

[Hen95] J. Hensen. Modelling coupled heat and airflow: Ping-pong vs onions. In *Proceedings of the 16th AIVC Conference*, pages 253–262, Palm Springs, USA, Sept. 1995. IEA Air Infiltration and Ventilation Centre.

[HL11] J. Hensen and R. Lamberts. *Building Performance Simulation for Design and Operation*. Spon Press, London; New York, Jan. 2011.

[HLK17] T. Hong, M. Lee, and J. Kim. Analysis of Energy Consumption and Indoor Temperature Distributions in Educational Facility Based on CFD-BES Model. *Energy Procedia*, 105:3705–3710, May 2017. doi:10.1016/j.egypro.2017.03.858.

[HMK+23] T. Hong, J. Malik, A. Krelling, W. O'Brien, K. Sun, R. Lamberts, and M. Wei. Ten questions concerning thermal resilience of buildings and occupants for climate adaptation. *Building and Environment*, 244:110806, Jan. 2023. doi: 10.1016/j.buildenv.2023.110806.

[HOAI2021] Verordnung über die Honorare für Architekten- und Ingenieurleistungen (Honorarordnung für Architekten und Ingenieure – HOAI), Jan. 2021.

[HP21] M. Hadavi and H. Pasdarshahri. Impacts of urban buildings on microclimate and cooling systems efficiency: Coupled CFD and BES simulations. *Sustainable Cities and Society*, 67:102740, Apr. 2021. doi:10.1016/j.scs.2021.102740.

[HR24] A. Hochberger and V. Richter. Automated IFC-based mesh refinement and quality control for indoor airflow simulations using OpenFOAM. In *35. Forum Bauinformatik, Fbi 2024*, pages 284–291, Technische Universität Hamburg, Institut für Digitales und Autonomes Bauen, Sept. 2024. Technische Universität Hamburg, Institut für Digitales und Autonomes Bauen. doi:10.15480/882.13503.

[IPCC23] H. Lee, K. Calvin, D. Dasgupta, G. Krinner, A. Mukherji, P. W. Thorne, C. Trisos, J. Romero, P. Aldunce, K. Barrett, G. Blanco, W. W. Cheung, S. Connors, F. Denton, A. Diongue-Niang, D. Dodman, M. Garschagen, O. Geden, B. Hayward, C. Jones, F. Jotzo, T. Krug, R. Lasco, Y.-Y. Lee, V. Masson-Delmotte, M. Meinshausen, K. Mintenbeck, A. Mokssit, F. E. Otto, M. Pathak, A. Pirani, E. Poloczanska, H.-O. Pörtner, A. Revi, D. C. Roberts, J. Roy, A. C. Ruane, J. Skea, P. R. Shukla, R. Slade, A. Slangen, Y. Sokona, A. A. Sörensson, M. Tignor, D. van Vuuren, Y.-M. Wei, H. Winkler, P. Zhai, Z. Zommers, J.-C. Hourcade, F. X. Johnson, S. Pachauri, N. P. Simpson, C. Singh, A. Thomas, E. Totin, P. Arias, M. Bustamante, I. Elgizouli, G. Flato, M. Howden, C. Méndez-Vallejo, J. J.

Pereira, R. Pichs-Madruga, S. K. Rose, Y. Saheb, R. Sánchez Rodríguez, D. Ürge-Vorsatz, C. Xiao, N. Yassaa, A. Alegría, K. Armour, B. Bednar-Friedl, K. Blok, G. Cissé, F. Dentener, S. Eriksen, E. Fischer, G. Garner, C. Guivarch, M. Haasnoot, G. Hansen, M. Hauser, E. Hawkins, T. Hermans, R. Kopp, N. Leprince-Ringuet, J. Lewis, D. Ley, C. Ludden, L. Niamir, Z. Nicholls, S. Some, S. Szopa, B. Trewin, K.-I. van der Wijst, G. Winter, M. Witting, A. Birt, M. Ha, J. Kim, E. F. Haites, Y. Jung, R. Stavins, D. J. A. Orendain, L. Ignon, S. Park, Y. Park, A. Reisinger, D. Cammaramo, A. Fischlin, J. S. Fuglestvedt, J. RobinB. Matthews, and C. Péan. IPCC, 2023: Climate Change 2023: Synthesis Report. Contribution of Working Groups I, II and III to the Sixth Assessment Report of the Intergovernmental Panel on Climate Change [Core Writing Team, H. Lee and J. Romero (eds.)]. IPCC, Geneva, Switzerland. Technical report, Jan. 2023. doi:10.59327/IPCC/AR6-9789291691647.

[ISO17772-1] ISO 17772-1:2017-06: Energy performance of buildings - Indoor environmental quality - Part 1: Indoor environmental input parameters for the design and assessment of energy performance of buildings. ISO. 2017.

[ISO17772-2] ISO/TR 17772-2:2018-04: Energy performance of buildings - Overall energy performance assessment procedures - Part 2: Guideline for using indoor environmental input parameters for the design and assessment of energy performance of buildings. ISO. Switzerland, 2018.

[ISO52120-1] ISO 52120-1: Energy performance of buildings - Contribution of building automation, controls and building management - Part 1: General framework and procedures. International Organization for Standardization (ISO). Switzerland, Jan. 2021.

[ISO7730] ISO 7730: Ergonomics of the thermal environment - Analytical determination and interpretation of thermal comfort using calculation of the PMV and PPD indices and local thermal comfort criteria. Nov. 2005.

[JCG20] N. L. Jones, I. Chaires, and A. Goehring. Detailed Thermal Comfort Analysis from Preliminary to Final Design. In V. Corrado, E. Fabrizio, A. Gasparella, and F. Patuzzi, editors, *Proceedings of Building Simulation 2019: 16th Conference of IBPSA*, Building Simulation Conference Proceedings, pages 2675–2682. IBPSA, Jan. 2020. doi:10.26868/25222708.2019.210875.

[JCM+21] N. Jones, I. Chaires, I. Mackenzie, T. Arioto, and A. Goehring. Predicting thermal comfort for diverse populations. In *2021 Building Simulation Conference*, Sept. 2021. doi:10.26868/25222708.2021.30601.

[JJBB13] M. F. Jentsch, P. A. James, L. Bourikas, and A. S. Bahaj. Transforming existing weather data for worldwide locations to enable energy and building performance simulation under future climates. *Renewable Energy*, 55:514–524, Jan. 2013. doi:10.1016/j.renene.2012.12.049.

[JLCZ19] A. Jiang, X. Liu, E. Czarnecki, and C. Zhang. Hourly weather data projection due to climate change for impact assessment on building and infrastructure. *Sustainable Cities and Society*, 50:101688, Jan. 2019. doi:10.1016/j.scs.2019.101688.

[JMM+21] D. Jansen, P. Mehrfeld, D. Müller, E. Fichter, V. Richter, A. Barz, J. Brunkhorst, M. Dahncke, P. Jahangiri, C. Warnecke, J. Frisch, C. van Treeck, and B. L.

Bruno Lüdemann. BIM2SIM - Development of semi-automated methods for the generation of simulation models using Building Information Modeling. In *Proceedings of Building Simulation 2021: 17th Conference of International Building Performance Simulation Association, Bruges, 1-3 September: To Be Published*. Jan. 2021. doi:10.26868/25222708.2021.30228.

[Joh16] R. W. Johnson, editor. *Handbook of Fluid Dynamics*. CRC Press Taylor & Francis Group, Boca Raton London New York, second edition, 2016.

[JRM+24] D. Jansen, V. Richter, L. Maier, J. Frisch, C. van Treeck, and D. Müller. Bim2sim: An Open-Source Framework for Automated Generation of Beps Models and Beyond from Bim Data, 2024. doi:10.2139/ssrn.5013181.

[KfW20] KfW. Anlage zum Merkblatt: Energieeffizient Bauen. Technische Mindestanforderungen. Kredit 153 600 000 3465, Frankfurt, 2020.

[KK17] M. Król and A. Król. Multi-criteria numerical analysis of factors influencing the efficiency of natural smoke venting of atria. *Journal of Wind Engineering and Industrial Aerodynamics*, 170:149–161, Nov. 2017. doi:10.1016/j.jweia.2017.08.012.

[Klo16] J. H. Klote. Smoke Control. In M. J. Hurley, D. Gottuk, J. R. Hall, K. Harada, E. Kuligowski, M. Puchovsky, J. Torero, J. M. Watts, and C. Wieczorek, editors, *SFPE Handbook of Fire Protection Engineering*, pages 1785–1823. Springer New York, New York, NY, 2016. doi:10.1007/978-1-4939-2565-0_50.

[KLZ16] K. Katić, R. Li, and W. Zeiler. Thermophysiological models and their applications: A review. *Building and Environment*, 106:286–300, Sept. 2016. doi:10.1016/j.buildenv.2016.06.031.

[KNO+20] T. Krijnen, F. Noardo, K. A. Ohori, H. Ledoux, and J. Stoter. Validation and Inference of Geometrical Relationships in IFC. In *Proceedings of the 37th International Conference of CIB W78*, CIB W78 Proceedings, pages 98–111. Eduardo Toledo Santos and Sergio Scheer, Jan. 2020. doi:10.46421/2706-6568.37.2020.paper008.

[KSA18] C. Karmann, S. Schiavon, and E. Arens. Percentage of commercial buildings showing at least 80% occupant satisfied with their thermal comfort. 2018.

[KSG24] Bundes-Klimaschutzgesetz (KSG), 2024.

[KSS97] W. Krüger, A. Seidl, and H. Speyer. Mathematische Nachbildung des Menschen: RAMSIS 3D Softdummy. In *Mathematische Nachbildung des Menschen: RAMSIS 3D Softdummy*, number 135 in FAT Schriftenreihe. Autoverband, Frankfurt am Main, Germany, 1997.

[KWW+22] K.-Y. Kang, X. Wang, J. Wang, S. Xu, W. Shou, and Y. Sun. Utility of BIM-CFD Integration in the Design and Performance Analysis for Buildings and Infrastructures of Architecture, Engineering and Construction Industry. *Buildings*, 12(5):651, Jan. 2022. doi:10.3390/buildings12050651.

[KZS+18] J. Kim, Y. Zhou, S. Schiavon, P. Raftery, and G. Brager. Personal comfort models: Predicting individuals' thermal preference using occupant heating and cooling behavior and machine learning. *Building and Environment*, 129:96–106, Feb. 2018. doi:10.1016/j.buildenv.2017.12.011.

[LC22] L. K. Lawrie and D. B. Crawley. Development of Global Typical Meteorological Years (TMYx). http://climate.onebuilding.org, 2022.

[LCK+24] G. Lamberti, F. Contrada, A. Kindinis, F. Leccese, and G. Salvadori. Developing a new adaptive heat balance model to enhance thermal comfort predictions and reduce energy consumption. *Energy and Buildings*, 321:114663, Oct. 2024. doi:10.1016/j.enbuild.2024.114663.

[LCLZ21] X. Lan, J. Cao, G. Lv, and L. Zhou. Simulation method for indoor airflow based on the Industry Foundation Classes model. *Journal of Building Engineering*, 39:102251, Jan. 2021. doi:10.1016/j.jobe.2021.102251.

[LDKB05] T. Loga, N. Diefenbach, J. Knissel, and R. Born. Ein vereinfachtes, statistisch abgesichertes Verfahren zur Erhebung von Gebäudedaten für die energetische Bewertung von Gebäuden. Technical report, Darmstadt, Germany, Jan. 2005.

[LEEDv5] LEED v5 Rating System: Building Design and Construction: New Construction. LEED. Apr. 2024.

[LES20] Y.-C. Lee, C. M. Eastman, and W. Solihin. Rules and validation processes for interoperable BIM data exchange. *Journal of Computational Design and Engineering*, Jan. 2020. doi:10.1093/jcde/qwaa064.

[LGKR18] G. N. Lilis, G. Giannakis, K. Katsigarakis, and D. V. Rovas. A tool for IFC building energy performance simulation suitability checking. In J. Karlshøj and R. Scherer, editors, *eWork and eBusiness in Architecture, Engineering and Construction*, pages 57–64. CRC Press, Jan. 2018. doi:10.1201/9780429506215-8.

[LGR15] G. N. Lilis, G. I. Giannakis, and D. V. Rovas. Detection and semi-Automatic correction of geometric inaccuracies in IFC files. In *Proceedings of BS2015: 14th Conference of International Building Performance Simulation Association*. Jan. 2015.

[LGR17] G. N. Lilis, G. I. Giannakis, and D. V. Rovas. Automatic generation of second-level space boundary topology from IFC geometry inputs. *Automation in Construction*, 76:108–124, Jan. 2017. doi:10.1016/j.autcon.2016.08.044.

[LH24] L. Liu and Y. Huang. HVAC Design Optimization for Pharmaceutical Facilities with BIM and CFD. *Buildings*, 14(6):1627, June 2024. doi:10.3390/buildings14061627.

[LHW+25] H. Li, H. Hu, Z. Wu, X. Kong, and M. Fan. Modified predicted mean vote models for human thermal comfort: An ASHRAE database-based evaluation. *Renewable and Sustainable Energy Reviews*, 209:115042, Mar. 2025. doi:10.1016/j.rser.2024.115042.

[LLGX24] S. Li, Y. Li, W. Gao, and F. Xiao. A comprehensive study on the impacts of thermal comfort on occupants' thermophysiology and cognitive performances in a radiant cooling environment using physiological measurements. *Energy and Buildings*, 323:114771, Nov. 2024. doi:10.1016/j.enbuild.2024.114771.

[LO18] E. Laurien and H. Oertel. *Numerische Strömungsmechanik*. Springer Fachmedien Wiesbaden, Wiesbaden, 2018. doi:10.1007/978-3-658-21060-1.

[LPJK21] M. Lee, G. Park, H. Jang, and C. Kim. Development of Building CFD Model Design Process Based on BIM. *Applied Sciences*, 11(3):1252, Jan. 2021. doi:

10.3390/app11031252.

[LRW19] P. Lundqvist, M. Risberg, and L. Westerlund. Air heating system design for a sub-Arctic climate using a CFD technique. *Building and Environment*, 160:106164, Jan. 2019. doi:10.1016/j.buildenv.2019.106164.

[LRW22] P. Lundqvist, M. Risberg, and L. Westerlund. Indoor thermal climate after energy efficiency measures of a residential building in a sub-Arctic region: Comparing ANSYS CFX and IDA ICE methods. *Indoor and Built Environment*, 31(3):732–744, Mar. 2022. doi:10.1177/1420326X211030323.

[MAKH22] T. Mori, T. Akamatsu, K. Kuwabara, and M. Hayashi. Comparison of Indoor Environment and Energy Consumption before and after Spread of COVID-19 in Schools in Japanese Cold-Climate Region. *Energies*, 15(5):1781, Feb. 2022. doi:10.3390/en15051781.

[MCRM21] S. G. Melgar, A. S. Cordero, M. V. Rodríguez, and J. M. A. Márquez. Influence on indoor comfort due to the application of Covid-19 natural ventilation protocols for schools at subtropical climate during winter season. *E3S Web of Conferences*, 293:01031, 2021. doi:10.1051/e3sconf/202129301031.

[MDD03] C. Morgan and R. De Dear. Weather, clothing and thermal adaptation to indoor climate. *Climate Research*, 24:267–284, 2003. doi:10.3354/cr024267.

[MDRPM23] F. Matoseiro Dinis, R. Rodrigues, and J. Poças Martins. Development and validation of natural user interfaces for semantic enrichment of BIM models using open formats. *Construction Innovation*, Jan. 2023. doi:10.1108/CI-12-2022-0348.

[MEL23] A. Mediavilla, P. Elguezabal, and N. Lasarte. Graph-Based methodology for Multi-Scale generation of energy analysis models from IFC. *Energy and Buildings*, 282:112795, Jan. 2023. doi:10.1016/j.enbuild.2023.112795.

[MHMA22] T. Mamani, R. F. Herrera, F. Muñoz-La Rivera, and E. Atencio. Variables That Affect Thermal Comfort and Its Measuring Instruments: A Systematic Review. *Sustainability*, 14(3):1773, Jan. 2022. doi:10.3390/su14031773.

[MJvT+22] D. Müller, D. Jansen, C. van Treeck, E. Fichter, V. Richter, B. Lüdemann, P. Jahangiri, J. Brunkhorst, M. Dahnke, and C. Warnecke. BIM2SIM - Methodenentwicklung zur Erstellung von Simulationsmodellen aus Daten des Building Information Modeling: Gemeinsamer Endbericht. Technical report, Aachen, Jan. 2022.

[MLL+23] E. Mamulova, M. Loomans, R. Loonen, M. Schweiker, and H. Kort. Let's talk scalability: The current status of multi-domain thermal comfort models as support tools for the design of office buildings. *Building and Environment*, 242:110502, Aug. 2023. doi:10.1016/j.buildenv.2023.110502.

[MN23] N. V. S. K. Manapragada and J. Natanian. Parametric Integration of CFD-based Wind Pressure Coefficients into Building Energy Models: A Novel Workflow. *Journal of Physics: Conference Series*, 2600(3):032011, Nov. 2023. doi:10.1088/1742-6596/2600/3/032011.

[MOBR13] T. Maile, J. O'Donnell, V. Bazjanac, and C. Rose. BIM-Geometry Modelling Guidelines for Building Energy Performance Simulation. In *Proceedings of*

BS2013: 13th Conference of International Building Performance Simulation Association, Chambéry, France, August 26-28, pages 3242–3249. Jan. 2013.

[MRV+22] M. Miranda, P. Romero, V. Valero-Amaro, J. Arranz, and I. Montero. Ventilation conditions and their influence on thermal comfort in examination classrooms in times of COVID-19. A case study in a Spanish area with Mediterranean climate. *International Journal of Hygiene and Environmental Health*, 240:113910, Mar. 2022. doi:10.1016/j.ijheh.2021.113910.

[MSBB14] M. J. Moran, H. N. Shapiro, D. D. Boettner, and M. B. Bailey, editors. *Fundamentals of Engineering Thermodynamics*. Wiley, Hoboken, N.J, 8th edition, 2014.

[MSP18] A. Mediavilla, Y. Sebesi, and P. Philips. Deliverable 4.6: Integration with external tools (Energy Plus). Technical report, Mar. 2018.

[MSPT+24] A. Machard, A. Salvati, M. P. Tootkaboni, A. Gaur, J. Zou, L. L. Wang, F. Baba, H. Ge, F. Bre, E. Bozonnet, V. Corrado, X. Luo, R. Levinson, S. H. Lee, T. Hong, M. Salles Olinger, R. M. E. S. Machado, E. L. A. Da Guarda, R. K. Veiga, R. Lamberts, A. Afshari, D. Ramon, H. Ngoc Dung Ngo, A. Sengupta, H. Breesch, N. Heijmans, J. Deltour, X. Kuborn, S. Sayadi, B. Qian, C. Zhang, R. Rahif, S. Attia, P. Stern, and P. Holzer. Typical and extreme weather datasets for studying the resilience of buildings to climate change and heatwaves. *Scientific Data*, 11(1):531, May 2024. doi:10.1038/s41597-024-03319-8.

[MTC+20] N. Morozova, F. Trias, R. Capdevila, C. Pérez-Segarra, and A. Oliva. On the feasibility of affordable high-fidelity CFD simulations for indoor environment design and control. *Building and Environment*, 184:107144, Oct. 2020. doi:10.1016/j.buildenv.2020.107144.

[NAOKS21] F. Noardo, K. Arroyo Ohori, T. Krijnen, and J. Stoter. An Inspection of IFC Models from Practice. *Applied Sciences*, 11(5):2232, Mar. 2021. doi:10.3390/app11052232.

[Neg95] C. O. R. Negrão. *Conflation of Computational Fluid Dynamics and Building Thermal Simulation*. PhD thesis, University of Strathclyde, 1995. doi:10.48730/RWG5-YZ20.

[NIK+17] C. Nytsch-Geusen, A. Inderfurth, W. Kaul, K. Mucha, J. Rädler, M. Thorade, and C. Ribas Tugores. Template based code generation of Modelica building energy simulation models. In *Proceedings of the 12th International Modelica Conference, Prague, Czech Republic, May 15-17, 2017*, Linköping Electronic Conference Proceedings, pages 199–207. Linköping University Electronic Press, Jan. 2017. doi:10.3384/ecp17132199.

[NK21] C. N. Nielsen and J. Kolarik. Utilization of Climate Files Predicting Future Weather in Dynamic Building Performance Simulation – A review. *Journal of Physics: Conference Series*, 2069(1):012070, Jan. 2021. doi:10.1088/1742-6596/2069/1/012070.

[NKNR14] C. Nytsch-Geusen, C. Klempin, J. Nuñez v. Voigt, and J. Rädler. Integration of CAAD, thermal building simulation and CFD by using the IFC data exchange format. In *Proceedings of Building Simulation 2003: 8th Conference of IBPSA*, Eindhoven, Netherlands, 2003-08-11/2003-08-14.

[NPW+23] A. Nicolai, A. Paepcke, D. Weiß, H. Hirsch, S. Hirth, and H. Fechner. SIM-VICUS. https://www.sim-vicus.de/, Aug. 2023.

[NRTRT19] C. Nytsch-Geusen, J. Rädler, M. Thorade, and C. Ribas Tugores. BIM2Modelica - An open source toolchain for generating and simulating thermal multi-zone building models by using structured data from BIM models. In *Proceedings of the 13th International Modelica Conference, Regensburg, Germany, March 4–6, 2019*, Linköping Electronic Conference Proceedings, pages 33–38. Linköing University Electronic Press, Jan. 2019. doi:10.3384/ecp1915733.

[OSR+11] J. O'Donnell, R. See, C. Rose, T. Maile, and V. Bazjanac. SimModel: A domain data model for whole building energy simulation. In *Proceedings of Building Simulation 2011: 12th Conference of International Building Performance Simulation Association, Sydney, 14-16 November*. Jan. 2011.

[PCN+19] H. J. Poh, P.-H. Chiu, H. H. Nguyen, G. Xu, C. S. Chong, L. T. Lee, K. Po, P. P. Tan, N.-H. Wong, R. Li, S. F. Lee, and N. C. Wong. Airflow Modelling Software Development for Natural Ventilation Design - Green Building Environment Simulation Technology. *IOP Conference Series: Earth and Environmental Science*, 238:012077, Mar. 2019. doi:10.1088/1755-1315/238/1/012077.

[PDB20] T. Parkinson, R. Dear, and G. Brager. Nudging the adaptive thermal comfort model. *Energy and Buildings*, 206:109559, Jan. 2020. doi:10.1016/j.enbuild.2019.109559.

[Pin21] M. Pinterić. *Building Physics: From Physical Principles to International Standards*. Springer International Publishing, Cham, 2021. doi:10.1007/978-3-030-67372-7.

[PKLC20] G. Park, C. Kim, M. Lee, and C. Choi. Building Geometry Simplification for Improving Mesh Quality of Numerical Analysis Model. *Applied Sciences*, 10(16):5425, Jan. 2020. doi:10.3390/app10165425.

[PPCL24] D. S. Parker, K. Panchabikesan, D. B. Crawley, and L. K. Lawrie. Impact of newer climate data for technical analysis of residential building energy use in the United States. *Energy and Buildings*, 323:114828, Nov. 2024. doi:10.1016/j.enbuild.2024.114828.

[PU19] J. Pouriya and B. Umberto. Building energy demand within a climate change perspective: The need for future weather file. *IOP Conference Series: Materials Science and Engineering*, 609(7):072037, Sept. 2019. doi:10.1088/1757-899X/609/7/072037.

[PWO+18] S. Pinheiro, R. Wimmer, J. O'Donnell, S. Muhic, V. Bazjanac, T. Maile, J. Frisch, and C. van Treeck. MVD based information exchange between BIM and building energy performance simulation. *Automation in Construction*, 90:91–103, Jan. 2018. doi:10.1016/j.autcon.2018.02.009.

[PZL+23] Y. Pan, M. Zhu, Y. Lv, Y. Yang, Y. Liang, R. Yin, Y. Yang, X. Jia, X. Wang, F. Zeng, S. Huang, D. Hou, L. Xu, R. Yin, and X. Yuan. Building energy simulation and its application for building performance optimization: A review of methods, tools, and case studies. *Advances in Applied Energy*, 10:100135, June 2023. doi:10.1016/j.adapen.2023.100135.

[RB15] C. M. Rose and V. Bazjanac. An algorithm to generate space boundaries for

building energy simulation. *Engineering with Computers*, 31(2):271–280, Jan. 2015. doi:10.1007/s00366-013-0347-5.

[RBMV22a] K. Rykaczewski, L. Bartels, D. M. Martinez, and S. H. Viswanathan. Computational manikin for radiation simulation (male and female models covering 1-99% BMI and height diversity in US), 2022. doi:10.48349/ASU/ZCLKT6.

[RBMV22b] K. Rykaczewski, L. Bartels, D. M. Martinez, and S. H. Viswanathan. Human body radiation area factors for diverse adult population. *International Journal of Biometeorology*, 66(11):2357–2367, Nov. 2022. doi:10.1007/s00484-022-02362-7.

[RFA+21] V. Richter, E. Fichter, M. Azendorf, J. Frisch, and C. van Treeck. Algorithms for Overcoming Geometric and Semantic Errors in the Generation of EnergyPlus Input Files based on IFC Space Boundaries. In M. Disser, A. Hoffmann, L. Kuhn, and P. Scheich, editors, *32. Forum Bauinformatik 2021: Konferenzband*. Jan. 2021. doi:10.18154/RWTH-2021-09522.

[RFC23] E. Rodrigues, M. S. Fernandes, and D. Carvalho. Future weather generator for building performance research: An open-source morphing tool and an application. *Building and Environment*, 233:110104, Jan. 2023. doi:10.1016/j.buildenv.2023.110104.

[RHX+20] M. Rodríguez-Vázquez, I. Hernández-Pérez, J. Xamán, Y. Chávez, M. Gijón-Rivera, and J. M. Belman-Flores. Coupling building energy simulation and computational fluid dynamics: An overview. *Journal of Building Physics*, 44(2):137–180, Sept. 2020. doi:10.1177/1744259120901840.

[RIBA20] Royal Institute of British Architects. RIBA Plan of Work - Overview. Technical report, 2020.

[Ric19] V. Richter. Quality Measures for Evaluation of Building Energy Model Geometry. Master's thesis, RWTH Aachen University, Aachen, Jan. 2019.

[RLM+18] P. Remmen, M. Lauster, M. Mans, M. Fuchs, T. Osterhage, and D. Müller. TEASER: An open tool for urban energy modelling of building stocks. *Journal of Building Performance Simulation*, 11(1):84–98, Jan. 2018. doi:10.1080/19401493.2017.1283539.

[RLS+23] V. Richter, C.-L. Lorenz, M. Syndicus, J. Frisch, and C. van Treeck. Framework for automated IFC-based thermal comfort analysis based on IFC model maturity. In IBPSA, editor, *Proceedings of Building Simulation 2023: 18th Conference of IBPSA*, Building Simulation Conference Proceedings, 2023. doi:10.26868/25222708.2023.1173.

[RM22] K. Rewitz and D. Müller. Influence of gender, age and BMI on human physiological response and thermal sensation for transient indoor environments with displacement ventilation. *Building and Environment*, 219:109045, July 2022. doi:10.1016/j.buildenv.2022.109045.

[RMF+22] V. Richter, A. Malhotra, E. Fichter, A. Hochberger, J. Frisch, and C. van Treeck. Validation of IFC-based Geometric Input for Building Energy Performance Simulation. In *2022 Building Performance Analysis Conference and SimBuild*, volume 10 of *ASHRAE/IBPSA-USA Building Simulation Conference*, pages 287–297. ASHRAE/IBPSA-USA, 2022. doi:10.26868/25746308.2022.C033.

[RMM20] I. J. Ramaji, J. I. Messner, and E. Mostavi. IFC-Based BIM-to-BEM Model Transformation. *Journal of Computing in Civil Engineering*, 34(3):04020005, Jan. 2020. doi:10.1061/(ASCE)CP.1943-5487.0000880.

[RSFvT23] V. E. Richter, M. Syndicus, J. Frisch, and C. van Treeck. Extending the IFC-Based bim2sim Framework to Improve the Accessibility of Thermal Comfort Analysis Considering Future Climate Scenarios. *Applied Sciences*, 13(22):12478, Nov. 2023. doi:10.3390/app132212478.

[RvTF24] V. E. Richter, C. van Treeck, and J. Frisch. Extending an IFC-based Framework to include an Automated CFD-Setup using Pre-Computed Boundary Conditions. In *Proceedings of BauSim Conference 2024: 10th Conference of IBPSA-Germany and Austria*, volume 10 of *BauSim Conference*, pages 72–79, Vienna, Austria, September 2024. IBPSA-Germany and Austria. doi:10.26868/29761662.2024.10.

[RWH17] D. Risberg, L. Westerlund, and G. Hellström. Computational fluid dynamics simulation of indoor climate in low energy buildings: Computational set up. *Thermal Science*, 21(5):1985–1998, 2017. doi:10.2298/TSCI150604167R.

[SCA+17] S. Shahzad, J. K. Calautit, A. I. Aquino, D. S. Nasir, and B. R. Hughes. A user-controlled thermal chair for an open plan workplace: CFD and field studies of thermal comfort performance. *Applied Energy*, 207:283–293, Dec. 2017. doi:10.1016/j.apenergy.2017.05.118.

[SIA2024] SIA 2024: Standard-Nutzungsbedingungen für die Energie- und Gebäudetechnik. Swiss Society of Engineers and Architects. Zurich, 2006.

[SKCK23] P. Szałański, P. Kowalski, W. Cepiński, and P. Kęskiewicz. The Effect of Lowering Indoor Air Temperature on the Reduction in Energy Consumption and CO2 Emission in Multifamily Buildings in Poland. *Sustainability*, 15(15):12097, Aug. 2023. doi:10.3390/su151512097.

[SL13] S. Schiavon and K. H. Lee. Dynamic predictive clothing insulation models based on outdoor air and indoor operative temperatures. *Building and Environment*, 59:250–260, Jan. 2013. doi:10.1016/j.buildenv.2012.08.024.

[SLS+20] X. Shan, N. Luo, K. Sun, T. Hong, Y.-K. Lee, and W.-Z. Lu. Coupling CFD and building energy modelling to optimize the operation of a large open office space for occupant comfort. *Sustainable Cities and Society*, 60:102257, Jan. 2020. doi:10.1016/j.scs.2020.102257.

[SOT+23] C. Y. Siu, W. O'Brien, M. Touchie, M. Armstrong, A. Laouadi, A. Gaur, Z. Jandaghian, and I. Macdonald. Evaluating thermal resilience of building designs using building performance simulation – A review of existing practices. *Building and Environment*, 234:110124, Apr. 2023. doi:10.1016/j.buildenv.2023.110124.

[Sto71] J. A. J. Stolwijk. A mathematical model of physiological temperature regulation in a man. NASA Contractor Report CR-1855, New Haven, Connecticut, USA, Aug. 1971.

[Str11] R. Streblow. *Thermal Sensation and Comfort Model for Inhomogeneous Indoor Environments*. PhD thesis, E.ON Energy Research Center, RWTH Aachen University, Aachen, 2011.

[THZS18] W. Tian, X. Han, W. Zuo, and M. D. Sohn. Building energy simulation coupled with CFD for indoor environment: A critical review and recent applications. *Energy and Buildings*, 165:184–199, Apr. 2018. doi:10.1016/j.enbuild.2018.01.046.

[TKN+02] S.-i. Tanabe, K. Kobayashi, J. Nakano, Y. Ozeki, and M. Konishi. Evaluation of thermal comfort using combined multi-node thermoregulation (65MN) and radiation models and computational fluid dynamics (CFD). *Energy and Buildings*, 2002. doi:10.1016/S0378-7788(02)00014-2.

[TMP+23] J. Taylor, R. McLeod, G. Petrou, C. Hopfe, A. Mavrogianni, R. Castaño-Rosa, S. Pelsmakers, and K. Lomas. Ten questions concerning residential overheating in Central and Northern Europe. *Building and Environment*, 234:110154, Apr. 2023. doi:10.1016/j.buildenv.2023.110154.

[TNM+20] F. J. Tapiador, A. Navarro, R. Moreno, J. L. Sánchez, and E. García-Ortega. Regional climate models: 30 years of dynamical downscaling. *Atmospheric Research*, 235:104785, Jan. 2020. doi:10.1016/j.atmosres.2019.104785.

[TSM12] K. E. Taylor, R. J. Stouffer, and G. A. Meehl. An Overview of CMIP5 and the Experiment Design. *Bulletin of the American Meteorological Society*, 93(4):485–498, Apr. 2012. doi:10.1175/bams-d-11-00094.1.

[UN15] United Nations (UN). Paris Agreement. In *Paris Climate Change Conference*, Paris, 2015.

[USDoE21] U.S. Department of Energy. EnergyPlus Version 9.5.0 Documentation: Auxiliary Programs. Technical report, Jan. 2021.

[VDI2078] VDI 2078: Calculation of thermal loads and room temperatures (design cooling load and annual simulation). Verein Deutscher Ingenieure (VDI). Beuth Verlag GmbH, Berlin, June 2015.

[VDI6007-1] VDI 6007-1: Calculation of transient thermal response of rooms and buildings - Modelling of rooms. Verein Deutscher Ingenieure (VDI). Beuth Verlag GmbH, Berlin, June 2015.

[VDI6007-2] VDI 6007-2: Calculation of transient thermal response of rooms and buildings - Modeling of windows. Verein Deutscher Ingenieure (VDI). Beuth Verlag GmbH, Berlin, Mar. 2012.

[VDI6007-3] VDI 6007-3: Calculation of transient thermal response of rooms and buildings - Modelling of solar radiation. Verein Deutscher Ingenieure (VDI). Beuth Verlag GmbH, Berlin, June 2015.

[VDI6020] VDI 6020: Requirements to be met by calculation methods for the simulation of thermal-energy efficiency of buildings and building installations. Verein Deutscher Ingenieure (VDI). Beuth Verlag GmbH, Berlin, Dec. 2022.

[VDI6070] VDI 6070 Blatt 1 (Draft): Room book: General requirements and fundamentals, Jan. 2023.

[vTFW+21] C. van Treeck, E. Fichter, S. Weck-Ponten, J. Siwiecki, and A. Nouri. BIM für die Energiebedarfsermittlung und Gebäudesimulation. In A. Borrmann, M. König, C. Koch, and J. Beetz, editors, *Building Information Modeling*, pages 427–441. Springer Fachmedien Wiesbaden, Wiesbaden, 2021. doi:10.1007/

978-3-658-33361-4_22.

[vTr10] C. A. van Treeck. Introduction to Building Performance Modeling and Simulation: A basic introduction to modeling and numerical simulation of the energy and thermal quality performance of buildings using a geometry based zone model. Habilitation thesis, Feb. 2010.

[vTR07] C. van Treeck and E. Rank. Dimensional reduction of 3D building models using graph theory and its application in building energy simulation. *Engineering with Computers*, 23(2):109–122, Jan. 2007. doi:10.1007/s00366-006-0053-7.

[Wet11] M. Wetter. Co-simulation of building energy and control systems with the Building Controls Virtual Test Bed. *Journal of Building Performance Simulation*, 4(3):185–203, Sept. 2011. doi:10.1080/19401493.2010.518631.

[Wil22] W. M. Willems, editor. *Lehrbuch der Bauphysik: Wärme – Feuchte – Klima – Schall – Licht – Brand*. Springer Fachmedien Wiesbaden, Wiesbaden, 2022. doi:10.1007/978-3-658-34093-3.

[WLG+23] L. Wang, G. Li, J. Gao, X. Fang, C. Wang, and C. Xiong. Case Study: Impacts of Air-Conditioner Air Supply Strategy on Thermal Environment and Energy Consumption in Offices Using BES–CFD Co-Simulation. *Sensors*, 23(13):5958, June 2023. doi:10.3390/s23135958.

[WLWZ23] H. Wang, N. Lu, F. Wu, and J. Zhai. Coupling Computational Fluid Dynamics and EnergyPlus to Optimize Energy Consumption and Comfort in Air Column Ventilation at a Tall High-Speed Rail Station. *Sustainability*, 15(17):12948, Aug. 2023. doi:10.3390/su151712948.

[Wöl17] D. Wölki. *MORPHEUS: Modelica-based Implementation of a Numerical Human Model Involving Individual Human Aspects*. PhD thesis, RWTH Aachen University, 2017. doi:10.18154/RWTH-2017-04128.

[WW97] R. L. Wilby and T. Wigley. Downscaling general circulation model output: A review of methods and limitations. *Progress in Physical Geography: Earth and Environment*, 21(4):530–548, Jan. 1997. doi:10.1177/030913339702100403.

[WW09] L. Wang and N. H. Wong. Coupled simulations for naturally ventilated rooms between building simulation (BS) and computational fluid dynamics (CFD) for better prediction of indoor thermal environment. *Building and Environment*, 44(1):95–112, Jan. 2009. doi:10.1016/j.buildenv.2008.01.015.

[WWQ24] Z. Wang, H. Weng, and H. Qiu. Optimization Design of Air Distribution in Capacitor Rooms Based on BIM-CFD Combined Modeling and Simulation. In *2024 6th International Conference on Energy Systems and Electrical Power (ICESEP)*, pages 1202–1206, Wuhan, China, June 2024. IEEE. doi:10.1109/ICESEP62218.2024.10652141.

[XC22] Y. Xiong and H. Chen. Impacts of uneven surface heating of an ideal street canyon on airflows and indoor ventilation: Numerical study using OpenFOAM coupled with EnergyPlus. *Building Simulation*, 15(2):265–280, Feb. 2022. doi:10.1007/s12273-021-0788-5.

[YL17] H. Ying and S. Lee. A Framework for Rule-Based Validation of IFC Space Boundaries for Building Energy Analysis. In K.-Y. Lin, N. El-Gohary, and

P. Tang, editors, *Computing in Civil Engineering 2017: Information Modeling and Data Analytics*, pages 110–117. American Society of Civil Engineers, Reston, Jan. 2017. doi:10.1061/9780784480823.014.

[YL20] H. Ying and S. Lee. Automatic Detection of Geometric Errors in Space Boundaries of IFC-BIM Models Using Monte Carlo Ray Tracing Approach. *Journal of Computing in Civil Engineering*, 34(2):04019056, Jan. 2020. doi:10.1061/(ASCE)CP.1943-5487.0000878.

[YL21a] H. Ying and S. Lee. Generating second-level space boundaries from large-scale IFC-compliant building information models using multiple geometry representations. *Automation in Construction*, 126:103659, Jan. 2021. doi:10.1016/j.autcon.2021.103659.

[YL21b] H. Ying and S. Lee. A rule-based system to automatically validate IFC second-level space boundaries for building energy analysis. *Automation in Construction*, 127:103724, Jan. 2021. doi:10.1016/j.autcon.2021.103724.

[YLYT16] Y. Yan, X. Li, L. Yang, and J. Tu. Evaluation of manikin simplification methods for CFD simulations in occupied indoor environments. *Energy and Buildings*, 127:611–626, Sept. 2016. doi:10.1016/j.enbuild.2016.06.030.

[YM24] X. Yin and M. W. Muhieldeen. Evaluation of cooling energy saving and ventilation renovations in office buildings by combining bioclimatic design strategies with CFD-BEM coupled simulation. *Journal of Building Engineering*, 91:109547, Aug. 2024. doi:10.1016/j.jobe.2024.109547.

[YYN23] T. Yamamoto, T. Yamashita, and S. Niihara. Thermophysiological coupled analysis with COM, ES, and CFD. *Energy and Buildings*, 291:113132, July 2023. doi:10.1016/j.enbuild.2023.113132.

[ZC05] Z. J. Zhai and Q. Y. Chen. Performance of coupled building energy and CFD simulations. *Energy and Buildings*, 37(4):333–344, Apr. 2005. doi:10.1016/j.enbuild.2004.07.001.

[ZC15] Z. Zhai and Q. Chen. Strategies for coupling energy simulation and computational fluid dynamic programs. In *Proceedings of Building Simulation 2001: 7th Conference of IBPSA*, Rio de Janeiro, Brazil, 2001-08-13/2001-08-15.

[ZCZ23] N. Zhang, B. Cao, and Y. Zhu. An effective method to determine bedding system insulation based on measured data. *Building Simulation*, 16(1):121–132, Jan. 2023. doi:10.1007/s12273-022-0916-x.

[ZDS+23] Q. Zhang, Q. Deng, X. Shan, X. Kang, and Z. Ren. Optimization of the Thermal Environment of Large-Scale Open Space with Subzone-Based Temperature Setting Using BEM and CFD Coupling Simulation. *Energies*, 16(7):3214, Apr. 2023. doi:10.3390/en16073214.

[Zha03a] Z. Zhai. *Developing an Integrated Building Design Tool by Coupling Building Energy Simulation and Computational Fluid Dynamics Programs*. PhD thesis, Massachusetts Institute of Technology, Sept. 2003.

[Zha03b] H. Zhang. *Human Thermal Sensation and Comfort in Transient and Non-Uniform Thermal Environments*. PhD thesis, University of California, Berkeley, Berkeley, 2003.

[ZKOS07] S. Zhu, S. Kato, R. Ooka, and T. Sakoi. Development of a Computational Thermal Manikin Applicable in a Nonuniform Thermal Environment—Part 1: Coupled Simulation of Convection, Radiation, and Smith's Human Thermal Physiological Model for Sensible Heat Transfer from a Seated Human Body in Radiant Environment. *HVAC&R Research*, 13(4):661–679, July 2007. doi: 10.1080/10789669.2007.10390978.

[ZKT+23] Z. Zeng, J.-H. Kim, H. Tan, Y. Hu, P. Rastogi, J. Wang, and R. Muehleisen. A critical analysis of future weather data for building and energy modeling. In IBPSA, editor, *Proceedings of Building Simulation 2023: 18th Conference of IBPSA*, Building Simulation Conference Proceedings. Jan. 2023.

[ZLL21] Q. Zhao, Z. Lian, and D. Lai. Thermal comfort models and their developments: A review. *Energy and Built Environment*, 2(1):21–33, Jan. 2021. doi:10.1016/j.enbenv.2020.05.007.

[ZLWZ23] L. Zheng, W. Lu, L. Wu, and Q. Zhou. A review of integration between BIM and CFD for building outdoor environment simulation. *Building and Environment*, 228:109862, Jan. 2023. doi:10.1016/j.buildenv.2022.109862.

[ZLYZ13] R. Zhang, K. P. Lam, S.-c. Yao, and Y. Zhang. Coupled EnergyPlus and computational fluid dynamics simulation for natural ventilation. *Building and Environment*, 68:100–113, Oct. 2013. doi:10.1016/j.buildenv.2013.04.002.

[ZZW+22] L. Zhao, H. Zhang, Q. Wang, B. Sun, W. Liu, K. Qu, and X. Shen. Digital Twin Evaluation of Environment and Health of Public Toilet Ventilation Design Based on Building Information Modeling. *Buildings*, 12(4):470, Apr. 2022. doi:10.3390/buildings12040470.

A Appendix

A.1 Relationship between Research Questions and Research Hypotheses

Figure A.1 visualizes the relations between the RQs defined in the introduction of this dissertation and the related RHs defined in the respective chapters on BEPS, CFD, TC, and CC.

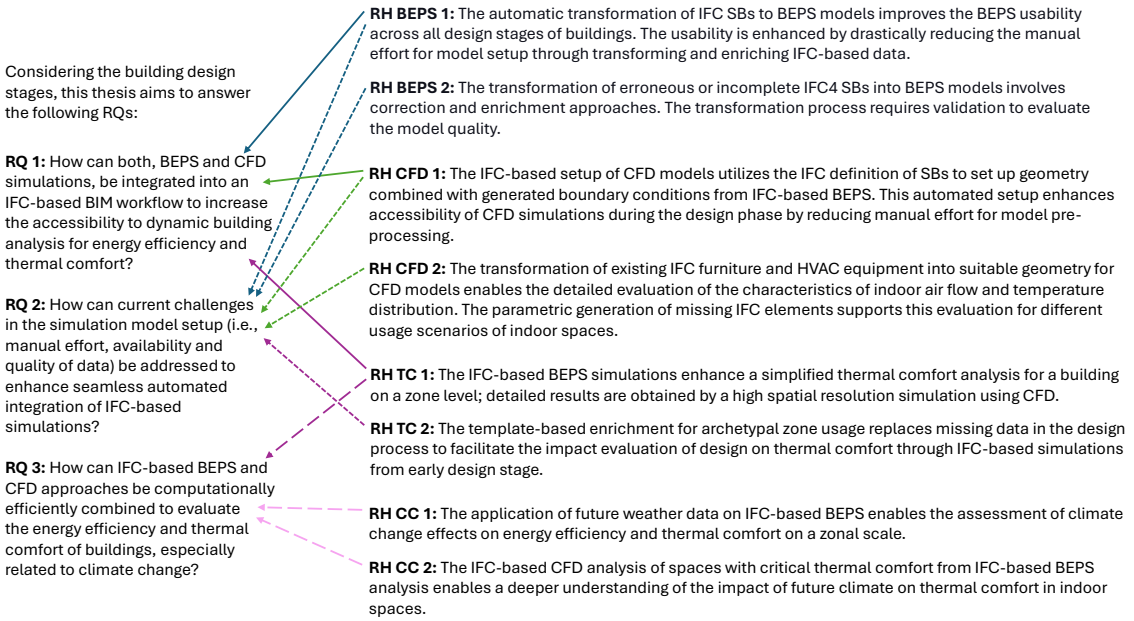

Figure A.1: Relations between research questions defined in the introduction and research hypotheses defined in the respective chapters.

A.2 Standards on Building Performance Evaluation

Table A.1 lists additional German and international standards for energy-efficient building design, which are an extension of the standards listed in Table 2.2.

Table A.1: German and International Regulations and Standards for Energy-Efficient Building Design, adapted and extended from [vTFW+21].

Regulation	Year	Title	Reference
DIN EN ISO 52000-1	2018	Energy performance of buildings - Overarching EPB assessment - Part 1: General framework and procedures	[DIN52000-1]
DIN EN ISO 52003-1	2018	Energy performance of buildings - Indicators, requirements, ratings and certificates - Part 1: General aspects and application to the overall energy performance	[DIN52003-1]
DIN EN ISO 52010-1	2018	Energy performance of buildings - External climatic conditions - Part 1: Conversion of climatic data for energy calculations	[DIN52010-1]
DIN EN ISO 52016-1	2018	Energy performance of buildings - Energy needs for heating and cooling, internal temperatures and sensible and latent heat loads - Part 1: Calculation procedures	[DIN52016-1]
DIN EN ISO 52017-1	2018	Energy performance of buildings - Sensible and latent heat loads and internal temperatures - Part 1: Generic calculation procedures	[DIN52017-1]
DIN EN ISO 52018-1	2020	Energy performance of buildings - Indicators for partial EPB requirements related to thermal energy balance and fabric features - Part 1: Overview of options	[DIN52018-1]
ISO 52120-1	2021	Energy performance of buildings - Contribution of building automation, controls and building management - Part 1: General framework and procedures	[ISO52120-1]

A.3 Handling Errors in the Automated IFC-based Setup of EnergyPlus Models

The following examples for common errors arising from translating IFC SBs to IDF are adapted from [RFA+21]:

- Geometric Errors
  - Non-watertight models caused by missing SBs, leading to gaps in the hull of thermal zones or IFC spaces
  - Overlapping shapes of spaces and SBs
  - SBs do not directly bound the related building element, but instead show a gap or are placed inside it
  - Incorrect surface normals (IFC SB-normals should point outwards the space)
  - Collinear and/or coincident vertices within the polygons defining the SB surfaces
- Semantic/Consistency Errors
  - Missing or incorrect link to the related building element
  - Missing or incorrect reference of the corresponding surface in another zone or relating space
  - Missing or incorrect reference to parent surface
  - Incorrect label for internal and external boundary conditions
  - Incorrect label for virtual and physical related building elements
- Errors due to differences in schema conventions and requirements
  - Vertex number of openings (windows, doors): maximum of 4 vertices allowed in IDF
  - Convexity: surfaces in IDF need to be defined as convex shapes to enable a correct shading calculation using EnergyPlus' PolygonClipping algorithm
  - Representation of inner loops within surfaces: EnergyPlus defines surfaces by a single polygon, while IFC allows to define additional polygons for inner loops
  - Geometric position of SBs (on surface or centerline of related building element)
  - Opening and base surface have the same area (child and parent), which is permitted in EnergyPlus.

Algorithm A.1 presents an algorithm to obtain these corresponding space boundaries by matching corresponding SBs within a given IFC file containing 2ndLevel space boundaries. The presented algorithm does not require corrected surface normals, but builds upon the relations between SB B and its relating building element E (e.g., Wall, Slab, Door). To find a matching corresponding space boundary B_c for the base space boundary B_0, the algorithm loops over all bounds B_i in the bound element of B_0, defined as E. Unless the current bound B_i is the base boundary, the surface areas of the boundaries are compared. If these areas match within a given tolerance, the distance of the center (d_{center}) of the space boundaries are evaluated. Prerequisite for further evaluation is that the distance is smaller than the minimum set tolerance for space boundary distance, and that it is also smaller than the

Algorithm A.1: Matching of corresponding SBs. [RFA+21]

```
Data: B_0, E
Result: B_c
tol_area := tolerance for difference in area of SBs;
tol_dist := tolerance for minimum distance of SBs;
d_min,local := initial value for local minimum distance;
B_c = [];
for B_i in E do
    if B_i != B_0 then
        if ||B_0,area − B_i,area|| < tol_area then
            d_center = ||B_0,center − B_i,center||;
            if (d_center < d_min,local) and
              (d_center < tol_dist) then
                d_min =
                  min(distance(||B_0,shape −
                  B_i,shape||));
                if d_min == d_center then
                    d_min,local = d_center;
                    B_c = B_i
                end
            end
        end
    end
end
```

initial minimum local distance, which should
be chosen according to the thickness of the related building element. If these prerequisites are fulfilled, the minimum distance of the shapes of B_0 and B_i is computed. If this distance is equal to the distance of the centers of the shapes, B_i is set as the corresponding boundary B_c. If the minimum distance of the shapes is smaller than the center distance, these bounds are not parallel, and thus, there is no valid matching pair of corresponding boundaries.

Algorithm A.2: Compute boundaries to generate airtight sets of SBs.

```
Data: S, E
Result: B_new
tol_area := tolerance for difference in surface areas;
tol_dist := tolerance for minimum distance of SB and
  space shape;
B_new = [];
E_area = 0;
for B_i in E do
    if B_i not has parent bound then
        E_area += B_i,area
    end
end
if abs(E_area - S_area) > tol_area then
    B_new,shape = S_shape for B_i in E do
        if B_new,area > 0 then
            if distance(B_new,shape, B_i,shape) < tol_dist
              then
                B_new,shape = cut(B_new,shape,
                  B_i,shape)
            end
        end
    end
    faces = getFacesOfShape(B_new,shape);
    if faces then
        B_new = createSpaceBoundaryInstances(faces);
        B_new = splitNonConvexBounds(B_new);
    end
end
```

Algorithm A.2 is included in the *PluginEnergyPlus* (cf. Section 2.5) to fill gaps in non-airtight sets of space boundaries. This approach relies on each space boundary B_i within the set of space boundaries E to be positioned on the surface of the space shape S_{shape}, which is compliant with the IFC schema. In this approach to create space boundaries B_{new} to fill the gap, first, the surface area of the set of space boundaries E_{area} is compared to the surface area S_{area} of the space itself. Only space boundary surface areas are considered for instances, which do not have a parent boundary, to not consider opening surfaces twice. If the surface area difference is below the threshold tol_{area}, it can be assumed that the set of space boundaries is airtight. This pre-check reduces the computational cost by ensuring that the following algorithm is only applied to sets of non-airtight space boundaries.

After the pre-check of applicability, the shape of the space S_{shape} is assigned to be the basis for the shape of missing space boundaries $B_{\text{new,shape}}$ that should be added as new boundaries. Iterating through all space boundaries E, for each new boundary B_i it is checked that the distance between the boundary B_i and the space shape $B_{\text{new,shape}}$ is below a threshold tol_{dist}, to ensure that B_i can be cut from $B_{\text{new,shape}}$. Once all boundaries have been cut from the space shape, or once the surface area of $B_{\text{new,area}}$ is zero, $B_{\text{new,shape}}$ is split into its individual faces. From these faces, new space boundary instances are created, and split into convex shapes to not cause errors in shadowing calculation.

A.4 Evaluation of the IFC-based BEPS Methods

Figure A.2 displays the heating setpoint temperatures applied for air temperature control in the FZK Haus simulation described in Section 2.7.1. These setpoints comply with the schedules visualized in Figure A.32 except for the bathroom setpoint which is increased to 24 °C. Figure A.3 visualizes the annual outdoor air temperature of the TMYx (2007-2021) weather file in a heatmap. Figure A.4 displays the space boundary validation in the presented validation tool for the modified FZK Haus using the IFC2SB Tool [Fic22].

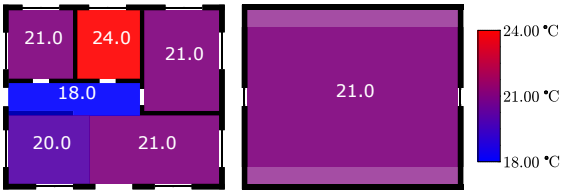

Figure A.2: Heating setpoint temperatures per space. All spaces have a night setback from 10pm to 6am to 18 °C, except for the bathroom, which has a night setback from 11pm to 5am to 20 °C.

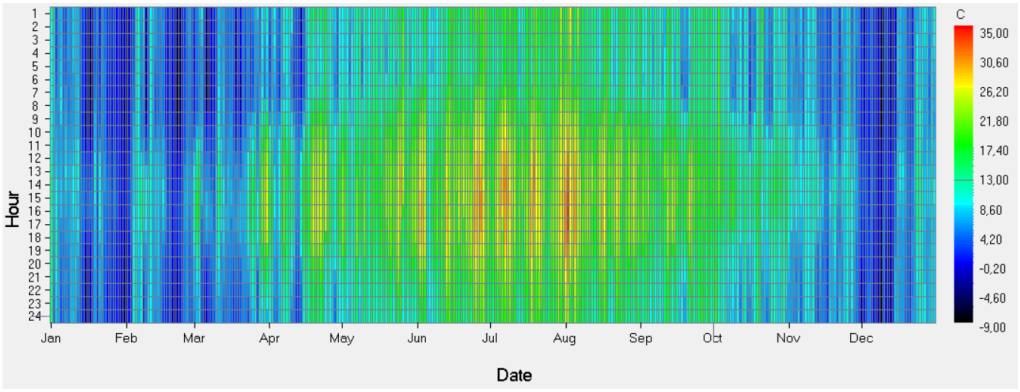

Figure A.3: Heatmap of outdoor air temperature of Cologne/Bonn Airport, TMYx (2007-2021), displayed in DesignBuilder Results Viewer.[1]

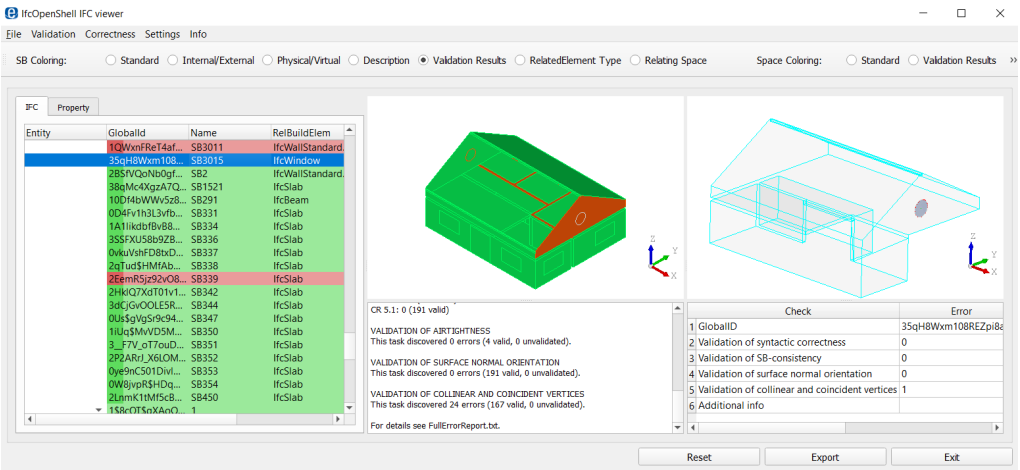

Figure A.4: Validation of space boundaries generated by [Fic22] for the FZK-Haus IFC4 file.

[1] DesignBuilder Results Viewer, Version 4.1, https://designbuilder.co.uk/download/previous-versions, accessed on June 05, 2025.

A.5 IFC-based CFD

A.5.1 Mesh Refinement Levels

Table A.2 displays the mesh refinement levels, i.e., minimum and maximum value, applied per surface type in the grid convergence analysis in Section 3.6.1. Table A.3 displays the parameters for the mesh refinement regions, including the minimum distance from the respective surface, up to which the minimum refinement level is applied, and the maximum distance, referring to the respective maximum refinement level.

Table A.2: Mesh refinement levels in the grid convergence test.

Surfaces	Min	Max
Floor	2	3
Inner Wall	2	3
Outer Wall	2	3
Roof	2	3
Window	2	3
Door	2	3
Heater surface	2	3
Inlet diffusor	2	5
Inlet/outlet diffusor	2	5
Inlet/outlet box	1	3
Inlet source	2	5
Outlet sink	2	5
Furniture	2	3
Person body parts	4	4

Table A.3: Mesh refinement regions in the grid convergence test. MinDistance and MaxDistance are stated in m.

Regions	MinDistance	Min	MaxDistance	Max
Heater porous media	-	0	-	3
Heater surface	0.05	3	0.15	2
In-/outlet source/sink	0.03	5	0.08	4
Furniture	0.03	3	0.6 (correct: 0.06)	2
Person	0.05	4	0.1	3

A.5.2 CFD for Occupied Space

Figure A.5 displays the air velocity distribution using LIC for the use case described in Figure 3.21. The horizontal slice is located at a height of 3.0 m, slicing through the air terminals. The visualization proves the functionality of the air terminals, as they all release an even airstream.

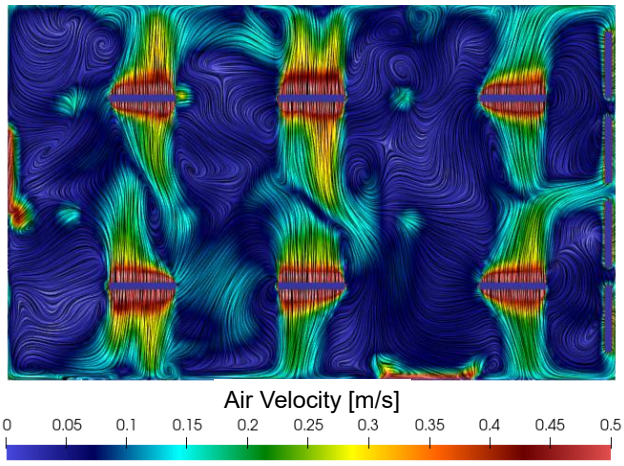

Figure A.5: Air velocity distribution (LIC) for sidewards outflow direction of slot diffusers in an occupied space. Horizontal slice through the domain at z=3.0 m, slice through the air terminals.

A.6 Thermal Comfort in EnergyPlus

In this section, the current capabilities of the EnergyPlus kernel are further analyzed, which is an excerpt from [RSFvT23]. EnergyPlus provides the implementation of the adaptive comfort analysis according to [DIN15251], which has been withdrawn. This standard is replaced by [DIN16798-1], which is not yet implemented in EnergyPlus. With the standard's transition, the methods for thermal comfort still rely on [ISO7730]. While methods to calculate the running mean outdoor temperature have not changed, the standards for acceptable temperatures have changed (cf. Table A.4), i.e., the lower boundary for each comfort category has been reduced by one degree Celsius, and thus, slightly cooler temperatures are defined to be acceptable. [RSFvT23]

Table A.4: Differences in running mean outdoor temperatures as setpoints for thermal comfort categories in [DIN15251, DIN16798-1], adapted from [RSFvT23].

	DIN EN 15251	DIN EN 16798-1
Category I, upper threshold	24.1…30.7 °C	
Category I, lower threshold	21.75…26.7 °C	19.1…25.7 °C
Category II, upper threshold	25.1…31.7 °C	
Category II, lower threshold	20.75…25.7 °C	18.1…24.7 °C
Category III, upper threshold	26.1…32.7 °C	
Category III, lower threshold	18.1…24.7 °C	17.1…23.7 °C
Applicability limits:		
Upper threshold	10…30 °C	
Lower threshold	15…30 °C	10…30 °C

For a valid analysis of adaptive thermal comfort according to [DIN16798-1], the comfort analysis has to be reimplemented, which is done based on the csv-output of the results. This reimplementation of the international standard [DIN16798-1] is extended by an additional adapted version covering the differences in the temperature limits stated in the NA as displayed in Figure 4.2.

A.7 Thermal Comfort Templates

A.7.1 Activity Parameters

Table A.5 presents the full list of derived activity levels for the extension of the TEASER templates. This list has initially been presented in [RSFvT23].

Table A.5: Deriving activity parameters for archetypal enrichment of thermal zones based on ASHRAE Fundamentals and ISO 7730, including a comparison to existing TEASER template values. Columns: (1) Room type according to TEASER templates, (2) Activity degree from TEASER templates (met), (3) Heat flow from TEASER templates (W/person), (4) Chosen activity type according to ASHRAE Fundamentals, Chapter 9 Table 4, (5) Chosen activity type according to ISO 7730, Table A.5 and B.1, (6) ASHRAE activity degree (met), (7) ISO 7730 activity degree (met), (8) Resulting combined activity degree (met), (9) Absolute deviation from TEASER activity degree (met), (10) Resulting heat flow (W/person), (11) Absolute deviation from TEASER heat flow (W/person). Initially presented in [RSFvT23].

(1) Room type	(2)	(3)	(4) ASHRAE Fundamentals	(5) ISO 7730	(6)	(7)	(8) Activity Degree (met)	(9)	(10) Heat flow (W/person)	(11)
Single office	1.2	70	Office, Typing	A.5, Single office	1.1	1.2	1.2	0.0	125	55
Group Office (between 2 and 6 employees)	1.2	70	Office, Typing	A.5, Landscape office	1.1	1.2	1.2	0.0	125	55
Open-plan Office (7 or more employees)	1.2	70	Office, Typing	A.5, Landscape office	1.1	1.2	1.2	0.0	125	55
Meeting, Conference, seminar	1.2	70	Office, Typing	A.5, Conference Room	1.1	1.2	1.2	0.0	125	55
Main Hall, Reception	1.2	70	Office Walking	B.1, Standing, light activity	1.7	1.6	1.7	0.5	178	108
Retail, department store	1.2	70	Office, Filing, Standing	A.5, Department store	1.4	1.6	1.5	0.3	157	87
Retail with cooling	1.2	70	Office, Filing, Standing	A.5, Department store	1.4	1.6	1.5	0.3	157	87
Class room (school), group room (kindergarden)	1.2	70	Office, Writing	A.5, Kindergarten	1	1.4	1.2	0.0	125	55
Lecture hall, auditorium	1.2	70	Office, Typing	A.5, Auditorium	1.1	1.2	1.2	0.0	125	55
Bed room	1.2	70	Resting, Sleeping	B.1, Reclining	0.7	0.8	0.8	0.4	84	14
Hotel room	1.2	70	Resting, Sleeping	B.1, Reclining	0.7	0.8	0.8	0.4	84	14
Canteen	1.2	70	Office, Filing, Seated	A.5, Cafeteria/restaurant	1.2	1.2	1.2	0.0	125	55
Restaurant	1.2	70	Office, Filing, Seated	A.5, Cafeteria/restaurant	1.2	1.2	1.2	0.0	125	55
Kitchen in non-residential buildings	1.2	70	Cooking	B.1, Standing, medium activity	1.8	2	1.9	0.7	199	129
Kitchen - preparations, storage	2	90	Cooking	B.1, Standing, medium activity	1.8	2	1.9	0.1	199	109
WC and sanitary rooms in non-residential buildings	1.2	70	Resting, Seated, quiet	B.1, Seated, relaxed	1	1	1	0.2	105	35
Further common rooms	1.2	70	Office, Typing	B.1, Sedentary activity	1.1	1.2	1.2	0.0	125	55
Auxiliary areas (without common rooms)	1.2	70	Office Walking	A.5, Department store	1.7	1.6	1.7	0.5	178	108
Traffic area	1.2	70	Office Walking	B.1, Walking, 2 km/h	1.7	1.9	1.8	0.6	188	118
Stock, technical equipment, archives	2	90	Office, Filing, Standing	B.1, Standing, light activity	1.4	1.6	1.5	0.5	157	67
Data center	1.2	70	Office, Filing, Standing	B.1, Standing, light activity	1.4	1.6	1.5	0.3	157	87
Commercial and industrial Halls - heavy work, standing activity	2	90	Machine work, heavy	B.1, Walking, 5 km/h	4	3.4	3.7	1.7	387	297
Commercial and industrial Halls - medium work, standing activity	1.6	80	Machine work, light (electrical industry)	B.1, Standing, medium activity	2.2	2	2.1	0.5	220	140
Commercial and industrial Halls - light work, standing activity	1.2	70	Machine work, sawing	B.1, Standing, light activity	1.8	1.6	1.7	0.5	178	108
Spectator area (theater and event venues)	1.2	70	Resting, Seated, quiet	A.5, Auditorium	1	1.2	1.1	0.1	115	45
Foyer (theater and event venues)	1.2	70	Resting, Standing, relaxed	B.1, Standing, light activity	1.2	1.6	1.4	0.2	146	76
Stage (theater and event venues)	2	90	Dancing, social	B.1, Walking, 3 km/h	3.2	2.4	2.8	0.8	293	203
Exhibition, congress	1.2	70	Office, Filing, Standing	A.5, Department store	1.4	1.6	1.5	0.3	157	87
Exhibition room and museum conservational demands	1.2	70	Resting, Standing, relaxed	B.1, Standing, light activity	1.2	1.6	1.4	0.2	146	76

(1) Room type	(2)	(3)	(4) ASHRAE Fundamentals	(5) ISO 7730	(6)	(7)	(8) Activity Degree (met)	(9)	(10) Heat flow (W/person)	(11)
Library - reading room	1.2	70	Office, Reading, seated	B.1, Sedentary activity	1	1.2	1.1	0.1	115	45
Library - open stacks	1.2	70	Office, Filing, standing	B.1, Standing, light activity	1.4	1.6	1.5	0.3	157	87
Library - magazine and depot	1.2	70	Office, Filing, standing	B.1, Standing, light activity	1.4	1.6	1.5	0.3	157	87
Gym (without spectator area)	3	120	Calisthenics/exercise	B.1, Walking, 5 km/h	3.5	3.4	3.5	0.5	366	246
Parking garages (office and private usage)	0	35	Office Walking	B.1, Walking, 2 km/h	1.7	1.9	1.8	1.8	188	153
Parking garages (public usage)	0	35	Office Walking	B.1, Walking, 2 km/h	1.7	1.9	1.8	1.8	188	153
Sauna area	1.2	70	Resting, Seated, quiet	B.1, Seated, relaxed	1	1	1	0.2	105	35
Exercise room	3	120	Office, Writing	A.5, Classroom	1	1	1	2.0	105	15
Laboratory	1.2	70	Office, Filing, Seated	B.1, Sedentary activity	1.2	1.2	1.2	0.0	125	55
Examination- or treatment room	1.2	70	Office, Filing, standing	B.1, Standing, light activity	1.4	1.6	1.5	0.3	157	87
Special care area	1.2	70	Office, Lifting/packing	B.1, Standing, medium activity	2.1	2	2.1	0.9	220	150
Corridors in the general care area	1.2	70	Office Walking	B.1, Walking, 2 km/h	1.7	1.9	1.8	0.6	188	118
Medical and therapeutic practices	1.2	70	Office, Filing, Seated	B.1, Standing, light activity	1.2	1.6	1.4	0.2	146	76
Storehouse, logistics building	2	90	Office, Lifting/packing	B.1, Standing, medium activity	2.1	2	2.1	0.1	220	130
Living	1.2	70	Resting, Seated, quiet	B.1, Sedentary activity	1	1.2	1.1	0.1	115	45
Classroom	1	70	Office, Writing	A.5, Classroom	1	1.2	1.1	0.1	115	45

A.7.2 Clothing Parameters

Table A.6 presents the full list of derived clothing parameters for the extension of the TEASER templates. This list has initially been presented in [RSFvT23].

Table A.6: Deriving clothing parameters for archetypal enrichment of thermal zones based on ASHRAE Fundamentals and ISO 7730. Columns: (1) Room type according to TEASER templates, (2) Chosen clothing type according to ASHRAE Fundamentals, Chapter 9 Table 7, (3) Chosen clothing type according to ISO 7730, (4) ASHRAE clothing (clo), (5) ISO 7730 clothing (clo), (6) Resulting combined clothing parameter (clo), (7) Chosen surrounding insulation type, (8) Surrounding insulation (clo). Initially presented in [RSFvT23].

(1) Room type	(2) ASHRAE Fundamentals	(3) ISO 7730	(4)	(5)	(6) Clothing insulation (clo)	(7) Surrounding insulation description	(8) Surrounding insulation (clo)
Single office	Trousers, long-sleeved shirt	Underwear, shirt, trousers, socks, shoes	0.61	0.7	0.66	ISO 7730, C.3 Executive chair	0.15
Group Office (between 2 and 6 employees)	Trousers, long-sleeved shirt	Underwear, shirt, trousers, socks, shoes	0.61	0.7	0.66	ISO 7730, C.3 Standard office chair	0.1
Open-plan Office (7 or more employees)	Trousers, long-sleeved shirt	Underwear, shirt, trousers, socks, shoes	0.61	0.7	0.66	ISO 7730, C.3 Standard office chair	0.1
Meeting, Conference, seminar	Trousers, long-sleeved shirt, suit jacket	Underwear, shirt, trousers, socks, shoes	0.96	0.7	0.83	ISO 7730, C.3 Wooden stool	0.01
Main Hall, Reception	Trousers, long-sleeved shirt, suit jacket	Underwear with short sleeves and legs, shirt, trousers, jacket, socks, shoes	0.96	1	0.98	ISO 7730, C.3 Standard office chair	0.1
Retail, department store	Trousers, long-sleeved shirt, long-sleeved sweater, T-shirt	Panties, shirt, trousers, jacket, socks, shoes	1.01	1	1.01	None	
Retail with cooling	Trousers, long-sleeved shirt, long-sleeved sweater, T-shirt	Panties, shirt, trousers, jacket, socks, shoes	1.01	1	1.01	None	
Class room (school), group room (kindergarden)	Trousers, long-sleeved shirt	Underwear, shirt, trousers, socks, shoes	0.61	0.7	0.66	ISO 7730, C.3 Wooden stool	0.01
Lecture hall, auditorium	Trousers, long-sleeved shirt	Underwear, shirt, trousers, socks, shoes	0.61	0.7	0.66	ISO 7730, C.3 Wooden stool	0.01
Bed room	Walking shorts, short-sleeved shirt	Panties, T-shirt, shorts, light socks, sandals	0.36	0.3	0.33	Average based on Zhang, N. et al. (2023)	2
Hotel room	Walking shorts, short-sleeved shirt	Panties, T-shirt, shorts, light socks, sandals	0.36	0.3	0.33	Average based on Zhang, N. et al. (2023)	2

(1) Room type	(2) ASHRAE Fundamentals	(3) ISO 7730	(4)	(5)	(6) Clothing insulation (clo)	(7) Surrounding insulation description	(8) Surrounding insulation (clo)
Canteen	Trousers, long-sleeved shirt	Underwear, shirt, trousers, socks, shoes	0.61	0.7	0.66	ISO 7730, C.3 Wooden stool	0.01
Restaurant	Trousers, long-sleeved shirt	Underwear, shirt, trousers, socks, shoes	0.61	0.7	0.66	ISO 7730, C.3 Wooden stool	0.01
Kitchen in non-residential buildings	Long-sleeved overalls, T-Shirt	Underpants, shirt, trousers, smock, socks, shoes	0.72	0.9	0.81	None	
Kitchen - preparations, storage	Long-sleeved overalls, T-Shirt	Underpants, shirt, trousers, smock, socks, shoes	0.72	0.9	0.81	None	
WC and sanitary rooms in non-residential buildings	Trousers, long-sleeved shirt	Underwear, shirt, trousers, socks, shoes	0.61	0.7	0.66	None	
Further common rooms	Trousers, long-sleeved shirt	Underwear, shirt, trousers, socks, shoes	0.61	0.7	0.66	ISO 7730, C.3 Wooden stool	0.01
Auxiliary areas (without common rooms)	Trousers, long-sleeved shirt	Underwear, shirt, trousers, socks, shoes	0.61	0.7	0.66	None	
Traffic area	Trousers, long-sleeved shirt	Underwear, shirt, trousers, socks, shoes	0.61	0.7	0.66	None	
Stock, technical equipment, archives	Trousers, long-sleeved shirt	Underwear, shirt, trousers, socks, shoes	0.61	0.7	0.66	None	
Data center	Trousers, long-sleeved shirt	Underwear, shirt, trousers, socks, shoes	0.61	0.7	0.66	None	
Commercial and industrial Halls - heavy work, standing activity	Trousers, long-sleeved shirt	Underwear, shirt, trousers, socks, shoes	0.57	0.7	0.64	None	
Commercial and industrial Halls - medium work, standing activity	Trousers, long-sleeved shirt	Underwear, shirt, trousers, socks, shoes	0.57	0.7	0.64	None	
Commercial and industrial Halls - light work, standing activity	Trousers, long-sleeved shirt	Underwear, shirt, trousers, socks, shoes	0.57	0.7	0.64	None	
Spectator area (theater and event venues)	Trousers, long-sleeved shirt, suit jacket	Underwear, shirt, trousers, socks, shoes	0.96	0.7	0.83	ISO 7730, C.3 Wooden stool	0.01
Foyer (theater and event venues)	Trousers, long-sleeved shirt, suit jacket	Underwear, shirt, trousers, socks, shoes	0.96	0.7	0.83	None	
Stage (theater and event venues)	Trousers, long-sleeved shirt	Underwear, shirt, trousers, socks, shoes	0.61	0.7	0.66	None	
Exhibition, congress	Trousers, long-sleeved shirt, suit jacket	Underwear, shirt, trousers, socks, shoes	0.96	0.7	0.83	None	
Exhibition room and museum conservational demands	Trousers, long-sleeved shirt, suit jacket	Underwear, shirt, trousers, socks, shoes	0.96	0.7	0.83	None	
Library - reading room	Trousers, long-sleeved shirt	Underwear, shirt, trousers, socks, shoes	0.61	0.7	0.66	ISO 7730, C.3 Wooden stool	0.01
Library - open stacks	Trousers, long-sleeved shirt	Underwear, shirt, trousers, socks, shoes	0.61	0.7	0.66	None	
Library - magazine and depot	Trousers, long-sleeved shirt	Underwear, shirt, trousers, socks, shoes	0.61	0.7	0.66	None	
Gym (without spectator area)	Walking shorts, short-sleeved shirt	Underpants, shirt with short sleeves, light trousers, light socks, shoes	0.36	0.5	0.43	None	
Parking garages (office and private usage)	Trousers, long-sleeved shirt, long-sleeved sweater, T-shirt	Panties, shirt, trousers, jacket, socks, shoes	1.01	1	1.01	None	
Parking garages (public usage)	Trousers, long-sleeved shirt, long-sleeved sweater, T-shirt	Panties, shirt, trousers, jacket, socks, shoes	1.01	1	1.01	None	
Sauna area	Not applicable	Not applicable	0	0	0	ISO 7730, C.3 Wooden stool	0.01
Exercise room	Trousers, long-sleeved shirt	Underwear, shirt, trousers, socks, shoes	0.61	0.7	0.66	ISO 7730, C.3 Wooden stool	0.01
Laboratory	Long-sleeved overalls, T-Shirt	Underpants, shirt, trousers, smock, socks, shoes	0.72	0.9	0.81	ISO 7730, C.3 Wooden stool	0.01
Examination- or treatment room	Long-sleeved overalls, T-Shirt	Underpants, shirt, trousers, smock, socks, shoes	0.72	0.9	0.81	ISO 7730, C.3 Wooden stool	0.01
Special care area	Long-sleeved overalls, T-Shirt	Underpants, shirt, trousers, smock, socks, shoes	0.72	0.9	0.81	Average based on Zhang, N. et al. (2023)	2
Corridors in the general care area	Long-sleeved overalls, T-Shirt	Underpants, shirt, trousers, smock, socks, shoes	0.72	0.9	0.81	None	
Medical and therapeutic practices	Long-sleeved overalls, T-Shirt	Underpants, shirt, trousers, smock, socks, shoes	0.72	0.9	0.81	ISO 7730, C.3 Wooden stool	0.01
Storehouse, logistics building	Long-sleeved overalls, T-Shirt	Underwear, shirt, trousers, socks, shoes	0.72	0.7	0.71	None	
Living	Trousers, long-sleeved shirt	Underwear, shirt, trousers, socks, shoes	0.61	0.7	0.66	ISO 7730, C.3 Executive chair	0.15
Classroom	Trousers, long-sleeved shirt	Underwear, shirt, trousers, socks, shoes	0.61	0.7	0.66	ISO 7730, C.3 Wooden stool	0.01

A.8 IFC-based Analysis of Thermal Comfort

This section includes supporting material and further analysis of the IFC-based thermal comfort methods.

A.8.1 Analyzing the System Sizing Impact on Simulation Results

The choice of sizing options for heating and cooling capacities in BEPS using EnergyPlus impacts the resulting heating and cooling demand of the building. Within the *bim2sim* tool, several combinations of sizing options are available. The default option is the choice of design period for the autosizing of the cooling capacity, while the heating capacity is unlimited, i.e., the power follows the heating demand of calculated during runtime in BEPS. The cooling design period can set to typical or extreme summer days, which is by default applied using EnergyPlus internal autosizing. If no autosizing should be applied to define the heating and cooling capacities, the use of calculated capacities can be enforced. The resulting capacities represent the maximum heat or cooling loads observed on the typical or extreme design day, respectively. In order to evaluate existing systems impacted by future weather scenarios, the weather files for sizing and simulation can independently be defined.

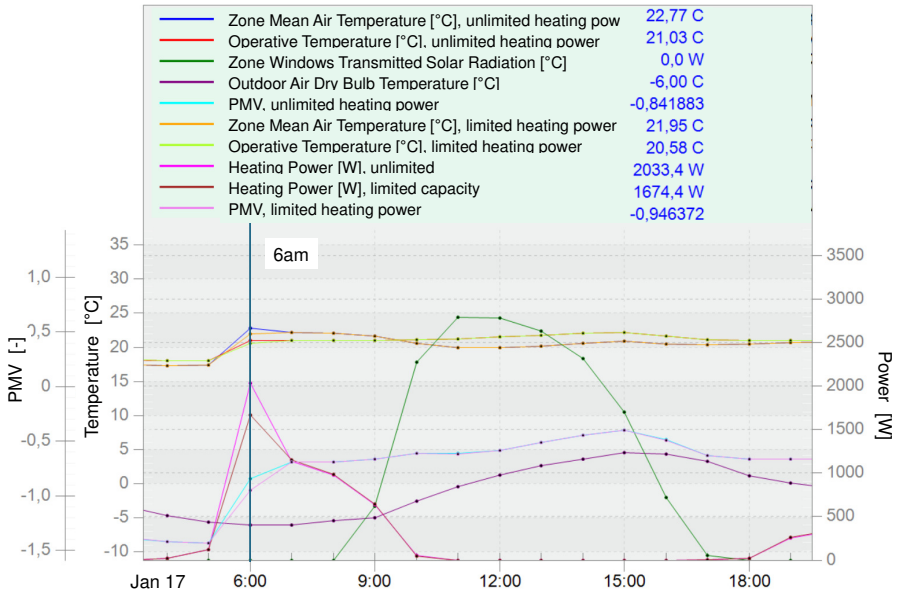

Figure A.6: EnergyPlus results for the south-east office space on Jan 17, 6am, sized and simulated using TMYx (2007-2021) weather data for Cologne/Bonn Airport. Visualization adapted from DesignBuilder Results Viewer.[2]

In Figure A.6, two related heating scenarios are compared for the south-east *E01-13 Group office* in the DigitalHub, simulated without external shading elements generated from external space boundaries. While the first option uses a heating capacity without limits, the second option uses a heating capacity limited to the extreme design day system sizing. As a result, the heating power at 6am after the night setback is about 350 W higher for the unlimited case, directly reaching the requested operative temperature of 21 °C. The case with the limited capacity reaches an operative temperature of 20.58 °C in this timestep, resulting in a 0.1 lower PMV

[2] DesignBuilder Results Viewer, Version 4.1, https://designbuilder.co.uk/download/previous-versions, accessed on June 05, 2025.

than the unlimited case. The unlimited heating capacity results in an annual heating energy consumption of 29.93 kWh/(m^{2}a), which is reduced by 2.05 kWh/(m^{2}a) for using extreme day system sizing (cf. Table A.10), while only slightly increasing the number of hours with a PMV below -0.5 on the top floor (1 to 155 hours per space and year).

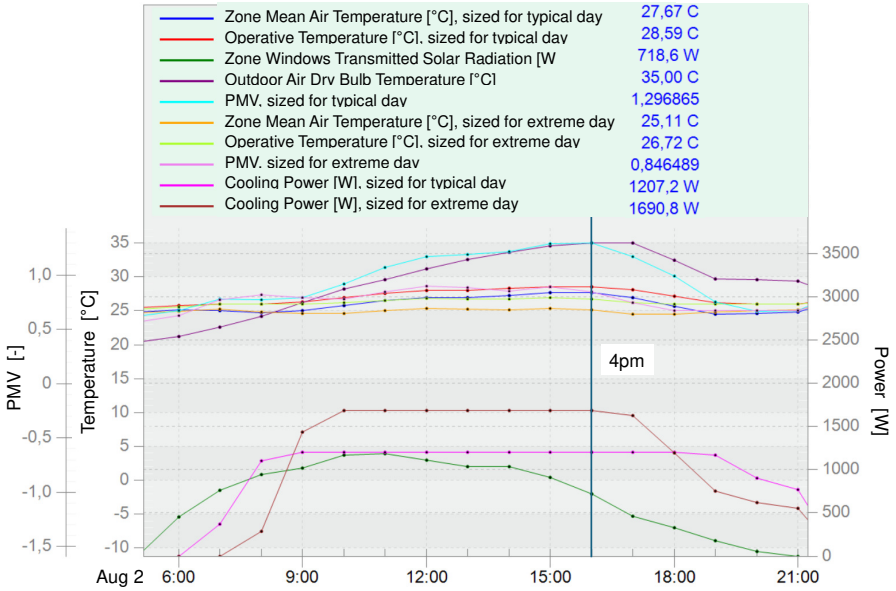

Figure A.7: EnergyPlus results for the south-east office space on Aug 2, 4pm, sized and simulated using TMYx (2007-2021) weather data for Cologne/Bonn Airport.

Figure A.7 compares the cooling scenarios. As both cooling capacities are limited, the cooling capacity sized for an extreme summer day results in a higher thermal comfort in space, than the cooling capacity sized for a typical summer day. While the extreme-day sized capacity is reached from 10am to 4pm and resulted in an operative temperature of 26.72 °C (0.72 K above acceptable) and a PMV of 0.85, the typical-day sized capacity has been reached for additional three hours, leading to an operative temperature of 1.67 K above the acceptable limit and a PMV of 1.30. Thus, the choice of sizing option is crucial to maintain thermal comfort during extreme summer periods, which is even more critical due to an increase of summer extreme weather conditions caused by global warming. Both cooling scenarios are analyzed regarding local thermal comfort. See Appendix A.8.5 for the typical-day sized cooling capacity, and Section 4.7.4 for the extreme-day sized cooling. The extreme-day cooling capacity is further evaluated in Section 5.4.3 on its performance in the future climate scenario SSP5-8.5, using the prediction for the year 2050.

A.8.2 Annual Thermal Comfort in the FZK Haus

Figure A.8 displays the adaptive thermal comfort according to [DIN16798-1], NA in the FZK Haus for the full year, including both occupied and unoccupied hours. An evaluation of the occupied hours is presented in Figure 4.8.

A.8.3 Annual Thermal Comfort in the DigitalHub using Extreme Day System Sizing

The following results are based on a system sizing for the extreme days of the TMYx weather file. All other evaluations have been executed similarly to the procedure described in Section 4.7.2,

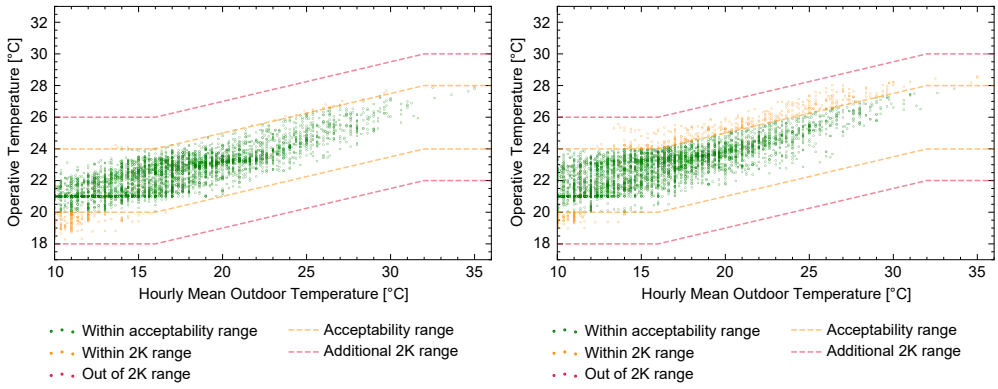

(a) Living (full)

(b) Single office (full)

Figure A.8: Evaluation of adaptive thermal comfort according to DIN EN 16798-1, NA, for the *Living* space and the *Single office*. Results are displayed for all hourly timesteps of the year, in contrast to the evaluation of the occupied hours displayed in Figure 4.8.

and these also use the DigitalHub model without external shadings, using the KfW40 constructions. See Appendix A.8.1 for an analysis of the sizing choice impact on the energy demand and thermal comfort.

For this extreme-day-sized setup, an annual heating energy consumption of 27.88 kWh/(m^{2}a) and a cooling energy consumption of 1.81 kWh/(m^{2}a) have been simulated, resulting in a total energy consumption of 58.35 kWh/(m^{2}a), including additional electric energy, 9.63 kWh/(m^{2}a) for lighting and 19.03 kWh/(m^{2}a) for electric equipment (cf. Table A.10). The electric energy demand is not affected by the applied system sizing for typical or extreme days, as they depend on the floor area and the schedules defined in the TEASER templates. Figure A.9 shows the annual heating and cooling energy consumption for the spaces on the top floor of the DigitalHub.

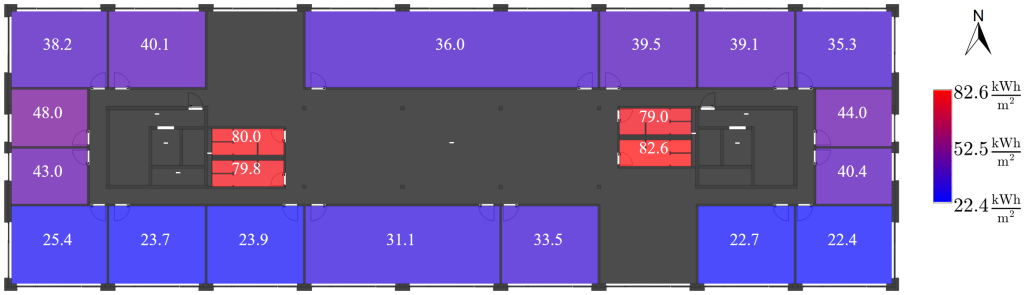

(a) Heating energy in kWh/(m^2 a)

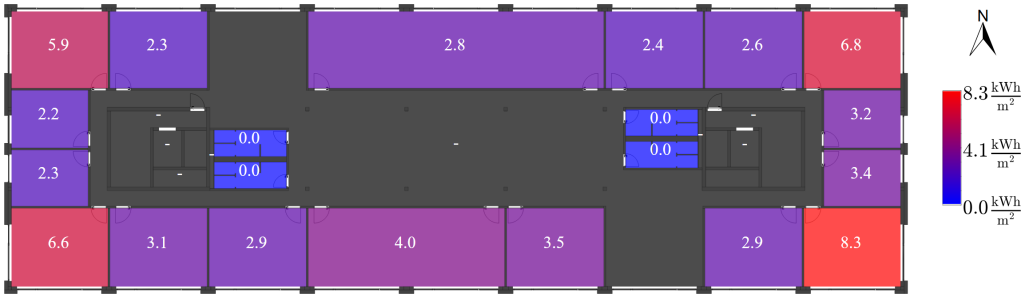

(b) Cooling energy in kWh/(m^2 a)

Figure A.9: Heating and cooling energy consumption on the top floor, no external shadings. Operative temperature setpoints of 21 °C/26 °C during the occupied hours, and 18 °C/36 °C otherwise, for heating/cooling, respectively.

The annual mean PMV does not differ from the mean PMV presented in Figure 4.13. The evaluation of the PMV above and below the Category II thresholds defined in [DIN16798-1] in Figure A.10 shows minor changes compared to the results obtained from the typical day sizing (cf. Figure 4.13).

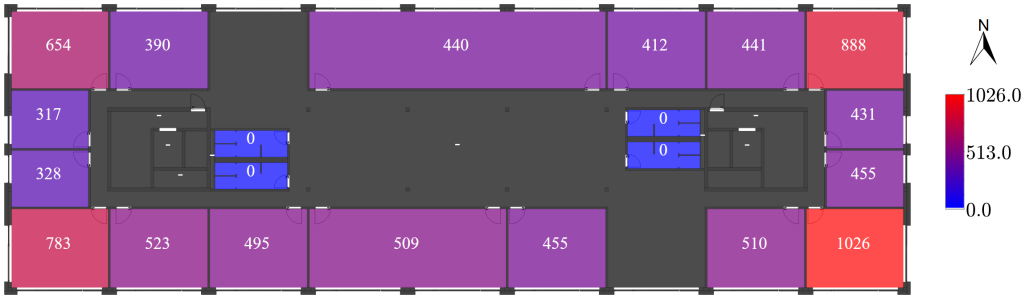

(a) Number of hours for $PMV > 0.5$.

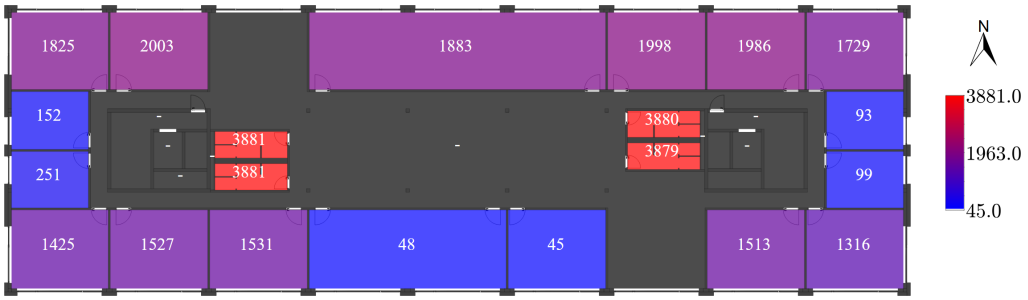

(b) Number of hours for $PMV < -0.5$.

Figure A.10: Number of hours above and below Category II ($-0.5 < PMV < 0.5$) for the occupied hours on the top floor, without external shading.

Figure A.11 visualizes the degree-hours exceeding the Category II limits of [DIN16798-1]. As the analyzed cooling system has been sized for an extreme summer day, the degree-hours observed for the south-east and north-east corner offices have been decreased by 0.2% each compared to the typical-day-sized system in Figure 4.16, i.e. a reduction from 377.9 Kh to 358.1 Kh for the north-east office, and a reduction from 563.5 Kh to 546 Kh for the south-east office. However, even though the extreme day sizing reveals a slight reduction of the degree-hours, still five offices exceed the acceptable threshold of 1% degree-hours.

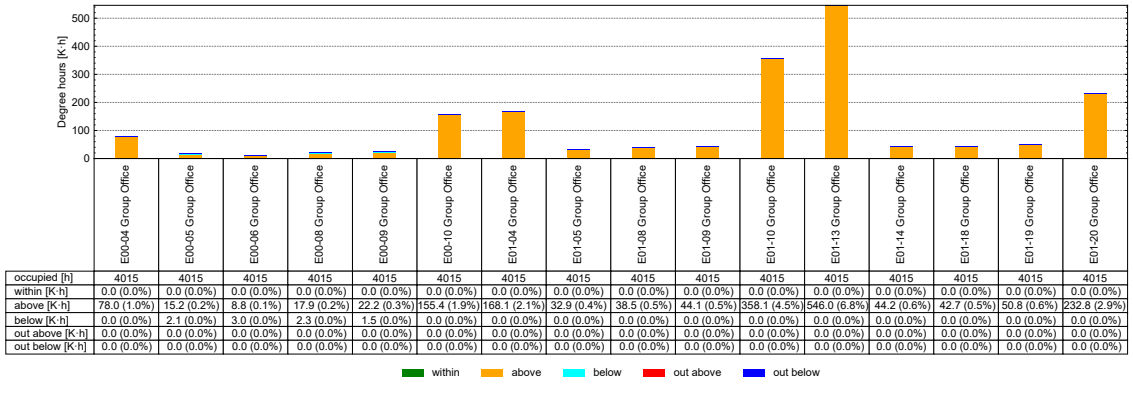

	E00-04 Group Office	E00-05 Group Office	E00-06 Group Office	E00-08 Group Office	E00-09 Group Office	E00-10 Group Office	E01-04 Group Office	E01-05 Group Office	E01-08 Group Office	E01-09 Group Office	E01-10 Group Office	E01-13 Group Office	E01-14 Group Office	E01-18 Group Office	E01-19 Group Office	E01-20 Group Office
occupied [h]	4015	4015	4015	4015	4015	4015	4015	4015	4015	4015	4015	4015	4015	4015	4015	4015
within [K·h]	0.0 (0.0%)	0.0 (0.0%)	0.0 (0.0%)	0.0 (0.0%)	0.0 (0.0%)	0.0 (0.0%)	0.0 (0.0%)	0.0 (0.0%)	0.0 (0.0%)	0.0 (0.0%)	0.0 (0.0%)	0.0 (0.0%)	0.0 (0.0%)	0.0 (0.0%)	0.0 (0.0%)	0.0 (0.0%)
above [K·h]	78.0 (1.0%)	15.2 (0.2%)	8.8 (0.1%)	17.9 (0.2%)	22.2 (0.3%)	155.4 (1.9%)	168.1 (2.1%)	32.9 (0.4%)	38.5 (0.5%)	44.1 (0.5%)	358.1 (4.5%)	546.0 (6.8%)	44.2 (0.6%)	42.7 (0.5%)	50.8 (0.6%)	232.8 (2.9%)
below [K·h]	0.0 (0.0%)	2.1 (0.0%)	3.0 (0.0%)	2.3 (0.0%)	1.5 (0.0%)	0.0 (0.0%)	0.0 (0.0%)	0.0 (0.0%)	0.0 (0.0%)	0.0 (0.0%)	0.0 (0.0%)	0.0 (0.0%)	0.0 (0.0%)	0.0 (0.0%)	0.0 (0.0%)	0.0 (0.0%)
out above [K·h]	0.0 (0.0%)	0.0 (0.0%)	0.0 (0.0%)	0.0 (0.0%)	0.0 (0.0%)	0.0 (0.0%)	0.0 (0.0%)	0.0 (0.0%)	0.0 (0.0%)	0.0 (0.0%)	0.0 (0.0%)	0.0 (0.0%)	0.0 (0.0%)	0.0 (0.0%)	0.0 (0.0%)	0.0 (0.0%)
out below [K·h]	0.0 (0.0%)	0.0 (0.0%)	0.0 (0.0%)	0.0 (0.0%)	0.0 (0.0%)	0.0 (0.0%)	0.0 (0.0%)	0.0 (0.0%)	0.0 (0.0%)	0.0 (0.0%)	0.0 (0.0%)	0.0 (0.0%)	0.0 (0.0%)	0.0 (0.0%)	0.0 (0.0%)	0.0 (0.0%)

Figure A.11: Adaptive over-temperature degree-hours for all group offices in the DigitalHub.

A.8.4 Local Thermal Comfort in the FZK Haus in Heating Period

This section provides additional results for the evaluation of local thermal comfort in the FZK Haus during the heating period, which is presented in Section 4.7.3. Figure A.12 displays the BEPS results for the *EG-05 Living* room on the ground floor of the FZK Haus, for December 9, 8am, visualizing the large difference between mean air temperature and operative temperature in the case with the IWU 1960 constructions, resulting from the operative temperature control and low surface temperatures due to low U-values.

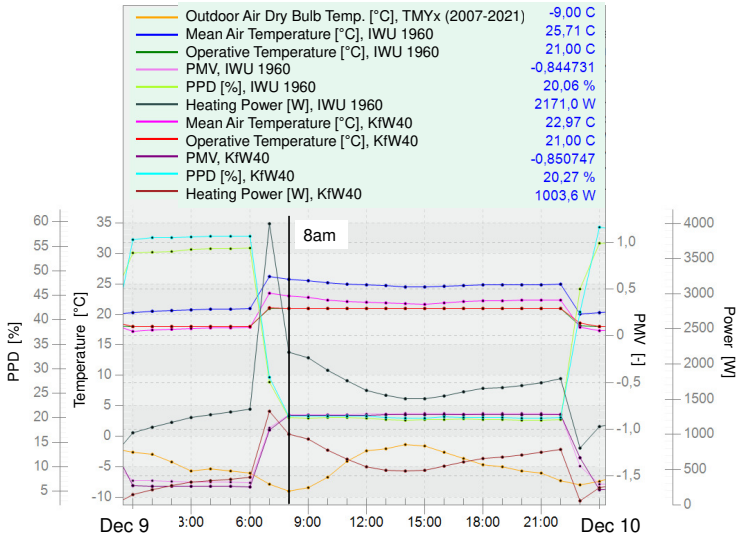

Figure A.12: Outdoor air temperature, zone air and operative temperature, PMV, PPD in the FZK Haus *Living* room (EG-05), using IWU 1960 and KfW40 constructions, simulated in EnergyPlus for the TMYx (2007-2021) weather data for Cologne/Bonn Airport, December 9, 8am.

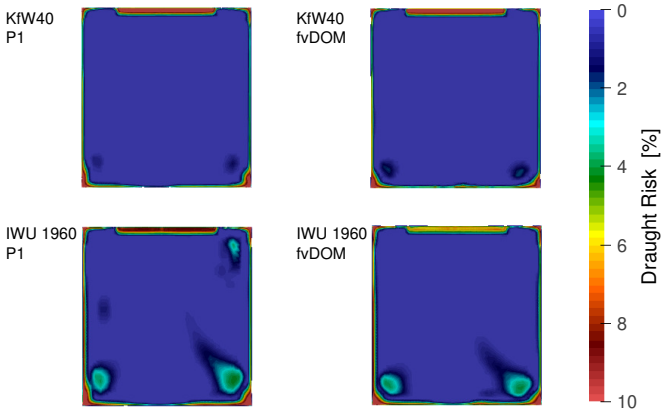

Figure A.13: FZK Haus, *Single office*. Draught risk at height of 1.1 m (head level) on January 17, 8am.

While this high temperature difference is included to represent the risk of extreme temperature deviations due to operative temperature control, the following results visualize the CFD results for the FZK office space on January 17, 8am. Here, Figure A.13 displays the DR, and Figure A.14 the air velocity exceeding the threshold according to [DIN16798-1], NA.

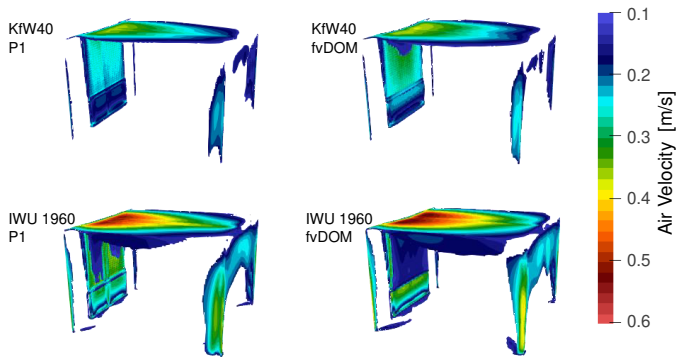

Figure A.14: FZK Haus, *Single office*. Air velocities larger acceptable limit of 0.13 m/s on January 17, 8am.

A.8.5 Local Thermal Comfort in the DigitalHub using Typical Day System Sizing

This section presents an analysis of the local thermal comfort for the south-east *E01-13 Group office* at the top floor of the DigitalHub based on the EnergyPlus model without external shadings. The heating and cooling systems are autosized for typical summer and winter days of the TMYx (2007-2021) weather file, which is also used for the annual BEPS simulation.

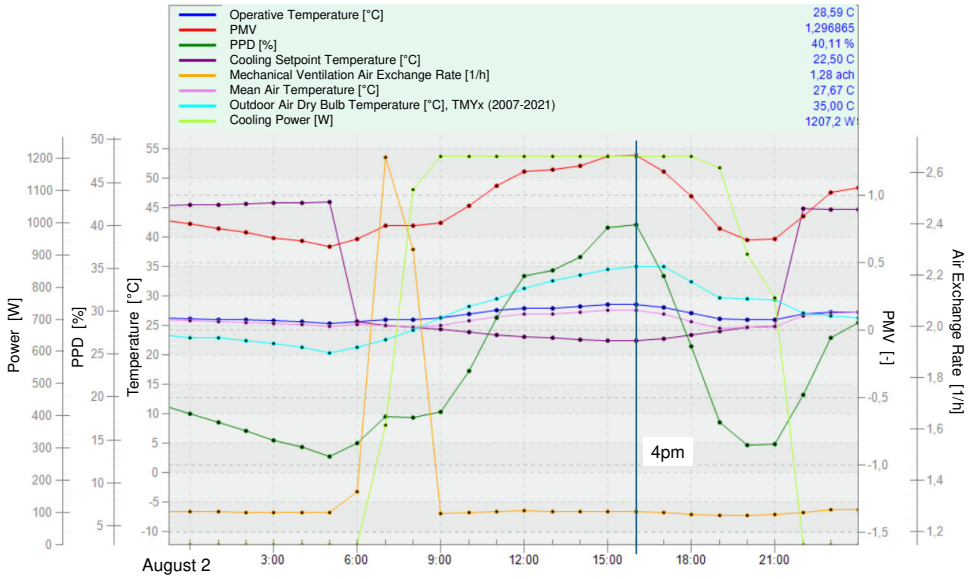

Figure A.15: EnergyPlus results for the south-east office space on August 2, 4pm. T_{op} = 301.74 K, T_{mean} = 300.82 K, T_{inlet} = 295.65 K for TMYx (2007-2021) weather data for Cologne/Bonn Airport.

The BEPS results for August 2, 4pm in Figure A.15 show operative temperatures exceeding the cooling setpoint limit of 26 °C, as the cooling systems have been sized for typical summer days to prevent oversizing, rather than for extreme summer days. Comparing these results to the simulated air temperatures in CFD (using the OpenFOAM model generated from BEPS for the same timestep), displayed in Figure A.16, the operative temperature only shows a small error (0.25/0.3 K), while the error of the mean air temperature is slightly larger (ca. 0.7 K) for both cases.

Since the resulting mean indoor air temperature is high (about 28 °C) in both cases, the vertical temperature stratification is low (cf. Figure A.16). This is also visible in the analysis of the vertical air temperature difference in Figure A.17, which results in a maximum vertical air temperature

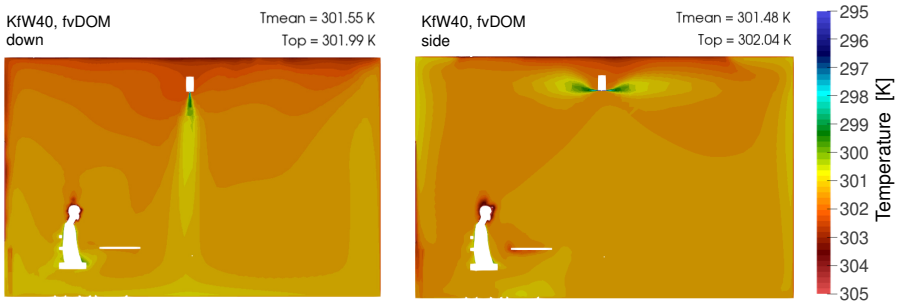

Figure A.16: Air Temperature distribution for August 2, 4pm.

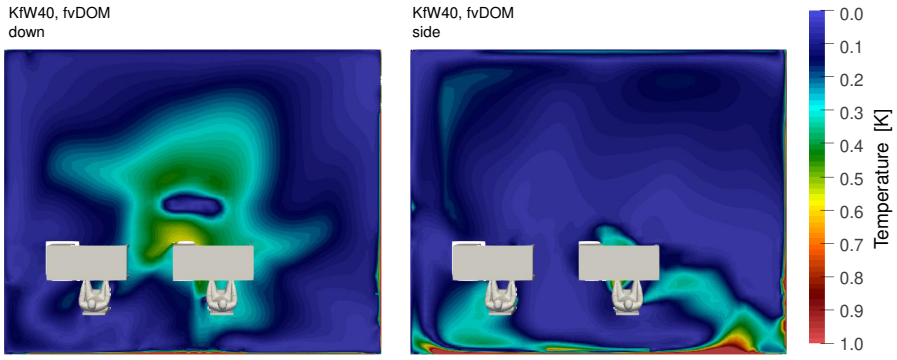

Figure A.17: Vertical air temperature difference between head and feet level.

difference of 0.6 K for the downward facing outflow, and an even lower maximum vertical difference of 0.3 K for the sidewards outflow. However, the sidewards outflow fails to properly mix the air in the space, resulting in a larger AoA than for the downward outflow (Figure A.18a), but also lower DR than the downward outflow (cf. Figure A.18b).

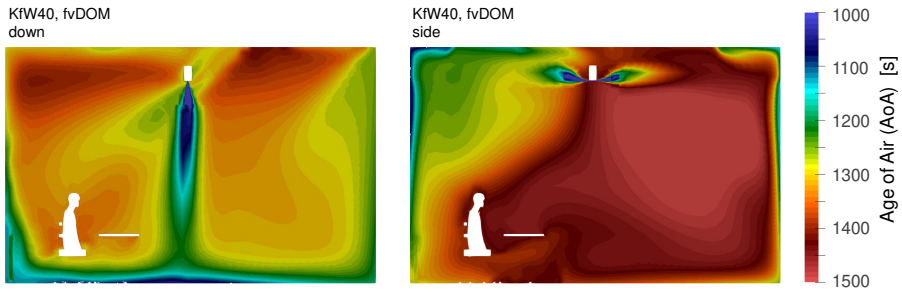

(a) Age of Air

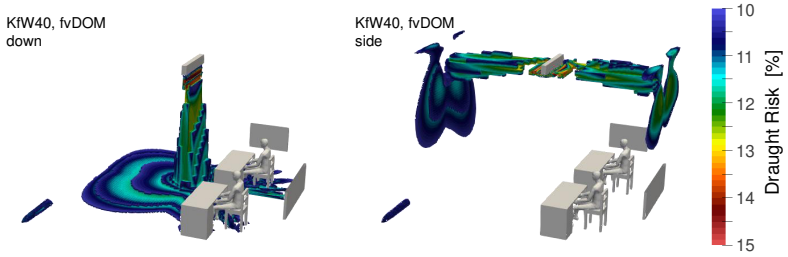

(b) Draught risk

Figure A.18: Vertical temperature difference, air velocities, and draft risk for August 2, 4pm.

The predicted mean PMV and PPD values in Figure A.19 from spatially high-resolved CFD

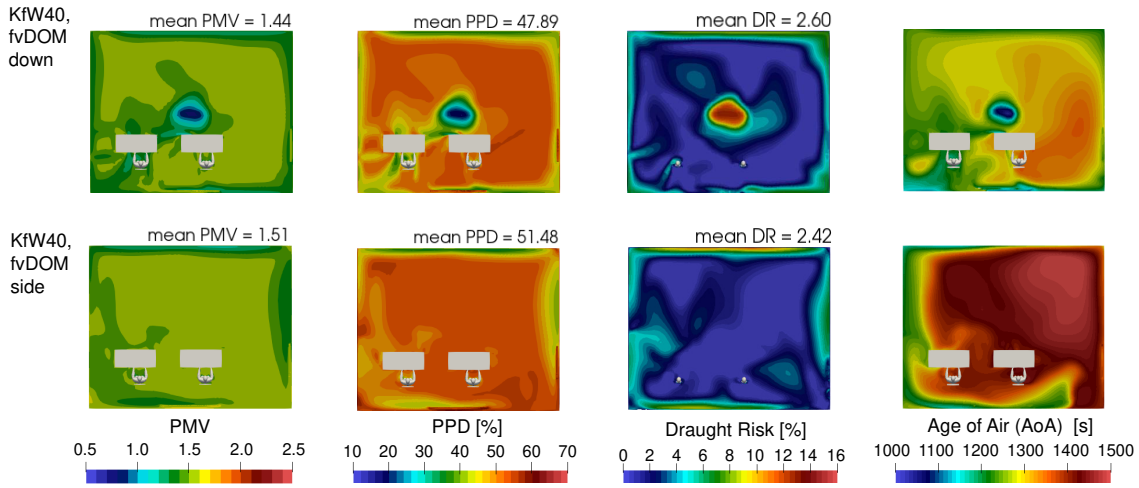

Figure A.19: PMV, PPD, and Age of Air at a height of 0.6 m and DR at a height of 1.1 m in the south-east office space for down- (top) and sidewards (bottom) outflow direction. Simulated for August 2, 4pm, sized and simulated using typical days of TMYx (2007-2021) weather data for Cologne/Bonn Airport.

simulation are higher (PMV of 1.44/1.51 vs. 1.30 and PPD 47.89%/51.48% vs. 40.11%) than those predicted in the EnergyPlus simulation (Figure A.15). The accuracy of the simulated CFD results under the IFC-based BEPS and CFD setups requires validation with measured data to ensure the correct interpretation of both, the BEPS and CFD results to prevent under- or overestimation of (local) thermal discomfort. The evaluation of the DR on head level (1.1m) in Figure A.19 visualizes the low DR, which is only estimated to 2.5%. The evaluation further additionally shows the difference in the air mixing in the space, as the AoA is a lot higher in the sidewards-facing flow than for the downward flow.

Evaluating the local thermal comfort for a hot summer day exceeding the cooling capacity limits visualized the low air temperature stratification caused by the comparatively low cooling capacity. The overall dissatisfaction with the indoor thermal comfort is comparatively high (up to 50%) and are mainly caused by high indoor air temperatures, as DR and vertical temperature differences are comparatively low. These exceeded cooling capacity limits of HVAC systems in operated buildings are likely to be a common issue in future climate scenarios.

A.8.6 Local Thermal Comfort in the DigitalHub using Extreme Day System Sizing

This section provides additional results on the case in Section 4.7.4, which analyzes the local thermal comfort in the DigitalHub, evaluating the system-sizing and simulation for the extreme day of the TMYx weather file.

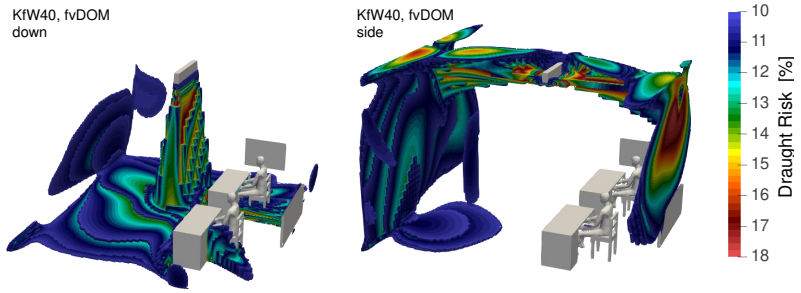

(a) Draught Risk (DR) above the Category I limit (10%, Cat II: 15%) defined in [DIN16798-1], NA

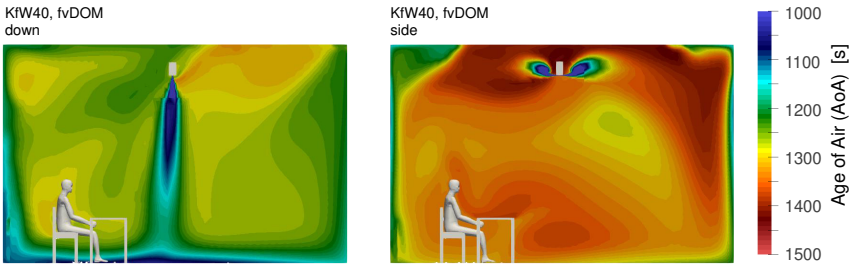

(b) Age of Air

Figure A.20: Draught Risk and Age of Air in the south-east office space for down- and sidewards outflow direction. Simulated for August 2, 4pm, sized and simulated using extreme summer day of TMYx (2007-2021) weather data for Cologne/Bonn Airport.

Figure A.20a visualizes the increased DR for the downward-facing outflow, while the sideward-facing outflow only minorly affects the DR in the occupied zone of the space. Figure A.20b displays the increased AoA for the sideward-facing outflow compared to the downward outflow, as the sideward-facing outflow results in an incomplete mixture of air.

A.9 Future Climate Scenarios

A.9.1 BEPS-based Thermal Comfort in Future Climate

This section provides additional results for the BEPS-based assessment of the impact of climate change on the thermal performance of buildings. This section includes the results for the DigitalHub, using system sizing for typical days of the SSP5-8.5 scenario prediction for the year 2050. In this section, both cases of shading are analyzed. First, the case without external shading elements, then, the case with external shading elements generated from external space boundaries using the IFC2SB tool by [Fic22].

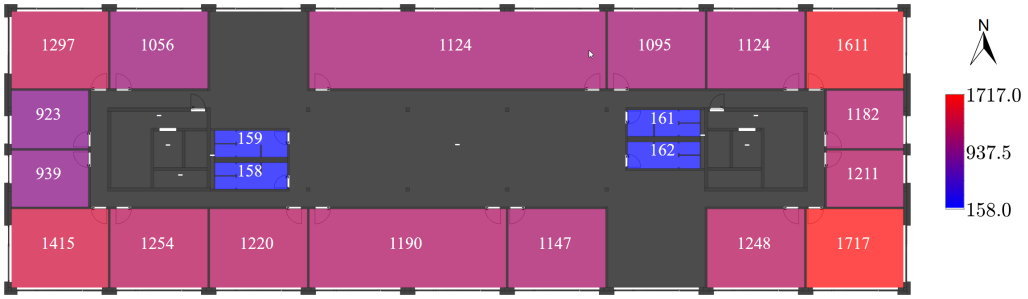

(a) Number of hours for $PMV > 0.5$.

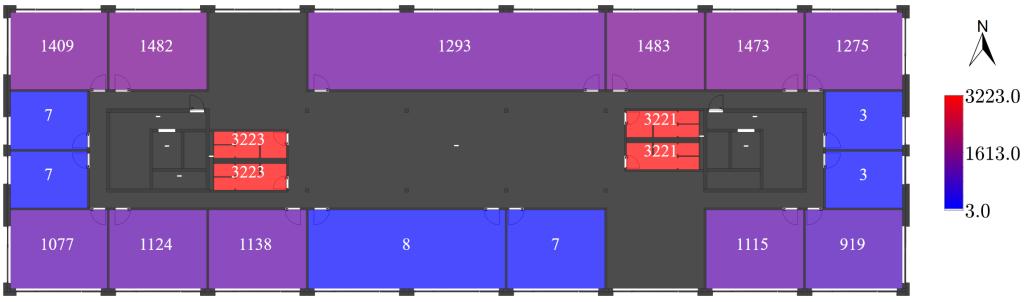

(b) Number of hours for $PMV < -0.5$.

Figure A.21: Number of hours above and below Category II ($-0.5 < PMV < 0.5$) for the occupied hours on the top floor, without external shading, for the SSP5-8.5 (2050) climate scenario.

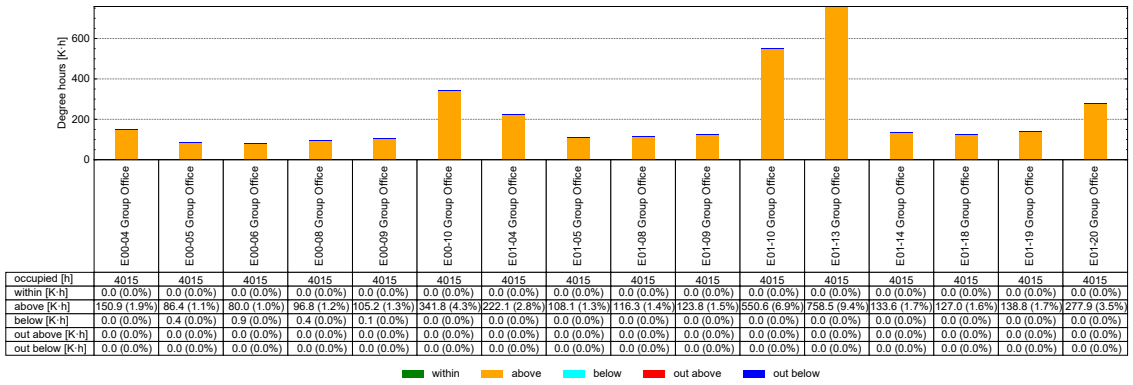

	E00-04 Group Office	E00-05 Group Office	E00-06 Group Office	E00-08 Group Office	E00-09 Group Office	E00-10 Group Office	E01-04 Group Office	E01-05 Group Office	E01-08 Group Office	E01-09 Group Office	E01-10 Group Office	E01-13 Group Office	E01-14 Group Office	E01-18 Group Office	E01-19 Group Office	E01-20 Group Office
occupied [h]	4015	4015	4015	4015	4015	4015	4015	4015	4015	4015	4015	4015	4015	4015	4015	4015
within [K·h]	0.0 (0.0%)	0.0 (0.0%)	0.0 (0.0%)	0.0 (0.0%)	0.0 (0.0%)	0.0 (0.0%)	0.0 (0.0%)	0.0 (0.0%)	0.0 (0.0%)	0.0 (0.0%)	0.0 (0.0%)	0.0 (0.0%)	0.0 (0.0%)	0.0 (0.0%)	0.0 (0.0%)	0.0 (0.0%)
above [K·h]	150.9 (1.9%)	86.4 (1.1%)	80.0 (1.0%)	96.8 (1.2%)	105.2 (1.3%)	341.8 (4.3%)	222.1 (2.8%)	108.1 (1.3%)	116.3 (1.4%)	123.8 (1.5%)	550.6 (6.9%)	758.5 (9.4%)	133.6 (1.7%)	127.0 (1.6%)	138.8 (1.7%)	277.9 (3.5%)
below [K·h]	0.0 (0.0%)	0.4 (0.0%)	0.9 (0.0%)	0.4 (0.0%)	0.1 (0.0%)	0.0 (0.0%)	0.0 (0.0%)	0.0 (0.0%)	0.0 (0.0%)	0.0 (0.0%)	0.0 (0.0%)	0.0 (0.0%)	0.0 (0.0%)	0.0 (0.0%)	0.0 (0.0%)	0.0 (0.0%)
out above [K·h]	0.0 (0.0%)	0.0 (0.0%)	0.0 (0.0%)	0.0 (0.0%)	0.0 (0.0%)	0.0 (0.0%)	0.0 (0.0%)	0.0 (0.0%)	0.0 (0.0%)	0.0 (0.0%)	0.0 (0.0%)	0.0 (0.0%)	0.0 (0.0%)	0.0 (0.0%)	0.0 (0.0%)	0.0 (0.0%)
out below [K·h]	0.0 (0.0%)	0.0 (0.0%)	0.0 (0.0%)	0.0 (0.0%)	0.0 (0.0%)	0.0 (0.0%)	0.0 (0.0%)	0.0 (0.0%)	0.0 (0.0%)	0.0 (0.0%)	0.0 (0.0%)	0.0 (0.0%)	0.0 (0.0%)	0.0 (0.0%)	0.0 (0.0%)	0.0 (0.0%)

Figure A.22: Degree-hours for the DigitalHub without external shading elements, typical-day-sized and simulated for the SSP5-8.5 (2050) scenario.

Figure A.21 displays the number of hours above and below PMV Category II for the DigitalHub without external shadings in the SSP5-8.5 (2050) scenario. The degree-hours of the DigitalHub without external shading elements are displayed in Figure A.22. Figure A.23 displays the number

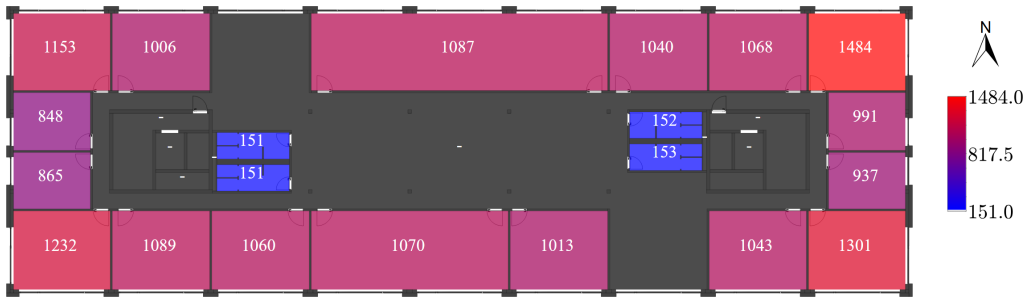

(a) Number of hours for $PMV > 0.5$.

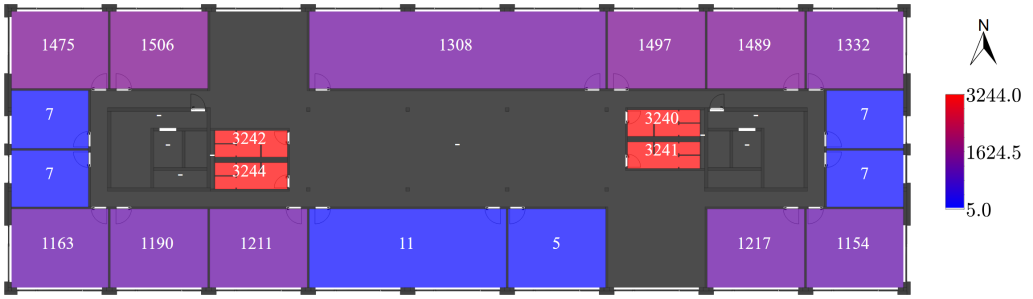

(b) Number of hours for $PMV < -0.5$.

Figure A.23: Number of hours above and below Category II ($-0.5 < PMV < 0.5$) for the occupied hours on the top floor, with external shading, for the SSP5-8.5 (2050) climate scenario.

occupied hours with PMV above and below the acceptable limits defined in [DIN16798-1], NA, for the DigitalHub use case with external shadings. Heating and cooling capacities are sized for a typical day in the SSP5-8.5 weather scenario. The degree-hours of the DigitalHub with external shading elements are displayed in Figure A.24.

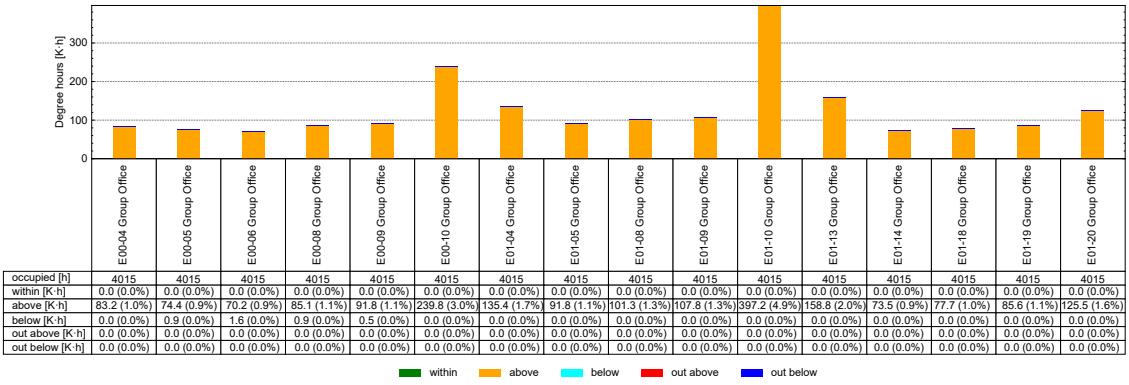

Figure A.24: Degree-hours for the DigitalHub with external shading elements, typical-day-sized and simulated for the SSP5-8.5 (2050) scenario.

Figure A.25 displays the heatmap of the PMV and the adaptive thermal comfort for the case with external shadings. Both metrics are evaluated for the categories defined in [DIN16798-1], NA, for the DigitalHub use case with external shadings for the south-east office on the top floor. Heating and cooling capacities are sized for a typical day in the SSP5-8.5 weather scenario.

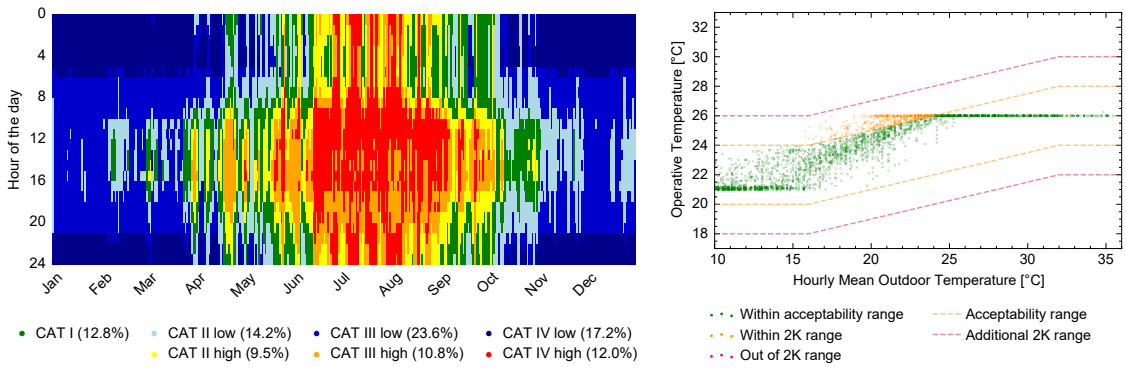

(a) Heatmap with PMV Categories.

(b) Adaptive thermal comfort.

Figure A.25: Group office top floor, south-east corner according to [DIN16798-1], NA, SSP5-8.5 (2050), with external shadings.

A.9.2 Local Thermal Comfort using a Future Typical Summer Day for System Sizing

Figure A.26 displays the BEPS results for the south-east office on the top floor. The cooling rate is twice the height of the TMYx (2007-2021) case (cf. Appendix A.8.5). Both of these cases are sized for typical summer days within their respective weather files. The SSP5-8.5 case does not reach the maximum cooling capacity limit, which results in better overall thermal comfort for SSP5-8.5 simulation than the TMYx case in Appendix A.8.5.

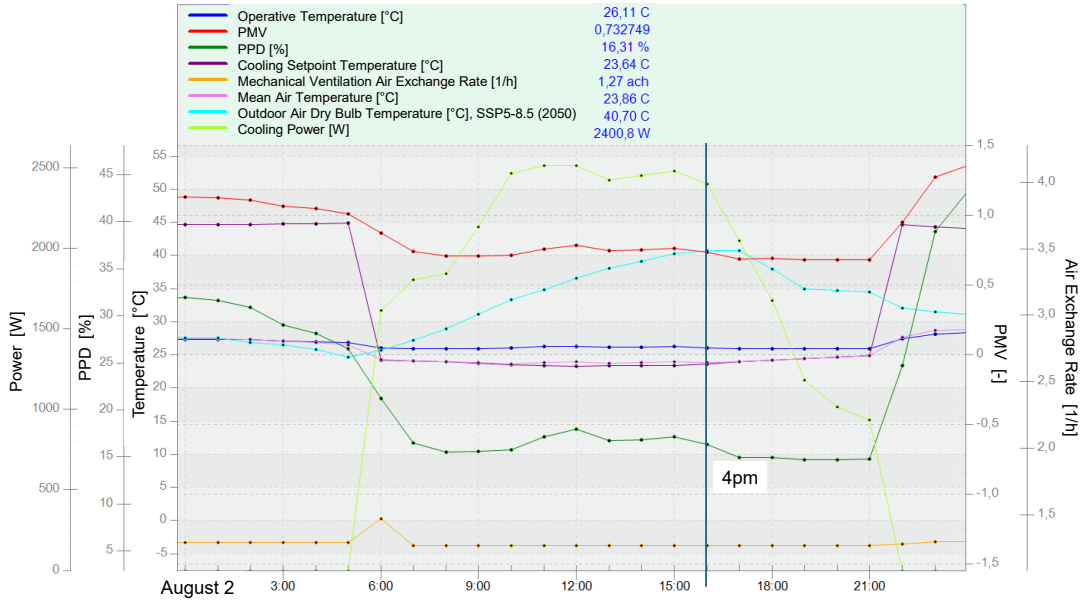

Figure A.26: EnergyPlus results for the south-east office space on August 2, 4pm. T_{op} = 299.26 K, T_{mean} = 296.79 K, $T_{set,cool}$ = 296.79 K in SSP5-8.5 (2050) scenario for Cologne/Bonn Airport, maximum cooling capacity is sized for a typical summer day of the applied weather scenario.

Figure A.27 displays the air temperature distribution in the south-east office. The downwards-facing outflow leads to a higher stratification than the sidewards-facing outflow. This difference in stratification is also visible in the vertical air temperature difference between head and feet level, displayed in Figure A.28. The vertical air temperature difference in Figure A.28 visualizes the differences for the vertical temperature distribution between the downward- and

sideward-facing outflow. However, both scenarios are within the acceptable range of vertical air temperature difference according to [DIN16798-1], NA.

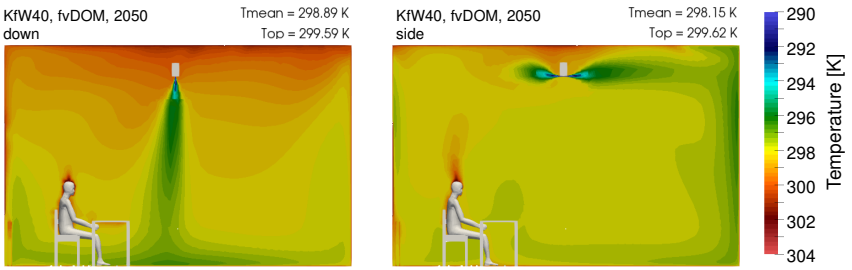

Figure A.27: Air temperature distribution in south-east office on August 2, 4pm, in SSP5-8.5 (2050) scenario, maximum cooling capacity is sized for a typical summer day of the applied weather scenario.

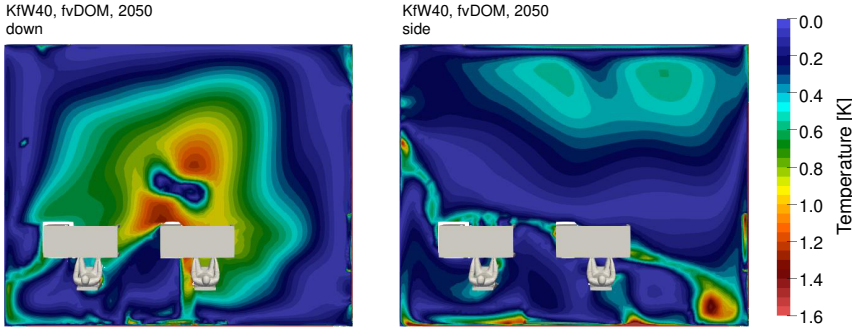

Figure A.28: Air temperature difference between head and feet level in south-east office on August 2, 4pm, in SSP5-8.5 (2050) scenario, maximum cooling capacity is sized for a typical summer day of the applied weather scenario.

Figure A.29 displays the air velocity exceeding the Category II threshold of [DIN16798-1], NA, 0.2 m/s. For the downward-facing outflow (left), the area above the floor shows increased air velocity, as well as the area around the occupants. Here, the occupants are increasingly affected by the air velocities. In the sideward-facing outflow case, only one of the occupants is affected by the increased air velocities, while also large parts of the floor surface show increased air velocities, which exceed the acceptable Category II range.

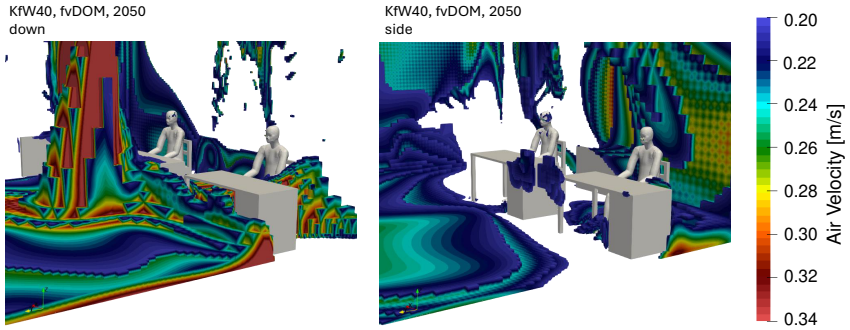

Figure A.29: Air velocity exceeding the Category II [DIN16798-1], NA limit of 0.2 m/s in south-east office on August 2, 4pm, in SSP5-8.5 (2050) scenario, maximum cooling capacity is sized for a typical summer day of the applied weather scenario.

Figure A.30 displays the resulting PMV, PPD, AoA, and DR, for the downward-facing outflow case (left) and the sideward-facing case (right). The resulting PMV in the occupied area is larger

for the downward-facing outflow (i.e., about 0.9), which is also reflected in the larger PPD (i.e., about 23%), compared to the sideward-facing outflow, where the PMV reaches about 0.85 in the occupied area, and the PPD is about 20% in the occupied area. The resulting DR is similar in both cases, showing a DR below 5% in large parts of the space. However, the downward-facing flow shows an increased local DR at the center of the space (25%), while the sideward-facing outflow shows an increased DR close to the walls (12%). The downward-facing airflow leads to a better mixture of air in the space, which is visible from the evaluation of the AoA in both cases. While the AoA is about 1200 s, i.e., about 20 minutes, the AoA in the sideward-facing case is about 1330 s in parts of the space, while other regions that are close to the overflow outlet underneath the door, which is located on the top-left of the view, show more similar AoA than the downward-facing case.

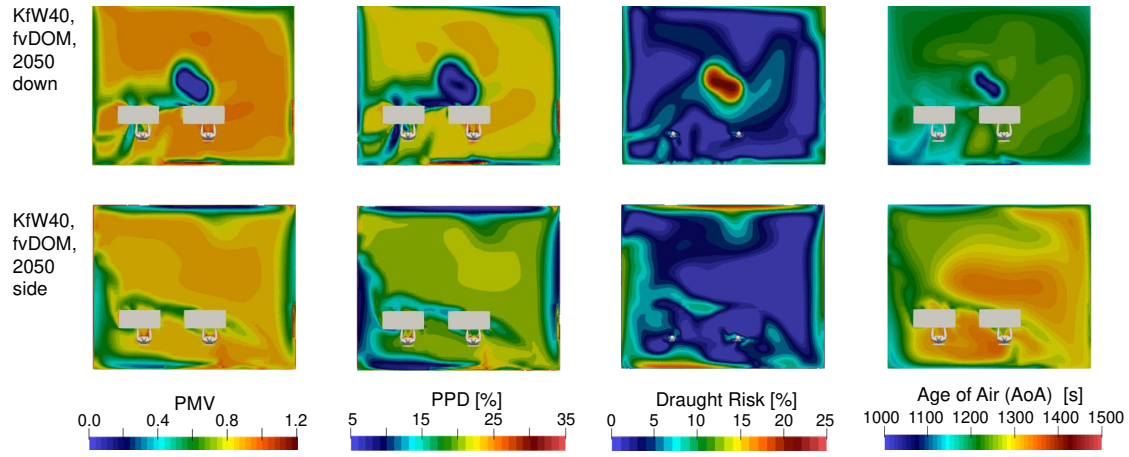

Figure A.30: PMV, PPD, and Age of Air at a height of 0.6 m and DR at a height of 1.1 m in the south-east office space for down- and sidewards outflow direction. Simulated for August 2, 4pm, in SSP5-8.5 (2050) scenario. Maximum cooling capacity is sized for a typical summer day of the applied weather scenario.

A.9.3 Future Local Thermal Comfort using a Historical Extreme Summer Day for System Sizing

The results of the CFD analysis of future local thermal comfort using heating and cooling capacities from TMYx-extreme-day-sized systems are presented and discussed in Section 5.4.3. As an addition to these results, Figure A.31 displays the prediction of the DR.

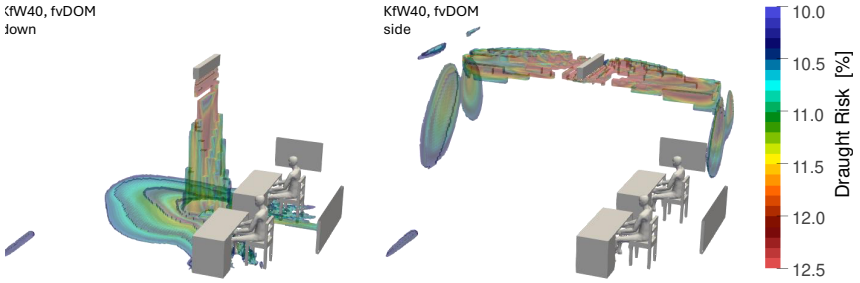

Figure A.31: Draught risk above the Category I threshold (10%, Category II: 15%) defined in [DIN16798-1], NA, in the south-east office space for down- and sidewards outflow direction. Simulated for August 2, 4pm, sized using extreme summer day of TMYx (2007-2021), simulated for SSP5-8.5 (2050) for Cologne/Bonn Airport.

A.10 Supplementary Material on Use Conditions

This section includes supplementary material for the simulations in Chapter 2, Chapter 4, and Chapter 5 for the template-based enrichment of the FZK Haus and the Digital Hub. The parameter stated in Table A.7 and in Table A.8 represent the maximum occupancy (calculated from the respective space area), lighting power, and mechanical equipment power based on their respective use conditions profiles. These profiles state the fraction of the maximum occupancy or power stated in the table.

A.10.1 FZK Haus

This section provides supplementary material for the template-based enrichment of the use conditions in the FZK Haus. Table A.7 shows the parameters of the use conditions. Figure A.32 shows the heating profiles, Figure A.33 the cooling profiles, Figure A.34 the occupancy profiles, Figure A.35 the machines profile, and Figure A.36 the lighting profile.

Table A.7: Input parameters within the template-based enrichment of use conditions in the FZK Haus, adapted from the original TEASER-Templates and the adaptations presented in [RSFvT23].

	Activity degree met	Heat flow rate (occupants) W/person	Machines W/m^2	Lighting W/m^2	Area per occupant m^2	Clothing clo	Clothing (surrounding) clo
Single office	1.2	125	7	3.33	14	0.66	0.15
Bedroom	0.8	84	4	2.00	10	0.33	2.00
Kitchen residential	1.9	199	40	1.33	5	0.81	0.00
WC residential	1.0	105	0	1.33	10	0.66	0.00
Traffic area	1.8	188	0	0.67	10	0.66	0.00
Living	1.1	115	2	0.50	50	0.66	0.15

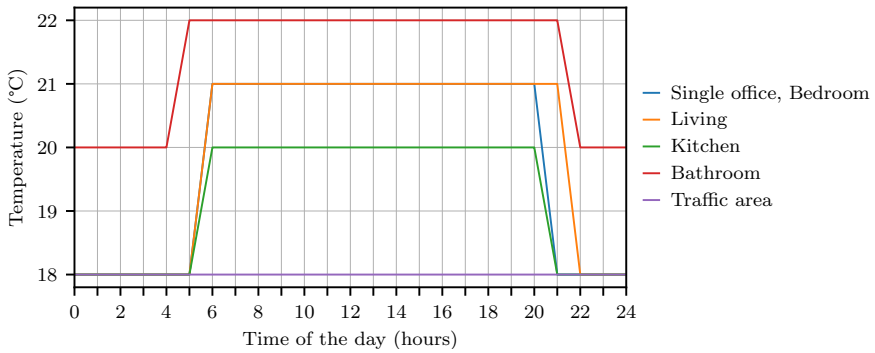

Figure A.32: FZK Haus heating profiles.

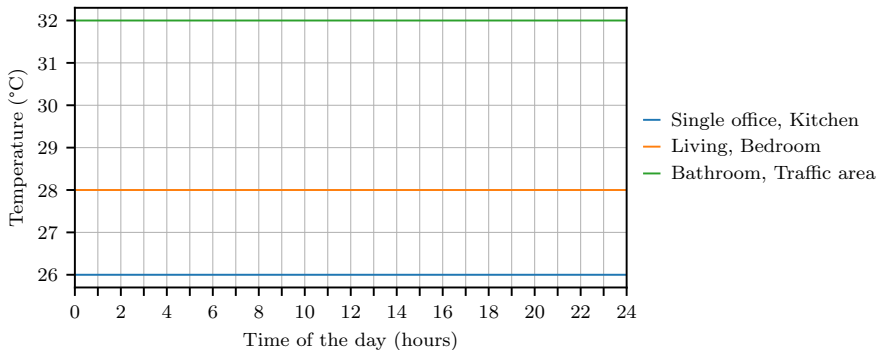

Figure A.33: FZK Haus cooling profiles.

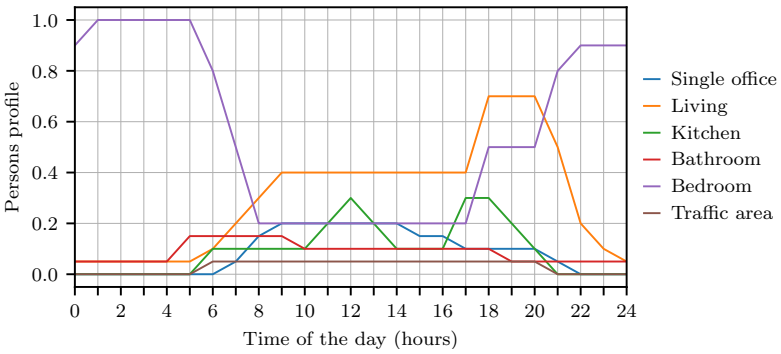

Figure A.34: FZK Haus occupancy profiles.

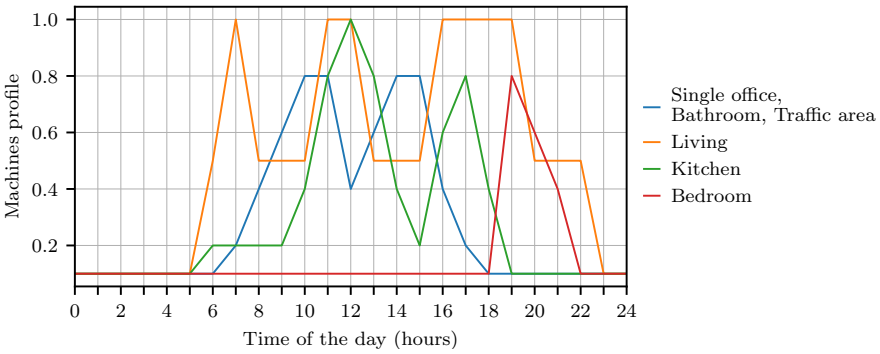

Figure A.35: FZK Haus machines profiles.

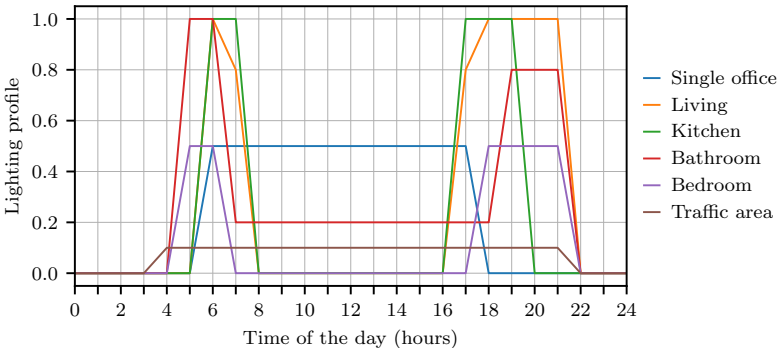

Figure A.36: FZK Haus lighting profiles.

A.10.2 DigitalHub

This section includes supplementary material for the simulations in Chapter 4 and Chapter 5 for the template-based enrichment of the DigitalHub. Figure A.37 displays the floor plans of the three-storey building. Table A.8 shows the parameters of the use conditions. Figure A.38 shows the heating profiles, Figure A.39 the cooling profiles, Figure A.40 the occupancy profiles, Figure A.41 the machines profile, and Figure A.42 the lighting profile.

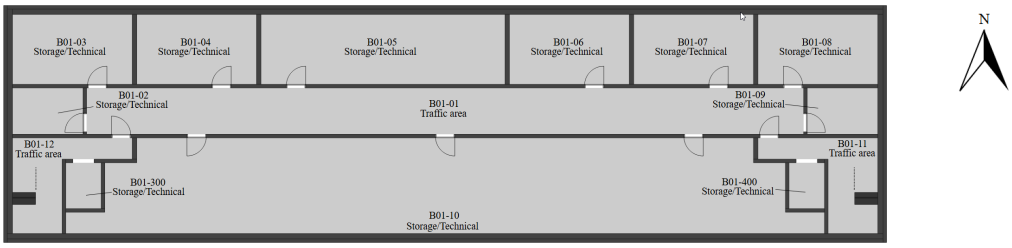

(a) Basement (B01)

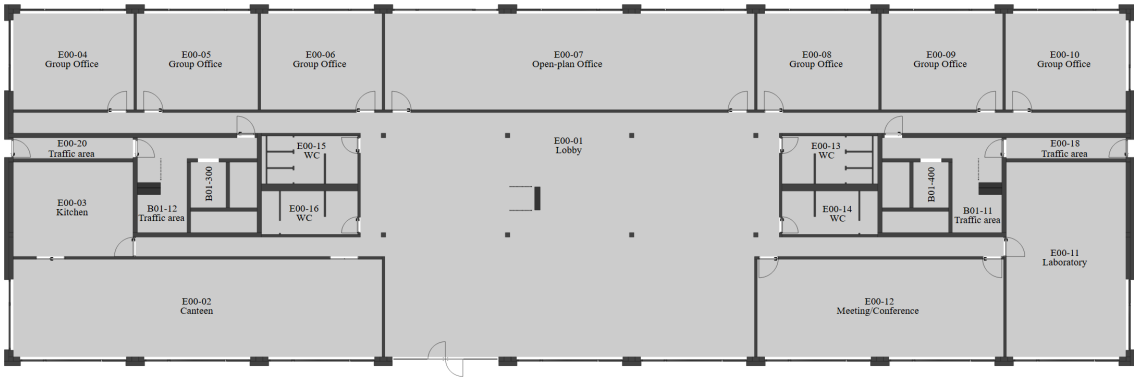

(b) Ground floor (E00)

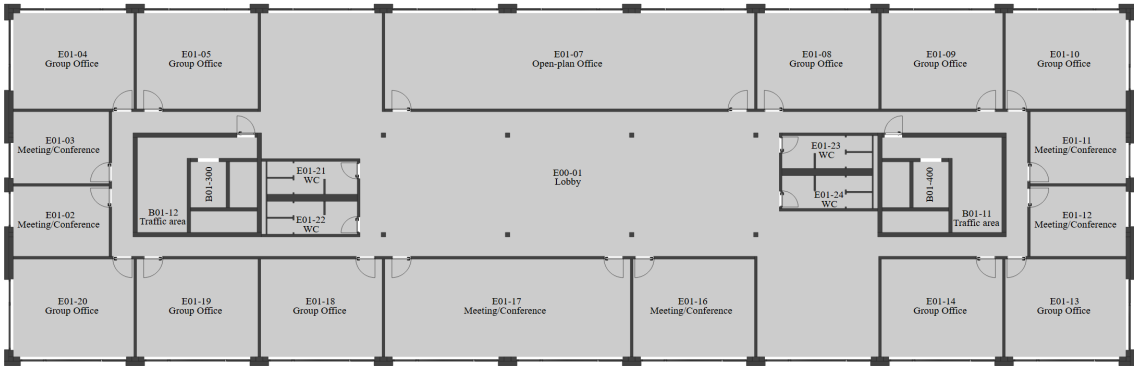

(c) First floor (E01)

Figure A.37: Floor plan of the DigitalHub.

Table A.8: Input parameters within the template-based enrichment of use conditions in the DigitalHub, adapted from the original TEASER-Templates.

	Activity degree met	Heat flow rate (occupants) W/person	Machines W/m^2	Lighting W/m^2	Area per occupant m^2	Clothing clo	Clothing (surrounding) clo
Group Office	1.2	125	7	3.33	14.00	0.66	0.10
Open-plan Office	1.2	125	10	3.33	10.00	0.66	0.10
Meeting	1.2	125	2	3.33	3.00	0.83	0.01
Lobby	1.7	178	4	2.00	12.00	0.98	0.10
Traffic area	1.8	188	0	0.67	10.00	0.66	0.00
Storage/Technics	1.5	157	0	0.67	40.00	0.66	0.00
Canteen	1.2	125	2	1.33	2.00	0.66	0.01
Laboratory	1.2	125	18	3.33	15.00	0.81	0.01
WC	1.0	105	0	1.33	10.00	0.66	0.00
Kitchen	1.9	199	300	3.33	2.00	0.81	0.00

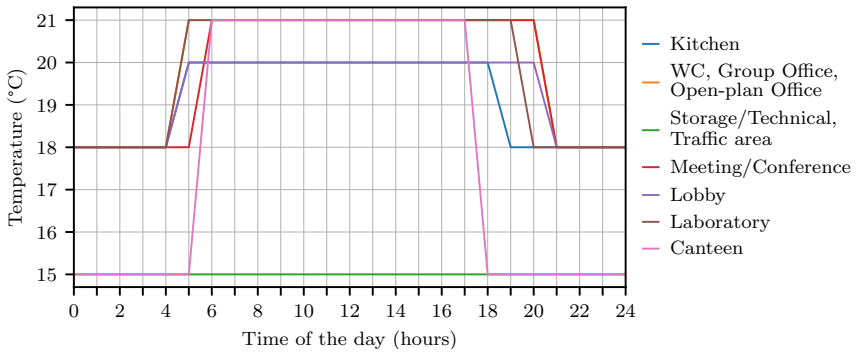

Figure A.38: DigitalHub heating profiles.

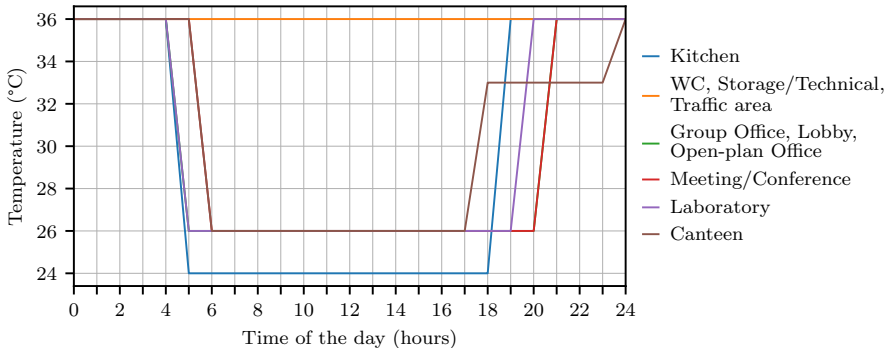

Figure A.39: DigitalHub cooling profiles.

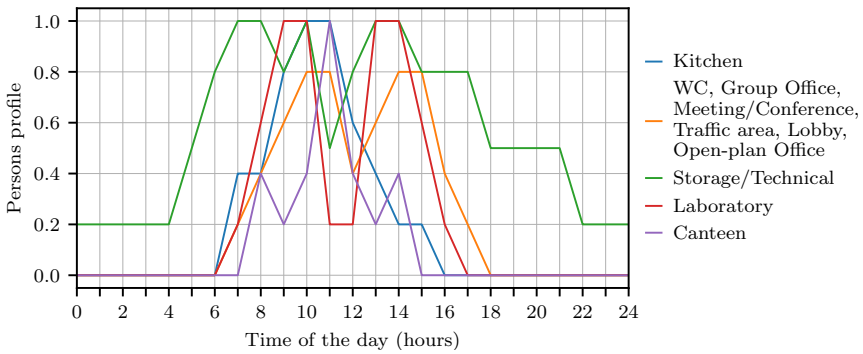

Figure A.40: DigitalHub occupancy profiles.

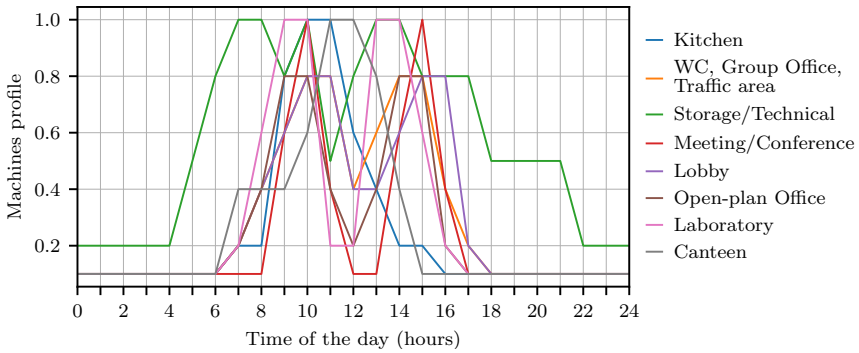

Figure A.41: DigitalHub machines profiles.

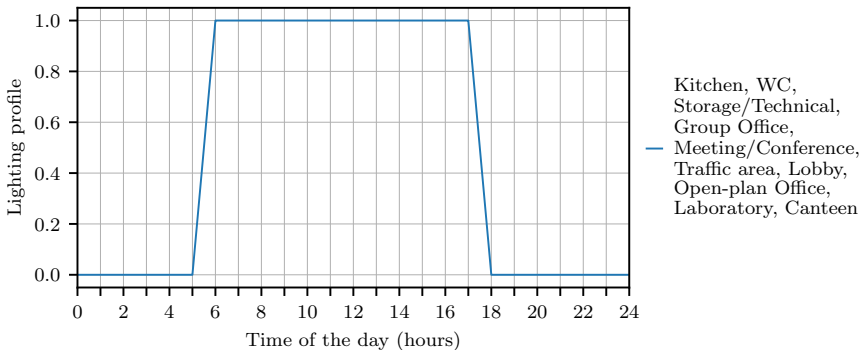

Figure A.42: DigitalHub lighting profiles.

A.11 Overview on BEPS Results

Table A.9: Overview on simulation results across all FZK Haus use cases.

Category			FZK	FZK	FZK	FZK	FZK	FZK
Location in Text	Section		2.7.3	4.7.1a / 4.7.3	4.7.1b	4.7.3	5.4.1a	5.4.1b
Weather	Location		Cologne/Bonn	Cologne/Bonn	Cologne/Bonn	Cologne/Bonn	Cologne/Bonn	Cologne/Bonn
Weather	Weather Scenario		TMYx (2007-2021)	TMYx (2007-2021)	TMYx (2007-2021)	TMYx (2007-2021)	SSP8-5 (2050)	SSP8-5 (2080)
Construction	ConstructionType		IWU heavy	KFW 40	KFW 40	IWU heavy	KFW 40	KFW 40
Construction	Year (if applicable)		1960			1960		
Construction	GlazingType		Wood / double glazing	Triple Glazing	Triple Glazing	Wood / double glazing	Triple Glazing	Triple Glazing
Construction	U-Value ExtWall	$W/(m^2 K)$	1.27	0.134	0.134	1.27	0.134	0.134
Construction	U-Value Ground	$W/(m^2 K)$	1.98	0.192	0.192	1.98	0.192	0.192
Construction	U-Value Roof	$W/(m^2 K)$	2.17	0.095	0.095	2.17	0.095	0.095
Construction	U-Value ExtDoor	$W/(m^2 K)$	1.291	1.291	1.291	1.291	1.291	1.291
Construction	U-Value IntWall	$W/(m^2 K)$	1.613	0.703	0.703	1.613	0.703	0.703
Construction	U-Value IntFloor	$W/(m^2 K)$	1.632	0.534	0.534	1.632	0.534	0.534
Construction	U-Value IntDoor	$W/(m^2 K)$	1.157	1.157	1.157	1.157	1.157	1.157
Construction	U-Value ExtWindow	$W/(m^2 K)$	2.7	0.799	0.799	2.7	0.799	0.799
Shading	Shading Control Activation	W/m^2	None	150	150	150	150	150
Shading	Exterior Shading (SBs)		None	None	None	None	None	None
Ventilation	Natural/Mechanical		Natural	Natural	Natural	Natural	Natural	Natural
Setpoints	Heating	°C	18/20/21/24	18/20/21/22	18/20/22	18/20/21/22	18/20/21/22	18/20/21/22
Setpoints	Cooling	°C	None	None	None	None	None	None
Setpoint control	Operative / air temperature		air	operative	operative	operative	operative	operative
System Sizing	Heating Sizing		Unlimited	Unlimited	Unlimited	Unlimited	Unlimited	Unlimited
System Sizing	Cooling Sizing		None	None	None	None	None	None
System Sizing	Sizing Weather		same	same	same	same	same	same
Energy	Total Energy	$kWh/(m^2 a)$	168.03	52.77	57.12	233.92	41.18	35.73
	Total Heating Energy	$kWh/(m^2 a)$	150.14	34.89	39.23	216.04	23.29	17.85
	Total Cooling Energy	$kWh/(m^2 a)$	0	0	0	0	0	0
	Total Electric Energy	$kWh/(m^2 a)$	17.88	17.88	17.88	17.88	17.88	17.88

Table A.10: Overview on simulation results across all DigitalHub use cases.

Category			DH	DH	DH	DH	DH	DH
Location in Text	Section		4.7.2a / A.8.5	4.7.2b	A.8.3 / 4.7.4	5.4.2a	5.4.2b	5.4.3
Weather	Location		Cologne/Bonn	Cologne/Bonn	Cologne/Bonn	Cologne/Bonn	Cologne/Bonn	Cologne/Bonn
Weather	Weather Scenario		TMYx (2007-2021)	TMYx (2007-2021)	TMYx (2007-2021)	SSP8-5 (2050)	SSP8-5 (2050)	SSP8-5 (2050)
Construction	ConstructionType		KFW 40	KFW 40	KFW 40	KFW 40	KFW 40	KFW 40
Construction	Year (if applicable)							
Construction	GlazingType		Triple Glazing	Triple Glazing	Triple Glazing	Triple Glazing	Triple Glazing	Triple Glazing
Construction	U-Value ExtWall	$W/(m^2 K)$	0.134	0.134	0.134	0.134	0.134	0.134
Construction	U-Value Ground	$W/(m^2 K)$	0.192	0.192	0.192	0.192	0.192	0.192
Construction	U-Value Roof	$W/(m^2 K)$	0.095	0.095	0.095	0.095	0.095	0.095
Construction	U-Value ExtDoor	$W/(m^2 K)$	1.291	1.291	1.291	1.291	1.291	1.291
Construction	U-Value IntWall	$W/(m^2 K)$	0.703	0.703	0.703	0.703	0.703	0.703
Construction	U-Value IntFloor	$W/(m^2 K)$	0.534	0.534	0.534	0.534	0.534	0.534
Construction	U-Value IntDoor	$W/(m^2 K)$	1.157	1.157	1.157	1.157	1.157	1.157
Construction	U-Value ExtWindow	$W/(m^2 K)$	0.799	0.799	0.799	0.799	0.799	0.799
Shading	Shading Control Activation	W/m^2	150	150	150	150	150	150
Shading	Exterior Shading (SBs)		None	Yes	None	None	Yes	None
Ventilation	Natural/Mechanical		Mechanical	Mechanical	Mechanical	Mechanical	Mechanical	Mechanical
Setpoints	Heating	°C	21	21	21	21	21	21
Setpoints	Cooling	°C	26	26	26	26	26	26
Setpoint control	Operative / air temperature		operative	operative	operative	operative	operative	operative
System Sizing	Heating Sizing		Unlimited	Unlimited	ExtremeWinter	Unlimited	Unlimited	ExtremeWinter
System Sizing	Cooling Sizing		Auto TypSummer	Auto TypSummer	ExtremeSummer	Auto TypSummer	Auto TypSummer	ExtremeSummer
System Sizing	Sizing Weather		same	same	same	same	same	TMYx (2007-2021)
Energy	Total Energy	kWh/m²/a	61.61	64.1	58.35	61.17	61.73	57.22
	Total Heating Energy	kWh/m²/a	29.93	33.09	27.88	20.84	23.07	19.67
	Total Cooling Energy	kWh/m²/a	3.02	2.36	1.81	11.67	10.00	8.89
	Total Electric Energy	kWh/m²/a	28.66	28.66	28.66	28.66	28.66	28.66

A.12 Weather Data Statistics

Table A.11 shows an overview on the annual weather data statistics. Invalid values, i.e., humidity > 100% and direct normal radiation > solar constant (1367 W/m^2) (cf. Section 5.4) are highlighted and indicate the need for correction of both the data sets and the generation method.

Table A.11: Statistics on the annual weather data sets for Cologne/Bonn Airport. Observed invalid values are displayed in *italics*.

			TRY 2015	TMYx (2007-2021)	TRY 2045 (cold)	TRY 2045	TRY 2045 (hot)	SSP5-8.5 (2050)	SSP5-8.5 (2080)
Dry Bulb Temperature	°C	mean	10.6	11.2	11.0	11.7	12.3	14.3	16.0
		median	10.5	11.0	10.7	11.3	11.5	13.7	15.3
		min	-9.0	-9.0	-7.9	-6.9	-4.5	-4.6	-2.4
		max	31.0	35.0	36.5	31.9	36.5	40.7	41.6
Humidity	%	mean	77.1	74.5	75.8	76.4	74.0	73.2	72.9
		median	81.0	77.0	80.0	81.0	78.0	76.0	76.0
		min	22.0	19.0	17.0	17.0	12.0	22.0	22.0
		max	100.0	100.0	100.0	100.0	100.0	*108.0*	*110.0*
Direct Normal Radiation	W/m^2	mean	99.8	140.5	117.1	105.8	139.7	158.4	163.2
		median	0.0	0.0	0.0	0.0	0.0	1.0	1.0
		min	0.0	0.0	0.0	0.0	0.0	0.0	0.0
		max	998.3	888.0	971.7	962.7	964.8	*1980.0*	*1988.0*
Diffuse Horizontal Radiation	W/m^2	mean	64.0	52.6	64.4	63.4	62.7	67.4	66.1
		median	4.0	5.0	4.5	4.0	5.0	1.0	1.0
		min	0.0	0.0	0.0	0.0	0.0	0.0	0.0
		max	539.0	344.0	446.0	455.0	463.0	443.0	443.0
Longwave Sky Radiation	W/m^2	mean	311.8	316.1	310.1	316.7	312.5	353.8	362.8
		median	315.0	319.0	314.0	321.0	315.0	355.0	364.0
		min	183.0	192.0	173.0	183.0	195.0	208.0	218.0
		max	413.0	419.0	423.0	409.0	422.0	509.0	515.0
Wind Direction	°	mean	180.8	180.8	183.6	191.7	174.6	180.8	180.8
		median	160.0	160.0	160.0	180.0	158.0	160.0	160.0
		min	0.0	0.0	0.0	0.0	0.0	0.0	0.0
		max	360.0	360.0	360.0	360.0	360.0	360.0	360.0
Wind Speed	m/s	mean	3.3	3.4	3.3	3.3	3.1	3.3	3.3
		median	3.0	3.1	3.0	3.0	2.8	3.0	3.0
		min	0.1	0.0	0.1	0.2	0.0	0.0	0.0
		max	11.7	17.0	14.5	11.7	14.9	17.4	16.7
Pressure	Pa	mean	100643	100121	100726	100638	100811	100062	100102
		median	100600	100121	100700	100700	100900	100115	100100
		min	97800	100031	98100	95900	97100	99561	99635
		max	103100	100214	102800	103200	103500	100301	100461

Figure A.43 illustrates the outdoor air temperature and the direct normal radiation using violin plots. This visualization technique was adapted from [BHM$^+$20]. The visualization of the outdoor air temperature in Figure A.43a and the daily maximum direct normal radiation in Figure A.43b seem to match well with their respective boxplots in Figure 5.1 and Figure 5.2. However, the violin plot of all direct normal radiation values in Figure A.43c shows unexpected

characteristics for the SSP5-8.5 weather data, illustrated by the low mean and median values. Here, the high radiation peaks (cf. Figure 5.3) in the mornings are in the upper inter-quartile range, which is excluded from the violin representation. These violin plots underline the need for future research on generating future weather data, and further evaluation of their impact on the simulation results on different temporal scales. It is expected that these errors in direct normal radiation hardly affect the annual simulation results, but become visual on the thermal performance of buildings in weekly or daily evaluations.

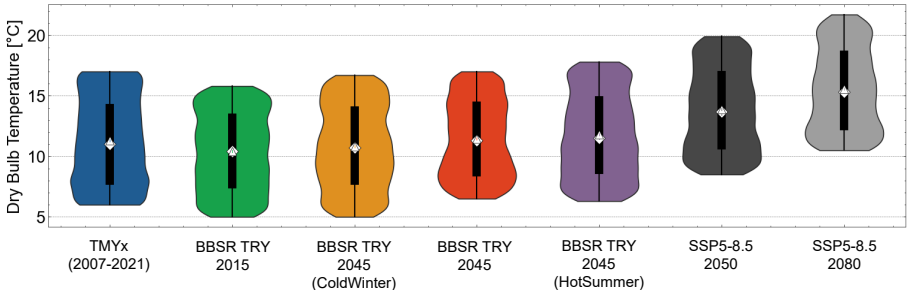

(a) Outdoor air temperature.

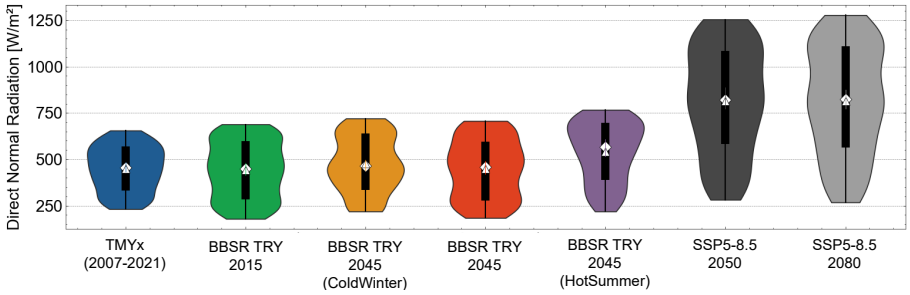

(b) Direct normal radiation, daily maximum values.

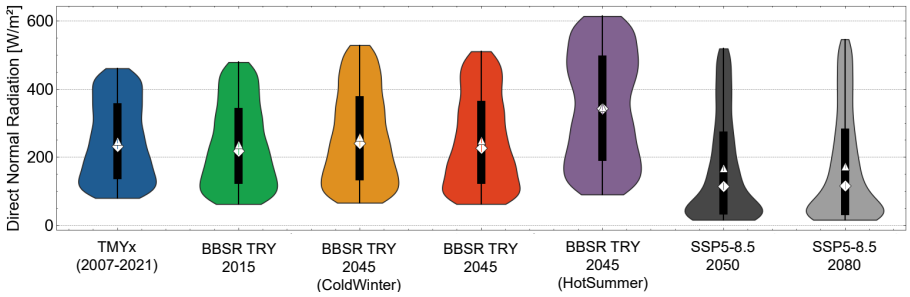

(c) Direct normal radiation.

Figure A.43: Violin plots of temperature and direct normal radiation for historical and future weather data for the Cologne/Bonn Airport. The violins are limited by upper and lower quartiles, the boxes are illustrate 1.5 of the inter-quartile range. Diamonds represent the median, triangles the mean value.